The Dissertation Committee for He Sun Certifies that this is the approved version of the following dissertation:

Studies of Unusual Catalysis: A Tale of Four Enzymes from Diverse Biosynthesis Pathways

Committee:

Hung-wen Liu, Supervisor

Eric V. Anslyn

Walter L. Fast

Sean M. Kerwin

Christian P. Whitman

Studies of Unusual Catalysis: A Tale of Four Enzymes from Diverse Biosynthesis Pathways

by

He Sun, B.S.;M.S.Ch.

Dissertation

Presented to the Faculty of the Graduate School of

The University of Texas at Austin

in Partial Fulfillment

of the Requirements

for the Degree of

Doctor of Philosophy

The University of Texas at Austin

December 2013

Acknowledgements

In the journey to my PhD, I have received tremendous support from people here and aboard. Without them, I wouldn't have been able to write this dissertation. Therefore, before I start to discuss my research, I would like to thank all of them for their years of help, support, and advice that lifted me up to this point.

First of all, I would like to thank my adviser Dr. Hung-wen (Ben) Liu for having me in his wonderful laboratory. Ben has provided me with an invaluable research environment, opportunities to learn from colleagues with diverse expertise, and the freedom to work on challenging and important scientific questions. His passion and dedication to the research greatly encouraged me while perusing my PhD. I also want to thank Dr. Yung-nan Liu for her years of care and support. Yung-nan taught me cloning and protein purification techniques when I started my studies and helped me purify many of the proteins used in my research. She is really kind and takes care of everyone in the lab.

I would also like to thank both former and present Liu lab members for their great help and support. I am sincerely grateful to our current postdoctoral scholar Dr. Mark W. Ruszczycky. Mark gave me immense help both in research projects and scientific writing and presentations. His thorough logical approach towards scientific questions inspires me a lot and is a good model for me to learn from. I especially appreciate Mark for generously proofreading this whole dissertation. I am also very grateful to the former graduate student Dr. Eita Sasaki. Eita taught me a lot in my graduate studies from designing experiments to specific hands-on skills. He is also my Japanese teacher and a good friend. Special thanks also need to be given to Drs. Yasushi Ogasawara, Steven

Mansoorabadi, Christopher Thibodeaux, Wei-chen Chang, Sei-hyun Choi, and Ying Zhou. Yasushi taught me a lot of useful skills and gave helpful suggestions for my research. Steve helped me with my department presentation and candidacy examination. Chris introduced me to the UDP-galactopyranose mutase project and provided me the flavin analogues used in the studies. Wei-chen and Sei were the synthetic experts in the lab, and several compounds used in the assays or as standards were provided by them. I had great time with Ying before she graduated and learned a lot from her. I want to thank all the current Liu Lab members as well. Specially, Chia-I, Meilan, Anthony, Mel, Ke-yi, and Geng-min. Chia-I, Anthony, and Geng-min kindly proofread part of this dissertation, and they are very helpful in discussions of my research projects. Meilan is a very nice friend to have and helps me a lot in my daily life. Mel helped me in my course work, and Ke-yi provided useful information in both research and life.

I am grateful to all the committee members. They are excellent teachers, and I have learned a lot from their lectures. I would especially like to thank Dr. Walter L. Fast for his support and encouragement during my rotation in his group. I would also like to thank Mr. Steven D. Sorey in the Nuclear Magnetic Resonance Facility in UT Chemistry Department for his great assistance in the positional isotope exchange experiments. Lastly, I would like to thank my former advisors Dr. Kang Zhao at Tianjin University and Dr. Zhaohui (Sunny) Zhou at Northestern University for their long-term support and encouragement.

Finally, I want to say thank you to my parents in China and my husband in Dallas. They have been very understanding and supportive of all my decisions, and this dissertation is dedicated to them as a gift for their love.

Studies of Unusual Catalysis: A Tale of Four Enzymes from Diverse Biosynthesis Pathways

He Sun, Ph. D.

The University of Texas at Austin, 2013

Supervisor: Hung-wen Liu

The diverse reactions that enzymes catalyze have fascinated enzymologists for decades. Continuing investigations in the biosynthesis of both primary and secondary metabolites have led to the discovery of enzymes that employ unusual ways to mediate bio-transformations. Exploration of such atypical biological catalysts is not only important for a comprehensive understanding of the natural products biosynthesis, but also providing new insights that are potentially valuable for developing novel compounds with enhanced biological activities. This dissertation describes the characterization of four enzymes that demonstrate unusual catalytic properties in different biosynthesis pathways.

UDP-galactopyranose mutase (UGM) is required for cell wall biosynthesis in many microorganisms. It uses the common cofactor flavin adenine dinucleotide (FAD) in an unusual manner. Positional isotope exchange and kinetic linear free energy relationship studies provide a direct experimental evaluation of the nucleophilic participation by reduced FAD during UGM catalysis. MoeZ from *Amycolatopsis orientalis* is a unique sulfur carrier protein (SCP) activating enzyme that participates in the metabolism of sulfur. Unlike reported pathway specific homologues, MoeZ can

activate multiple SCPs from different biosynthesis pathways found in *A. orientalis*. Herein, the enzyme is characterized biochemically, and a disulfide intermediate is suggested as part of its catalytic cycle for sulfur transfer from thiosulfate to SCPs. The last two enzymes, Fom3 and OxsB, belong to the cobalamin-dependent radical SAM class of enzymes. While these enzymes are believed to operate with unprecedented chemistry, they remain poorly understood and understudied. Fom3 is proposed to methylate an unactivated carbon center in the biosynthesis of fosfomycin, which is a clinically relevant antibiotic. OxsB is responsible for the biosynthesis of oxetanocin A, an oxetane ring containing nucleoside that exhibits antiviral activity. Efforts have been made to isolate active Fom3 and reconstitute the *in vitro* activity of OxsB. Reductive cleavage of SAM by the latter enzyme has been demonstrated for the first time and is described in this dissertation.

Table of Contents

List of Tables

List of Figures

Chapter 1: Nucleophilic Participation of Reduced Flavin Coenzyme in the Mechanism of UDP-Galactopyranose Mutase

1.1. INTRODUCTION

1.1.1. Occurrence and significance

Sugars are found ubiquitously in all living organisms where they play pivotal roles in structural integrity, energy storage, fertilization and development, cell proliferation and organization, host-pathogen interactions, inflammation, as well as immune responses.[1] In eukaryotes, a relatively small collection of monosaccharides dominate the carbohydrate chemistry of primary metabolism (see Fig. 1-1, **1-1** to **1-12**). In contrast, the development of extensive secondary metabolic pathways in prokaryotes has led to a much more diverse array of sugar structures. Thus, more than a hundred monosaccharide units have been reported in these organisms, including dexoy-, amino-, nitro-, and sulfur containing sugars.[2-3]

Within the great diversity of structures among glycoconjugates, hexoses are typically found in the pyranosyl form (e.g., **1-4**). However, during the last two decades, the furanosyl form (e.g., **1-12**) of the hexose unit has also attracted interest, because they are important structural components in a variety of microorganisms including a number of pathogenic ones. Furthermore, hexofuranose has not been found in mammals. This distribution of glycofuranosyl conjugates and their derivatives suggests unique opportunities for new drug development.[4]

Hexofuranosyl conjugates found in nature

Hexofuranosyl conjugates are important metabolic and structural constituents of many bacteria, protozoa, fungi, plants, and archaea. D-Galactofuranose (Fig. 1-2, Gal*f* **1-**

13) and D-fructofuranose (Fru*f* **1-14**) are the more frequently observed structures, whereas D-glucofuranose (Glu*f* **1-15**), D-fucofuranose (Fuc*f* **1-17**), 2-acetamido-2-deoxy-D-galactofuranose (Gal*f*NAc **1-16**), and D-streptose (**1-18**) are much less common.[4-5]

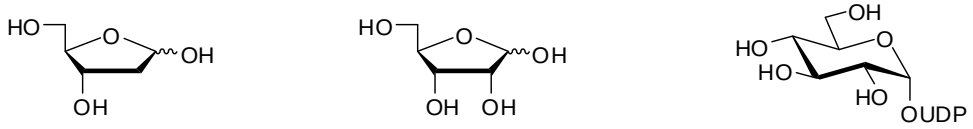

2-deoxy-D-ribose **1-1**

D-ribose **1-2**

UDP-D-glucose **1-3**

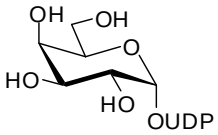

UDP-D-galactose (UDP-Gal*p*) **1-4**

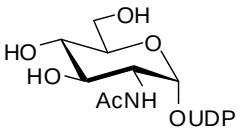

UDP-2-*N*-acetyl-D-glucosamine **1-5**

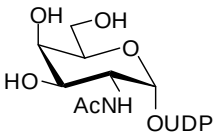

UDP-2-*N*-acetyl-D-galactosamine **1-6**

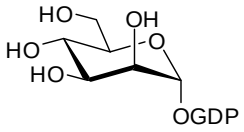

GDP-D-mannose **1-7**

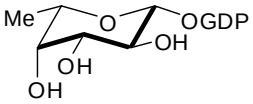

GDP-L-fucose **1-8**

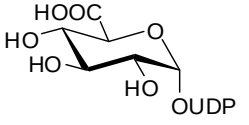

UDP-D-glucuronic acid **1-9**

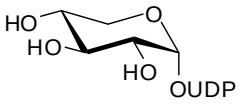

UDP-D-xylose **1-10**

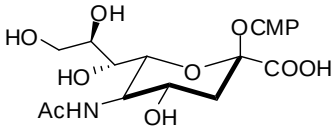

CMP-*N*-acetyl-neuraminic acid **1-11**

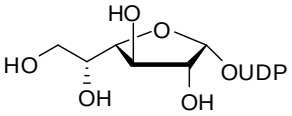

UDP-D-galactofuranose (UDP-Gal*f*) **1-12**

Figure 1-1: Examples of some sugars commonly used in primary metabolism.

An important example of a Gal*f* containing polysaccharides is arabinogalactan from the cell wall of *Mycobacterium tuberculosis* (Fig. 1-3 **A**). It contains a galactan chain of approximately 35 Gal*f* residues that is essential for the viability and virulence of *M. tuberculosis*.[6] Given the global prevalence of tuberculosis (World Health Organization Media Center) and the increasing incidence of multidrug resistant strains,[7] blocking the biosynthesis of Gal*f* appears to be an attractive alternative mechanism for new therapeutics.[8-9] The Gal*f* moiety is also present in some eukaryotic pathogens in the form of glycoconjugates such as lipophosphoglycan (LPG), glycoinositol phospholipids (GIPLs), and mucin-like proteins. These pathogens include *Trypanosoma cruzi*, the causative agent of Chagas diseas, and *Leishmania major*, the parasites that infects more than 10 million people worldwide through sand-fly mediated transmission.[10] Although less abundant, Gal*f* unit has also been observed in some species of fungus, such as *Aspergillus fumigates*, which is an important pathogen for immunodeficient patients. In fact, Gal*f* containing polysaccharides have been studied as markers for early diagnosis of clinical fungal infections.[11]

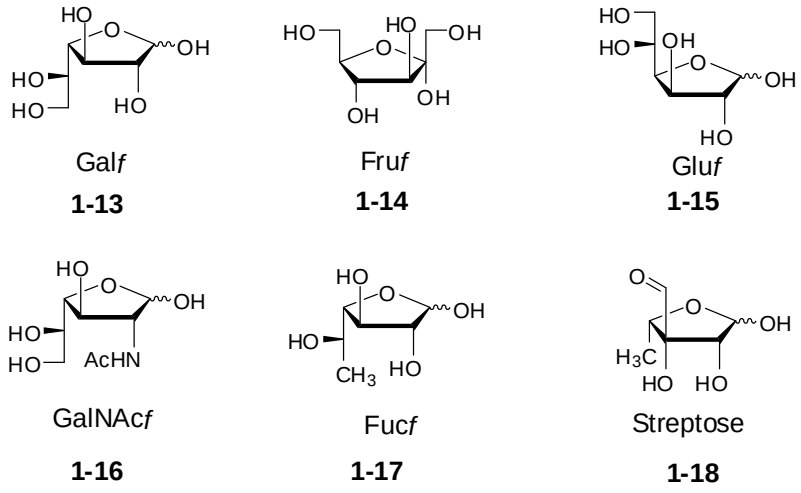

Figure 1-2: Structures of hexofuranoses observed in naturally occurring glycans.

In addition to the pathogenic microorganisms described above, hexofuranose containing glycans are also widely distributed among a number of other species including bacteria (both Gram-positive and Gram-negative), plants, algae, marine sponges, starfish, and archaebacteria. A selection of some of the interesting structures involving hexofuranoses is provided in Fig. 1-3. Here, the biological functions and activities of these glycans are briefly described and the furanose moieties are colored in red.[12]

Biosynthesis of hexofuranosyl conjugates

The biological construction of glycosidic linkages is typically catalyzed by glycosyltransferases (GTs), which couple activated sugars to the target acceptor molecules. Activated sugars are usually represented by nucleotide monophosphate (NMP) or nucleotide diphosphate (NDP) derivatives. For hexofuranosyl NDPs, they are most often biosynthesized from pyranosyl NDPs precursors in reactions catalyzed by specific mutases (except for D-Ara*f* conjugates whose biosynthesis also relies on polyisoprenyl donors in *Actinomycetales*).[12]

A well studied example is UDP-Gal*f*, the biological activated donor for the Gal*f* residue. The mutase responsible for the key ring contraction step converting UDP-Gal*p* to UDP-Gal*f* is UDP-galactopyranose mutase (UGM). UGM is a flavoenzyme that uses a reduced flavin cofactor to catalyze this redox-neutral isomerization (Fig. 1-4 **A**),[13] and it is the mechanism of this reaction in particular that represents the focus of this chapter.

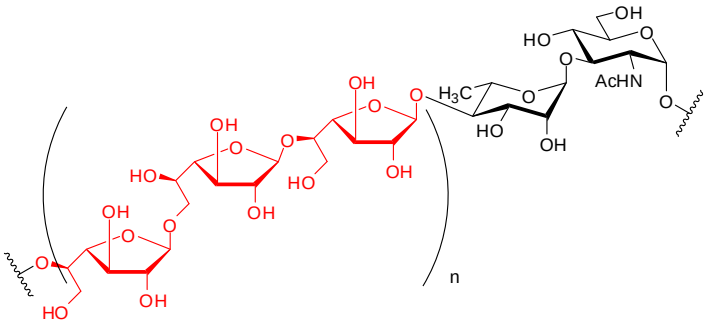

A. Fragment of arabinogalactan from mycobacteria cell wall.

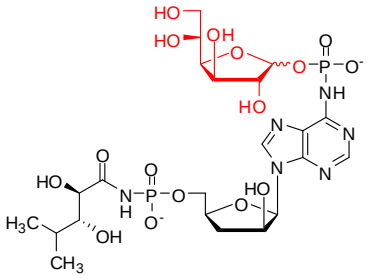

B. Anitbiotic agrocin 84 from *Agrobacterium tumefaciens* K84 strain.

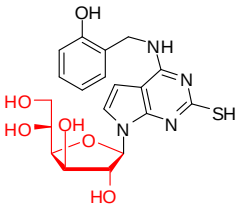

C. New purine derivative presenting cytokinin activity isolated from *Zantedeschia aethiopica.*

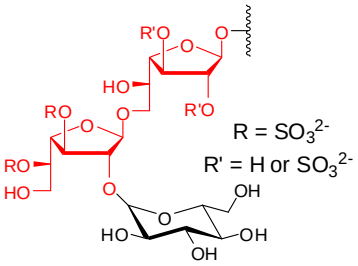

D. Sulfated polysaccharide-peptidoglycan fragment from *Arthrobacter sp.* that was shown to have antitumor activity.

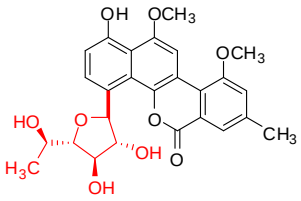

E. Gilvocarcin V from *Streptomyces gilvotanareus* that contains antibiotic and antitumor activity.

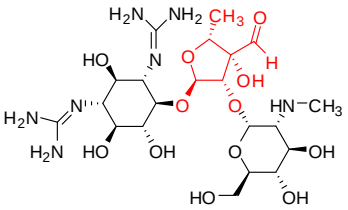

F. Aminoglycoside antibiotic streptomycin from *S. griseus.*

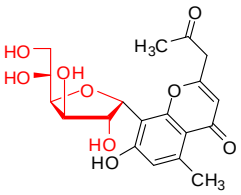

G. First natural C-glucofuranosyl chromone isolated from the leaves of *Aloe barbadensis*.

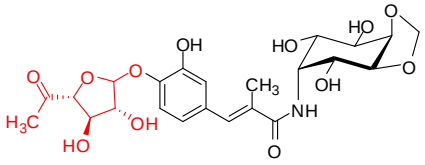

H. Antibiotic hygromycin A from Streptomyces hygroscopicus NRRL 2388.

Figure 1-3: Selected hexofuranosyl containing glycans and natural products.

A number of other important mutases similar to UGM have also been described. For example, UDP-*N*-acetyl-galactopyranose mutase (UNGM) has been recently described as a UGM homolog from *Campylobacter jejuni* 11168.[14] UNGM can accommodate both UDP-Gal and UDP-GalNAc. Interestingly, UDP-Gal is a better substrate for UNGM although only Gal*f*NAc residues have been found in the capsular polysaccharide glycoconjugates of *C. jejuni*.[15] The mechanism of UNGM is thought to be similar to that of UGM and the *N*-acetyl group is stabilized by the active site arginine residue (Fig. 1-4 **B**).[14] Likewise, TDP-fucopyranose mutase (Fcf2) from *E. coli* O52 has also been reported and shown to possess 60% identity to the *Klebsiella pneumonia* UGM. (Fig. 1-4 **C**).[16] Another identified mutase is UDP-arabinopyranose mutase (UAM), which catalyzes the interconversion of UDP-Ara*p* and UDP-Ara*f* (Fig. 1-4 **D**).[17] Arabinofuranose (Ara*f*) is another major component of glycoconjugates found in microorganisms and plant cell walls. Unlike UGM and UNGM, UAM does not require a cofactor for its activity. Recent studies suggest that in functional UAMs an arginyl residue is reversibly glycosylated with a single glycosyl residue, and that this residue is required for mutase activity.[18] While additional furanosyl units beyond those noted above have also described in biological systems, their biosyntheses are even less well understood.

With regard to the GTs that transfer the furanosyl moiety to the target acceptor, only the ones that are involved in the mycobacterial cell wall biosynthesis have been characterized. They are GlfT1 and GlfT2 and use UDP-Gal*f* as the donor in *M. tuberculosis*.[12] GlfT1 catalyzes attachment of the first two Gal*f* residues to the peptidoglycan anchor and GlfT2 catalyzes the subsequent polymerization of the galactan in a processive manner.[19]

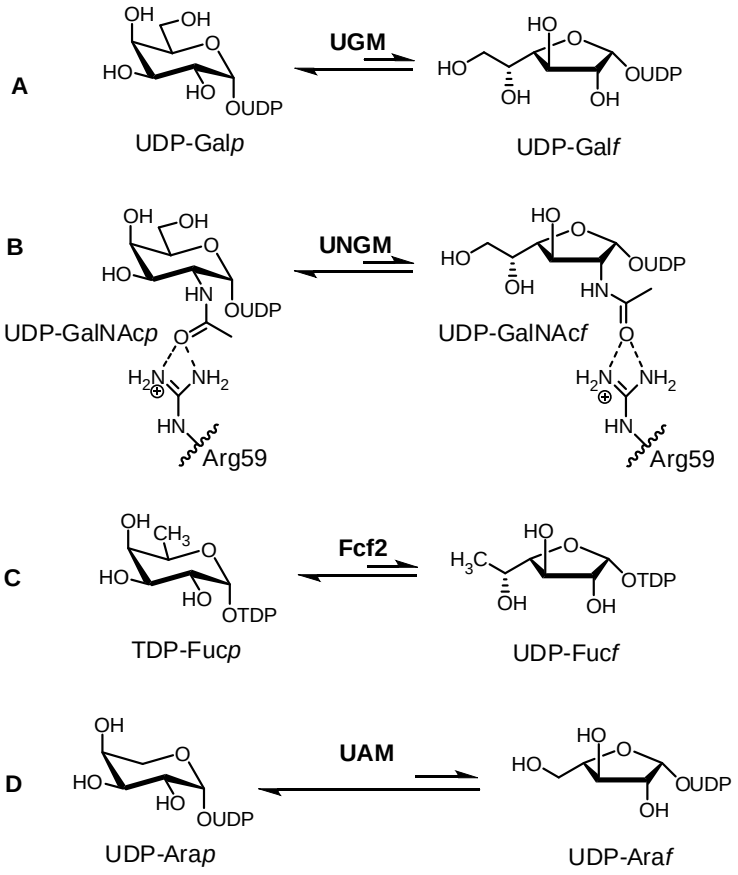

Figure 1-4: Reversible ring contraction/expansion reactions catalyzed by NDP-glycopyranose mutases.

1.1.2. Mechanistic hypotheses for UGM

UGM from *E. coli* was initially characterized in 1996.[20] Soon after, UGMs were also discovered in other prokaryotes such as *Klebsiella pneumonia* and *Mycobacterium tuberculosis*.[21-22] Recently, eukaryotic UGMs especially from human pathogens have begun to receive more attention. (e.g., *Trypanosoma cruzi* and *Aspergillus spp.*)[23-24] One key reason for the renewed interest in UGM is the recognition that the enzyme is required by the pathogens (for the biosynthesis of activated cell wall precursors) but not for mammals. Understanding the reaction mechanism of UGM is extremely important for

inhibitors design. Moreover, the reversible reaction catalyzed by UGM is also interesting from a purely biochemical point of view. As mentioned above, UGM requires the reduced flavin coenzyme (FAD_{red}, **1-24**) to catalyze a redox-neutral isomerization. This has raised questions about the catalytic function of the coenzyme during turnover.

The versatility of flavoenzymes

Flavoenzymes utilize flavin mononucleotide (FMN, **1-20**) and/or flavin adenine dinucleotide (FAD, **1-21**) as prosthetic groups to catalyze a wide range of chemical transformations. FMN and FAD are the biologically active forms of riboflavin (**1-22**), which is more commonly known as vitamin B_2 and is an essential dietary component for humans. In fact, the human genome contains 90 genes that encode flavoenzymes, and about 60% of them are associated with human disorders caused by mutations in the pertinent gene.[25]

Flavoenzymes are known to mediate a variety of oxidation/reduction reactions critical to different aspects of metabolism such as photosynthesis, aerobic respiration, denitrification, and sulfur respiration.[26] Compared to other essential cofactors involved in redox transformations such as nicotinamide coenzymes (NAD(P)/NAD(P)H) (hydride transfer only) and both heme- and non-heme iron-dependent enzymes (obligate to only one-electron transfer), the tricyclic isoalloxazine structure of the flavin cofactor allows it to access both two- and one-electron transfer reactions.[27] Therefore, the isoalloxazine ring of FAD (or FMN) can exist in three different oxidation states (Fig. 1-5): an oxidized form (FAD **1-21**), a one-electron-reduced neutral semiquinone ($FADH^{\bullet}$ **1-23**), and a two-electron-reduced hydroquinone (FAD_{red} or $FADH_2$ **1-24**).

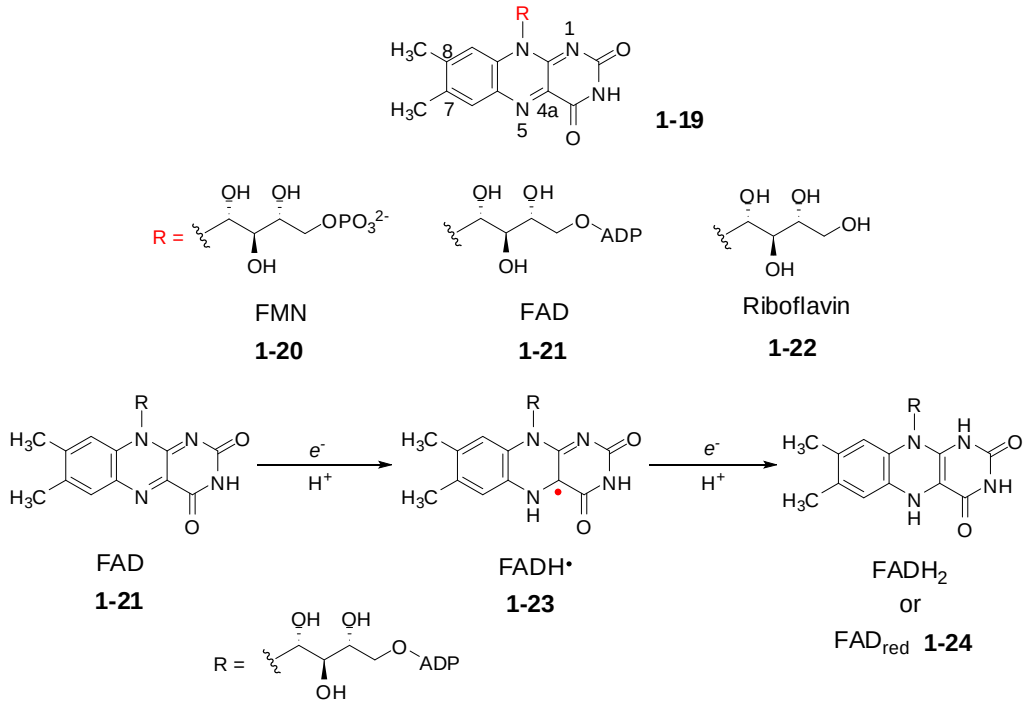

Figure 1-5: Structures of different forms of flavins and the three oxidation states of FAD.

Common types of redox reactions catalyzed by flavoenzymes are shown in Fig. 1-6. In the reductive half reactions, the bound flavin is reduced and the substrate is oxidized. Examples include desaturation reactions; amine, alcohol, and thiol oxidations; disulfide formations; as well as oxidizing NADPH to NADP. In the reoxidative half reactions, the reduced flavin generated from the reductive half reactions will be oxidized. Many flavoenzymes are also capable of reacting directly with molecular oxygen leading to the formation of a flavin-4a-OOH adduct. This adduct can then be used to carry out oxygenation reactions such as Baeyer-Villiger ring expansions, olefin epoxidations, halogenations via HOCl generation, and oxidative Favorskii rearrangements.[27]

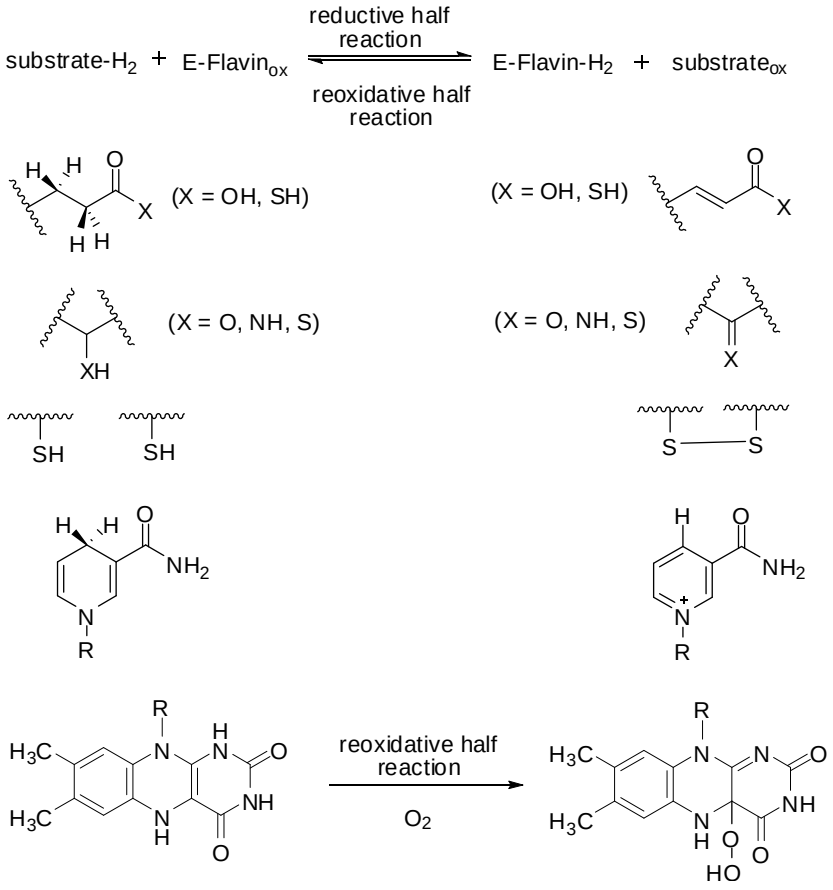

Figure 1-6: Common redox reactions catalyzed by flavoenzymes.

Noncanonical roles of flavin cofactor

Other than playing a redox role, recent findings have also suggested novel functions for flavin cofactor, especially in the case of net redox neutral reactions. For example, a class of FAD-containing TPP-dependent enzymes, such as CDP-4-aceto-3,6-dideoxygalactose synthase (CADS or YerE), utilize the flavin for structural purposes in order to maintain the integrity of the enzyme active site.[28] Similar cases where the flavin appears to be used in a purely structural manner have been reported for acetohydroxyacid synthase and glyoxylate carbo-ligase.[29]

Another non-redox role for the flavin cofactor is acid/base catalysis as in the case of type II isopentenyl diphosphate isomerase[30-31] and chorismate synthase, although in the latter case this has yet to be fully established.[32] Another instance where reduced FAD has been suggested to operate as an acid/base catalyst is in the reaction catalyzed by NikD, which catalyzes an aromatization reaction in the biosynthesis of nikkomycin and the proposed mechanism of NikD is shown in Fig. 1-7.[33] Recently, another flavin dependent enzyme named CrtY was reported and catalyzes the cyclization of lycopene in carotenoids formation in *Pantoea ananatis*. This enzyme can take either reduced FAD or FMN to catalyze the reaction, though higher rates of catalysis are reported with FAD_{red}.[34] An active site Glu residue is proposed to function as the general acid/base catalyst in the CrtY reaction, whereas the anionic form of FAD_{red} is hypothesized to stabilize a cationic intermediate (see Fig. 1-8).[35]

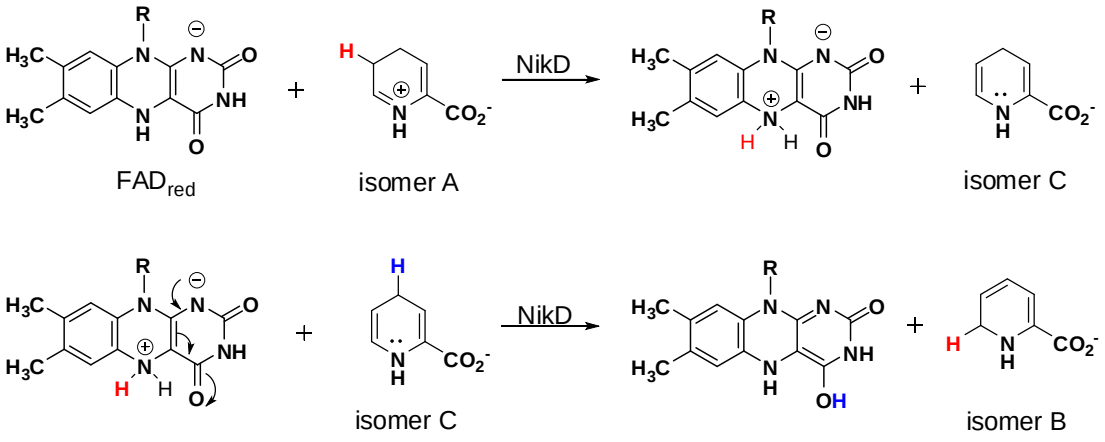

Figure 1-7: Proposed mechanism for NikD reaction.

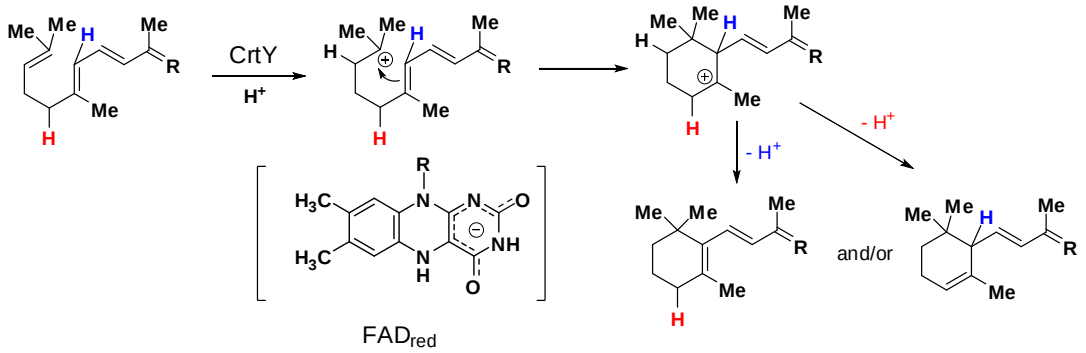

Figure 1-8: Propose mechanism for the CrtY catalyzed reaction. Whether the reaction mechanism is via a stepwise or concerted pathway was not clear.

Recent studies have also demonstrated that the N5 nitrogen of the flavin cofactor can form a covalent iminium adduct during enzyme turnover. One example is alkyl-dihydroxyacetonephosphate synthase (ADPS), a key enzyme in ether phospholipid biosynthesis.[35] This flavoenzyme catalyzes the net replacement of an ester linkage with an ether linkage using a tightly bound FAD cofactor (see Fig. 1-9). Here, the N5 nitrogen of FAD undergoes nucleophilic attack by a conjugate base of the acyl DHAP substrate. Participation of the N5 lone pair expels the acyl moiety to form an iminium intermediate. Addition of the long-chain alcohol followed by release of the FAD cofactor then gives the alkyl DHAP product.[36] The reaction mechanism of ADPS is analogous to the reductive half reaction of nitroalkane oxidase, where an overall redox change is involved.[27]

Another redox reaction involving a covalent flavin adduct intermediate is the unique tRNA methyltransferase TrmFO.[37] Typically, the methyl donor for tRNA methylation is *S*-adenosyl-L-methionine (SAM). However, in some Gram-positive bacteria, methylenetetrahydrofolate (CH_2THF) serves as the methyl donor. Recently, TrmFO from *Bacillus subtilis* was purified and studied *in vitro*.[38] TrmFO is a flavoenzyme that utilizes reduced FAD to generate 5-methyluridine at position 54

(m^5U_{54}) in the tRNA transcript. The flavin has been hypothesized to act as an intermediary during the methyl transfer reaction as shown in Fig. 1-10. During each turnover, FAD_{red} is oxidized upon reducing a methylene functionality to a methyl such that NAD(P)H is required to reduce the cofactor for further catalysis. The last example involving a substrate-flavin adduct will be UGM, and its mechanism will be discussed in detail in the following section.

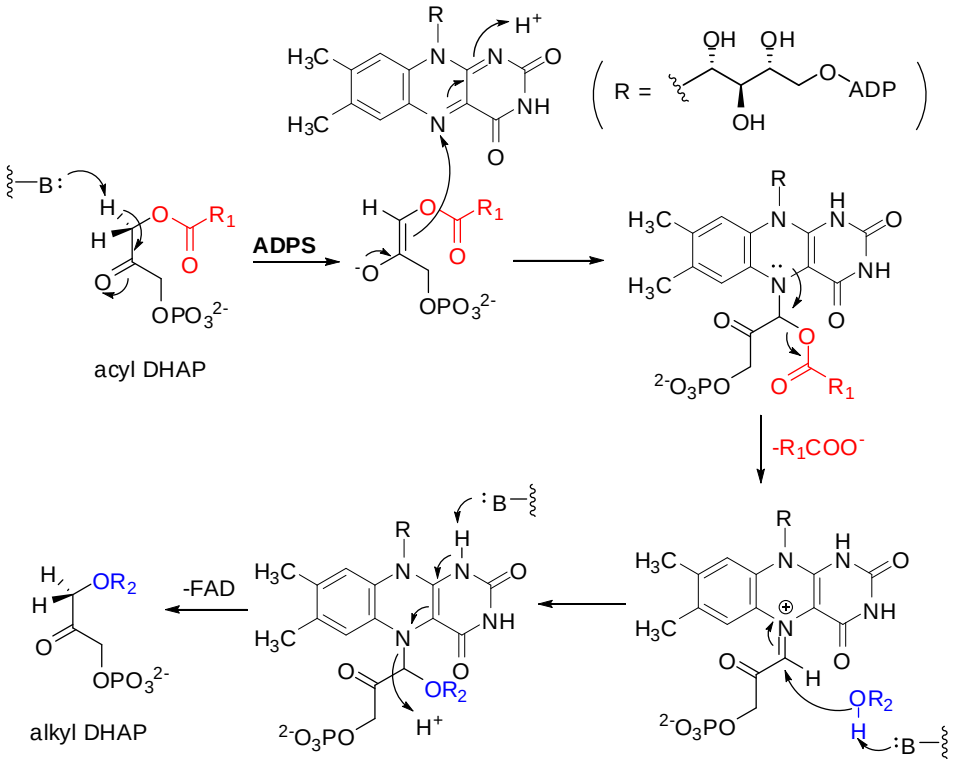

Figure 1-9: Proposed mechanism for ADPS. FAD serves as an electrophile in a redox neutral reaction forming a covalent FAD-substrate intermediate.

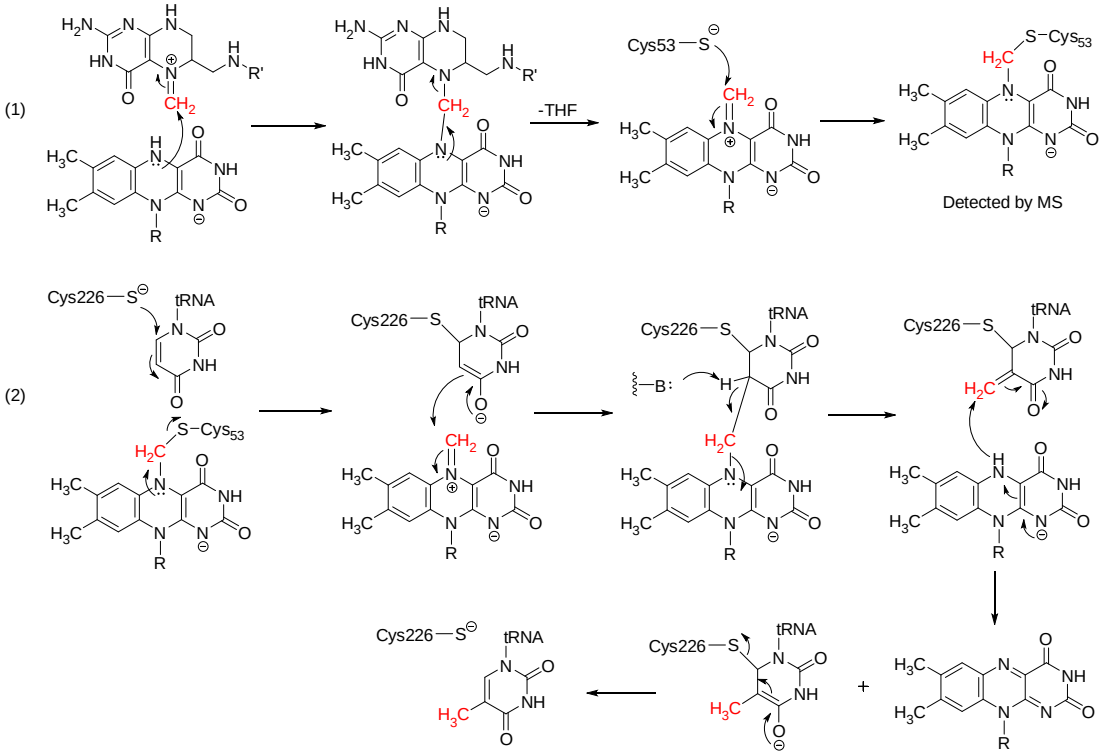

Figure 1-10: Proposed mechanism for the TrmFO catalyzed methylation reaction. (1) Formation of the covalent flavin intermediate. (2) Transfer the methylene group to the tRNA substrate and hydride transfer to complete the methylation.

A flavin-substrate covalent adduct is an intermediate in the UGM catalytic cycle

Several previous studies have provided important insights into the chemical mechanism of the UGM catalyzed reaction. Purified UGM from *E. coli* demonstrated a rate enhancement of more than two orders of magnitude in the presence of dithionite, suggesting reduced FAD is required for catalysis.[13] Given the redox properties of FAD, the mechanistic proposal envisioned for UGM shown in Fig. 1-11. However, this hypothesis was refuted by the following studies: (1) Using positional isotope exchange (PIX) studies, Blanchard and co-workers demonstrated that the anomeric C1-OP$_\beta$ bond is broken and reformed during turnover.[39] (2) Although rate reduction was observed,

fluorinated analogues UDP-[2-F]Gal*f*/*p* and UDP-[3-F]Gal*f*/*p* could be turned over by UGM.[40-41] At this point, the mechanism of UGM was proposed to involve a bi-cyclo acetal intermediate (**1-25**) as shown in Fig. 1-12, though the identity of the enzyme nucleophile was not clear.

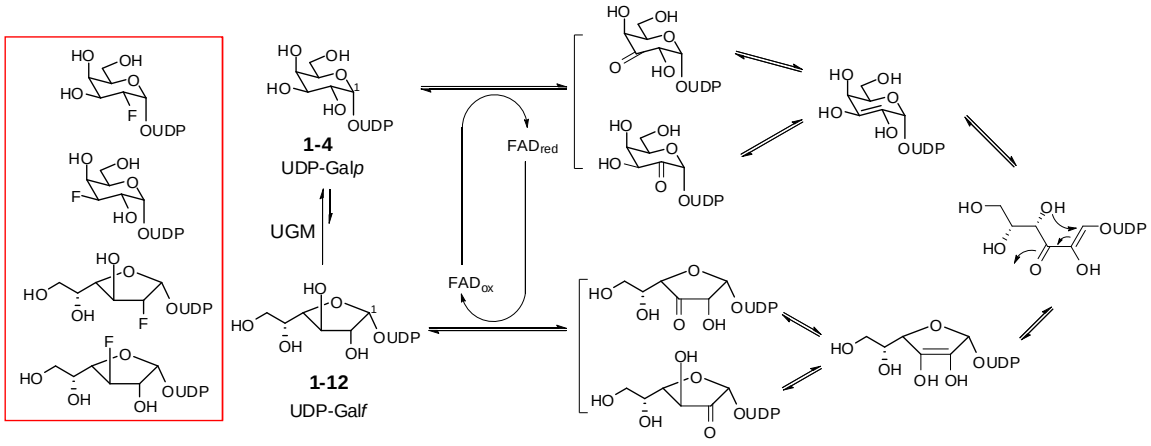

Figure 1-11: Early mechanistic hypothesis for UGM involving oxidation and reduction of the substrate.

Later, Huang *et al.* were able to reconstitute activity when apo-UGM, from which FAD had been removed, was incubated with 1-deaza-FAD but not 5-deaza-FAD.[42] This result suggested the importance of the N5 nitrogen of FAD, and a radical pathway leading to formation of a flavin-substrate iminium intermediate was proposed as shown in Fig. 1-14 (pathway C). Soon after, using $NaCNBH_3$ as a chemical quenching agent, Soltero-Higgin *et. al.* trapped species **1-26** (verified by mass)**,** providing more direct evidence for the intermediacy of the iminium ion (**1-27**) in the UGM catalytic cycle shown in Fig. 1-14.[43] Combined with the observation that a synthetic bi-cyclo acetal species could not be accepted by UGM as a substrate, the earlier hypothesis shown in Fig. 1-12 was firmly ruled out.[44]

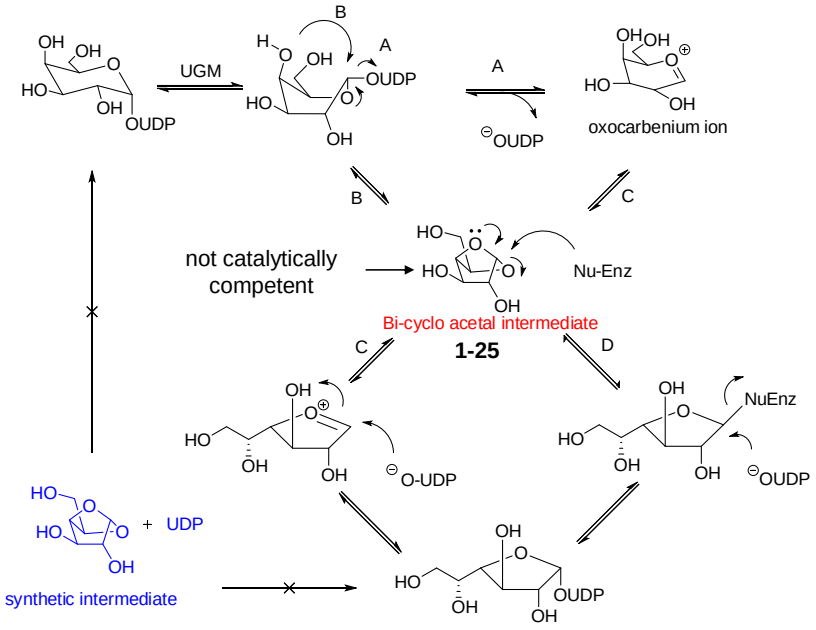

Figure 1-12: Hypothesis for UGM mechanism involving a bi-cyclic intermediate.

Characterization of species **1-26** by ^{1}H-NMR helped to verify its identity.[45] Structures of reduced UGM determined in the presence of UDP-Gal*p* by saturation transfer difference NMR spectroscopy[46] and X-ray crystallography[45] revealed that the N5 nitrogen of FAD_{red} is in close proximity to the anomeric carbon of the substrate (Fig. 1-13), providing compelling evidence for the participation of N5 in nucleophilic attack at C1 of the substrate to form **1-28** and **1-29** during turnover.

Although the existence of an iminium FAD-substrate covalent intermediate has become well accepted, the detailed mechanism underlying its formation is still under debate. Three mechanistic hypotheses have been proposed to address this issue as shown in Fig. 1-14. Generation of these intermediate flavin adducts may occur via nucleophilic attack by N5 of FAD_{red} at the anomeric carbon of **1-4** (or **1-12**) concerted with cleavage of the C1-OP_{β} bond (Fig. 1-14, *path A*), which is reminiscent of typical S_N2-type substitutions. Alternatively, formation of **1-28** and **1-29** may take place in a stepwise

fashion similar to S_N1-type substitutions (Fig. 1-14, *path B*), where elimination of UDP to produce an oxocarbenium intermediate (such as **1-30**) precedes the nucleophilic attack by N5. It is also possible that the electron deficient nature of **1-30** could facilitate single-electron transfer (SET) from FAD_{red} to form a radical pair (such as **1-31** and **1-33**), followed by covalent bond formation to afford the intermediates (Fig. 1-14, *path* C).

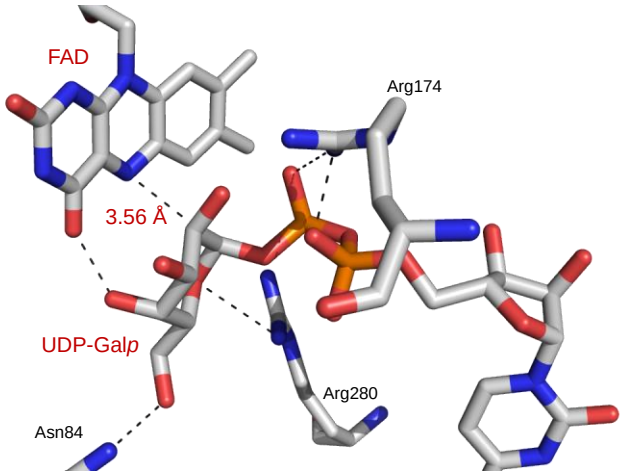

Figure 1-13: A representative view of the UGM active site under reducing conditions with both FAD_{red} and UDP-Gal*p* bound. (PDB: 3INT) The distance between the N5 of FAD_{red} and the C1 of UDP-Gal*p* is approximately 3.6 Å.

Indirect evidence for an oxocarbenium intermediate has come in the form of a significant rate reduction observed with fluorinated UDP-galactose analogues[40-41] and the inability of UGM to displace UDP from the linear substrate analog UDP-galactitol.[47] However, whether these substrate analogs bind in the active site with the appropriate configuration for catalysis is not clear. One example for this potential concern is UDP-CH_2-Gal*p*. This phosphono analog of UDP-Gal*p* showed a binding mode distinct from that of the natural substrate, although methylenephosphonates are a well established isosteric replacement for the phosphate group.[48] Although the observation of neutral flavin semiquinone (**1-23**) in the presence of UDP-Gal*p* has been reported, its catalytic

relevance has not been demonstrated.[49] While the result that apo-UGM could be reconstituted with 1-deaza-FAD but not 5-deaza-FAD was consistent with a SET route,[42] it was also in agreement with pathways involving Lewis acid/base chemistry. Furthermore, a UDP-Gal*p*/*f* radical species has not been observed by EPR, and the X-ray crystal structure of reduced FAD and UDP-Gal*p* bound to UGM is consistent with all three hypotheses (see Fig. 1-13).

1.1.3. Thesis statement

This chapter discusses mechanistic studies of UGM. This enzyme uses reduced FAD to catalyze the reversible interconversion of UDP-Gal*p* and UDP-Gal*f*. UGM is required by a number of pathogens for the biosynthesis of UDP-Gal*f*, which is needed for cell wall biosynthesis and is absent in mammals. Results from previous studies by different research groups have provided evidence for the existence of an FAD-Gal*f*/*p* adduct as an intermediate in the catalytic cycle. These findings are consistent with Lewis acid/base chemistry involving nucleophilic attack by the N5 nitrogen of FAD_{red} at the C1 position of UDP-Gal*f*/*p*. However, the mechanism by which the covalent adduct is formed remains unresolved, and three different pathways have been proposed. (Fig. 1-14)

In this chapter, PIX and linear free energy relationships (LFERs) studies are described in an attempt to further investigate the role of the N5 nitrogen of FAD_{red} during UGM catalysis. Together, the results of these experiments are most consistent with an S_N2-type displacement of UDP from the substrate by N5 of FAD_{red} (Fig. 1-14, *path A*).

UGM is an attractive drug target and several different UGM analogs have been developed with this aim in mind.[50-51] Detailed understanding of the reaction mechanism will provide more information for the design of inhibitors. Moreover, the chemical reaction catalyzed by UGM involves novel usage of the flavin cofactor. The results from

this chapter will for this reason also be useful in understanding more about this important class of biocatalysts.

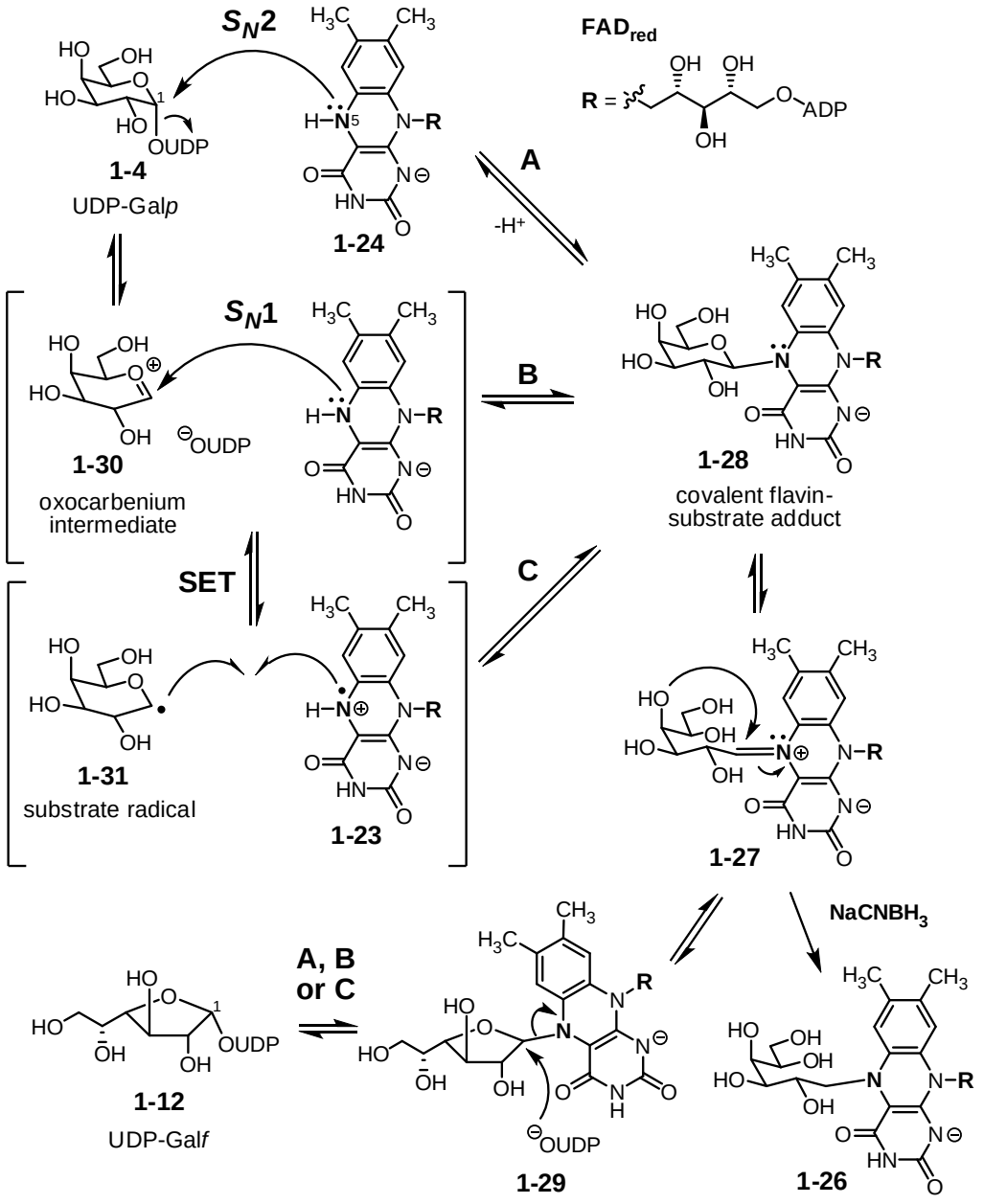

Figure 1-14: Putative chemical mechanisms for UGM catalysis.

1.2. MATERIALS AND METHODS

1.2.1. General

Protein concentrations were determined by the Bradford method using bovine serum albumin (BSA) as the standard.[52] The relative molecular mass and purity of the enzyme samples were determined using 12% SDS-PAGE. DNA sequencing was performed by the Core Facilities of the Institute of Cellular and Molecular Biology at University of Texas at Austin. The general methods and protocols for recombinant DNA manipulations were followed by Sambrook and coworkers.[53] NMR spectra were acquired on Varian NMR spectrometers (400, 500, or 600-MHz) at the Nuclear Magnetic Resonance Facility in the Department of Chemistry and Biochemistry at the University of Texas at Austin. Mass spectra were obtained at the Mass Spectrometry Core Facility in the Department of Chemistry and Biochemistry at the University of Texas at Austin. Except for ^{13}C NMR peak deconvolution and integration, all data analysis was performed with programs written and implemented using the GNU Octave numerical analysis software, which is available as freeware at the website www.gnu.org/software/octave.[54]

Materials

Vectors pET24b(+) and pET28b(+) were purchased from Novagen (Madison, WI). Enzymes and molecular weight standards used for molecular cloning were from Invitrogen (Carlsbad, CA) or New England Biolabs (Ipswich, MA). Nickel-nitrilotriacetic acid (Ni-NTA) resin and kits for DNA gel extraction and spin miniprep were obtained from Qiagen (Valencia, CA). *Pfu* DNA polymerase was purchased from Stratagene (La Jolla, CA). Enzymes used in the preparation of [1-^{13}C, 1-^{18}O]UDP-Gal*p* were acquired from Sigma-Aldrich (St. Louis, MO) except for galactose kinase (GalK). D-[1-^{13}C]Galactose (99%) was from Cambridge Isotope Laboratories (Andover, MA) and

$H_2{}^{18}O$ (95%, normalized) was from Fluka (St. Louis, MO). Other chemicals and reagents were products of either Sigma-Aldrich or Thermo Fisher Scientific (Waltham, MA). Amicon YM10 Centrifugal Filter Units were from EMD Millipore (Darmstadt, Germany). The bacteria strains *E. coli* DH5α used for cloning was from Invitrogen, and *E. coli* BL21 Star™ (DE3) used for protein overexpression was from Novagen (Madison, WI). The *glf* gene encoding recombinant pQZ-1 and UDP-Gal*f* were prepared by Dr. Kenji Itoh. The genomic DNA of *E. coli* K-12 used to clone GalK was provided by Dr. Christopher J. Thibodeaux. All flavin analogs were provided by Dr. Christopher J. Thibodeaux and Dr. Wei-chen Chang.[31]

Instrumentation

The pH values were measured using a Corning pH meter 240 from Fisher Scientific, or colorpHast® indicator strips from EM Science (Gibbstown, NJ). Agarose gel electrophoresis apparatus was from Bio-Rad (Richmond, CA) and Fisher Scientific. Centrifugation procedures were carried out using either an Avanti J-25 or Avanti JE-255 unit from Beckman-Coulter (Arlington Heights, IL) for large volumes, and an Eppendorf (Enfield, CT) 5415 D or 5415 R for small volumes. Photography of agarose gels was performed with a Kodak EDAS 290 apparatus connected to a PC running Kodak 1D 3.5 software using a FBTIV-88 transilluminator from Thermo Fisher Scientific. PCR was performed using an Eppendorf Mastercycler Gradient from Brinkman Instruments. The Synergy HT Multi-Mode Microplate Reader was from Bio-TEK (Winooski, VT). Ultraviolet-visible (UV) spectra were obtained using either Beckman DU650 or Agilent 8433 spectrophotometers (Santa Clara, CA). High-performance liquid chromatography (HPLC) was performed on a Beckman Coulter System Gold equipped with a UV detector. Varian Microsorb-MV 100-5 C18 HPLC columns (250 × 4.6 mm) were

purchased from Varian Inc. (Palo Alto, CA). DNA concentrations were measured using a NanoDrop ND-1000 UV-vis instrument from Thermo Fisher Scientific.

1.2.2. UGM expression and purification

The recombinant plasmid pQZ-1 containing the *glf* gene from *E. coli* was used to transform *E. coli* BL21 Star^{TM} (DE3) for overexpression of UGM as a *C*-terminal His_6-fusion protein. Cells were cultured in LB medium containing 50 mg/liter kanamycin at 37 °C until the absorbance at 600 nm reached 0.6. Protein overexpression was induced by the addition of isopropyl β-D-thiogalactopyranoside to 0.1 mM, and the culture was allowed to incubate for an additional 18 h at 18 °C. The cells were then harvested by centrifugation at 4500 × 15 min and stored at –80 °C.

All purification steps were carried out at 4 °C following the manufacturer's protocol for Ni-NTA resin with minor modifications. Specifically, the thawed cells were resuspended in lysis buffer (50 mM potassium phosphate (KPi), pH 7.5, 10% (v/v) glycerol, 300 mM NaCl, and 10 mM imidazole) and then disrupted by sonication. The resulting supernatant was centrifuged at 16,000 × g for 30 min and subjected to Ni-NTA purification. The collected protein was dialyzed against 3 × 1 L of 100 mM KPi, pH 7.5 containing 15% glycerol. The protein solution was then flash-frozen in liquid nitrogen and stored at –80 °C until use.

1.2.3. Cloning, expression and purification of GalK

The *galk* gene was PCR-amplified from *E. coli* K12 genomic DNA with engineered *Nde*I and *BamH*I restriction sites.[55] The sequence of the forward primer was 5′-GGGAATTC**CATATG**AGTCTGAAAGAAAAAACACAATCTC-3′ (the restriction site is in bold, and the start codon is underlined). The sequence of the reverse primer was 5′-CGC**GGATCC***TCA*GCACTGTCCTGCTCCTTG-3′ (the stop codon is in italics).

PCR-amplified gene fragments were digested and purified from a DNA gel and then ligated into a pre-digested pET28b(+) vector. The resulting plasmid, GalK/pET28b(+), was used to transform *E. coli* BL21 star (DE3) for protein overexpression. The GalK was expressed as an *N*-terminal-His_6-tagged protein. The expression and purification method is identical to that of UGM, while Tris buffer pH 8.0 was used instead of KPi and 10% (v/v) glycerol was used in the dialysis buffer.

1.2.4. Preparation of double-labeled UDP-Gal*p*

Double-labeled [1-^{13}C, 1-^{18}O]-UDP-Gal*p* was prepared according to published methods with slight modification.[39, 55-56] First, the double labels were introduced by incubating 100 mg D-[1-^{13}C]galactose with 200 μL of $H_2{}^{18}O$ (95%, normalized; Fluka) at 55 °C for 2 days to yield the double labeled galactose. The double-labeled UDP-Gal*p* was then synthesized enzymatically as shown in Fig. 1-15. A solution of 80 mM double-labeled galactose was treated with pyruvate kinase (PK) and GalK in the presence of 125 mM phosphoenolpyruvate (PEP) and 6 mM ATP in 50 mM Tris buffer (pH 7.5) with 5 mM $MgCl_2$, 2 mM $MnCl_2$, 5 mM KCl, and 5 mM DTT to generate double-labeled galactose 1-phosphate. The enzymes were removed using YM10 centrifugal filtration after complete consumption of the labeled galactose as monitored by TLC. The filtrate was adjusted to pH 8.5 with NaOH and treated with galactose-1-phosphate uridylyltransferase (GalT), UDP-glucose pyrophosphorylase (UGP), and inorganic pyrophosphatase (PPase) in the presence of 0.6 mM UDP-glucose (UDP-Glc) and 100 mM UTP to form UDP-[1-^{13}C, 1-^{18}O]Gal*p*. The reaction was monitored by HPLC (see below for conditions). Enzymes were then removed by filtration and the product was purified using a DEAE-cellulose column eluted with a 0 – 0.1 M gradient of NH_4HCO_3 in

water. The fractions were checked by HPLC to confirm the presence of product using unlabeled UDP-Gal*p* as a standard.

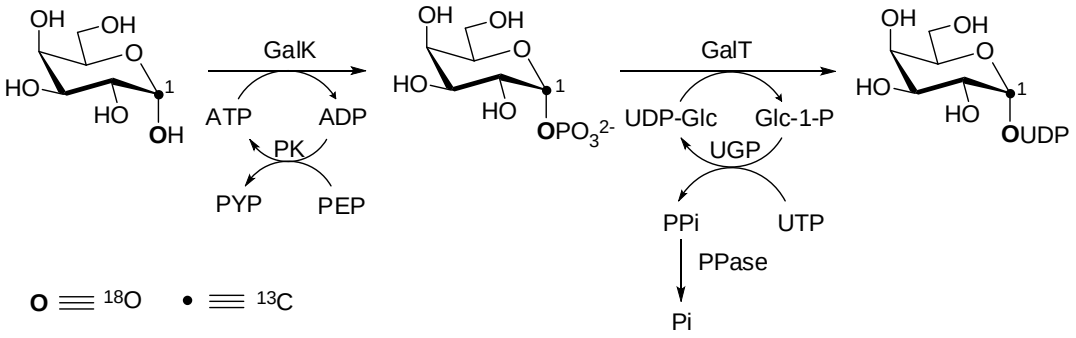

Figure 1-15: Scheme for enzymatic synthesis of double-labeled UDP-Gal*p*.

1.2.5. Preparation of apo-UGM and reconstitution with other FAD analogues

FAD was removed from the purified enzyme by the addition of a 2.6-fold volume excess of 3 M KBr in 20% glycerol to a 10 mg/mL enzyme stock in storage buffer.[42] The resulting mixture was incubated on ice for 2 min before precipitating the enzyme by the addition of a 1.8-fold volume excess of saturated ammonium sulfate (pH 2.5). The enzyme precipitate was pelleted by centrifugation at 18,000 × *g* for 10 min. The clear yellow supernatant containing released FAD was decanted, and the protein pellet was redissolved in 4 mL of storage buffer. The high salt treatment was repeated a second time, and the resulting apo-UGM was dialyzed against storage buffer (100 mM KPi, pH 7.5, 15% glycerol). Reconstitution of UGM with FAD analogues was carried out by incubating a 2.5 mg/mL solution of apo-UGM with an excess of cofactor analogue for 15 min at room temperature. The reconstituted enzyme/cofactor solution was then diluted with storage buffer to a concentration compatible with the enzyme assays. In the LFER studies, the molar ratio of cofactor to apo-UGM was about 100:1.

1.2.6. PIX Time course experiments

PIX experiments were carried out at 27 °C in NMR tubes containing 50 mM KPi (pH 7.5), 10% D_2O (for locking the ^{13}C NMR signal), 7 mM $Na_2S_2O_4$ (determined by UV at 315 nm using $\varepsilon = 6900\ M^{-1}cm^{-1}$),[57] and approximately 14 mM double-labeled UDP-Gal*p* in a total volume of approximately 630 µL. Apo-UGM was pre-incubated with the respective cofactor for 15 min before dilution into the reaction solution. In the 5-deaza-FAD/UGM and apo-UGM samples, the final enzyme concentration was 15 µM, and the 5-deaza-FAD concentration was approximately 820 µM. In the FAD/UGM positive control, the final enzyme and FAD concentrations were 10 and 220 µM, respectively. All ^{13}C NMR spectra were recorded using a 600-MHz Varian NMR spectrometer except for the reaction with apo-UGM, which were recorded using a 500-MHz Varian NMR.

1.2.7. Kinetic assay

Initial rates for the conversion of UDP-Gal*f* to UDP-Gal*p* by reconstituted UGM were determined according to a previously described discontinuous assay with slight modifications.[41] Reactions were run in 50 mM KPi buffer (pH 7.5) containing 7 mM $Na_2S_2O_4$ and 10 – 500 µM UDP-Gal*f* in a total volume of 30 µL. The temperature was maintained at 37 °C using a water bath. Enzyme concentrations varied from 0.015 to 0.2 µM depending on the analogue tested. Reactions were initiated upon the addition of UDP-Gal*f*, quenched with a 3-fold excess of methanol, and centrifuged to remove precipitates. The resulting supernatant were dried in a speed vacuum concentrator and re-suspended in HPLC buffer A prior to analysis. The fraction of reaction was determined based on the relative integrations of the UDP-Gal*f* and UDP-Gal*p* peaks and used to calculate the initial rate of reaction.

1.2.8. HPLC conditions

HPLC analysis was performed at room temperature using a Varian Microsorb-MV 100-5 C18 column (250 × 4.6 mm) with UV detection at 262 nm. Solvent A contained 50 mM KPi and 2.5 mM tetrabutylammonium hydrogen sulfate (pH 6.9) in H_2O, and solvent B contained 50 mM KPi and 2.5 mM tetrabutylammonium hydrogen sulfate (pH 6.9) in 50% H_2O/acetonitrile. Isocratic elution was performed at 96% solvent A at a flow rate of 1 mL/min.[58]

1.2.9. Preparation and verification of 7/8-substituted FAD analogues

The 7/8-substituted FAD analogues used in this study were prepared according to published methods.[31] The identity of each compound was verified by ^{1}H NMR and ^{31}P NMR spectroscopy as well as by high resolution electrospray ionization mass spectrometry.

1.3. RESULTS AND DISCUSSION

1.3.1. Purification and characterization of UGM and GalK

UGM and apo-UGM

C-terminal His_6-tagged UGM was purified to near homogeneity (Fig. 1-16). The purified enzyme has a bright yellow color and a distinct UV-vis absorption (peaks at 380 nm and 450 nm), indicating the presence of a tightly bound FAD cofactor (Fig. 1-17). The yield was about 50 mg per liter of culture. The molecular weight of UGM was estimated to be 45 kDa as judged by SDS-PAGE, which correlated well with the calculated molecular weight of 45,014 Da including the His_6 tag. After high salt denaturation and renaturation to remove the cofactor, apo-UGM appeared colorless. No detectable FAD signal could be observed in UV-vis spectra of apo-UGM (see Fig. 1-17). Before the PIX assay, activities of the reconstituted enzymes were compared with the as isolated UGM and no enzyme control in the reverse direction (from UDP-Gal*f* **1-12** to UDP-Gal*p* **1-4**). As expected, only UGM reconstituted with FAD showed similar activity to the as isolated holo-UGM. Both apo-UGM and UGM reconstituted with 5-deaza-FAD showed no conversion in 2 min similar to the no enzyme control (see Fig. 1-18).

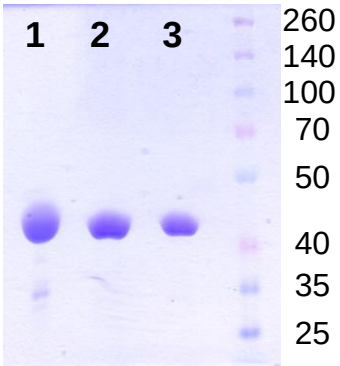

Figure 1-16: 10% SDS-PAGE of GalK and UGM: lane 1, GalK; lane 2, apo-UGM; lane 3, UGM as isolated.

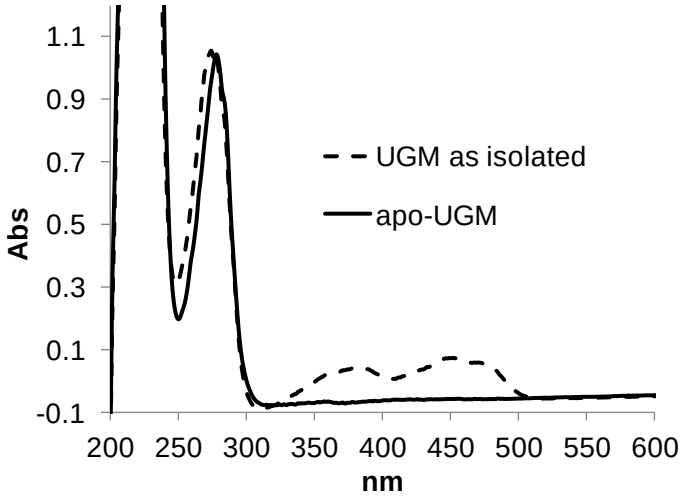

Figure 1-17: UV-vis spectra of UGM as isolated and apo-UGM.

GalK

N-terminal His_6-tagged GalK was purified with a major band near 43 kDa as judged by SDS-PAGE (Fig. 1-16), in agreement with the calculated molecular weight of 43,605 Da. About 5 mg protein was obtained from a 4 L culture. The activity of GalK was confirmed by incubating the expressed enzyme with 4 mM D-galactose and 50 mM ATP. After 30 min at 37 °C, the D-galactose (R_f = 0.6) was completely converted to its monophosphate (R_f = 0.1) as indicated by TLC. TLC was developed in *n*-butanol/ethanol/water with a ratio of 5:3:2 and stained with phosphomolybdic acid (PMA).

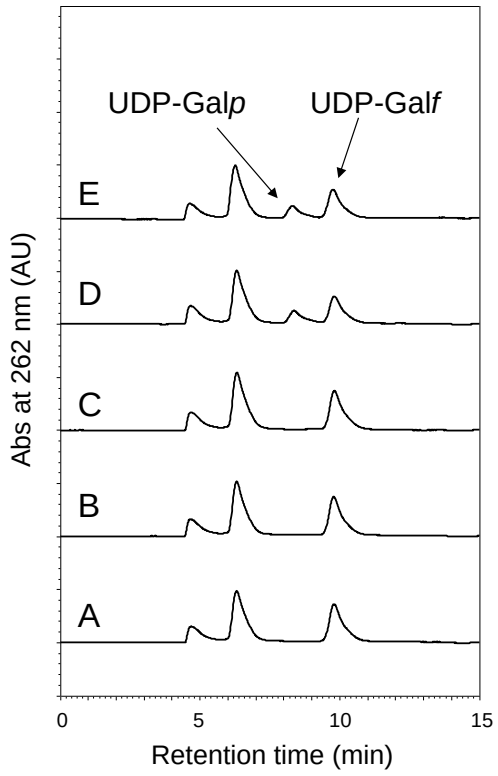

Figure 1-18: HPLC chromatograph for UGM activity assay. (A) No enzyme (B) apo-UGM (C) UGM reconstituted with 5-deaza-FAD (D) UGM reconstituted with FAD (E) UGM as isolated. The reaction condition was same for all samples: 20 mM Tris pH 7.5, 7 mM $Na_2S_2O_4$, 60 μM UDP-Gal*f*, and 50 nM enzyme if present. Incubations were at 37 °C for 2 min.

1.3.2. Characterization of double-labeled UDP-Gal*p*

The synthesized UDP-[1-^{13}C, 1-^{18}O]Gal*p* was determined to be 95% pure based on HPLC analysis. The extent of isotopic double-label incorporation into the UDP-Gal*p* product was determined by ^{1}H NMR (Fig. 1-19) and ^{13}C NMR (Fig. 1-20) spectrometries and confirmed by high resolution electrospray ionization mass spectrometry (negative-ion mode), demonstrating peaks at *m*/*z* 566.0518 and 568.0530, corresponding to the ^{16}O (calculated *m*/*z* 566.0511) and ^{18}O (calculated *m*/*z* 568.0553) isotopologues, respectively.

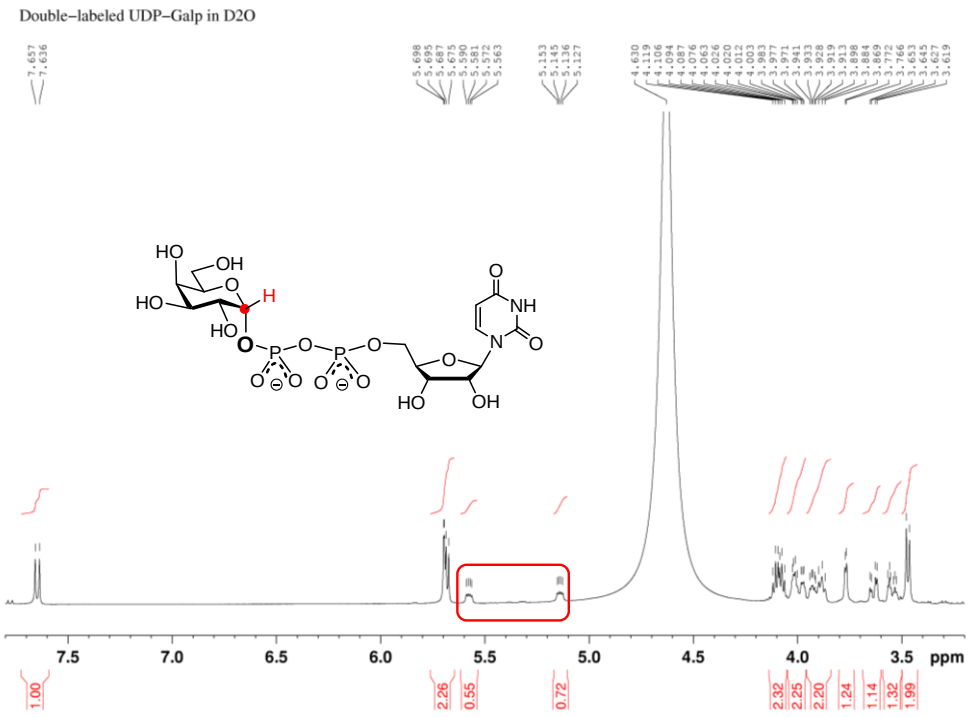

Figure 1-19: ^{1}H NMR (400 MHz, D_2O) of double-labeled UDP-Gal*p*. The C1 proton is highlighted in red, and the corresponding NMR signal split by the ^{13}C at C1 is boxed.

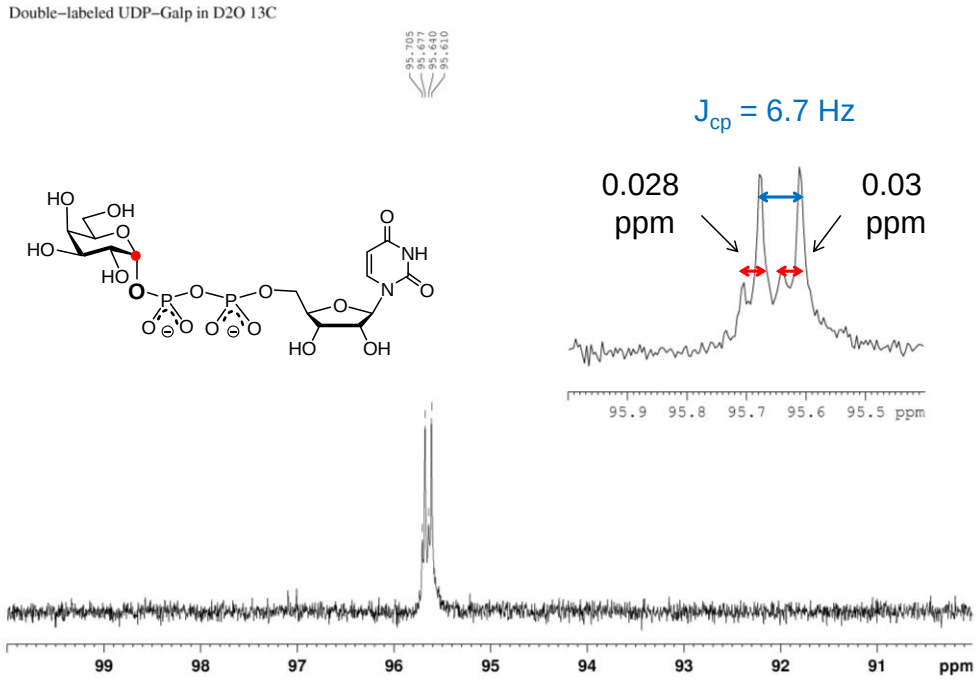

Figure 1-20: ^{13}C NMR (100 MHz, D_2O) of double-labeled UDP-Gal*p*. The coupling constant of the C1 carbon and the β-phosphorus is 6.7 Hz. The 0.03 ppm chemical shift difference between C1 attached to ^{16}O versus ^{18}O matches the description in the reference for the double-labeled UDP-Gal*p*.[39]

The C1 ^{13}C NMR signal of UDP-Gal*p* is split into a doublet by the adjacent β-phosphate and demonstrates an upfield shift of approximately 0.03 ppm when the anomeric oxygen is replaced with ^{18}O. The resulting two doublets were deconvoluted and integrated using the Varian VnmrJ software and a multicomponent fit with Lorentzian line shapes. ^{13}C NMR and mass spectrometry results indicated that the double-labeled UDP-Gal*p* (**1-34**) was prepared with approximately 99% incorporation of ^{13}C at C1 and 77 ± 4% incorporation of ^{18}O at the bridging C1–OP_β position. This value was determined from a single sample measured twice (N = 2) using the 600 MHz NMR on two separate consecutive days.

1.3.3. PIX experiment

Rationale

Evidence for the cleavage of the anomeric bond of UDP-Gal*p* during turnover by UGM was first provided by Blanchard and co-workers using PIX.[39] In this study, incubation of UGM with UDP-[1-^{13}C]Gal*p* enriched with ^{18}O at the bridging oxygen between C1 and the β-phosphate (**1-34**) was monitored by ^{13}C NMR spectroscopy. When ^{18}O is replaced with ^{16}O at the bridging position (see **1-35**), a well resolved downfield shift of the ^{13}C1 resonance occurs, with the change in the ratio of the ^{13}C–^{18}O and ^{13}C–^{16}O signals during turnover indicative of bond cleavage and reformation (Fig. 1-21). It has also been shown that UGM reconstituted with 5-deaza-FAD does not catalyze the interconversion of UDP-Gal*f* and UDP-Gal*p*.[42] This observation was initially interpreted as support for a mechanism involving SET (Fig. 1-14, *path C*), because 5-deaza-FAD is restricted to 2-electron processes.[59] Nevertheless, this indirect evidence does not exclude the possibility of a nucleophilic role for N5 of FAD_{red} and, in particular, an S_N2-type process if it is required for expulsion of the UDP moiety.

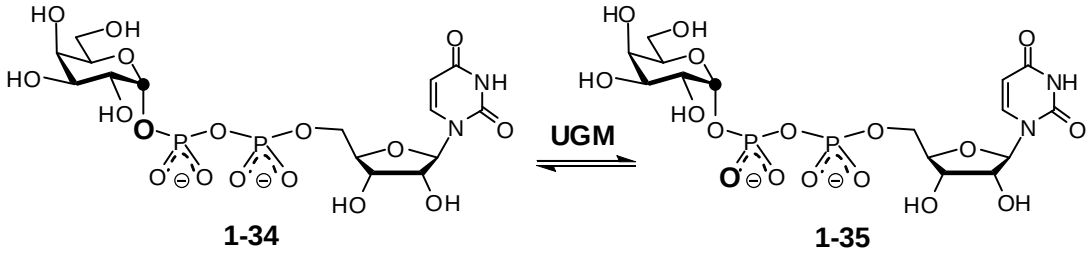

Figure 1-21: Rationale for PIX experiments.

As an initial test of the hypothesis that the N5 nitrogen is directly involved in the cleavage of the anomeric bond of UDP-Gal*p* to form the flavin-substrate adduct (**1-28**

and **1-29**), we considered the ability of UGM to utilize 5-deaza-FAD to catalyze PIX of the P_β oxygens in UDP-Gal*p*. If an oxocarbenium intermediate (**1-30)** is involved in the mechanism (*pathway B* and *C*), anomeric bond cleavage would be independent of nucleophile attack by the N5 nitrogen. Thus, PIX of labeled substrate (**1-34**) would still be expected for UGM reconstituted with 5-deaza-FAD, although no corresponding UDP-Gal*f* product would be expected to form. However, if the mechanism is a concerted process (*pathway A*), then nucleophilic attack by the N5 nitrogen would be required for cleavage of the anomeric bond. In this scenario, both PIX and UDP-Gal*f* formation would be impaired. This hypothesis rests on the assumption that 5-deaza-FAD will not perturb substrate binding, which has been justified in an earlier study where both 5-deaza-FAD and 1-deaza-FAD were both found to bind UGM tightly with equilibrium dissociation constants similar to that of FAD, i.e., approximately 10 nM.[42]

PIX results

PIX experiments were conducted under reducing conditions (7 mM sodium dithionite) in NMR tubes. The change in the fraction (*f*) of ^{18}O *versus* ^{16}O bound to $^{13}C1$ was monitored *versus* time (*t*) by ^{13}C NMR spectroscopy. As shown in Fig. 1-21, the fraction of ^{18}O at the bridging C1–OP_β position is expected to ultimately reach an equilibrium value of $f_{eq} = 0.26$ upon complete scrambling of the P_β oxygens (the product of the initial ^{18}O enrichment in our double-labeled UDP-Gal*p* substrate and the statistical factor of one-third). In the presence of 10 μM UGM reconstituted with FAD_{red}, PIX scrambling (**1-34**↔**1-35**) was > 90% complete within 20 min of incubation. In contrast, PIX was considerably slower in the presence of either 15 μM apo-UGM or UGM reconstituted with 5-deaza-FAD_{red}, occurring over a time scale of > 7 h. No PIX scrambling was observed over a 24-h period when UGM was omitted from the reaction

solution. A representative graph was shown in Fig. 1-22 to compare the PIX results in different conditions in short incubation time.

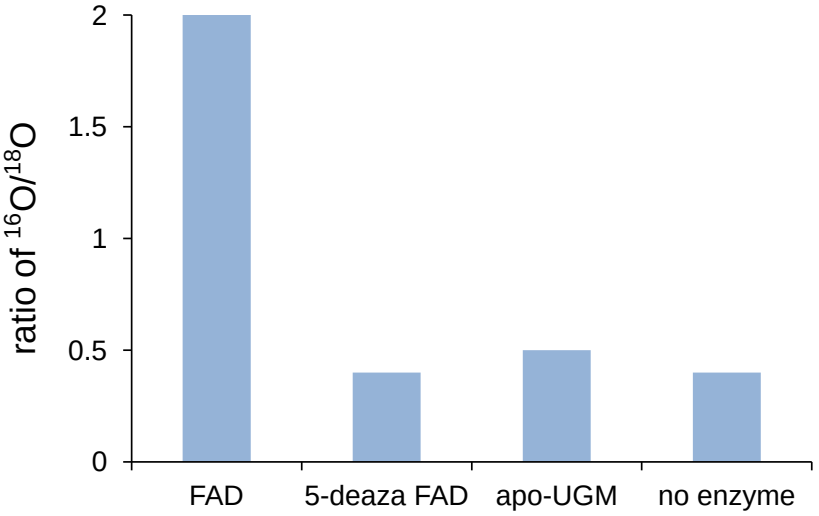

Figure 1-22: PIX results after short time (~20 min) for comparison. The values were calculated based on the peak area of ^{13}C NMR after deconvolution. Note that value of 2 indicated that isotope scrambling reached to equilibrium.

Since both 5-deaza-FAD reconstituted UGM and apo-UGM showed slow PIX over time, it was followed over 8 h. (Fig. 1-23) This permitted f to be measured every 60 min and subsequently fit using equation 1.1 to extract the first-order rate constant for PIX[60]:

Equation 1.1 $$f = f_{eq} + \Delta f \exp(-k_{PIX}\, t)$$

In this equation, f_{eq} is the final value of f after complete equilibration of the exchangeable oxygens, and Δf is the difference between the initial value of f and f_{eq}. The first-order rate constant, k_{PIX}, describes the approach to the PIX equilibrium under the experimental conditions and is equivalent to the positional exchange rate[61] normalized for the total initial substrate concentration, which was held constant and saturating in the experiments. The parameters k_{PIX} and Δf were both allowed to float during nonlinear fitting, whereas

f_{eq} was fixed at 0.257, (Fig. 1-24). Fitting employed the standard Gauss-Newton algorithm of iterative linearization assuming constant additive error.[62]

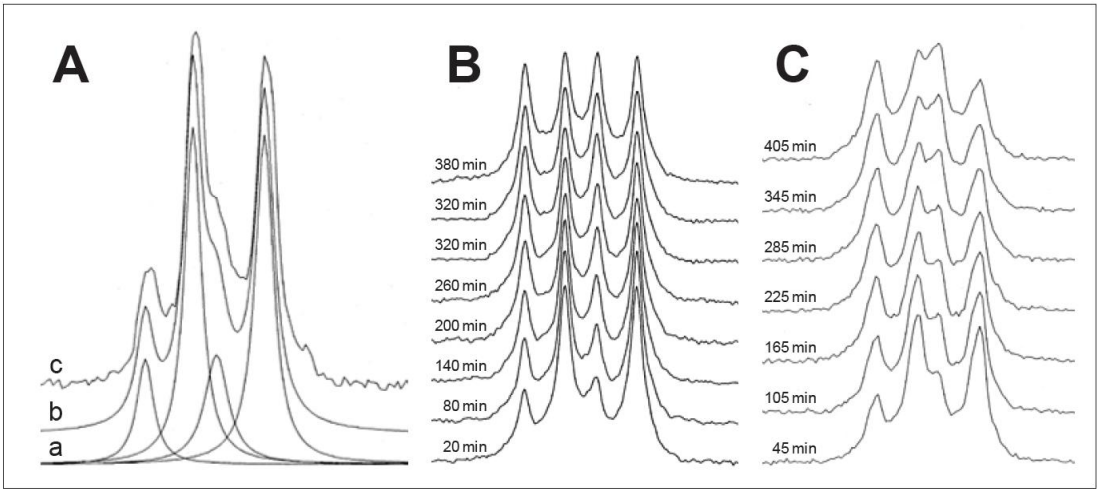

Figure 1-23: Representative ^{13}C NMR spectra used to determine fractional enrichment of ^{18}O at the bridging position in the double-labeled UDP-Gal*p*. (A) 600 MHz ^{13}C NMR of labeled substrate with the deconvoluted peaks (a), composite (b) and observed spectrum (c). (B) 500 MHz ^{13}C NMR spectra obtained during PIX equilibration of the doubly labeled substrate in the presence of apo-UGM. (C) 600 MHz ^{13}C NMR spectra obtained during PIX equilibration of the doubly labeled substrate in the presence of UGM reconstituted with 5-deaza-FAD.

The observed values of k_{PIX} for apo-UGM and UGM reconstituted with 5-deaza-FAD_{red} were 0.0015 ± 0.0001 and 0.0017 ± 0.0001 min^{-1}, respectively, and are approximately 100-fold smaller than the k_{PIX} for UGM reconstituted with FAD_{red}. The latter value was obtained from the observation of approximately 31% labeling of ^{18}O at the bridging position after 20 min incubation with 10 μM UGM reconstituted with FAD_{red}, namely, using the parameters f_{eq} = 0.257 and Δf = 0.514, in equation 1.1, one obtained k_{PIX} = 0.112 min^{-1}. After correction for the relative enzyme concentrations (i.e., a difference of 1.5-fold) used in the different assays, the final adjusted estimate was then

0.17 min^{-1}, which is approximately 100-fold greater than the observed values of k_{PIX} determined for apo-UGM and UGM reconstituted with 5-deaza-FAD. According to a two-tailed *t*-test, these latter values of k_{PIX} are significantly different from zero ($p < 0.0001$); however, they are not significantly different from one another ($p > 0.3$).

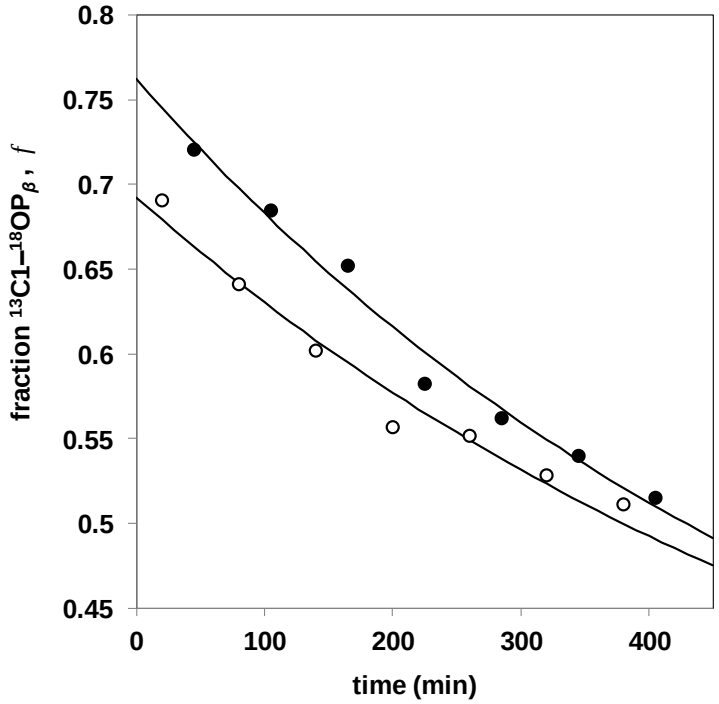

Figure 1-24: Comparison of PIX rates for apo-UGM (open circles) versus UGM reconstituted with 5-deaza-FAD (solid circles). Each time course is a plot of the fraction, *f*, of UDP-Gal*p* possessing ^{18}O at the bridging C1−OP_β position as determined by ^{13}C NMR versus time.

The PIX results suggested 5-deaza-FAD was unable to substitute for FAD_{red} in catalyzing PIX of the P_β oxygens. Although over a longer period of time, PIX was still observed, the PIX rate was no different compared to the background rate observed with apo-UGM. These results are most consistent with the conclusion that the N5 nitrogen of FAD_{red} is necessary for cleavage of the anomeric C1–OP_β bond. Thus, attack at C1 of the

substrate by N5 (Fig. 1-14, *pathway A*) is expected to be concerted with the elimination of the UDP moiety.

Evaluation of the background PIX

The background PIX of 5-deaza-FAD is most likely due to residual holo-UGM in the apo-UGM preparation, which is consistent with the tight binding of FAD to UGM. Formation of UDP-Gal*f* was observed in all the reactions after 24 h with the exception of the no enzyme control (Fig. 1-25). Despite some overlap of the UDP-Gal*f* peak (Fig. 1-25, c) with the tail of the UDP-Gal*p*) peak (Fig. 1-25, b), peak integrations indicated about 5% conversion in the case of both UGM reconstituted with 5-deaza-FAD and UGM reconstituted with FAD. This is consistent with the previously reported fractional conversion of ca. 7% at equilibrium.[39] No significant turnover was detected during short incubation times with UGM reconstituted with 5-deaza-FAD (Fig. 1-18, trace C). Therefore, it is likely that a residual amount of FAD was still present in the apo-UGM.

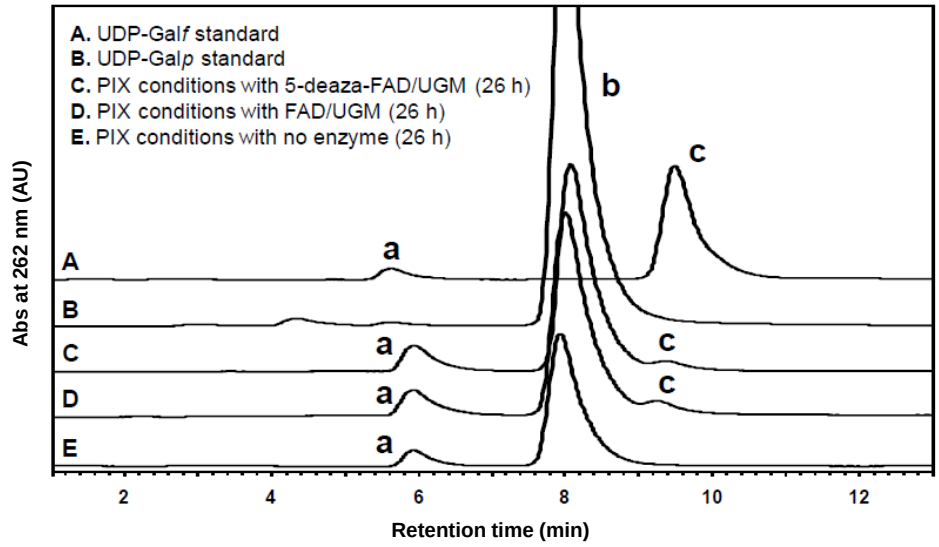

Figure 1-25: HPLC chromatograms to test for formation of UDP-Gal*f* during the PIX experiment with UGM reconstituted with 5-deaza-FAD.

Peak a is uridine monophosphate (UMP), peak b is the UDP-Gal*p* substrate and peak c is the UDP-Gal*f* product. Incubations corresponding to traces C, D and E were conducted under PIX conditions for 26 h before HPLC analysis. As the HPLCs were run on different days, i.e., following the individual PIX experiments, there was some variability in retention time; therefore, the traces have been shifted along the abscissa to facilitate comparison.

To further test this hypothesis, a new batch of apo-UGM was prepared by increasing number of the precipitation step to further remove the potential FAD in the isolated enzyme. Formation of UDP-Gal*f* still occurred with the newly prepared apo-UGM, however, at a slower relative rate. (Fig. 1-26) This result is consistent with the hypothesis that residual FAD remains in the apo-UGM preparations such that it might be difficult to obtain completely pure apo-UGM.

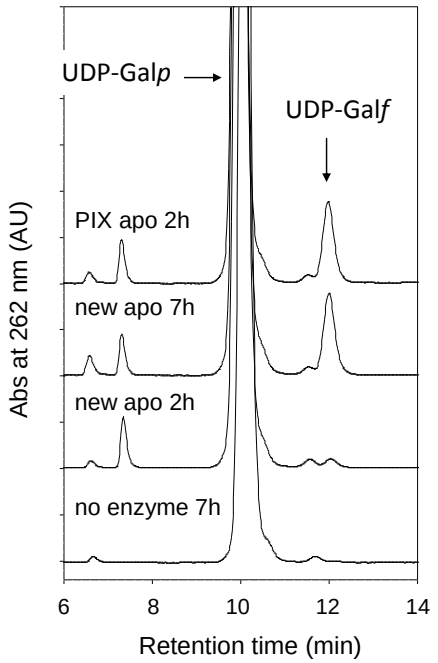

Figure 1-26: HPLC chromatograms for comparing relative activities of different batches of apo-UGM. "PIX apo" was used for PIX experiments following precipitation twice to remove FAD; "new apo" was precipitated four times instead of twice to further remove FAD. Reaction conditions: 1 mM UDP-Gal*p*, 7 mM $Na_2S_2O_4$, 50 mM KPi pH 7.5, 10 μM apo-UGM when present.

1.3.4. LFER study

Rationale

To further characterize the role of the N5 nitrogen of FAD_{red} during the UGM catalyzed isomerization more, kinetic LFERs associated with changes in the nucleophilicity of the N5 nitrogen were examined. Our rationale is that if adduct **1-28** (or **1-29**) is formed via an S_N2-type substitution (Fig. 1-14, *path A*), and if this step is at least partially rate-limiting during steady-state turnover, then changes in the nucleophilicity of the N5 nitrogen should be reflected in the rate of steady-state turnover. In contrast, the rate of steady-state turnover is expected to be much less sensitive to the nucleophilicity of N5 if adduct formation proceeds by an S_N1 or a SET pathway (Fig. 1-14, *paths B* and *C*), where formation of the oxocarbenium species (**1-30**) is expected to be substantially rate-limiting. Thus, as the electron density at the N5 nitrogen of FAD_{red} is decreased by substitution of the isoalloxazine moiety, a decrease in the steady-state reaction rate is expected for mechanism A, whereas little or no effect is expected for mechanisms B and C (shown in Fig. 1-27).

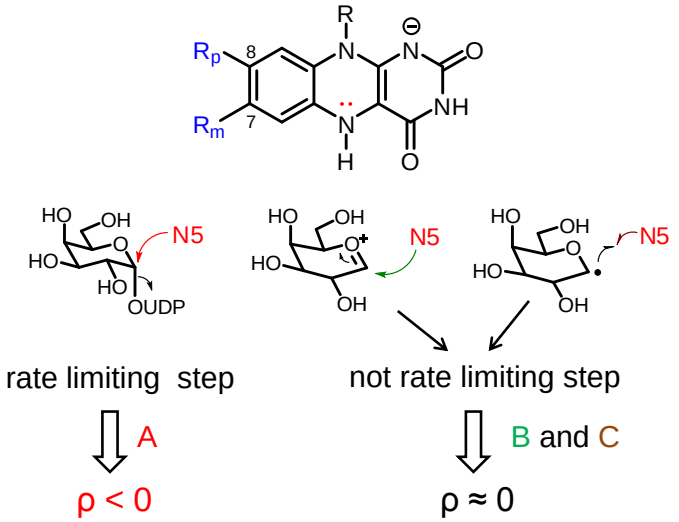

Figure 1-27: Rationale of LFER study.

Estimation of steady state kinetic parameters

To test this hypothesis, six FAD analogues (Fig. 1-28) containing electron-withdrawing or electron-donating groups at positions 7 and/or 8 of the isoalloxazine moiety (*meta* and *para*, respectively, to the N5 position) were chemo-enzymatically synthesized according to published procedures.[31] Following reconstitution of apo-UGM with each FAD analog, the turnover number (k_{cat}) for conversion of UDP-Gal*f* to UDP-Gal*p* (Fig. 1-4A in reverse direction) was determined from plots of the initial rate (v_i) *versus* initial UDP-Gal*f* concentration (s_i) according to the structural relation,

Equation 1.2 $$v_i = k_{cat} s_i e_0 / (K_M + s_i)$$

where e_0 is the total enzyme concentration, and K_M is the Michaelis constant. Nonlinear regression of equation 1.2 on the initial rate measurements was performed using the standard Gauss-Newton algorithm of iterative linearization assuming constant additive error. Convergence was determined when the maximal change among the fitted parameters was less than 0.1%. The variance and covariance of each fitted parameter were obtained from the asymptotic variance-covariance matrix of the converged fit under the linear approximation.[62-63] The estimated standard deviation of each parameter, i.e., the standard error, is then the square root of the associated variance. It is well know that parameter confidence intervals are underestimated by least-squares nonlinear regression methods.[64-65] Therefore, all confidence intervals and *p*-values should be considered nominal. Initial rates and corresponding fits using equation 1.2 are provided in Fig. 1-29. The corresponding steady state parameters obtained from the fits are listed in Table 1-1.

In the steady state kinetic studies, the molar ratio of cofactor to apo-UGM was approximately 100:1. Controls were also performed with ratios of 1000:1 for the 8-OMe-FAD and 7-Cl-FAD analogues versus apo-UGM. No significant differences were

observed in the fitted kinetic parameters, implying that the variations in k_{cat} were not a result of subsaturating flavin concentrations.

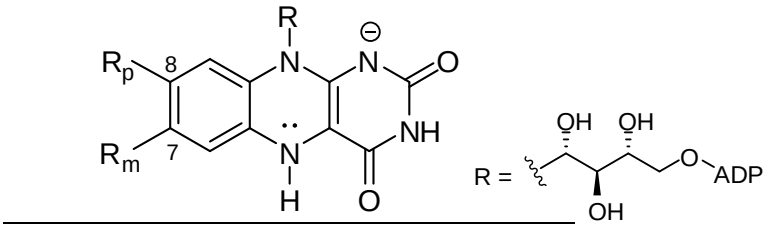

FAD: R_p=Me, R_m=Me
8-OMe-FAD: R_p=OMe, R_m=H
7-OMe-FAD: R_p=H, R_m=OMe
8-Cl-FAD: R_p=Cl, R_m=H
7-Cl-FAD: R_p=H, R_m=Cl
7-CF_3-FAD: R_p=H, R_m=CF_3

Figure 1-28: Chemo-enzymatic synthesized FAD analogs.

FAD analogue	k_{cat} (s^{-1})	K_M (μM)	k_{cat}/K_M (s^{-1} μM^{-1})
FAD	14.9 ± 1.4	32 ± 9.6	0.46 ± 0.10
8-OMe-FAD	8.0 ± 1.6	520 ± 180	0.0150 ± 0.0021
7-OMe-FAD	4.59 ± 0.56	380 ± 85	0.0120 ± 0.0013
8-Cl-FAD	1.21 ± 0.23	130 ± 60	0.0089 ± 0.0025
7-Cl-FAD	1.23 ± 0.34	140 ± 100	0.0087 ± 0.0039
7-CF_3-FAD	0.229 ± 0.022	25.8 ± 8.2	0.0088 ± 0.0022

Table 1-1: Steady state parameters obtained for the UGM catalyzed conversion of UDP-Gal*f* to UDP-Gal*p* following reconstitution with the different FAD analogues. All values are reported ± one standard error.

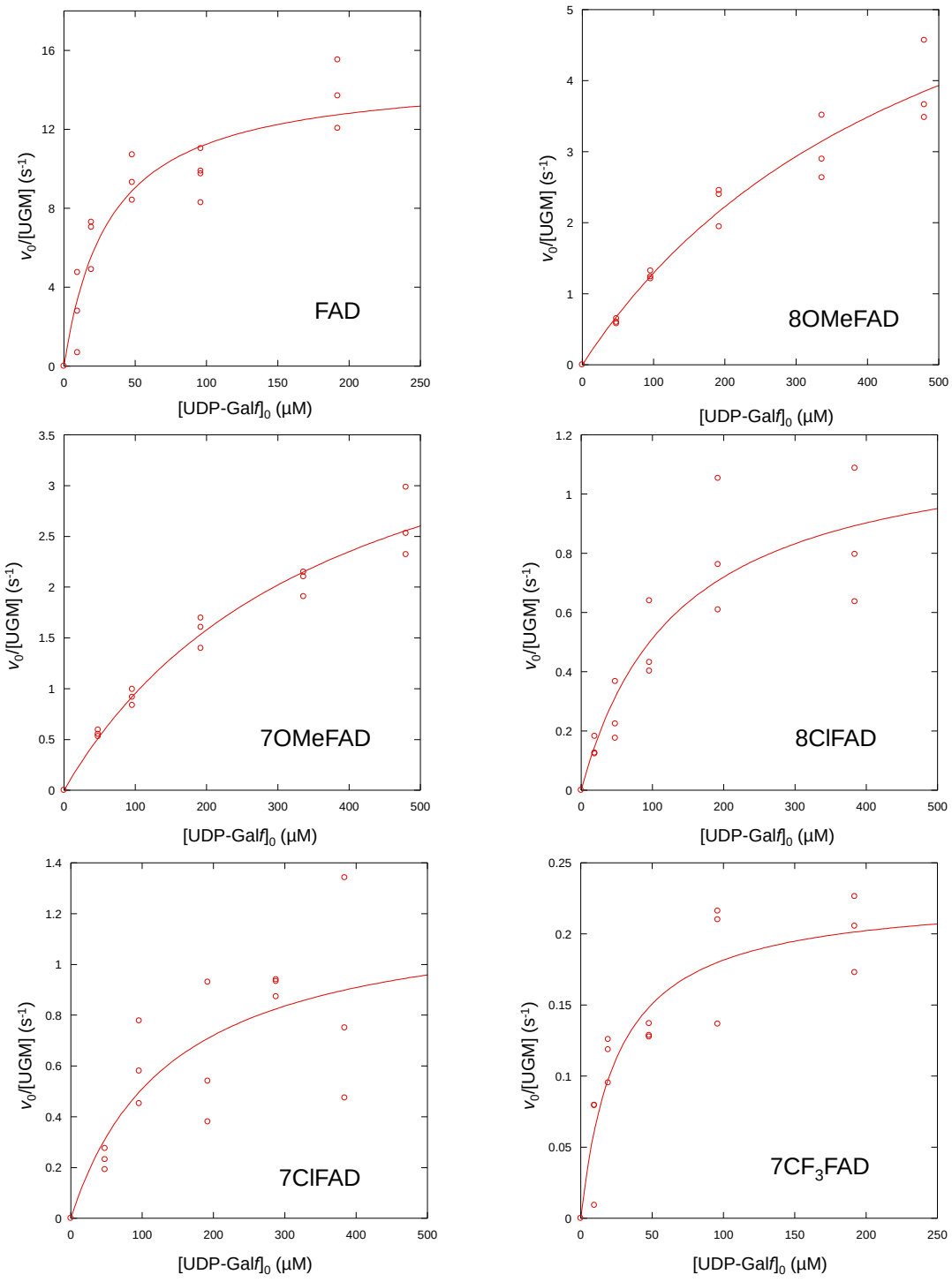

Figure 1-29: Plots of initial rate versus UDP-Gal*f* concentration for the UGM catalyzed conversion of UDP-Gal*f* to UDP-Gal*p*.

Initial rates have been normalized for UGM concentration in the individual assays. Each initial rate is based on three replicate trails. Solid lines represent the fits to equation 1.2.

LFERs on the steady state kinetic parameters

The nucleophilicity of the N5 nitrogten is represented as the sum of the σ_m and σ_p substituent constants for the substituent at the *meta* and *para* positions, respectively, of the FAD analogues. These substituent constants are based on the ionization of phenylacetic acid in water.[66] Except for the *para*-methoxy substituent, these values are nearly identical to the Hammett substituent constants obtained for ionization of benzoic acid in water.[67] In the case of *p*-methoxy, σ_p is significantly more negative with benzoic acid likely due to hydrogen bond stabilization of a *trans*-quinoidal resonance structure in H_2O.[68] (Table 1-2) Although a better correlation was obtained with the values of σ_m and σ_p based on ionization of phenylacetic acid, the same conclusions were drawn with those based on benzoic acid. Previous studies of many flavoenzymes[31, 69-71] and model systems[72] reconstituted with 7- and 8-substituted flavin analogues have established precedence for significant LFERs correlating Hammett substituent constants with a variety of parameters related to flavin structure and reactivity.

FAD analogue	σ_{BA}	σ_{PA}	$\log_{10}(k_{cat})$	$\log_{10}(k_{cat}/K_M)$
FAD	−0.24	−0.22	1.173 ± 0.041	−0.336 ± 0.094
8-OMe-FAD	−0.27	−0.12	0.906 ± 0.089	−1.812 ± 0.059
7-OMe-FAD	0.12	0.13	0.662 ± 0.053	−1.921 ± 0.047
8-Cl-FAD	0.23	0.27	0.083 ± 0.082	−2.05 ± 0.12
7-Cl-FAD	0.37	0.37	0.09 ± 0.12	−2.06 ± 0.19
7-CF_3-FAD	0.43	0.42	−0.641 ± 0.042	−2.06 ± 0.11

Table 1-2: Values used in the Hammett plot. $\sigma = \sigma_m + \sigma_p$ are listed for both ionization of benzoic acid (σ_{BA})[67] and phenylacetic acid (σ_{PA})[66,73].

The resulting Hammett plot of $\log_{10}(k_{cat})$ *versus* σ_{PA} (the sum of the substituent constants at positions 7 and 8 of the FAD analogues based on the ionization of phenylacetic acid in water) is shown in Fig. 1-30. On the basis of an analysis of variance, we found no evidence for either unequal expression of *para versus meta* effects in the LFER, *i.e.* $\rho_m \neq \rho_p$,[69] or non-additivity, *i.e.* higher order terms of σ. The value of the susceptibility factor (ρ) estimated from the linear correlation was −2.4 ± 0.4 and was significantly different from zero ($p < 0.01$).

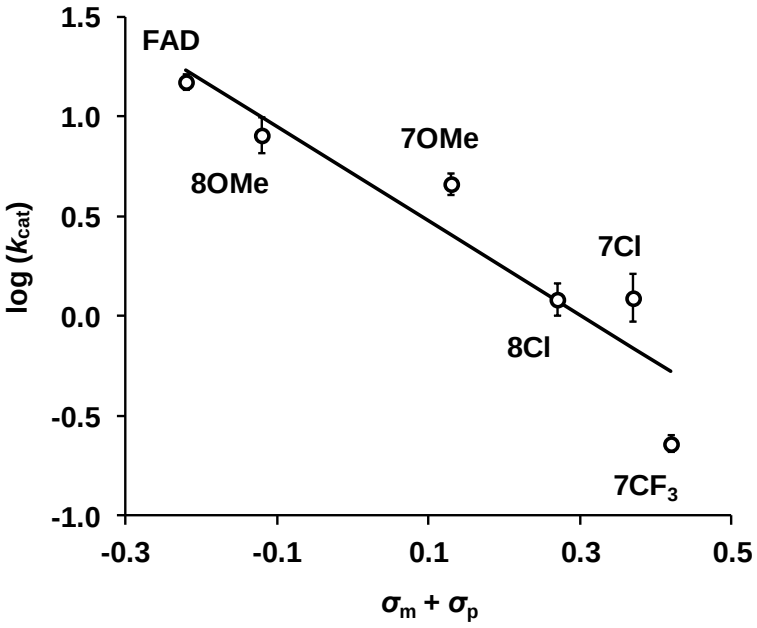

Figure 1-30: Hammett plot for the correlation of $\log_{10}(k_{cat})$ versus the sum of σ_p and σ_m. The fit was obtained from unweighted least squares linear regression, and error bars denote one standard error of $\log_{10}(k_{cat})$ above and below the observed value.

A linear correlation of $\log_{10}(k_{cat})$ for the UGM-catalyzed reaction *versus* the sum of σ_m and σ_p for the FAD analogues was observed with a slope of −2.4 ± 0.4. This implies that the rate of steady-state turnover by UGM is indeed sensitive to the electron density at

N5 of FAD_{red}. The large negative ρ value suggests a substantial decrease in electron density on the flavin in the transition state of the step(s) that limits steady-state turnover. This result is more consistent with a concerted mechanism (Fig. 1-14, *pathway A*), because discrete oxocarbenium intermediate formation (Fig. 1-14, *pathway B* and *C*) would be independent of the attacking nucleophile. Of course, alone, the results of LFER studies cannot distinguish between rate-limiting S_N2-type adduct formation (**1-12** → **1-29**) and iminium intermediate formation (**1-29** → **1-27**). However, the PIX experiments strongly suggest that if an S_N1-type mechanism were operative, then cleavage of the anomeric bond to form an oxocarbenium intermediate (**1-30**) would be energetically demanding and contribute significantly to limiting k_{cat}. Because this step is significantly impaired when the N5 nitrogen of FAD_{red} is absent in the active site of UGM, the most consistent interpretation of our PIX and LFER studies is that adduct formation (**1-12** → **1-29**) occurs by a concerted reaction that is mediated by the N5 nitrogen of FAD_{red}.

Consideration of k_{cat}/K_M in the LFER study

The preceding discussion focused primarily on k_{cat} rather than k_{cat}/K_M for two primary reasons. First, given the relationships between the observed and true values of the steady state parameters, the observed value of k_{cat}/K_M is influenced by the degree to which UGM is saturated with the FAD analogues whereas k_{cat} is not as long as the analogue is in excess of the enzyme. The kinetic equation for the UGM reaction can be written as:

Equation 1.3
$$E_{apo} \underset{-\ FAD_{red}}{\overset{+\ FAD_{red}}{\rightleftharpoons}} E_{holo} \underset{-\ UDP\text{-}Gal\mathit{f}}{\overset{+\ UDP\text{-}Gal\mathit{f}}{\rightleftharpoons}} E_M \xrightarrow[-\ UDP\text{-}Gal\mathit{p}]{K_{cat}} E_{holo}$$

where E_{apo} and E_{holo} denote apo-UGM and holo-UGM, respectively, and E_M denotes the ternary Michaelis complex of holo-UGM and substrate UDP-Gal*f*. The parameter k_{cat} is equal to the reciprocal sum of the reciprocal net rate constants for all intermediates other than free E_{holo} and E_{apo}.[74] Therefore, k_{cat} implicitly represents all chemical steps from the Michaelis complex E_M up to and including dissociation of the UDP-Gal*p* product, which is considered kinetically irreversible under the experimental conditions. Solving for the steady state rate, *v*, of product formation in the above kinetic equation yields:

Equation 1.4 $$v = k_{cat} e_0 s / ((K_D^{FAD}/c + 1)\, K_M + s)$$

where e_0, c and s respectively denote the concentrations of total UGM, the FAD_{red} cofactor and UDP-Gal*f* substrate. The factor K_M is the Michaelis constant for UDP-Gal*f* combining with holo-UGM. The factor K_D^{FAD} is the equilibrium constant for dissociation of E_{holo}, such that $e_0/(K_D^{FAD}/c + 1)$ denotes the concentration of E_{holo} as $s \rightarrow 0$. In terms of the UDP-Gal*f* substrate, the observed steady state kinetic parameters are given by:

Equation 1.5 $$(k_{cat})_{obs} = k_{cat}$$
$$(k_{cat} / K_M)_{obs} = (1 / (K_D^{FAD} / c + 1)) \bullet (k_{cat} / K_M)$$

Therefore, $(k_{cat})_{obs}$ is independent of the coenzyme concentration, whereas $(k_{cat}/K_M)_{obs}$ depends on both the coenzyme concentration and binding affinity of the coenzyme.

Second, k_{cat}/K_M, unlike k_{cat}, is susceptible to differences in the ability of UDP-Gal*f* to form a Michaelis complex in the presence of the analogues. This binding step may be perturbed by affects unrelated to the LFER of interest, e.g., steric clashes rather than the electron density at the N5 nitrogen. In fact, the Hammett plot for $\log(k_{cat}/K_M)$ versus σ

gave a much diminished negative ρ value with a "outlier" represented by the natural cofactor FAD. (Fig. 1-31) This anamolous result is not likely to be caused by undersaturation of UGM with the FAD analogues, because in the control reactions, where 1000-fold (vs. 100-fold) 7-Cl-FAD and 8-OMe-FAD analogues were used, no significant changes were observed in either k_{cat}/K_M or k_{cat}.

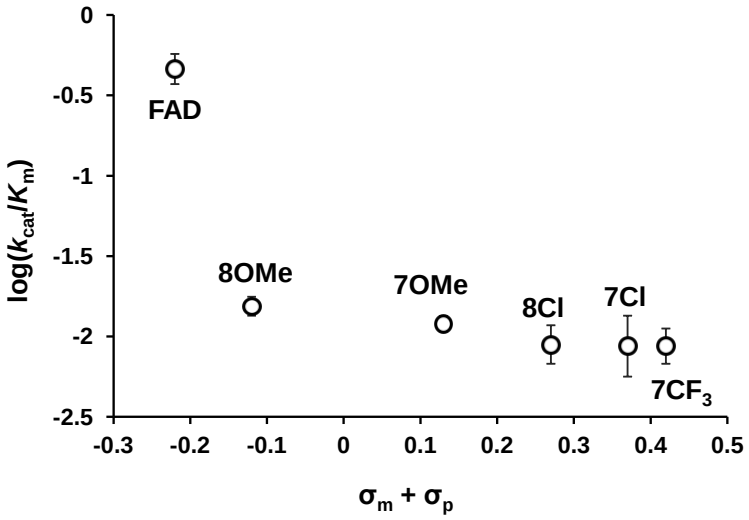

Figure 1-31: LFER plot for $\log(k_{cat}/K_M)$ versus $\sigma = \sigma_m + \sigma_p$. Error bars denote ± one standard error.

For these reasons, our current hypothesis is that an effect not represented by σ, such as steric clashes, leads to poor binding of the UDP-Gal*f* substrate in the presence of different flavin analogues making this step strongly rate limiting under *V*/*K* conditions. Therefore, only k_{cat}, representing all the steps after binding of cofactors and UDP-Gal*f*, was considered in the LFER study.

1.4. CONCLUSION

Positional isotope exchange (PIX) studies indicated that UGM reconstituted with 5-deaza-FAD_{red} is unable to catalyze PIX of the bridging C1–OP_β oxygen of UDP-Gal*p*, suggesting a direct role for the FAD_{red} N5 nitrogen in this process. In addition, analysis of kinetic linear free energy relationships (LFERs) of k_{cat} versus the nucleophilicity of N5 of FAD_{red} gave a slope of -2.4 ± 0.4. These observations represent a direct experimental evaluation of nucleophilic participation by FAD_{red} during UGM catalysis. Together, these findings are most consistent with a mechanism in which the covalent FAD_{red}-Gal*p*/*f* intermediates (**1-28**/**1-29**) are formed through a concerted S_N2-type displacement involving the N5 nitrogen of FAD_{red} as the nucleophile (Fig. 1-14 *pathway A*). Although we cannot completely rule out the existence of oxocarbenium ion intermediate (**1-30**), PIX and LFER studies using different flavin analogues strongly suggest that if such an intermediate does arise during the catalytic cycle, it is transient and very short lived.

UGM utilizes reduced flavin to mediate a chemical transformation that does not involve redox chemistry, illustrating the catalytic versatility of the ubiquitous flavin coenzyme. Our studies toward the mechanism of flavin-substrate covalent adduct formation provide a more detail mechanistic picture of UGM catalysis that will be helpful in the study of eukaryotic UGMs.[75] Moreover, our findings also help to explain the pharmacologically unsatisfactory results obtained with UGM inhibitors that mimic a transition state for generation of an oxocarbenium intermediate.[76-78] Therefore, analogues that specifically target the nucleophilic addition step may offer more promising leads for developing inhibitors of UGM activity.

Chapter 2: Characterization and Mechanistic Implications of MoeZ: a common activating enzyme involved in sulfur trafficking in actinobacteria

2.1. INTRODUCTION

2.1.1. Occurrence and significance

Sulfur is an essential element for all living organisms. It exists in a wide range of compounds such as amino acids, antioxidants, enzyme cofactors, nucleic acids, metal clusters, and a diverse array of secondary metabolites as natural products (examples of sulfur containing biomolecules are listed in Fig. 2-1 and Fig. 2-2). These compounds exhibit a variety of bioactivities and many of them are crucial for life.

The thiol (R-SH) group of cysteine (**2-1**) can function as either a Lewis acid or base in addition to its role as an important redox functionality, for example, in the formation of disulfide (R-S-S-R) bonds. In contrast to cysteine, methionine (**2-2**) contains a thioether (R_1-S-R_2) that is generally more hydrophobic than related thiols; however, thioethers can also act as nucleophiles similar to free thiols. These two amino acids are not only essential components of proteins but are also important precursors in the biosyntheses of other primary metabolites. For example, glutathione (GSH, **2-3**) contains cysteine and is an important cellular antioxidant, whereas *S*-adenosyl-L-methionine (SAM **2-5**), the versatile cofactor discussed in Chapter 3, is directly synthesized from methionine and ATP.

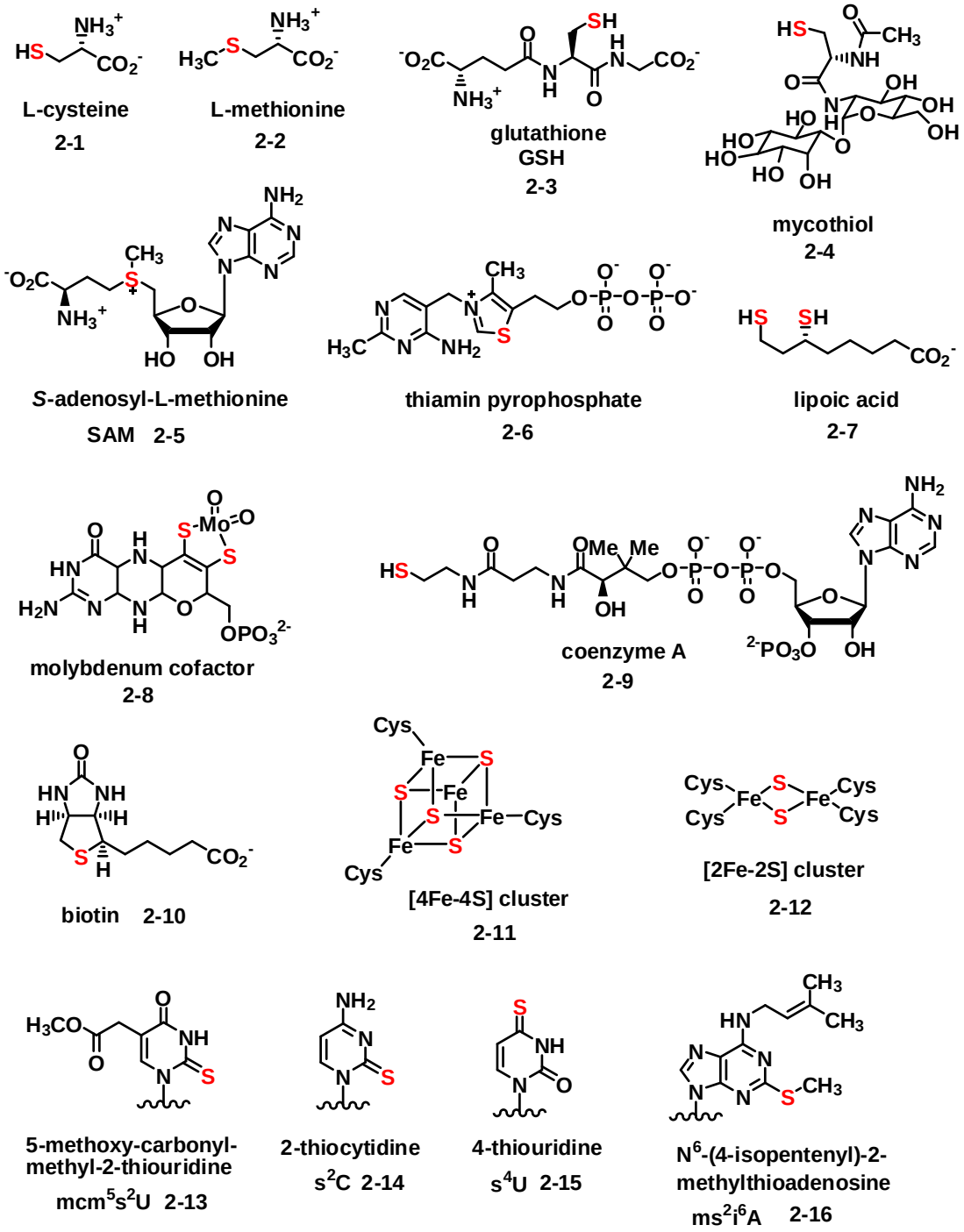

Figure 2-1: Selected sulfur-containing biological compounds.

In addition to SAM, a number of other enzyme cofactors also contain sulfur. Thiamin (vitamin B_1) pyrophosphate (**2-6**) plays a key role in the metabolism of carbohydrates and the biosynthesis of branched chain amino acids. The two sulfur atoms of lipoic acid (**2-7**) can alternate between reduced and oxidized states during the oxidative decarboxylation of α-keto acids. The molybdenum cofactor (Moco, **2-8**) required by several essential enzymes such as sulfite oxidase and aldehyde oxidase also contains two sulfur atoms, which are coordinated to molybdenum. The thiol group of coenzyme A (**2-9**), which functions as an acyl carrier in fatty acid metabolism, is the key component in the thioester linkage (R_1-$COSR_2$) of the fatty acyl derivatives of this cofactor. As a final example, a sulfur atom plays an important structural role in biotin (vitamin B_7, **2-10**), which is yet another cofactor in primary metabolism.[79]

Moreover, sulfur is also a component of iron-sulfur clusters (such as **2-11** and **2-12**). Along with playing a structural role, these clusters serve as redox-active complexes essential to a number of biological processes. Besides, several tRNA modifications involve sulfur incorporation (**2-13 to 2-16**). These modified nucleosides are important for gene expression and codon recognition.[80]

Sulfur is also found in a variety of secondary metabolites. Some selected examples are shown in Fig. 2-2. Penicillin (**2-17**) and cephalosporin (**2-18**) are commonly used antibiotics. The plant natural product salacinol (**2-24**) isolated from *Salacia reticulate* belongs to a class of thiosugars bearing a sulfonium cation core and a monosulfated polyhydroxylated acyclic chain. This class of compounds can act as inhibitors of α-glucosidase and demonstrate antihyperglycemic properties with potential for the treatment of type II diabetes.[81] Lincomycin A (**2-20**) from *Streptomyces lincolnensis* exhibits antimicrobial activity, and its semi-synthetic derivative, clindamycin, is a widely-used, FDA-approved antibiotic. Both of them contain a C_8-sugar backbone

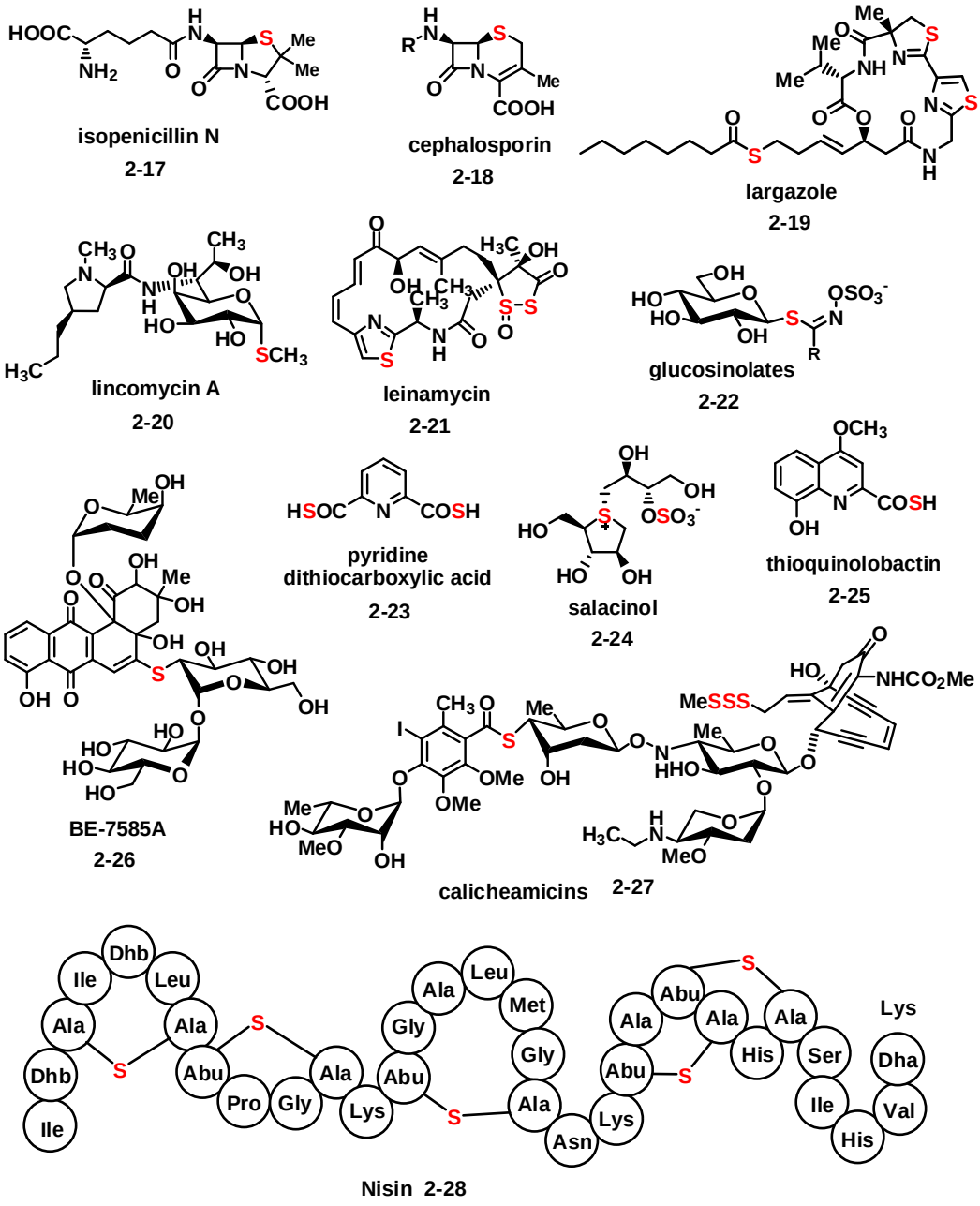

Figure 2-2: Selected sulfur-containing secondary metabolites.

with a C-1-thioether. The antitumor antibiotic leinamycin[82] (**2-21**) and the promising anticancer natural product largazole[83] (**2-19**) both contain a thiazole ring moiety. Calicheamicin (**2-27**) from *Micromonospora echinospora subsp. Calichensis*, the potent antitumor agent, contains a C-4-thiosugar and polysulfide moiety BE-7585A (**2-26**) from *Amycolatopsis orientalis subsp. Vinearia BA-07585* possesses 2-thiosugar group, is a potential antitumor agent due to its thymidylate synthase inhibition activity.[84] Nisin (**2-28**), a lanthipeptide contains thioether linkage, has been used as antibacterial agent in the food industry for more than 40 years.[85]

2.1.2. Sulfur incorporation mechanism

Although the structures of sulfur-containing biomolecules have been long known, the biosynthetic processes that lead to incorporation of sulfur into these compounds have just recently begun to be elucidated in detail. Essentially two mechanisms are currently recognized as underlying biochemical sulfur insertion reactions. The first involves Lewis acid/base case chemistry, where bisulfide (HS^-), a thiolate ($R\text{-}S^-$), a protein persulfide ($R\text{-}S\text{-}S^-$), or a protein thiocarboxylate ($R\text{-}COS^-$) acts as the nucleophilic sulfur donor. The second mechanism involves radical chemistry, and this class of reactions is catalyzed by radical-SAM enzymes, which are discussed in the next chapter.

Sulfur incorporation using bisulfide as the sulfur donor

Plants and microorganisms assimilate sulfate (**2-29**) from the environment and convert it to bisulfide (**2-31**) as a direct sulfur source in cysteine (**2-1**) biosynthesis. The enzyme catalyzing this reaction is *O*-acetylserine sulfhydrylase (OASS), a pyridoxal 5′-phosphate (PLP, **2-32**) dependent enzyme. The reaction mechanism is typical for PLP-dependent enzymes and is shown in Fig. 2-3.[86] The product L-cysteine (**2-1**) can then be used as the sulfur-bearing component in the biosynthesis of other primary metabolites

such as methionine and GSH. Although this is a well-known pathway for the biosynthesis of L-cysteine, it is not the only way this essential amino acid is constructed in nature. Two novel cysteine biosynthetic pathways have recently been reported which employ other sulfur donors such as protein persulfides in archaea[87-88] and protein thiocarboxylates in *Actinomyces*.[89]

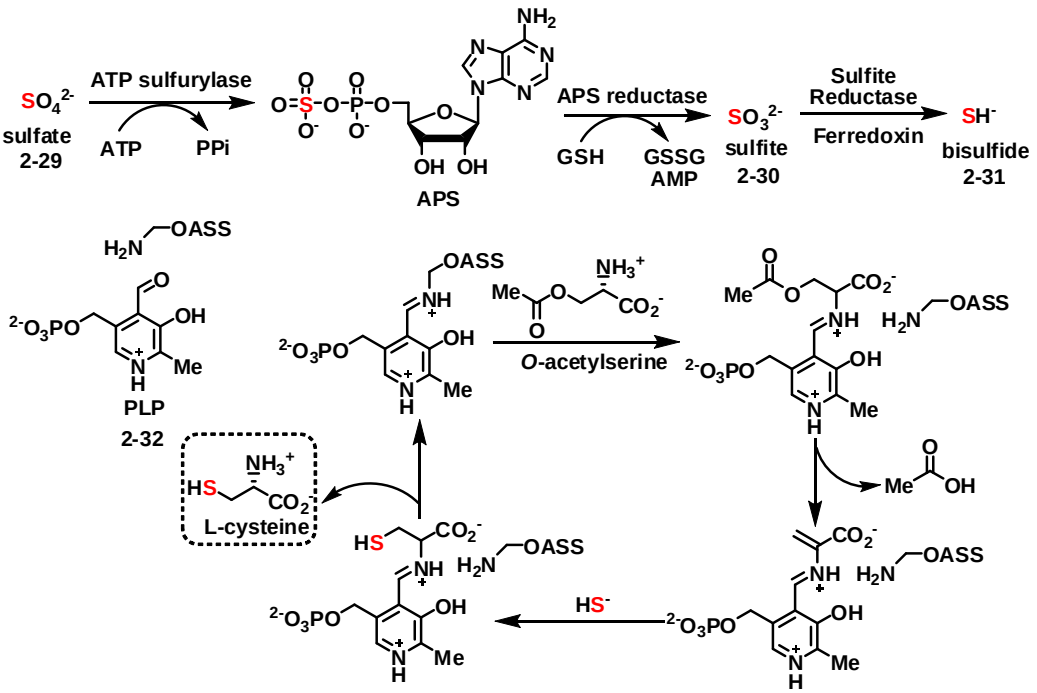

Figure 2-3: Mechanism of OASS where bisulfide acts as the sulfur donor.

Sulfur incorporation using a thiol group as the sulfur donor

An alkyl thiol group in either an enzyme active site (e.g., a cysteine residue) or a free thiol containing molecule in the cell (e.g., cysteine **2-1**, GSH **2-3**, and mycothiol **2-4**) can also be employed as a sulfur donor without complete incorporation of the thiol-bearing species. For example, the eukaryotic enzyme THI4p from *Saccharomyces cerevisiae* transfers a hydrosulfide equivalent from an active site cysteine residue to its

substrate in the biosynthesis of the thiazole ring in thiamine (see Fig. 2-4).[90] In doing so, THI4p functions as a suicide enzyme, because each turnover converts the active site cysteine residue into an inactive dehydroalanine in a process mediated by iron.[91] Nevertheless, the reaction mediated by THI4p in eukaryotes takes place of six separate enzyme catalyzed reactions required in prokaryote thiazole biosynthesis. The biosynthesis of C-1-thioglucosides (e.g., glucosinolates **2-16**) serves as an example of sulfur transfer from small molecule donors such as L-cysteine or GSH.[92]

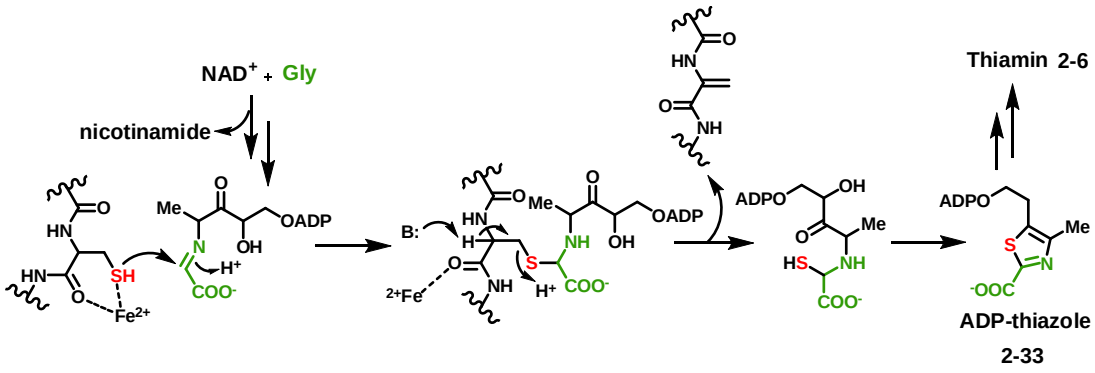

Figure 2-4: Proposed mechanism for THI4p using active site cysteine as sulfur donor. The thiazole ring here is biosynthesis by one enzyme THI4p using NAD^+, glycine, and its active site cysteine residue.

Sulfur incorporation using a protein persulfide as the sulfur donor

High concentration of free bisulfide is considered toxic *in vivo*, in contract, persulfide group bound to a large protein (protein persulfide, R-S-SH) is the bisulfide equivalent nature created to overcome this problem. In fact, protein persulfide has been considered as a key component in cellular sulfur trafficking. Cysteine desulfurases and rhodanese homology domain proteins are the two currently recognized protein families that can convert their active site cysteine residues to a persulfide- group.

Cysteine desulfurases (e.g., IscS, NifS, CsdA, and SufS) are PLP-dependent enzymes catalyzing the transfer of a hydrosulfide equivalent from L-cysteine to an active site cysteine residue. The resulting cysteine persulfide residue in the cysteine desulfurase can then be used to transfer the hydrosulfide to a thiol acceptor in another protein forming a new persulfide in a process known as sulfur relay. The protein persulfides can also react with the activated *C*-terminal of a sulfur carrier protein to form a protein thiocarboxylate.[93] The mechanisms of cysteine desulfurase and sulfur relay are shown in Fig. 2-5. In this manner, the cysteine desulfurases participate in several different biosynthetic pathways such as iron-sulfur cluster assembly,[94] selenium incorporation, *t*-RNA modification, and the biosynthesis of thiamin and molybdopterin.[79]

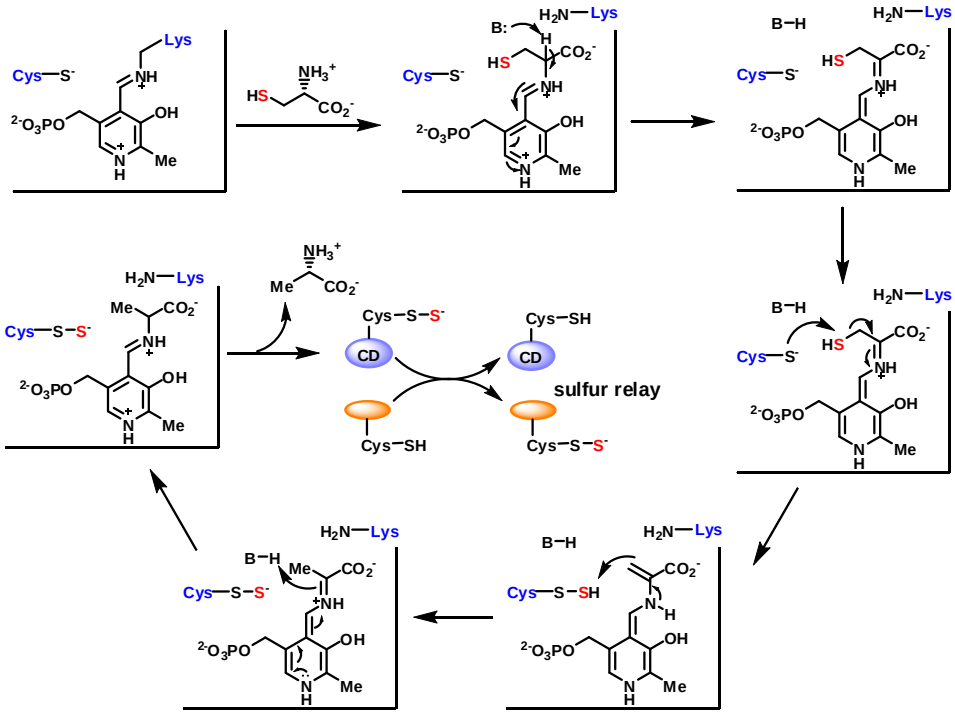

Figure 2-5: General mechanism of cysteine desulfurases (CD) and sulfur relay.

Analogy to cysteine desulfurases, rhodanese homology domain (RHOD) proteins can also form protein persulfide group in their active sites. Differently, this process does not cost free cysteine but transfers the sulfur atom from thiosulfate or another protein persulfide. Rhodaneses, also known as thiosulfate:cyanide sulfurtransferases, are enzymes that catalyze sulfur transfer from thiosulfate (**2-34**) to an active site cysteine residue as shown in Fig. 2-6.[95-96] Bioinformatics analysis has shown that rhodanese homology domains exit in about 500 genes from three major evolutionary phyla, although the thiosulfate:cyanide sulfurtransferase activity varies in different cases.[95] Mutagenesis studies of the conserved active site loop CRXGX[R/T] of a RHOD protein MOCS3 suggested that, the first cysteine residue (underlined) is responsible for forming a persulfide group during catalysis, and the last amino acid determines the relative activity of the thiosulfate sulfurtransfer.[97] Based on their results, RHOD protein with an R/T residue at the six position of the active site loop is likely to be 500-fold more active than the one with a D residue.[97] So far, several RHOD proteins have been characterized, including ThiI, MOCS3, Uba4, YbbB, and YnjE. Along with cysteine desulfurases, these proteins play important roles in cofactor biosynthesis and tRNA modification.[88, 98-101]

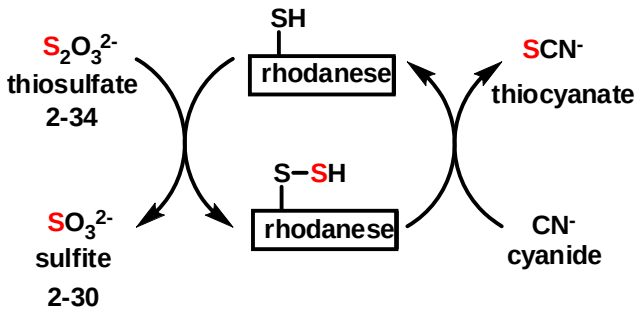

Figure 2-6: General reaction scheme for rhodanese activity.

For example, both cysteine desulfurase (IscS) and a rhodanese homology domain protein (ThiI) are required for sulfur incorporation during the biosynthesis of 4-thiouridine (**2-15**) in *E. coli* (see Fig. 2-7).[102] IscS uses cysteine as the sulfur donor to oxidize an active site cysteine residue to a cysteine persulfide. The sulfane sulfur of the persulfide group is then transferred to an active site cysteine residue of ThiI (Cys_{456}). ThiI then participates in two reactions leading to the conversion of the uridine-8 residue in tRNA to a 4-thiouridine residue. The first reaction is adenylation of uridine-8 to form an activated intermediate. The second reaction is substitution of the adenylate moiety with the sulfane sulfur from the ThiI-Cys_{456}-S-SH residue. Currently, there are two working hypothesis for the mechanism of the latter sulfur incorporation reaction. In the first mechanism, the protein persulfide directly attacks the activated tRNA substrate and AMP is released to form a covalent enzyme-substrate disulfide complex. Then an adjacent active site cysteine (Cys_{344}) attacks the disulfide intermediate to generate the 4-thiouridine product (s^4U **2-15**) and a Cys_{456}-S-S-Cys_{344} disulfide linkage (see Fig. 2-7 A). Reduction of the internal disulfide bond will then regenerate ThiI completing the catalytic cycle. Alternatively, bisulfide generated in situ via formation of the Cys_{456}-S-S-Cys_{344} disulfide may instead represent the sulfur nucleophile responsible for elimination of the adenylate moiety and formation of product without a covalent enzyme-substrate intermediate (see Fig. 2-7 B).

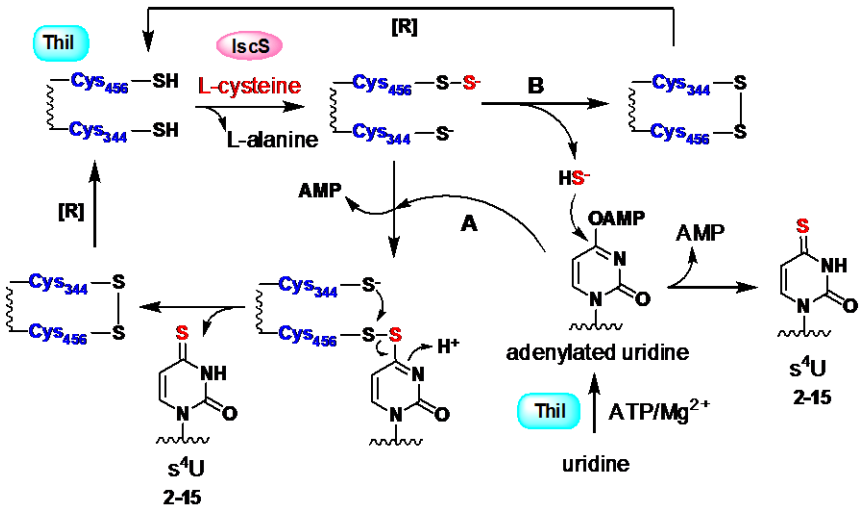

Figure 2-7: Proposed mechanism for 4-thiouridine biosynthesis.

Sulfur incorporation using a protein thiocarboxylate as the sulfur donor

In contrast with thiamine biosynthesis in eukaryotes, the immediate sulfur donor for thiazole (**2-38**) formation in prokaryotes is a protein thiocarboxylate.[90] Formation of this sulfur donor requires two enzymes, the sulfur carrier protein ThiS and its activation enzyme ThiF, as shown in Fig. 2-8.[84] The *C*-terminal carboxylate group of ThiS is first adenylated by ATP in a reaction catalyzed by ThiF. The terminal sulfur of the persulfide group on cysteine desulfurase IscS then substitutes the AMP moiety of the adenylated ThiS to form the ThiS thiocarboxylate (**2-35**). Upon formation, the nucleophilic thiocarboxylate can then add to the carbonyl of the ThiG/DXP complex (**2-36**). An *S*-*O* shift of the ThiS *C*-terminal acyl functionality completes incorporation of the free thiol. Following elimination of the ThiS carboxylate, the thiol-bearing ThiG adduct (**2-37**) is coupled with dehydroglycine to complete the formation of the thiazole ring.

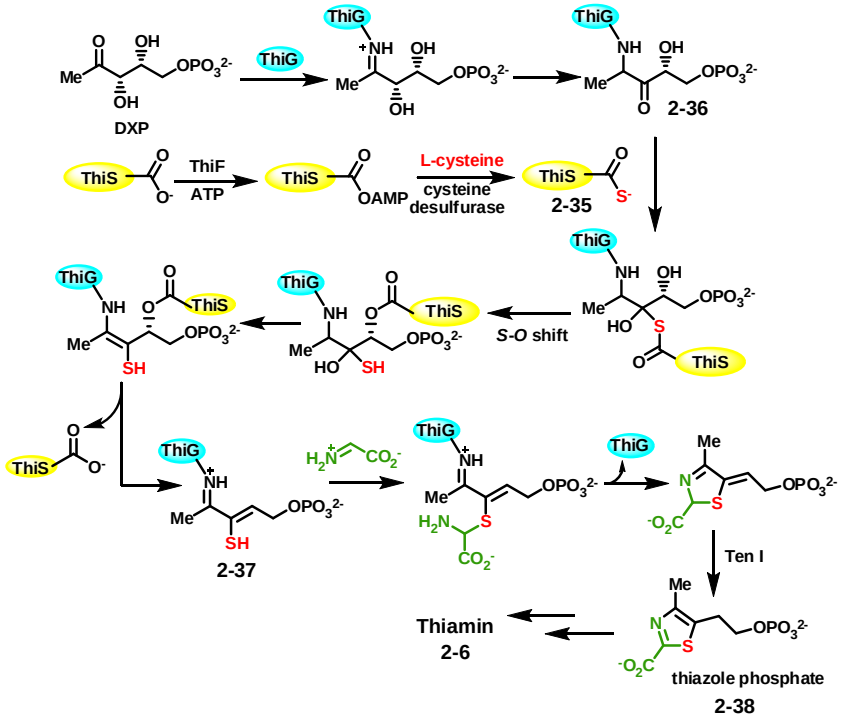

Figure 2-8: Proposed mechanism for thiazole formation in prokaryotes using a protein thiocarboxylate as the sulfur donor.

As illustrated above, ThiS is an example of a sulfur carrier protein, which bears a thiocarboxylate sulfur donor in its activated form. Sulfur carrier proteins represent an increasingly recognized class of proteins characterized by the following features: (1) small size with approximately 65-100 amino acids in their primary sequence; (2) a flexible Gly-Gly sequence at the *C*-terminus; and (3) a β-grasp fold structure.[103] The activation of sulfur carrier proteins requires ATP, a sulfur source, and an activation enzyme (e.g., ThiF in the case of ThiS).[103]

Interestingly, sequence, structure and activation of sulfur carrier proteins are analogy to eukaryotic ubiquitin (Ub), which is a small protein that can be used as a donor to conjugate other proteins via the formation of an amide bond as shown in Fig. 2-9 D.[104-107] In fact, protein ubiquitination are highly conserved in eukaryotes and controls an

enormous range of physiological processes. Thus, misregulation of this system is known to be associated with a number of diseases in humans.[108] The resemble of two distinct processes suggest the evolutionary linkage between bacterial sulfur carrier proteins and eukaryotic Ub and ubiquitin-like proteins (Ubls).[109-111] This hypothesis is supported by the discovery of ubiquitin-like proteins that function in both sulfur transfer and protein conjugation in prokaryotes and archaea.[112-113] Listed in Fig. 2-9 and Fig. 2-10 are the sulfur carrier proteins and activating enzymes reported so far, including those involved in the biosynthesis of primary metabolites such as thiamin pyrophosphate (**2-6**),[114-115] molybdopterin (**2-8**),[109,116-117] L-cysteine (**2-1**),[89,118] L-methionine (**2-2**),[119] 2-thioribothymidine,[109-110,120] and 5-methoxycarbonylmethyl-2-thiouridine (**2-13**).[111-112,121] Also included are those sulfur carrier proteins involved in the formation of secondary metabolites such as pyridine dithiocarboxylic acid (**2-23**),[122-123] thioquinolobactin (**2-25**)[124], and compound BE-7585A (**2-26**).[84]

Sulfur incorporation involving radical SAM chemistry

So far, there are three types of sulfur insertion reactions that have been recognized to involve radical SAM enzymes. The first type utilizes a protein coordinated [2Fe-2S] cluster as the sulfur donor and is involved in the biosynthesis of biotin (**2-10**)[125-126] and lipoic acid (**2-7**).[126] The second type catalyzes tRNA methylthiolation, and is observed in the biosynthesis of N^6-(4-isopentenyl)-2-methylthioadenosine (**2-15**).[126] Finally, radical SAM enzymology has also been characterized in an alternative mechanism of thioester bond formation, as is the case with bacteriocin subtilosin A biosynthesis.[127] These enzymes will discussed more fully in Chapter 3, where radical SAM enzymes are considered in general.

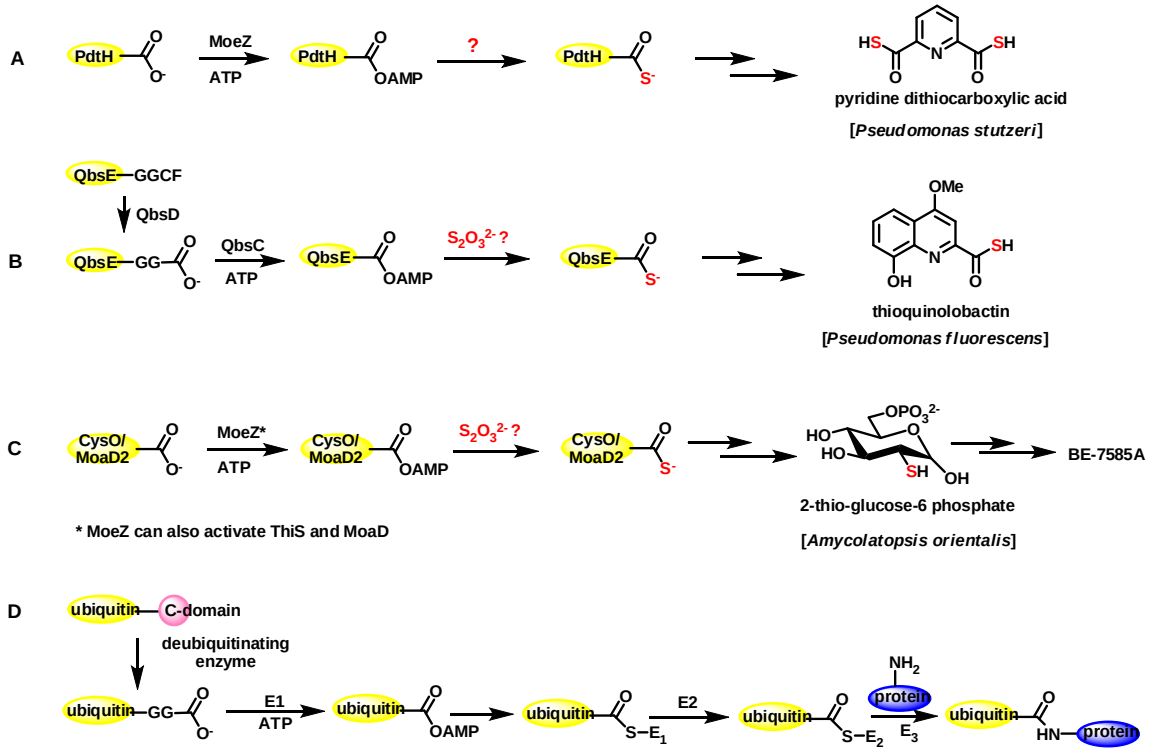

Figure 2-9: Sulfur carrier proteins and their activating enzymes involved in secondary metabolism (A-C) and the eukaryotic ubiquitination pathway (D).

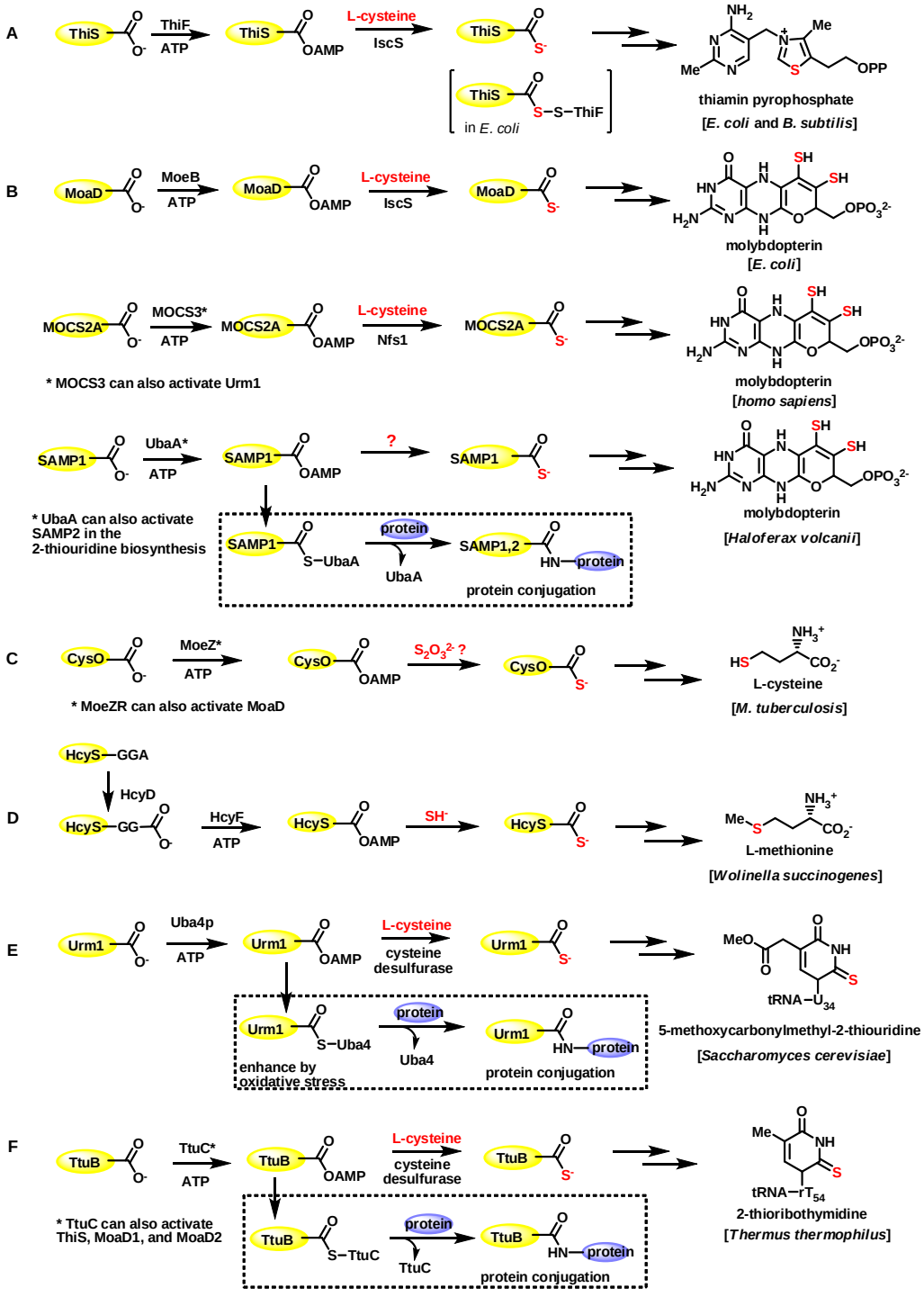

Figure 2-10: Sulfur carrier proteins and their activating enzymes involved in primary metabolism.

2.1.3. MoeZ mediated sulfur transfer in actinobacteria

Biosynthesis of 2-thioglucose in BE-7585A

Recently, the biosynthesis of the sulfur-containing compound BE-7585A (**2-24**) from *Amycolatopsis orientalis subsp. Vinearia BA-07585* was investigated.[3,84,128-129] In the BE-7585A biosynthetic gene cluster, *bexX*, a gene whose product shares moderate sequence similarity to thiazole synthase ThiG in *Bacillus subtilis* (Fig. 2-8), was identified. This gene was later demonstrated to encode a thiosugar synthase involved in the biosynthesis of the 2-thiosugar moiety shown in Fig. 2-11. Unlike the thiamin biosynthetic genes in *B. subtilis*, a gene encoding the required sulfur carrier protein and its activating enzyme are not found in the same cluster as *bexX*.

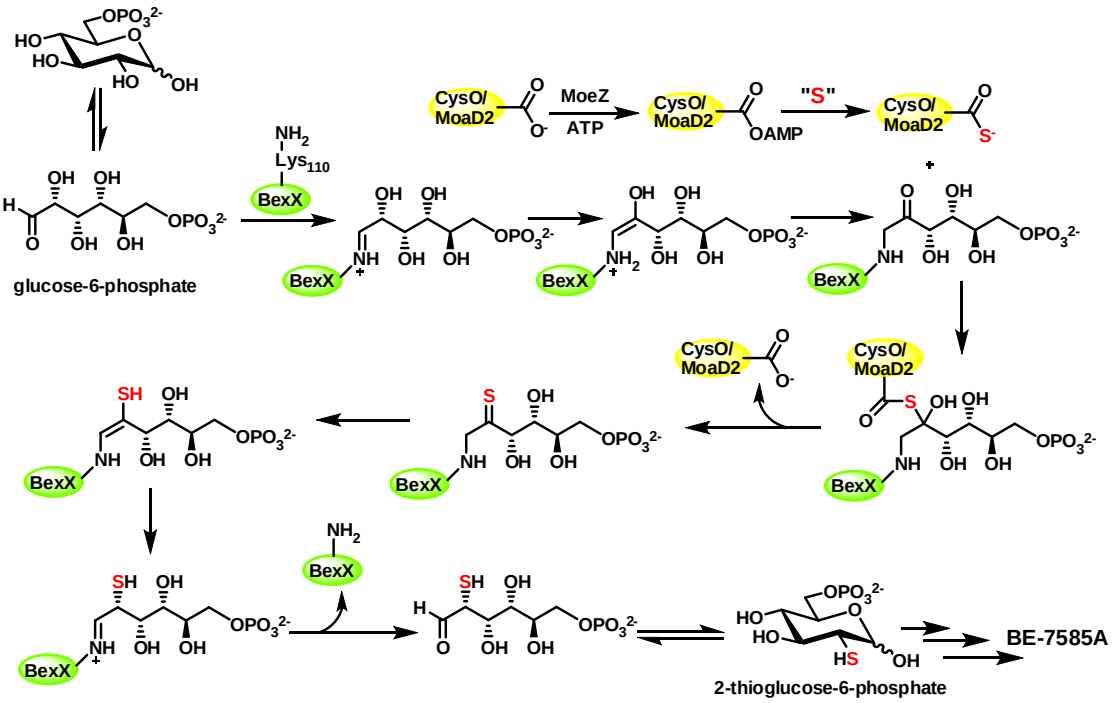

Figure 2-11: Proposed biosynthetic pathway for 2-thioglucose in BE-7585A.

In fact, whole genome sequencing of *A. orientalis* identified only four genes annotated as encoding sulfur carrier proteins. These include *thiS* in the putative thiamin biosynthesis cluster, *cysO* in the putative cysteine biosynthesis cluster, *moaD* in the putative molybdopterin biosynthesis cluster, and *moaD2* which does not appear to be related to any particular biosynthetic pathway. Surprisingly, in each of these putative primary metabolite biosynthetic gene clusters, no corresponding activating enzyme is present. Instead, BLAST analysis identified MoeZ as the only activating enzyme encoded in the genome of *A. orientalis*, and subsequent experiments have shown that MoeZ is able to activate all four sulfur carrier proteins to their thiocarboxylate form. Interestingly, only two of them, CysO and MoaD2, can transfer a sulfur atom to glucose-6-phosphate.[84]

Sequence homology of MoeZ

MoeZ from *A. orientalis* is composed of an *N*-terminal E1-like domain, which ostensibly catalyzes an adenylation reaction, and a *C*-terminal rhodanese homology domain (RHOD). Presence of the *C*-terminal RHOD implies that MoeZ may directly generate a protein-persulfide from thiosulfate (Fig. 2-6). Although it is also possible that L-cysteine and a cysteine desulfurase are responsible for the protein-persulfide formation (Fig. 2-7).

The sequence alignment of MoeZ with selected sulfur carrier protein activating enzymes is shown in Fig. 2-12. Based on sequence homology, MoeZ from *A. orientalis* exhibits the greatest similarity to MoeZ from *M. tuberculosis* and *P. stutzeri*, as well as QbsC from *P. fluorescens*, which all contain two distinct domains. Compared to human MOCS3 and *Saccharomyces cerevisiae* Uba4 (Fig. 2-10, B and E), two enzymes that are relatively well characterized, MoeZ does not contain the dual CXXC motif for zinc-binding. Furthermore, the thiosulfate sulfurtransferase activity of MoeZ is predicted to be

much higher than those of MOCS3 and Uba4 based on sequence of the active site loop.[84,97] Both MOCS3 and Uba4 are capable of utilizing thiosulfate as a sulfur source *in vitro*; however, the physiological sulfur donor has been proposed to be L-cysteine and cysteine desulfurase Nfs1 in case of MOCS3.[130-132] This hypothesis is based on the relatively slow observed sulfur transfer efficiency from thiosulfate catalyzed by MOCS3.[132] Since the RHOD of MoeZ is expected to demonstrate greater thiosulfate sulfur transfer activity, we hypothesize that thiosulfate might be the physiological sulfur donor in case of MoeZ.

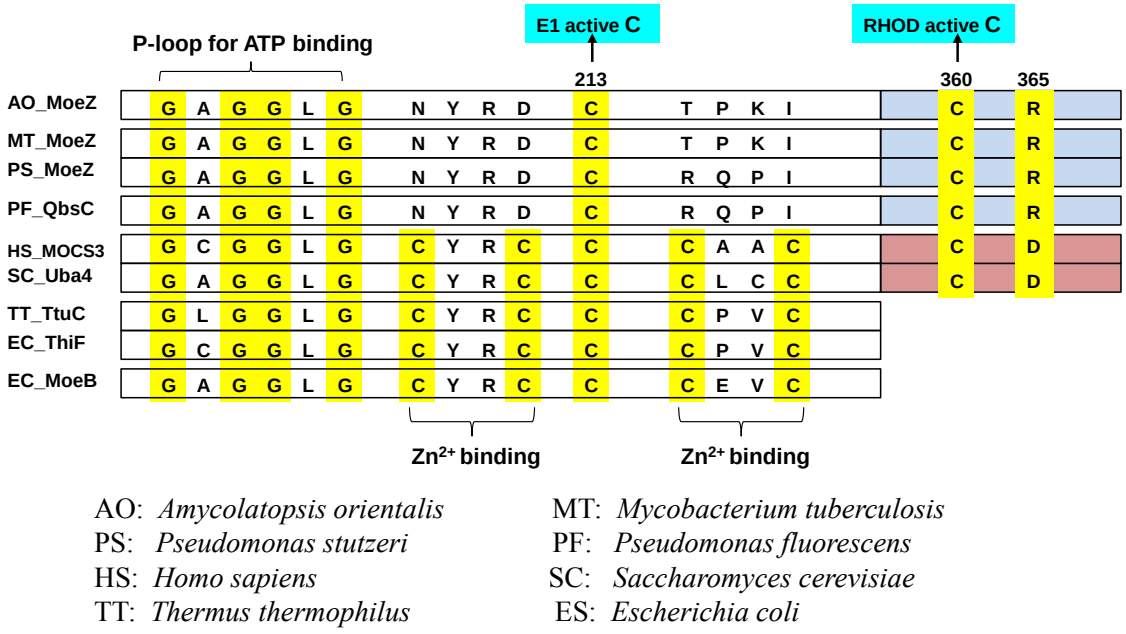

Figure 2-12: Sequence alignment of selected sulfur carrier protein activating enzymes from different organisms.

Proposed mechanisms for MoeZ in A. orientalis

Based on the results of sequence alignment and knowledge of other sulfur carrier protein (SCP) activating enzymes, we have proposed the mechanisms shown in Fig. 2-13 for the MoeZ catalyzed sulfur transfer reaction using thiosulfate as the sulfur source.

Overall, the E1-like domain of MoeZ is believed to utilize ATP to activate the substrate SCP via an adenylation reaction, and the RHOD of MoeZ is believed to generate an active site protein persulfide functionality using thiosulfate as the sulfur donor. The terminal sulfur of the protein persulfide group is transferred to the adenylated SCP in some manner to form a thiocarboxylate group concomitant with displacement of the adenylate from the substrate and formation of a disulfide linkage within MoeZ.

There are four possible mechanisms involving the conserved cysteine residues of MoeZ. In pathway A, a MoeZ-SCP thioester intermediate is formed at Cys_{213} of MoeZ, whereas a protein persulfide using thiosulfate occurs at Cys_{360}. The sulfane sulfur of the persulfide group then attacks the thioester intermediate resulting in an acyl disulfide intermediate (I) at Cys_{360}. The cysteine residue at Cys_{213} then forms an internal disulfide bond with Cys_{360} eliminating the SCP thiocarboxylate. The proposed formation of a thioester intermediate is reminiscent of ubiquitination (Fig 2-9 D) and has also been suggested by others.[133] Thorough review of reported SCP activating systems offers controversial results regarding the existence of this species as well as its mechanistic importance.[112,120-121,132] Since the mechanism of MoeZ and its homologues has not been investigated, the existence and significance of this thioester intermediate is of our interest.

In pathways B and C, only the acyl disulfide intermediate is formed during the reaction. The difference between these two routes lies on the residue of acyl disulfide bond formation. It could be at site Cys_{360}, where the protein persulfide is generated (*pathway B*). It could also be at Cys_{213}, which first accepts the sulfane sulfur from the Cys_{360} persulfide to generate a Cys_{213} persulfide (*pathway C*). The rationale for pathway B is based on the similar nucleophilicity of alkyl persulfides versus thiols. We include pathway C, because an acyl disulfide-linked ThiF-ThiS adduct (Fig. 2-10 A) from *E. coli* has been detected using Fourier transform mass spectrometry.[114] Although MoeZ

contains an additional RHOD compared to ThiF (Fig. 2-12), the fact that ThiS in *A. orientalis* can be activated by MoeZ makes this possibility worth considering. In pathway D, no covalent MoeZ-SCP intermediate is formed. Instead, bisulfide is released directly upon formation of the internal disulfide bond between Cys_{213} and the Cys_{360} persulfide, similar to mechanism B of ThiI catalyzed sulfur incorporation into tRNA (Fig. 2-7). Bisulfide itself then serves as the nucleophile during attack at the adenylated SCP to give the thiocarboxylate product.

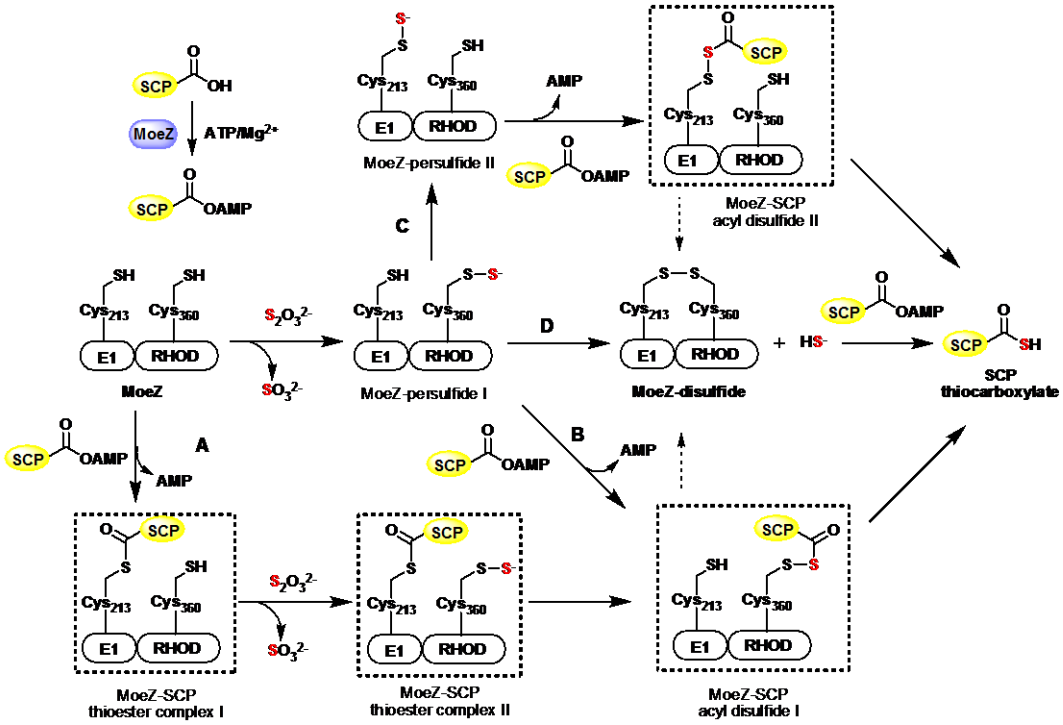

Figure 2-13: Proposed mechanism for MoeZ catalyzed sulfur transfer in *A. orientalis*. Boxed species are potential MoeZ-SCP covalent conjugates.

Alternative sulfur sources for MoeZ from A. orientalis

As RHOD can function as both a thiosulfate sulfur transferase and a protein persulfide acceptor, another possible sulfur source for MoeZ catalyzed SCP thiocarboxylate formation is either L-cysteine or L-cystine via the action of a cysteine

desulfurase as shown in Fig. 2-14 B & C. In fact, five cysteine desulfurase homologues (CD 1-5) have been found in the genome of *A. orientalis*, and initial assays have suggested that CD2 or CD4 uses cysteine as the sulfur donor while CD3 uses cystine.[84]

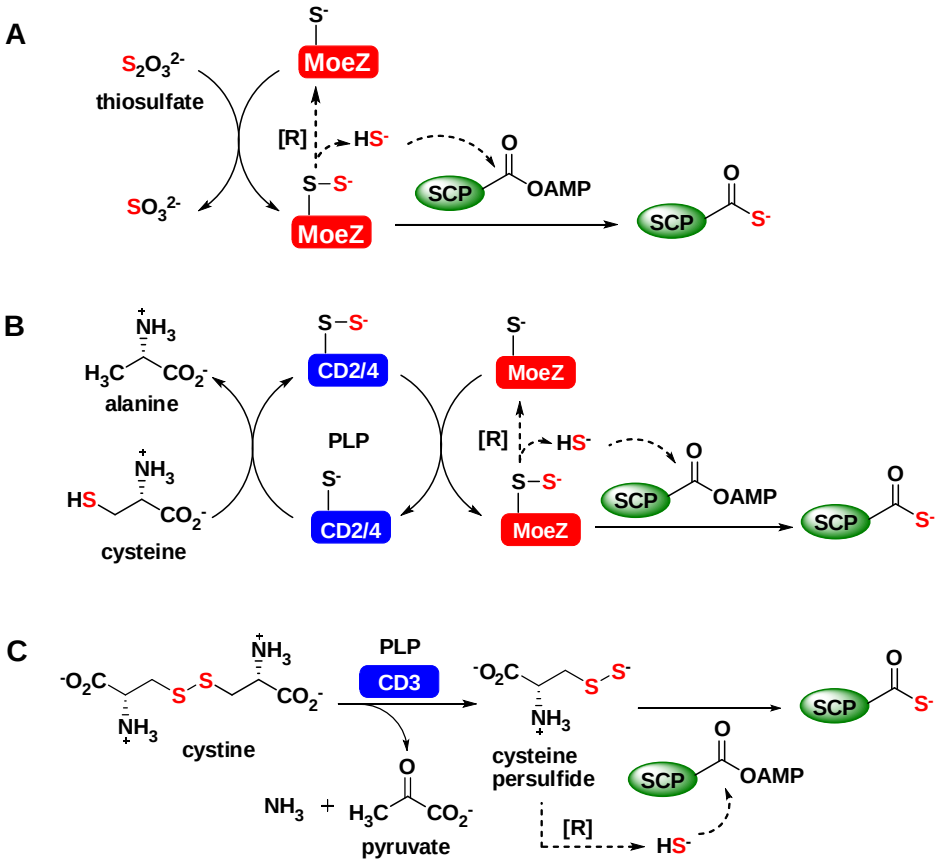

Figure 2-14: Potential sulfur sources for MoeZ catalyzed SCP thiocarboxylate formation.

2.1.4. Thesis statement

Sulfur containing compounds are present in a wide range of living systems as amino acids, antioxidants, metal clusters, cofactors, and natural products. Although the importance of these compounds is well appreciated, little was understood regarding the trafficking and incorporation of sulfur into target scaffolds until the last decade. Only very recently has the incorporation of sulfur into thiosugars been clarified through

biosynthesis studies of the angucycline-type natural product BE-7585A from *Amycolatopsis orientalis*, which bears a 2-thiosugar moiety.[84,128-129] An important finding of this work is that the thiosugar synthase BexX utilizes sulfur carrier proteins from other primary metabolite biosynthetic pathways rather than one specific for the biosynthesis of BE-7585A. Based on the results from genome mining, the sulfur carrier protein activating enzyme MoeZ responsible for producing the activated sulfur donor for the BexX catalyzed reaction is shared among different biosynthetic pathways. The focus of this chapter will be the characterization and mechanistic study of MoeZ, with emphasis on how the sulfur atom is transferred from thiosulfate to the sulfur carrier proteins. The MoeZ chemistry may also be applied to the chemoenzymatic synthesis of selenosugars and will also be investigated as an alternative to existing synthetic methods.[134]

Sequence alignment of MoeZ and its reported homologues suggests that two cysteine residues (Cys_{213} and Cys_{360}) may be important for sulfur trafficking. Results from mutagenesis studies and gel shift assays are most consistent with the following hypothesis (see Fig. 2-13A): (1) MoeZ catalyzes adenylation of SCPs in the presence of ATP and Mg^{2+}. The two conserved cysteine residues are not important for this activity. (2) A thioester covalent conjugate between the MoeZ Cys_{213} and the SCP is then generated via elimination of the adenylate moiety. (3) A Cys_{360} persulfide is produced via sulfur transfer from thiosulfate. This activity is identical to a typical rhodanese enzyme. (4) The Cys_{360} persulfide subsequently attacks the Cys_{213}-thioester releasing the SCP thiocarboxylate product and forming an internal disulfide bond in the active site of MoeZ.

2.2. MATERIALS AND METHODS

2.2.1. General

DNA sequencing was performed by the Core Facilities of the Institute of Cellular and Molecular Biology at the University of Texas at Austin. The general methods and protocols for recombinant DNA manipulation were followed according to Sambrook and coworkers.[53] Mass spectroscopy was performed at the Mass Spectrometry Core Facility in the College of Pharmacy at the University of Texas at Austin. Vector NTI Advance 10.1.1 from Invitrogen was used for sequence alignments.

Materials

The materials used for molecular cloning as well as protein expression and purification are the same as those described in Chapter 1. PCR primers were purchased from Integrated DNA Technologies, Inc (Coralville, IA). All chemicals and reagents were purchased from Sigma-Aldrich Chemical Co. (St. Louis, MO), Thermo Fisher Scientific (Waltham, MA), or VWR (Radnor, PA), and were used without further purification unless otherwise specified. The Milli-Q lab water purification system was purchased from EMD Millipore (Darmstadt, Germany). Compressed gases and liquid nitrogen were obtained from Airgas (Austin, TX). The Mini-Protein II vertical system used for SDS-PAGE, the Mini-Trans-Blot Cell used for blotting transfer, the GelAir gel drying system, and all related accessories were purchased from Bio-Rad (Richmond, CA). The CarboPac PA1 high-performance liquid chromatography column was a product of Thermo Fisher Scientific. The recombinant vectors encoding genes *moeZ*, *thiS*, *cysO*, *moaD*, *moaD2*, and *bexX* were previously prepared by Dr. Eita Sasaki.[84]

Instrumentation

Experiments described in this chapter utilized a number of instruments in addition to those mentioned in Chapter 1. Cell disruption was performed using a Fisher 550 Sonic Dismembrator from Thermo Fisher Scientific. A standard bench heat block and mini vortexer were purchased from VWR. Incubators were products of New Brunswick from Eppendorf (Enfield, CT). The glove-box used for anaerobic experiments was purchased from Coy Laboratory Products, Inc. (Grass Lake, MI). The glove-box was maintained under an atmosphere consisting of approximately 98% N_2 and 2% H_2 with an oxygen level less than 1 ppm. The catalyst used to remove the oxygen in the glove-box was regenerated about every two weeks by heating at 120 ºC for 2 h.

2.2.2. Preparation of competent cells

Competent cells were prepared using the rubidium chloride method.[53] Specifically, a single fresh colony of the appropriate *E. coli* strain was used to inoculate 5 mL of Luria-Bertani (LB) medium at 37 ºC. After about 10 h of growth, the resulting culture was used to inoculate 100 mL of SOB medium (per 100 mL H_2O: 2 g tryptone, 0.5 g yeast extract, 0.05 g NaCl, 19 mg KCl, and 0.2 mL 5 M NaOH; after autoclave 1 mL of autoclaved 1 M $MgCl_2$ and 1 mL of 1 M $MgSO_4$ were added) which was then grown at 18 ºC until the OD_{600} reached approximately 0.4. The culture was then divided into two 50 mL sterilized conical vials and chilled on ice for 15 min. After centrifugation at 3000 rpm for 10 min at 4 ºC, the supernatant was decanted and the cells were resuspended in 35 mL of cold, filtration-sterilized RF1 solution (per 100 mL H_2O: 0.29 g CH_3COOK, 0.99 g $MnCl_2•4H_2O$, 0.15 g $CaCl_2•2H_2O$, 1.2 g RbCl, and 15 g glycerol, pH 5.8 with 0.1 M acetic acid). The suspension was then incubated on ice for 15 min. After centrifugation and removal of the supernatant, the cell pellet was then resuspended in 8.5 mL of cold, filtration-sterilized RF2 solution (per 100 mL H_2O: 0.209 g MOPS, 1.1 g

$CaCl_2$•$2H_2O$, 0.12 g RbCl, 15 g glycerol, pH 6.8 with 2 M NaOH). The resulting suspension was then quickly aliquoted into pre-chilled, autoclaved tubes and stored at −80 ºC.

2.2.3. Cloning of MoeZ mutants

The site-specific C213A-*moeZ*, C223A-*moeZ*, and C360A-*moeZ* mutants were constructed using the QickChange site-directed mutagenesis kit from Stratagene. Plasmid *moeZ*/pET28b(+) was used as the DNA template. The PCR primers used in the mutation experiments are shown in Table 2-1. The resulting plasmids C213A-moeZ/pET28b(+), C223A-*moeZ*/pET28b(+), and C360A-*moeZ*/pET28b(+) were used to transform the *E. coli* BL21 star (DE3) strain for protein overexpression of the corresponding mutants.

Primer	Sequence
C213A-*moeZ*-forward	5’-CATGGTCCCCTCCGCCGCCGAGGGT-3’
C213A-*moeZ*-reverse	5’-GCCACCCTCGGCGGCGGAGGGGAC-3’
C223A-*moeZ*-forward	5’-CTGGGCGTGCTCGCCGCGTCCATCG-3’
C223A-*moeZ*-reverse	5’-GCCGATGGACGCGGCGAGCACGCCC-3’
C360A-*moeZ*-forward	5’-GATCGTCCTGCACGCCAAGTCGGGC-3’
C360A-*moeZ*-reverse	5’-GCGGGCGCCCGACTTGGCGTGCAGG-3’

* The codon for the mutated residue is underlined.

Table 2-1: Primers used for constructing MoeZ mutants.

2.2.4. Protein expression and purification

MoeZ and its mutants

Typically, a 10 mL culture of *E. coli* BL21 star (DE3) transformed with a plasmid encoding either *moeZ* (His_6 tag at *N*-terminus or His_6 tag at *C*-terminus) or one of its mutants (His_6 tag at *N*-terminus) was grown overnight in LB medium containing 50 μg/mL of kanamycin at 37 ºC. This small culture was then used to inoculate 1 L of LB medium. The large culture was subsequently incubated at 37 ºC with shaking (230 rpm) until the OD_{600} reached approximately 0.5. Expression of the target protein was then induced by the addition of isopropyl β-D-1-thiogalactopyranoside (IPTG) to a final concentration of 0.1 mM, and the culture was incubated at 18 ºC with shaking (120 rpm) for an additional 22 h. Following protein expression, the cells were harvested by centrifugation at 4500 × g for 15 min and stored at –80 ºC.

Protein purifications were carried out at 4 ºC using Ni-NTA resin according to the manufacturer's procedure with minor modifications. Specifically, a 5 g cell pellet was thawed and resuspended in 20 mL lysis buffer (50 mM Tris buffer, pH 8.0, 300 mM NaCl, 10 mM imidazole). The resulting mixture was sonicated using 10 × 10 s pulses at power 8 with a 30 s cooling time between each pulse. The resulting lysate was centrifuged at 16,000 × g for 30 min, and the supernatant was incubated with Ni-NTA resin for 1 hr at 4 ºC with gentle agitation. The resulting resin was loaded on to a column and washed with 150 mL wash buffer (50 mM Tris buffer, pH 8.0, 500 mM NaCl, 25 mM imidazole), the bound protein was eluted with 20 mL elution buffer (50 mM Tris buffer, pH 8.0, 300 mM NaCl, 250 mM imidazole). The concentrated fractions were pooled and dialyzed against 3 × 1 L dialysis buffer (50 mM Tris buffer, pH 8.0, 50 mM NaCl, 10% glycerol). The purified protein was then flash-frozen in liquid nitrogen and stored at −80 ºC until use. Protein concentration was determined by the Bradford assay

using bovine serum albumin as the standard.[52] Protein purity was estimated by sodium dodecyl sulfate polyacrylamide gel electrophoresis (SDS-PAGE).

Sulfur carrier proteins and cysteine desulfurases

Only *N*-terminal His_6-tagged recombinants of sulfur carrier proteins (ThiS, MoaD, MoaD2, and CysO from *A. orientalis* were prepared, because the *C*-terminal carboxylate represents the modification site. The expression and purification procedures regarding the sulfur carrier proteins were essentially identical to those used for the preparation of MoeZ and its mutants. Cysteine desulfurases (CD3 and CD4) were prepared by Dr. Eita Sasaki and the procedure was described in his dissertation.[84]

2.2.5. Characterization of MoeZ and its mutants

Spectrophotometric analysis of the adenylation reaction

The adenylation of sulfur carrier proteins catalyzed by MoeZ and its mutants was monitored using a coupled enzyme assay in the presence of an excess of NaSH.[84] As shown in Fig. 2-15, one molecule of AMP is released with the formation of each activated sulfur carrier protein. To detect formation of AMP continuously, adenylate kinase (AP) is present in the assay and converts one molecule of AMP and ATP to two molecules of ADP. ADP can then used to regenerate ATP in the reaction using pyruvate kinase (PK) and phosphoenol pyruvate (PEP). The resulting pyruvate can be converted to lactate in the presence of lactate dehydrogenase (LDH) and NADH. Therefore, release of one molecule of AMP will lead to the consumption of two molecules of NADH (ε_{340} = 6220 $M^{-1}cm^{-1}$), which can be monitored by UV-vis spectrometry at 340 nm. In this assay, an excess of NaSH was used as the sulfur source. Since bisulfide can react with adenylated SCP directly,[135] this condition allows formation of adenylated SCP as the rate limiting step to allow the adenylation process correlates consumption of NADH. Typical

reactions in a total volume of 120 µL contained 50 mM Tris buffer at pH 7.5, 1 mM $MgCl_2$, 2 mM PEP, 3 mM NaSH, 3 mM DTT, 0.15 mM NADH, 60 µM ATP, 4 µM MoeZ or MoeZ mutant, 40 µM ThiS (based on the concentration determined by Bradford assay), and about 0.3 unit of AP, PK, and LDH.

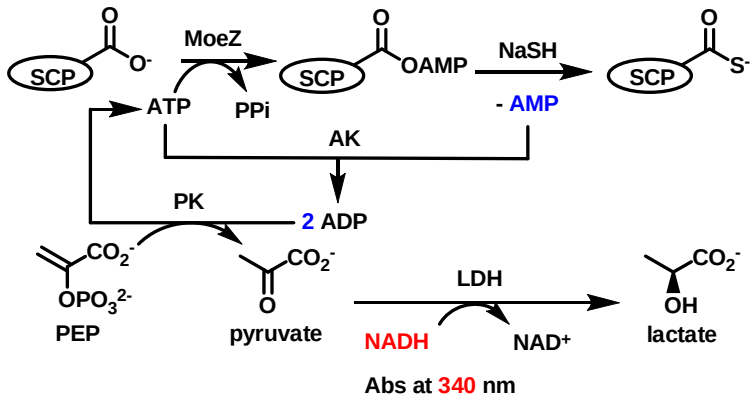

Figure 2-15: Colorimetric assay to detect formation of AMP during the MoeZ catalyzed sulfur transfer reaction in the presence of an excess of NaSH.

Thiosulfate:DTT oxidoreductase assay

The rhodanese activity of MoeZ and the MoeZ variants was measured by the method developed by Pecci *et al.*,[136] which measures the oxidation of DTT by UV-vis spectrometry at 285 nm as shown in Fig. 2-16 A. A typical reaction had a volume of 120 µL and contained 50 mM Tris buffer, pH 7.5, 50 mM freshly prepared DTT, approximately 0.5 to 2 µM of MoeZ or one of its mutants, and between 0 to 35 mM sodium thiosulfate. The reaction was initiated by the addition of MoeZ, and the background change in absorbance due to nonenzymatic oxidation of DTT was subtracted from each assay. Amount of the oxidized DTT can be determined using extinction coefficient of 275 $M^{-1}cm^{-1}$ at 285 nm.

Thiosulfate:KCN sulfurtransferase assay

Alternatively, the rhodanese activity of MoeZ could also be assessed using the assay developed by Sörbo *et al.*,[137] which measures the formation of thiocyanate from an alkyl persulfide and potassium cyanide colorimetrically as shown in Fig. 2-16 B. A typical reaction condition included 50 mM Tris buffer, pH 7.5, 50 mM KCN, approximately 0.6 to 2 μM of MoeZ or one of its mutants, and between 0 to 35 mM of sodium thiosulfate in a total volume of 100 μL. The reaction was initiated by the addition of enzyme and was quenched after 10 s by the addition of 50 μL of 15% formaldehyde in water. Then 150 μL of reagent (prepared by dissolving 1 g $Fe(NO_3)_3 \bullet 9H_2O$ and 2 mL 65% HNO_3 in 13 mL H_2O) was added for color development. As a control, a blank sample was prepared without the addition of enzyme and with the highest concentration of thiosulfate. All samples were read together in a 96-well plate using a plate reader. The extinction coefficient used to quantify the amount of $Fe(SCN)_3$ is 4200 $M^{-1}cm^{-1}$ at 460 nm.

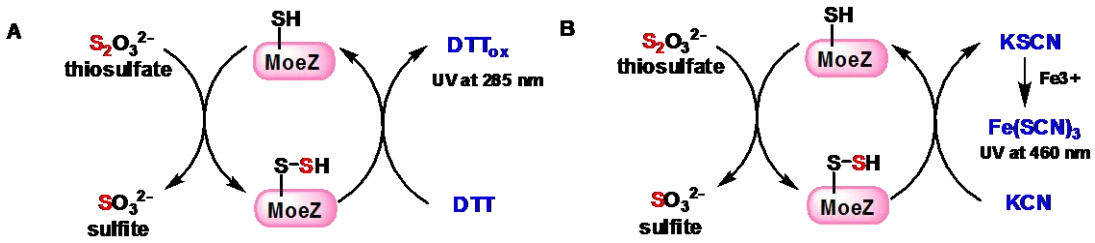

Figure 2-16: Two different assays to test the rhodanese activity of MoeZ and its mutants. (A) Detection of oxidized DTT. (B) Detection of thiocyanide formation.

2.2.6. Analysis of protein-protein conjugates by SDS-PAGE

In the proposed mechanisms, several covalent conjugates between MoeZ and the sulfur carrier protein are proposed. The molecular weight for MoeZ and the sulfur carrier

proteins are approximately 45 kDa and 10 kDa, respectively. Therefore, it should be possible to detect formation of protein-protein conjugates using SDS-PAGE. Since the acyl-disulfide bond is quite labile under reducing conditions, DTT was omitted when preparing the SDS-PAGE loading dye used for these assays. A typical assay was carried out in 10 μL 50 mM HEPES (pH 8.0) buffer. Details regarding the different reaction components of the conjugation reaction under consideration will be indicated with the results of SDS-PAGE for convenience. Following reaction, 10 μL SDS-PAGE loading dye (2X) is added as a quench and the resulting mixture was loaded directly onto the protein gel. Either a 12% or 15% SDS-PAGE gel was used for these analyses. A 12% gel gives good resolution at the 50 kDa region, where the protein conjugate was expected; however, such a gel results in loss of the sulfur carrier protein (especially ThiS) from the gel and a weak band. Therefore, the 15% gels were used to check for the presence or absence of the low molecular weight sulfur carrier protein.

2.2.7. Detection of sulfur carrier protein thiocarboxylate formation by ESI-MS catalyzed by MoeZ and its mutants

When a sulfur carrier protein is converted to its thiocarboxylate form, there is a 16 Da mass increase that can be detected by ESI-MS. To evaluate the importance of Cys_{213} and Cys_{360} for catalysis, a sulfur carrier protein (ThiS, or CysO, or MoaD2) was incubated with Cys213A-MoeZ or Cys360A-MoeZ mutant to see if formation of the protein thiocarboxylate product will be perturbed. As a control reaction, sulfur carrier protein was incubated with MoeZ under the same conditions. To avoid potential complication caused by bisulfide generated from reduction of protein persulfide, no reductants were used in the assay. Therefore, a stoichiometric excess of MoeZ was used to ensure complete conversion of the sulfur carrier protein to product would be possible. Reactions were carried out in the glove-box to minimize oxidation of cysteine residues.

Buffer and water used in the assay were made anaerobic by pre-equilibration with the anaerobic atmosphere in the glove-box for two days. A typical reaction included either 80 μM MoeZ, or 80 μM C213A-MoeZ mutant, or 80 μM C360A-MoeZ mutant in a buffer containing 4 mM ATP, 5 mM $MgCl_2$, 5 mM $Na_2S_2O_3$, 50 mM HEPES, pH 8.0, 12 mM Tris (from enzyme storage buffer), 500 mM glycerol (from enzyme storage buffer), and sulfur carrier protein (150 μM ThiS, or 100 μM MoaD2, or 100 μM CysO) in a total volume of 50 μL. The reaction was incubated in the glove-box at ~30 ºC for 30 min and then stopped by flash freezing in liquid nitrogen. Samples were then submitted to ESI-MS for analysis.

2.2.8. Free thiol content of MoeZ and its mutants determined by DTNB assay

5,5'-Dithiobis-(2-nitrobenzoic acid) (DTNB) titration[138] under folded and unfolded conditions in order to quantify the initial thiol oxidation in MoeZ and its mutants. The rationale of the assay is shown in Fig. 2-17. L-Cysteine was used to prepare a standard curve for free thiol quantitation. Assays performed under the folded condition contained ~10 μM MoeZ, 0.4 mM DTNB, 50 mM HEPES, pH 7.0 in a total volume of 120 μL. Assays performed under the unfolded condition contained ~10 μM MoeZ, 0.4 mM DTNB, 50 mM HEPES, pH 7.0, and 4 M urea or 5 M guanidinium chloride in a total volume of 120 μL. Reactions were incubated at room temperature for 5 min before taking the measurements at 412 nm.

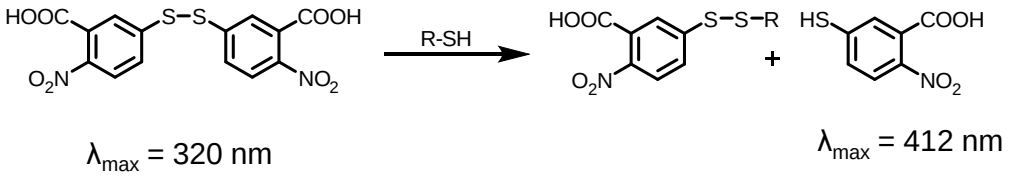

Figure 2-17: Reaction scheme of DTNB assay.

2.2.9. Methylene blue assay to detect disulfide formation *in situ*

A methylene blue assay[139-140] was used to determine if any bisulfide is released from MoeZ in the presence of thiosulfate. The principle behind the assay is that under acidic conditions bisulfide reacts with *N*,*N*-dimethyl-*p*-phenylenediamine (DMPD) in the presence of iron to form methylene blue as shown in Fig. 2-18. A typical assay solution contained 40 μM MoeZ or one of its mutants, 50 mM HEPES, pH 7.8, and 0.8 mM $Na_2S_2O_3$ in a total volume of 200 μL. Positive controls were prepared in parallel with the addition of 0.8 mM DTT to make sure the protein persulfide is generated under these conditions. To detect bisulfide in the assay, a 200 μL sample containing Na_2S (control) or assay solution was mixed with 600 μL of freshly prepared 1% $Zn(OAc)_2$ solution (w/v in water) in a microcentrifuge tube followed by the addition of 30 μL of 3 M NaOH. The resulting solution was incubated at room temperature for 1 h. A solution of 150 μL of freshly prepared DNPD reagent (0.1% in 5 M HCl) was then added, followed by 30 μL $FeCl_3$ (23 mM in 1.2 M HCl). The resulting reaction was vortexed and then incubated for 1 h at room temperature to develop color. The sulfur content was quantified by the absorbance at 670 nm with an extinction coefficient of 34,500 $M^{-1}cm^{-1}$.

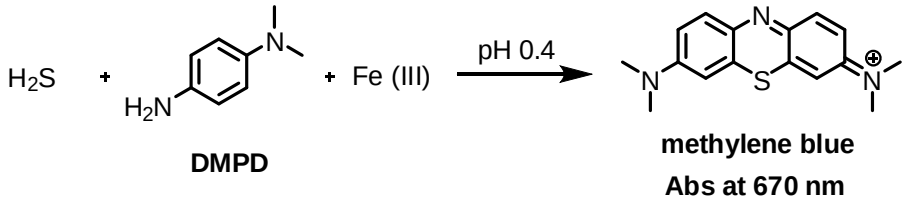

Figure 2-18: Reaction scheme of the methylene blue assay for the quantitation of hydrogen sulfide.

2.2.10. Enzymatic generation of 2-selenosugar and its detection

BexX reaction using sodium selenide

Based on the protocol to enzymatically synthesize 2-thioglucose (Fig. 2-11),[84] similar reactions were carried out to test whether a selenosugar can be produced by BexX. Reactions in a volume of 30 μL contained 100 μM *C*-His_6-BexX, 40 μM *N*-His_6-CysO or 40 μM *N*-His_6-MoaD2, 15 μM *N*-His_6-MoeZ, 3 mM ATP, 3 mM glucose-6-phosphate (G6P), 3 mM Na_2Se or NaSH (positive control to ensure all the enzyme were active), and 5 mM $MgCl_2$ in 50 mM NH_4HCO_3 buffer at pH 8.0. The reactions were performed both aerobically and in the glove-box with 7 h of incubation. Samples were stored at −20 ºC before analysis.

BexX reaction using L-selenocystine and cysteine desulfurases

Attempts to obtain selenosugars were also carried out using the protocol for 2-thiosugar production with CD3 from *A. orientalis* (Fig. 2-14).[84] Typically, a reaction in a volume of 30 μL contained 100 μM *C*-His_6-BexX, 40 μM *N*-His_6-CysO or *N*-His_6-MoaD2, 15 μM *N*-His_6-MoeZ, 3 mM ATP, 3 mM glucose-6-phosphate (G6P), 3 mM L-selenocystine or L-cystine (positive control to ensure the enzymes were active), 0.1 mM PLP, 40 μM *N*-His_6-CD3, 5 mM $MgCl_2$ in 50 mM NH_4HCO_3 buffer at pH 8.0. The reactions were performed both aerobically and in the glove-box with 7 h of incubation. The samples were then stored at −20 ºC before analysis.

Detection of selenosugars by mBBr derivatization and HPLC analysis

To detect formation of 2-selenosugars, reactions were treated with bromobimane (mBBr) according to a similar procedure previously described for the detection of 2-thioglucose as shown in Fig. 2-19.[84,141] A reaction mixture stored at −20 ºC was thawed, approximately 1 unit of calf intestinal alkaline phosphase (CIP) was added in order to

cleave the phosphate group to facilitate the HPLC analysis (in this way we can use synthetic 2-thioglucose as standard). The resulting solution was then incubated at 37 ºC for 1 h. Then about same volume of methanol was added to the sample and the precipitates were removed by centrifugation. To the supernatant was treated with 1 mM Tris(2-carboxyethyl)phosphine (TCEP) to prevent potential dimerization and then derivatized with 5 mM mBBr (powder was dissolved in MeOH to prepare stock solution). The resulting mixture was incubated for 30 min in the dark and then dried by speed vacuum. The sample was then resuspended with deionized water and centrifuged again prior to HPLC analysis. An analytical C18 column was used and the product was eluted with a gradient of water (solvent A) and acetonitrile (solvent B). The gradient was run from 15% to 30% B over 15 min, 30% to 80% B over 5 min, 80% to 15% B over 5 min, and then isocratic at 15% B for 10 min. The flow rate was 1 mL/min and the UV detector was set at 260 nm. Synthetic 2-thio-D-glucose[128] was used to prepare 2-thio-D-glucose-bimane as a standard for HPLC analysis.

2.2.11. ESI-MS analysis for protein selenocarboxylate formation

To investigate formation of protein selenocarboxylates, ESI-MS analysis was carried out for reactions between MoeZ and sulfur carrier proteins using L-selenocystine as the selenium donor. Detailed reaction conditions will be presented with MS results.

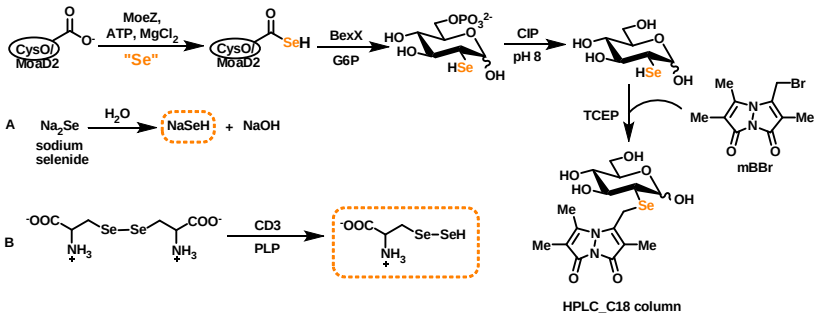

Figure 2-19: Reaction scheme for detection 2-selenoglucose.

Two potential selenium donors are boxed: (A) biselenide (B) selenocysteine perselenide.

2.2.12. Spectrophotometric analysis of CD3 and L-selenocystine

To ensure whether L-selenocystine can be taken as a substrate for CD3, detection of potential pyruvate formation was carried out by an enzyme couple assay shown in Fig. 2-20.[84] A 50 µL reaction contained 0.2 mM L-selenocystine or 0.5 mM L-cystine, 1 mM PLP, 20 µM CD3 (cysteine desulfurase homolog that functions as cystine lyase),[84] 1 mM $MgCl_2$, 2 mM DTT if any, in 50 mM Tris buffer at pH 7.5. The reaction was incubated at room temperature for 1 hr and then the color and the smell of the reaction were recorded. Reactions were quenched by boiling the samples for 30 s and the resulting precipitates were removed. To the 10 µL of supernatant was added 90 µL reaction solution containing 50 mM Tris buffer, pH 7.5, 2 mM $MgCl_2$, 120 µM NADH, 0.2 units lactate dehydrogenase (LDH). The resulting solution was incubated for 5 min before taking the UV-vis scan.

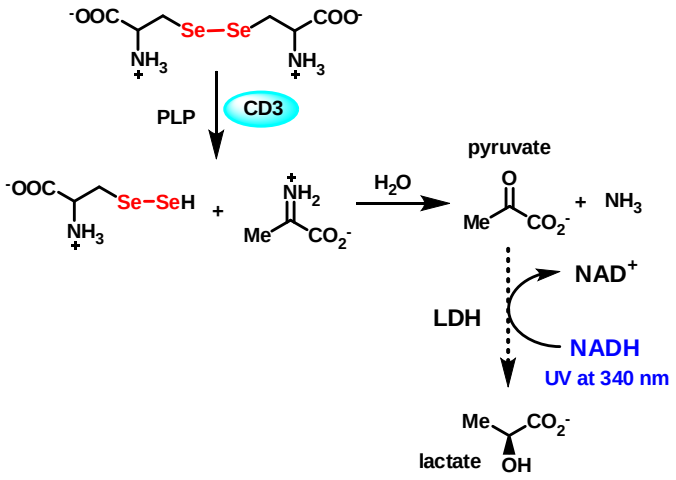

Figure 2-20: Reaction scheme proposed for CD3 and selenocystine.

2.3. RESULTS AND DISCUSSION

2.3.1. MoeZ variants expression and purification

N-His$_6$-MoeZ, *N*-His$_6$-C213A-MoeZ, *N*-His$_6$-C223A-MoeZ, and *N*-His$_6$-C2360A-MoeZ were purified to approximately 90% homogeneity based on SDS-PAGE analysis. The yield was approximately 30 mg per liter of cell culture for each protein. The 12% SDS-PAGE gels of the purified proteins under both reducing and non-reducing conditions are shown in Fig. 2-21. MoeZ appeared as two different forms on the gel under non-reducing conditions. This may be due to an internal disulfide bond formed within each MoeZ protein.

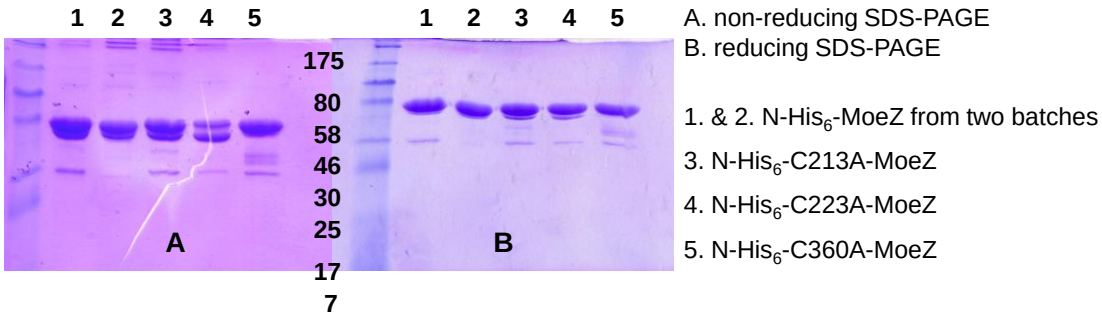

Figure 2-21: SDS-PAGE of MoeZ variants under both reducing and non-reducing conditions.

2.3.2. Assay for the adenylation activity of MoeZ and its mutants

The adenylation activity of MoeZ and its mutants was inferred using a colorimetric assay to monitor the production of AMP (indicated by the decrease of NADH at 340 nm) when MoeZ and its mutants were co-incubated with a sulfur carrier protein in the presence of sodium sulfide (see Fig. 2-15). Under identical conditions, the rate of AMP production appeared to be the same in the cases of MoeZ, C213A-MoeZ,

and C360A-MoeZas shown in Fig. 2-22, suggested that mutation at Cys213 and Cys360 had little effect on the adenylation activity of MoeZ.

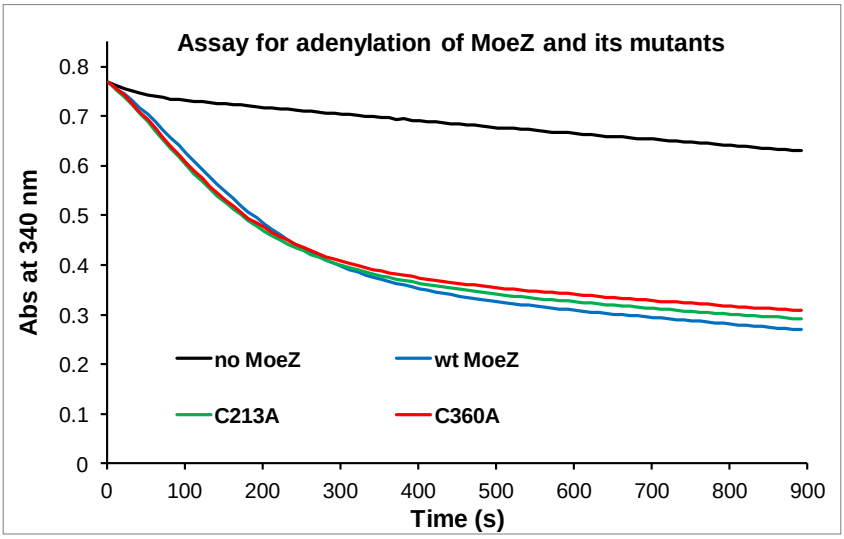

Figure 2-22: Relative adenylation activity measured by enzyme coupled assay. The decrease of absorption at 340 nm indicated release of AMP from the adenylation reaction catalyzed by MoeZ (compare to no MoeZ control).

2.3.3. Kinetic study of MoeZ rhodanese activity

The kinetic parameters for the rhodanese activity of MoeZ and its mutants were determined by using two different assays to measure the initial rate of MoeZ persulfide formation at different concentrations of sodium thiosulfate. Each assay was run in triplicate, and the data was fit using the following equation:

Equation 2.1 $$v_i = k_{cat} s_i e_0 / (K_M + s_i)$$

where e_0 is the concentration of MoeZ or its mutant, and K_M is the apparent Michaelis constant of thiosulfate in the reaction when keeping the sulfur acceptor KCN or DTT at

saturated concentration. The resulting plots are presented in Fig. 2-23, and the corresponding parameters obtained from the fits are listed in Table 2-2.

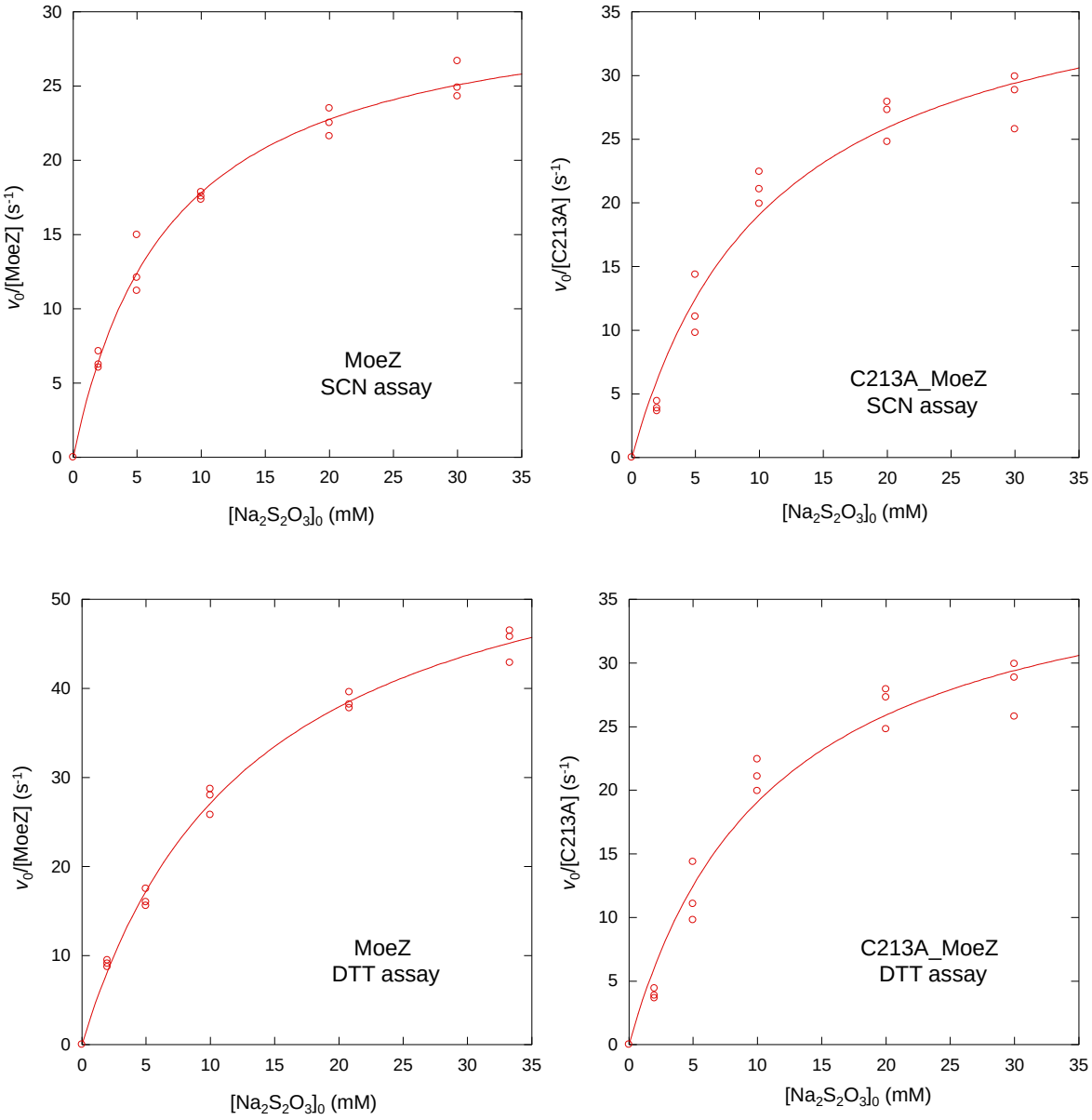

Figure 2-23: Plots of initial rate versus sodium thiosulfate concentration for the rhodanese activity of MoeZ and C213A-MoeZ. Initial rates have been normalized for enzyme concentration in the individual assays. The solid line represents the fits to equation 2.1.

Enzymes	KCN assay			DTT assay		
	k_{cat} (s^{-1})	K_M (mM)	k_{cat}/K_M ($mM^{-1}s^{-1}$)	k_{cat} (s^{-1})	K_M (mM)	k_{cat}/K_M ($mM^{-1}s^{-1}$)
MoeZ	32 ± 1	7.6 ± 0.7	4.2	63 ± 2	13 ± 1	4.8
C213A-MoeZ	40 ± 3	11 ± 2	3.6	59 ± 3	9 ± 1	6.5
C360A-MoeZ	Not detected			Not detected		

Table 2-2: Kinetic parameters for the rhodanese activity of MoeZ and its conserved cysteine mutants.

Under both assay conditions, no activity was observed when *N*-His_6-C360A-MoeZ was used. This suggests that Cys360 of MoeZ is the site of a protein persulfide formation as predicted based on sequence alignment (the conserved cysteine to form persulfide functionality in the active site six amino acid loop of RHOD). The kinetic parameters obtained via the two different assay systems were not very different. Furthermore, the catalytic efficiency (k_{cat}/K_M) of MoeZ with respect to rhodanese activity determined here is in the same range of those reported values for the MoeZ close homologues: QbsC from *P. fluorescens*[124] and MoeZ from *M. tuberculosis*[118] (2.5 $mM^{-1}s^{-1}$ and 1.35 $mM^{-1}s^{-1}$, respectively, as determined by the KCN assay).

2.3.4. Detection of protein conjugates using SDS-PAGE gel

Rationale

The mass range of MoeZ (~ 45 kDa) compared to sulfur carrier proteins (~ 10 kDa) makes detection of their covalent adducts possible using SDS-PAGE. Indeed, a similar strategy has been used to analyze other sulfur carrier protein activating enzymes.[110,120-121] One recently reported example is TtuC from *Thermus thermophilus* (Fig. 2-12). The authors were able to identify a protein thioester intermediate between TtuC and a sulfur carrier protein using non-reducing SDS-PAGE gel.[120] Therefore, we

decided to investigate whether a MoeZ-SCP intermediate forms as proposed in Fig. 2-13 using a similar protein gel methodology.

The potential protein conjugates can be categorized into two types: a MoeZ-SCP thioester intermediate and a MoeZ-SCP acyl disulfide intermediate. Although the mass difference of these two species is too small to distinguish by SDS-PAGE, they should still be distinguishable by their chemical properties. Specifically, the acyl disulfide bond is labile in the presence of tris-(2-carboxyethyl)-phosphine (TCEP) while the thioester bond is not.[142] TCEP is a commonly used reagent for reducing disulfide bonds using phosphine chemistry as shown in Fig. 2-24. Compared to other commonly used thiol based reducing agents for reduction of disulfide bonds such as dithiothreitol (DTT) and 2-mercaptoethanol (β-ME), TCEP is a much weaker nucleophile. Therefore, it will not react with thioesters.[143] When TCEP is not added to the reaction mixture, non-reducing SDS-PAGE should result in both types of conjugates appearing as a new band in the gel if they are present at detectable levels. The new band is likely to be a thioester intermediate if it remains unchanged upon addition of TCEP but disappears in the presence of DTT. In contrast, the new band is likely to be an acyl disulfide intermediate if it disappears when TCEP is added. If no adduct can be detected, then it is likely the reaction follows pathway D (Fig. 2-13), which can be followed up by testing for the release of bisulfide using the methylene blue assay. Of course, it is also possible the concentration of the intermediate is too low to be detected or the intermediate exists transiently.

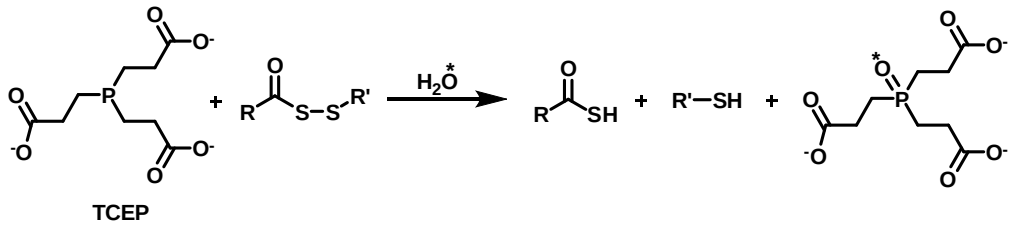

Figure 2-24: TCEP reduces acyl disulfides using phosphine chemistry.

Reaction of MoeZ with ThiS

As shown in Fig. 2-25, SDS-PAGE of reactions of MoeZ and its mutants with ThiS (MW ~ 8.7 kDa) showed formation of a new band at ~50 kDa, which is consistent with the predicted mass of a covalent complex between MoeZ-ThiS and C360A-MoeZ-ThiS. In the case of C213A-MoeZ, a very faint band also appeared around the 50 kDa reign, but with a much lower intensity. Formation of this new band was ATP-dependent and thiosulfate independent. The band slightly below 17 kDa is likely to be a ThiS dimer linked by DTT at the *C*-terminus, because it has been reported that adenylated sulfur carrier protein can form an adduct with reducing reagents such as DTT or β-mercaptoethanol.[120, 144] In support of this hypothesis is the observation that the band did not form in the absence of ATP or DTT (not shown in this gel). When 0.1 mM of thiosulfate was also present, the putative ThiS-DTT-ThiS conjugate disappeared in the MoeZ sample (lane 4), became weaker in the C213A-MoeZ sample (lane 8), and stayed about the same in the C360A-MoeZ sample (lane 12).

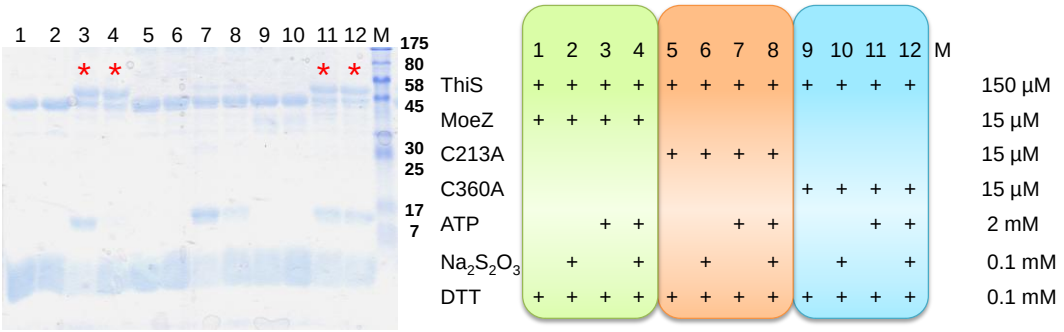

Figure 2-25: 15% Non-reducing SDS-PAGE of reactions between ThiS and MoeZ. The reaction conditions of each sample are listed. The reactions were incubated at room temperature for 2.5 h. The lanes labeled with an asterisk were the reactions gave strong signal of the new band.

To further characterize the new band at ~50 kDa, TCEP and DTT were added after the reaction. As shown in Fig. 2-26, the higher molecular weight band disappeared when the sample was treated with 10 mM DTT (lane 4) but remained unchanged when 5 mM TCEP (lane 3) was added to the sample. These results were consistent with a thioester intermediate between MoeZ and ThiS.

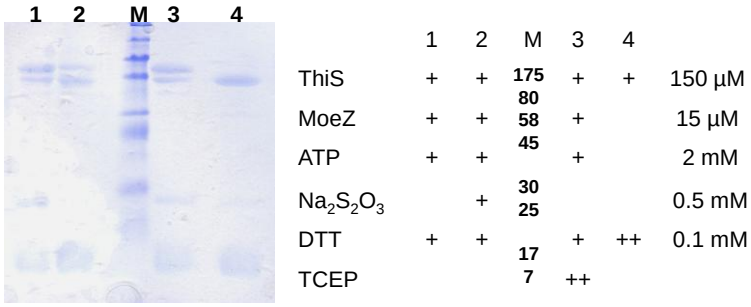

Figure 2-26: 15% Non-reducing SDS-PAGE of reactions between ThiS and MoeZ followed by treatment with TCEP and DTT. The reaction conditions of each sample are listed. The reactions were incubated at room temperature for 2 h. Lanes denoted with "++" were treated with the given reagent to cleave the protein conjugate linkage, namely, 10 mM TCEP or 5 mM DTT for 10 min at room temperature.

As expected, the results from the C223A-MoeZ mutant are similar to those obtained with the C360A-MoeZ as shown in Fig. 2-27, except that the conjugate at approximately 50 kDa became slightly weaker when 0.5 mM thiosulfate was also present. When shorter incubation time was used in the assay, no detectable protein conjugate formed in C213A-MoeZ mediated reaction (lane 3 and 4 in Fig. 2-27 compared to land 7 and 8 in Fig. 2-25). Taken together, the results from the non-reducing SDS-PAGE gel study of ThiS/ MoeZ system are most consistent with pathway A in Fig. 2-13.

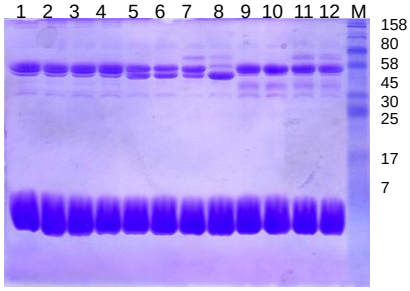

	1	2	3	4	5	6	7	8	9	10	11	12	M	
ThiS	+	+	+	+	+	+	+	+	+	+	+	+		150 µM
C213A	+	+	+	+										15 µM
C223A					+	+	+	+						15 µM
C360A									+	+	+	+		15 µM
ATP			+	+			+	+			+	+		2 mM
$Na_2S_2O_3$		+		+		+		+		+		+		0.5 mM
DTT	+	+	+	+	+	+	+	+	+	+	+	+		50 µM

Figure 2-27: 15% Non-reducing SDS-PAGE of reactions between ThiS and different MoeZ mutants. The reaction conditions of each sample are listed. The reactions were incubated at room temperature for 25 min. Only lanes 7–8, and lanes 11–12 had detectable new bands at ~50 kDa. Interestingly, in lane 7 and 8, distribution of the two bands changes upon addition of thiosulfate.

Reaction of MoeZ with MoaD2 and CysO

Since MoeZ can activate multiple sulfur carrier proteins (SCPs) from different biosynthesis pathways,[84] we also applied the same strategy used for ThiS to CysO and MoaD2. The molecular weight of CysO and MoaD2 are around 11.6 kDa and 12.5 kDa, respectively. Therefore, if a similar thioester intermediate is formed, a new band at ~57 kDa will be observed. However, no clear band corresponding to this mass was detected by non-reducing SDS-PAGE gel experiments when MoaD2 or CysO was incubated with MoeZ under identical conditions used for ThiS (data not shown here).

For better sensitivity, Western blot using anti *N*-His tag antibody was carried out for MoeZ and C213A-MoeZ with different SCPs in the presence and absence of ATP. The reactions were performed in the glove box to minimize the oxidation of the cysteine residues on MoeZ and C213A-MoeZ. A short incubation time 30 min was used to prevent formation of non-specific protein conjugates. Western blot results are presented in Fig. 2-28. In the case of ThiS, one band at ~50 kDa (lane 2, arrow pointed) appeared only in the MoaZ reaction when ATP was present, consistent with previous observations using coomassie staining. In the case of CysO and MoaD2, two new bands at ~90 kDa and ~50 kDa were observed for each condition (see Fig. 2-28, lane 4 for CysO and lane 6 for MoaD2, where the arrows pointed). However, new bands at similar molecular weights were also observed in the reaction of MoaD2 and C213A-MoeZ (lane 12, arrow pointed). This suggests that the adducts originate from non-specific bonding between surface cysteine residues and adenylated MoaD2.

The results of non-reducing SDS-PAGE gel assays for CysO and MoaD2 suggest formation of a small amount of thioester intermediate at Cys_{213} of MoeZ. However, the existence of other protein conjugates raises doubts as to whether the thioester intermediate is catalytically important or not. Therefore, the results imply pathway A (see Fig. 2-13) in the case of ThiS and MoeZ, but the mechanism of sulfur incorporation for the other two substrates CysO and MoaD2 remains uncertain.

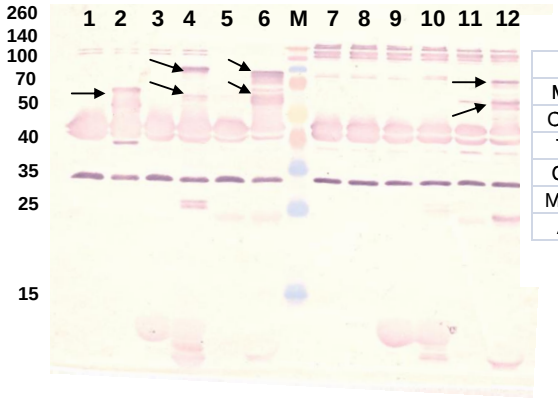

	1	2	3	4	5	6	M	7	8	9	10	11	12	
MoeZ	+	+	+	+	+	+								5 μM
C213A								+	+	+	+	+	+	5 μM
ThiS	+	+						+	+					50 μM
CysO			+	+						+	+			50 μM
MoaD2					+	+						+	+	50 μM
ATP		+		+		+			+		+		+	5 mM

Figure 2-28: 15% non-reducing SDS-PAGE of reactions between sulfur carrier proteins and MoeZ or C213A-MoeZ. Signal was detected by Western blotting using a murine monoclonal anti-polyHistidine antibody.

2.3.5. Cys213 and Cys360 are catalytically important residues for MoeZ

To further evaluate whether Cys_{213} of MoeZ is catalytically important for sulfur transfer from thiosulfate to sulfur carrier proteins, activity assays were carried out using wild type MoeZ (as a positive control), C213A-MoeZ mutant, or C360A-MoeZ mutant under single turnover conditions.

The reactions were carried out anaerobically to minimize the oxidization of cysteine residues by air. Formation of a protein thiocarboxylate was analyzed by ESI-MS and the results were shown in Fig. 2-29 and the expected masses of different SCP forms were listed in Table 2-3. In case of wild type MoeZ, thiocarboxylate forms of each SCP were the major species detected from each set of reaction (Fig. 2-29 A, C, E). However, no protein thiocarboxylates were detected in the sample using the C213A mutant of MoeZ under similar conditions (Fig. 2-29 B, D, F). Instead, glycerol adducts of the SCPs were the major species generated in the reactions. Glycerol that comes from enzymes added in the reactions, can function as nucleophile to liberate AMP from the activated

sulfur carrier proteins as shown in Fig. 2-30. The observation of SCP glycerol ester was consistent with the previous finding that the C213A mutation of MoeZ had almost no effect on its adenylation activity. The calculated mass is based on native protein with the *N*-terminal methionine residue removed, which is often the case in proteins recombinantly expressed in *E. coli*.[145] As shown in Fig. 2-30, another common observation is the mono-gluconoylation at the *N*-terminal amine of the *N*-His_6 tag fusion proteins expressed in *E. coli*.[146]

The C213A mutant of MoeZ has been demonstrated to have adenylation and rhodanese activity. Thus, the observation of this experiment that the C213A mutant does not facilitate formation of protein thiocarboxylate using thiosulfate in the absent of external reducing agent strongly indicates that Cys213 of MoeZ involved in the sulfur transfer process of MoeZ, consistent with the mechanism proposed in Fig. 2-13.

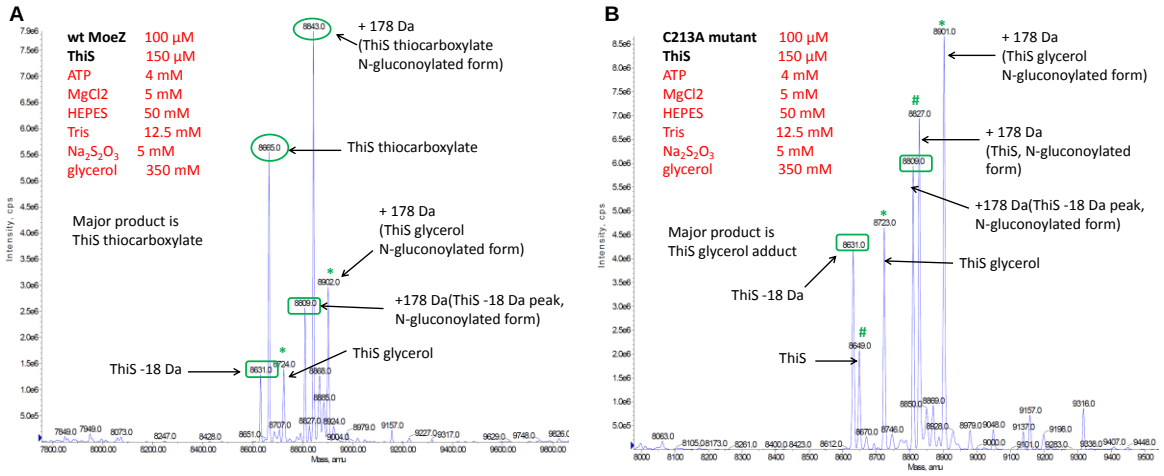

Figure 2-29: Deconvoluted ESI-MS spectra of sulfur carrier proteins activation by MoeZ and the C213A-MoeZ mutant using thiosulfate as the sulfur donor (A to B).

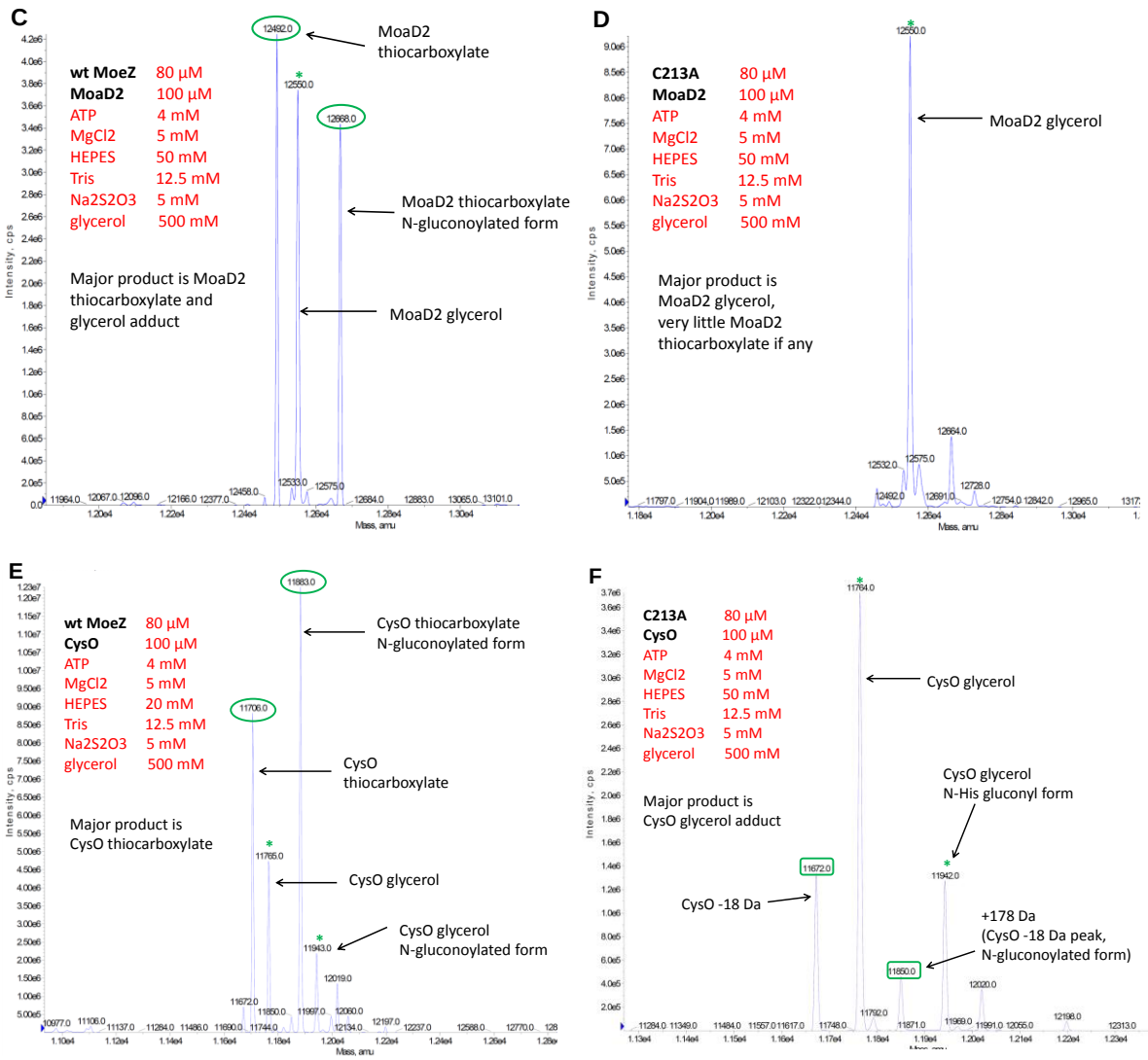

Figure 2-29: Deconvoluted ESI-MS spectra of sulfur carrier proteins activation by MoeZ and the C213A-MoeZ mutant using thiosulfate as the sulfur donor (C to F). Reaction conditions and major peaks identified (within ± 2 Da of the expected masses) are labeled.

SCP	Calculated Mass				Observed Mass		
	−COOH	−COSH	$-COC_3H_7O_3$		−COOH	−COSH	$-COC_3H_7O_3$
ThiS	8648	8664	8722	A	ND	8665	8724
				B	8649	ND	8723
MoaD2	12474	12490	12548	C	ND	12492	12550
				D	ND	ND	12550
CysO	11688	11704	11762	E	ND	11706	11765
				F	ND	ND	11764

Table 2-3: Calculated and observed masses of different forms of SCPs. A to F refers to the label from Fig. 2-29. ND refers to not determined. –COOH refers to unmodified sulfur carrier protein; −COSH refers to the thiocarboxylate derivative of the sulfur carrier protein; $-COC_3H_7O_3$ refers to sulfur carrier protein glycerol.

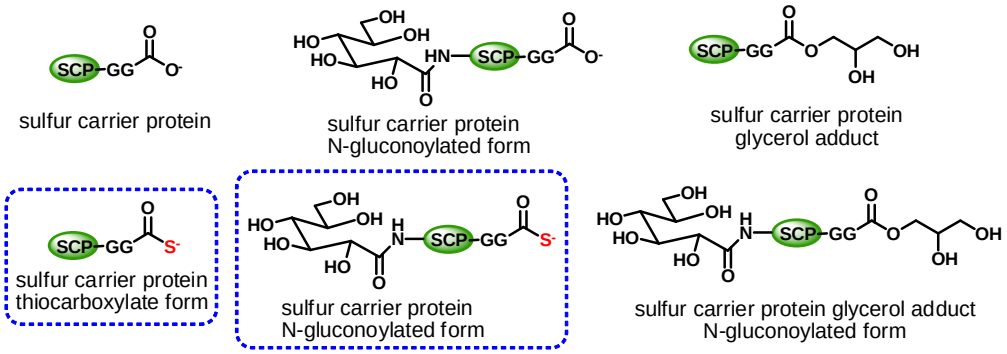

Figure 2-30: Proposed structures of the various sulfur carrier protein (SCP) forms existed in the ESI-MS spectra. The boxed structures are the possible products from SCPs activation by MoeZ, ATP, and thiosulfate.

The role of Cys_{360} of MoeZ as the site of protein persulfide formation from thiosulfate has been confirmed in the rhodanese assay where the Cys360A-MoeZ does not catalyze transfer of the sulfur atom from thiosulfate to MoeZ. To further confirm this result, Cys360A-MoeZ was incubated with CysO or MoaD2 under similar single turnover

assay conditions described for the wild type MoeZ. The reactions were analyzed by ESI-MS (shown in Fig. 2-31, a and b). As expected, no SCP thiocarboxylate was detected, and the major form of SCP is the glycerol ester from. Again, this result is in agreement with the previous finding that Cys360 of MoeZ does not affect adenylation activity but is essential for sulfur transfer from thiosulfate.

Overall, the single turnover assay of MoeZ catalyzed SCP activation strongly supported the role of the conversed cysteines Cys_{213} and Cys_{360} in mediating sulfur transfer from thiosulfate to SCP thiocarboxylate. This result alone supports but does not distinguish the proposed four mechanisms in Fig. 2-13. However, considering the protein gel results for ThiS and MoeZ, at least for this system, pathway A is most likely to be valid.

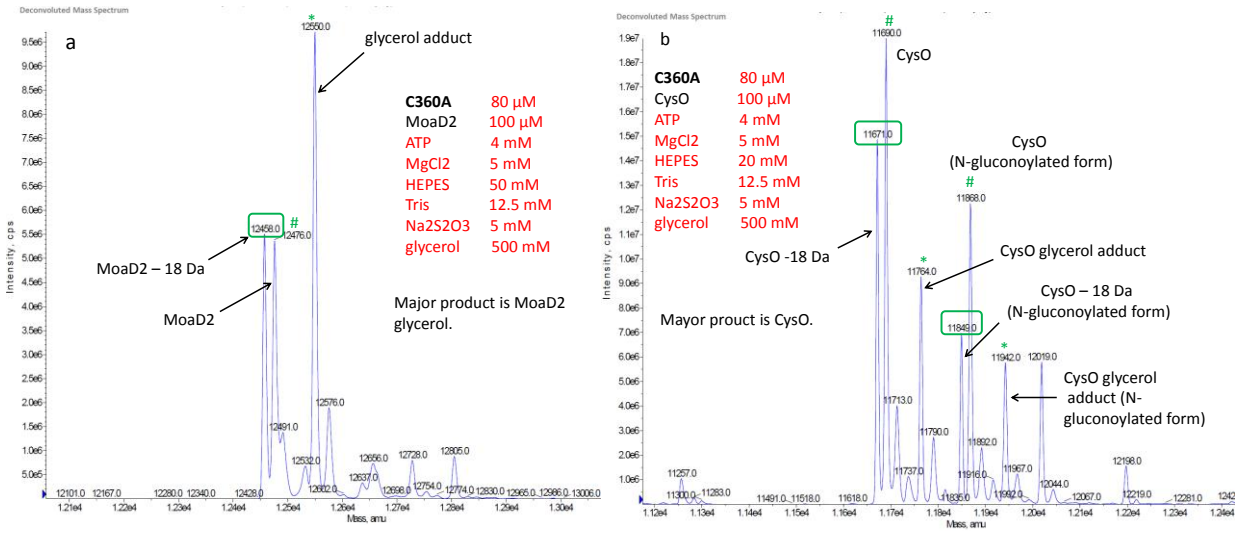

Figure 2-31: Deconvoluted ESI-MS spectra of sulfur carrier proteins activation by MoeZ and the C360A-MoeZ mutant using thiosulfate as the sulfur donor. Reaction conditions and major peaks identified (within ± 2 Da of the expected masses) are labeled.

2.3.6. Cysteine titration of MoeZ and its mutants

Based on the proposed mechanism, after each reaction turnover, MoeZ will be in an oxidized form characterized by an intramolecular disulfide bond. To evaluate this hypothesis, assays were carried out to quantify the number of free cysteine residues in MoeZ and it mutants using DTNB. However, the preliminary results from these experiments are ambiguous, because under both folded and unfolded (denatured) conditions, the number of free cysteine residues in both MoeZ and its mutants appears to be same and roughly equal to two (see Table 2-4). Given that four free cysteines are expected in wild type MoeZ and three in each of the mutants, these results are difficult to explain. Therefore, quantification of MoeZ and its mutants after the sulfur activation reaction was not performed.

	Folded condition	Unfolded condition	# of cysteine expected
MoeZ	1.77 ± 0.07	2.3 ± 0.2	4
C213A	1.8 ± 0.3	2.0 ± 0.3	3
C223A	1.5 ± 0.2	1.6 ± 0.4	3
C360A	2.2 ± 0.2	2.3 ± 0.3	3

Table 2-4: Number of free cysteine residues per monomer determined by DTNB assay for MoeZ and MoeZ mutants under both folded and unfolded conditions. The values listed in the table were the average of three measurements from different days. For each measurement, a standard curve prepared under corresponding conditions was used to infer the free thiol concentration. Protein concentrations were determined by Bradford assay.

2.3.7. *In situ* generation of bisulfide was not detected

To further evaluate pathway D in Fig. 2-13, an assay was designed to test for the formation of bisulfide when MoeZ is incubated with thiosulfate. If pathway D is valid, bisulfide would be released in the absence of a sulfur carrier protein after formation of

the protein persulfide bond. In this case, methylene blue formation will be detected when MoeZ is incubated with thiosulfate. As shown in Table 2-5, no detectable methylene blue was formed in the sample with thiosulfate and MoeZ or its mutants, which could be up to 40 μM. To ensure under similar condition, protein persulfide did form on MoeZ, DTT was added to another set of reactions as a control. Similar amount (more than one turnover) of methylene blue was formed in wild type MoeZ, C213A-MoeZ and C223A-MoeZ, but not in the C360A-MoeZ (less than 1 μM was formed). This result suggested that the protein persulfide formed on MoeZ was relatively resistant to the formation of an internal disulfide bond, which does not favor pathway D.

	$Na_2S_2O_3$ + DTT	$Na_2S_2O_3$
MoeZ	340 μM	0
C213A	356 μM	0
C223A	339 μM	0
C360A	0.3 μM	0

Table 2-5: Detection of methylene blue formation as a measure of bisulfide production in the reactions containing MoeZ or its mutants and sodium thisulfate. Control reactions containing DTT were also prepared in parallel. Samples were incubated at room temperature for 30 min before assay.

2.3.8. Enzymatic generation of a 2-selenosugar was not successful

As mentioned earlier, we are interested in knowing whether the biosynthetic machinery of 2-thiosugar can be reengineered to generate 2-selenosugar. The proposed strategy is shown in Fig. 2-19. In general, 2-thiosugar biosynthesis requires BexX, G6P, and CysO or MoaD2 thiocarboxylate. To obtain CysO or MoaD2 thiocarboxylates, a sulfur atom is incorporated from bisulfide, thiosulfate, cysteine, or cystine into the

activated adenylated SCP in a reaction catalyzed by MoeZ along with a suitable cysteine desulfurase.[84] Commercially available selenium sources include sodium selenide and L-selenocystine, which are analogous to bisulfide and cystine. Therefore, BexX catalyzed assays were performed with either sulfur sources (as a positive control) or seleno sources.

As shown in Fig. 2-32, in positive controls using NaSH or cystine and CD3 as sulfur sources (traces a & e), a 2-thiosugar-mBBr derivative was detected,[84] suggesting all the enzymes were active. However, in the parallel assays, where Na_2Se and seleocystine and CD3 were used to substitute the sulfur sources, no peak was observed in the retention time region for 2-thiosugar-mBBr (trace b & f). The results were similar when another potential sulfur carrier protein MoaD2 was used instead of CysO (traces c & g). Furthermore, the HPLC traces were identical to the ones where ThiS was used (traces d & h), and ThiS is a substrate for MoeZ to form thiocarboxylate, but not a substrate for BexX to generate 2-thiosugar.

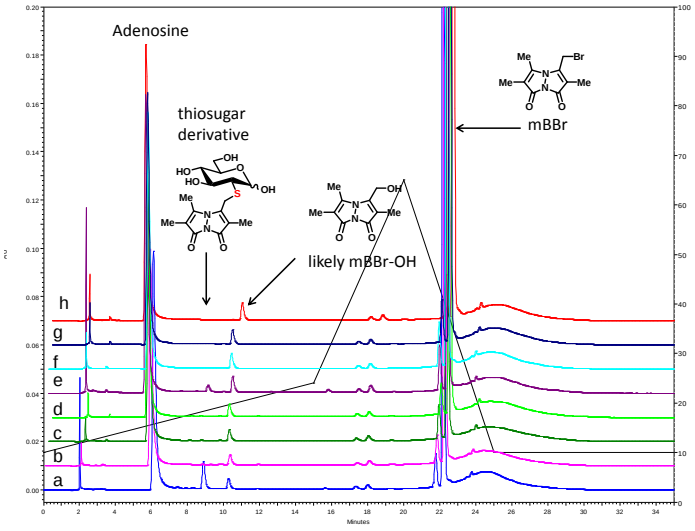

	a	b	c	d	e	f	g	h
NH_4HCO_3	+	+	+	+	+	+	+	+
$MgCl_2$	+	+	+	+	+	+	+	+
G6P	+	+	+	+	+	+	+	+
ATP	+	+	+	+	+	+	+	+
MoeZ	+	+	+	+	+	+	+	+
NaSH	+							
NaSe		+	+	+				
CysO	+	+			+	+		
MoaD2			+				+	
ThiS				+				+
BexX	+	+	+	+	+	+	+	+
PLP					+	+	+	+
CD3					+	+	+	+
cystine					+			
selenocystine						+	+	+

Figure 2-32: HPLC traces of the enzyme coupled reactions to generate 2-thioglucose and 2-selenoglucose.

The reactions were treated with alkaline phosphatase (CIP) to convert G6P to glucose and AMP to adenosine to facilitate the detection. 2-Thiosugar or 2-selenosugar generated in the reaction can then be derivatized by mBBr to facilitate detection by UV.

At this point, it is not clear why a seleno-sugar was not obtained. There are several possible reasons: (1) BexX cannot use CysO/MoaD2 selenocarboxylate as substrate; (2) CysO/MoaD2 selenocarboxylate is very unstable under studied condition; (3) Seleno sources used here cannot be converted to hydrogen selenide effectively to generate selenocarboxylate.

2.3.9. Preliminary results showed selenocarboxylate was unable to be generated using sodium selenide

Since formation of a selenosugar was not successful, attention was turned to determining whether a protein selenocarboxylate can be generated by replacing sodium sulfide with sodium selenide in the MoeZ activation reaction. As shown in Fig. 2-33 A, generation of one molecule of SCP carboxylate is associated with release of one molecule of AMP. Therefore, we applied the enzyme coupled assay we used earlier to examine whether addition of sodium selenide would facilitate the release of AMP.

When ThiS or CysO was incubated with MoeZ in the presence of ATP, addition of Na_2S greatly enhances the rate of AMP release (Fig. 2-33 B and C, black solid line) compared to when Na_2S is absent (Fig. 2-33, B and C, red solid line). However, this change did not occur when Na_2Se was added (Fig. 2-33, B and C, black dotted line). Therefore, this preliminary result suggests that generation of SCP selenocarboxylate from sodium selenide is most likely unsuccessful.

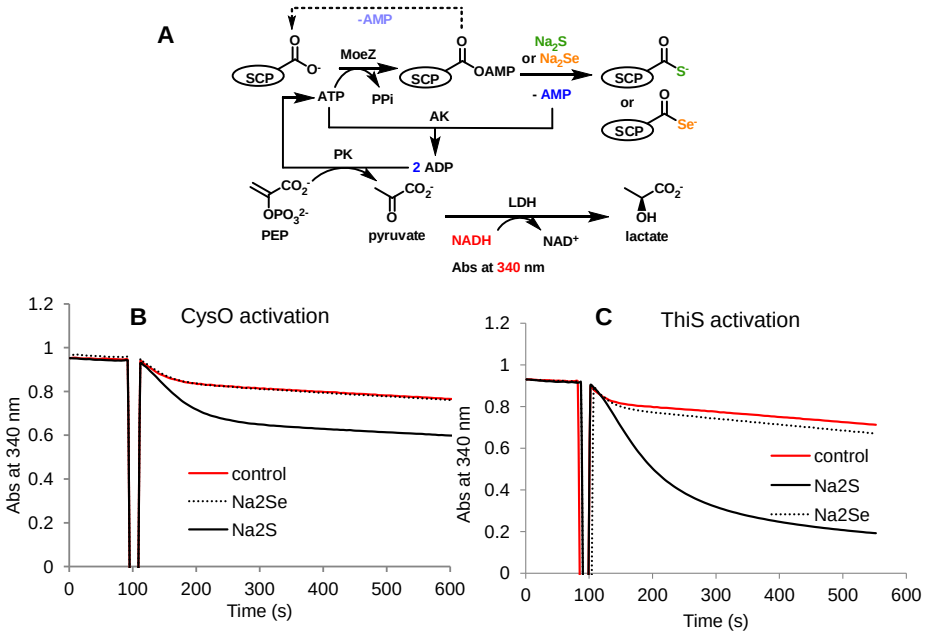

Figure 2-33: Coupled enzyme assay to indirectly detect formation of SCP selenocarboxylate. Reactions contained 50 mM HEPES, pH 8.0, 4 mM $MgCl_2$, 50 μM ThiS or 13 μM CysO, 3 μM MoeZ, 0.8 mM ATP, 1.2 mM PEP, 125 μM NADH, 2 mM Na_2S or Na_2Se if any. In the control reaction, no sulfur or selenium donor was added. Reaction was initiated by addition of ATP, where the sudden drop of the absorption occurred.

2.3.10. Preliminary results show selenocarboxylate is unable to be generated using selenocystine and CD3

Overexpression of five cysteine desulfurases found in *A. orientalis* gave four soluble proteins (CD1 to CD4) and it has been shown that cysteine together with CD3 and CD4 can be used to substituted for NaSH to generate 2-thioglucose-6-phophate.[84] CD3 has been suggested to function as a cystine lyase[147-150] (Fig. 2-14 C), while CD4 is likely to be a typical cysteine desulfurase (Fig. 2-14 B).[84] To test if these two systems can accept selenocystine and selenocysteine, MoaD2 was incubated with CD3 (in the absence of DTT) or CD4 (in the presence of DTT to reduce selenocystine to selenocysteine) in the reaction mixtures that also contained MoeZ, ATP, and selenocystine.

The resulting mixtures were subject to ESI-MS analysis. If incorporation of selenium is successful, a 63 Dalton mass increase is expected, which should be easily distinguished by ESI-MS analysis. As shown in Fig. 2-34 A, MoaD2 was the only major species detected when using CD4 and DTT. In case of CD3, two species were identified based on their masses: one is MoaD2 and the other is MoaD2 covalently linked to selenocysteine. Two possible structures of the second species (MoaD2-COSec and MoaD2-U) are shown in Fig. 2-34 B. Although mass spectroscopic data alone cannot distinguish between the two potential structures, precedent for an *N-S* shift used in native chemical ligation[151-152] suggests that this species is most likely to be MoaD2-U and it is likely formed via the scheme shown in Fig. 2-35.

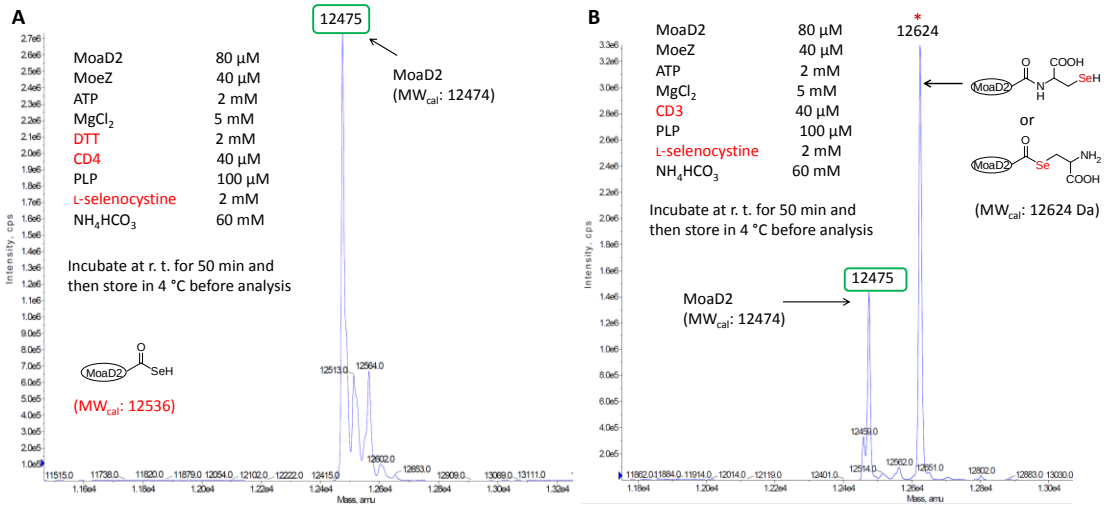

Figure 2-34: Deconvoluted ESI-MS spectra of MoeZ catalyzed MoaD2 activation in the presence of selenocystine and cysteine desulfurases. MoaD2 selenocarboxylate were not detected in both cases.

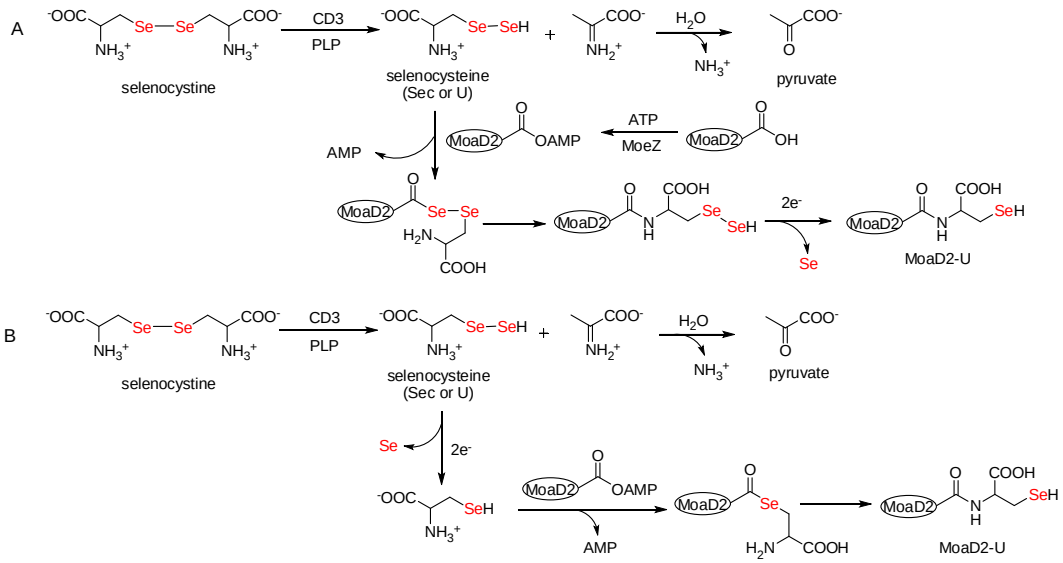

Figure 2-35: Rationale for the modification found in the reaction including MoaD2, MoeZ, ATP, CD3 and selenocystine. One potential electron source could be cysteine residues on the enzymes used in the assay.

Additional supporting information for the rationale shown in Fig. 2-35 is that an orange colored precipitate was observed in the reaction mixture, suggesting formation of selenium. To further confirm that CD3 could catalyzed the lyase activity of selenocystine, an enzyme coupled assay to detect pyruvate formation (Fig. 2-20) was applied. When cystine (0.5 mM) or selenocystine (0.2 mM) were incubated with CD3 (20 μM) for about 1 h, the concentration of pyruvate was determined to be about 280 μM and 70 μM, respectively. The later reaction turned to orange from slight yellow color and all the orange colored species precipitated after centrifugation. This preliminary test suggested that CD3 has lyase activity towards selenocystine.

The results above suggest that a SCP selenocarboxylate cannot be generated under the tested conditions and this is likely the reason for the failure to produce 2-selenosugars in the early trails. It seems that direct application of the 2-thiosugar biosynthetic pathway to the production of a 2-selenosugar is not feasible.

2.4. SUMMARY

Sulfur-containing biomolecules represent important components of many primary and secondary metabolic pathways. Biosynthesis of these molecules, especially the sulfur insertion step, reveals interesting chemistry and provides important information for understanding the biochemistry of this essential element in biological systems.

Recently, our group described the biosynthesis of the sulfur-containing natural product BE-7585A (**2-24**) from *Amycolatopsis orientalis* and in doing so demonstrated the biosynthesis of a 2-thiosugar for the first time. The 2-thiosugar synthase, BexX, utilizes sulfur carrier proteins (CysO or MoaD2) from primary metabolism pathway as the sulfur donors. Activation of the sulfur carrier proteins from different biosynthetic pathways was demonstrated to be catalyzed by a common enzyme, MoeZ. In this chapter, MoeZ was characterized, and the mechanism of MoeZ catalyzed sulfur carrier protein activation using thiosulfate was investigated.

Sequence alignment of MoeZ from *A. orientalis* indicates this enzyme belongs to a subclass of E1-like enzymes that does not have zinc binding sites and is fused with an active rhodanese domain, also known as MoeZR.[118] MoeZ has two conserved cysteine residues, Cys_{213} and Cys_{360}, each located in one of two domains. Neither cysteine is essential for adenylation activity; however, Cys360 is essential for the rhodanese activity. In the non-reducing SDS-PAGE gel assay, a protein conjugate between ThiS and MoeZ was identified. This covalent adduct was resistant to TCEP treatment but disappeared in the presence of an excess amount of DTT, implying that the linkage is through a thioester bond instead of an acyl disulfide bond. Similar amount of adduct was observed in C223A-MoeZ and C360A-MoeZ mutants but not in the C213A-MoeZ mutant, implied the site of thioester bond formation between ThiS and MoeZ is at Cys_{213}. The catalytic activity of this residue was further confirmed by a single turnover experiment in the

absence of external reductant. While wild type MoeZ showed protein thiocarboxylate formation with ThiS, MoaD2, and CysO substrates, no products were detected under the same assay condition using the C213A-MoeZ mutant. These results are most consistent with the mechanism shown in Fig. 2-36 (boxed part).

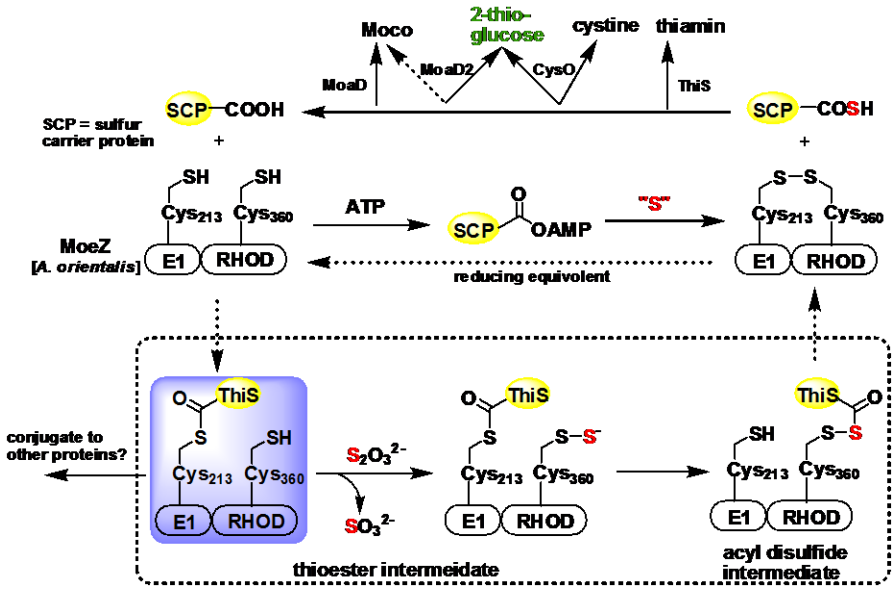

Figure 2-36: Summary of the reaction catalyzed by MoeZ from *A. orientalis*. "S" refers to sulfur source. It could be thiosulfate (studied in this chapter) or bisulfide (used in the adenylation assay). The reducing equivalent can be DTT or TCEP *in vitro*, and mycothiol *in vivo*.[153]

Although the evidence for the existence of CysO-MoeZ and MoaD2-MoeZ thioester intermediates is not strong, the non-reducing protein gel assay clearly revealed a thioester protein conjugate between ThiS and MoeZ. To our knowledge, this is the first example of an ubiquitin (Ub)-E1-like intermediate found in Actinomyces. The Ub-E1 like thioester intermediate may suggest the potential existence of isopeptide protein conjugates in actinobacteria, resembling the case of TtuC (a MoeZ homolog) from

thermobacteria.[113,120] Additional support for this hypothesis is that homolouges of the ubiquitination apparatus such as Ub-, E1-, E2-, and peptidase to remove Ub, have been found in the genome of actinobacteria.[154] Moreover, in this chapter, we provide the first *in vitro* evidence for the importance of the conserved cysteine in the E1-like domain in the sulfur carrier protein activation reaction.

In case of CysO and MoaD2, evidence for similar thioester intermediate is not strong, therefore, at this point it is difficult to define the activation mechanism of MoeZ. However, the involvement of the two conserved cysteine residues for sulfur trafficking among MoeZ is convincing when thiosulfate is used as sulfur donor. Unfortunately, attempt to enzymatically generate 2-selenosugar using the biosynthesis machineries for 2-thiosugar was not successful. The reason might be due to the instability of protein selenocarboxylate, or selenide in aqueous solution is not as good as sulfide in term of nucleophilicity.

MoeZ in *A. orientalis* functions as a common activating enzyme for multiple sulfur carrier proteins from different biosynthetic pathways. Characterization and mutagenesis studies have provided useful information of the sulfur trafficking mechanism, especially when thiosulfate is used as sulfur donor. Identification of a thioester intermediate further supports the evolutionary connection[107,110,112-113,133] between ubiquitination and bacterial sulfur transfer in actinobacteria.

Chapter 3: Studies of Cobalamin-dependent Radical SAM Enzymes: Fom3 in fosfomycin biosynthesis and OxsB in oxetanocin A biosynthesis

3.1. INTRODUCTION

3.1.1. *S*-Adenosyl-L-methionine (SAM or AdoMet): nature's versatile cosubstrate and cofactor

S-Adenosyl-L-methionine (SAM or AdoMet **2-4**) is one of the most efficient metabolites found in biological systems.[155] This small molecule was first discovered by Guilio Cantoni in 1952,[156] and since then it has been recognized to participate in a variety of important biological transformations. SAM is biosynthesized by the ligation of ATP and L-methionine (Met **2-2**) in a reaction catalyzed by SAM synthetase.[157] And all parts of the molecule can be efficiently used as a source for diverse reactions without waste.[158] A brief scheme is shown in Fig. 3-1 to represent the metabolic cycle and catalytic role of SAM.

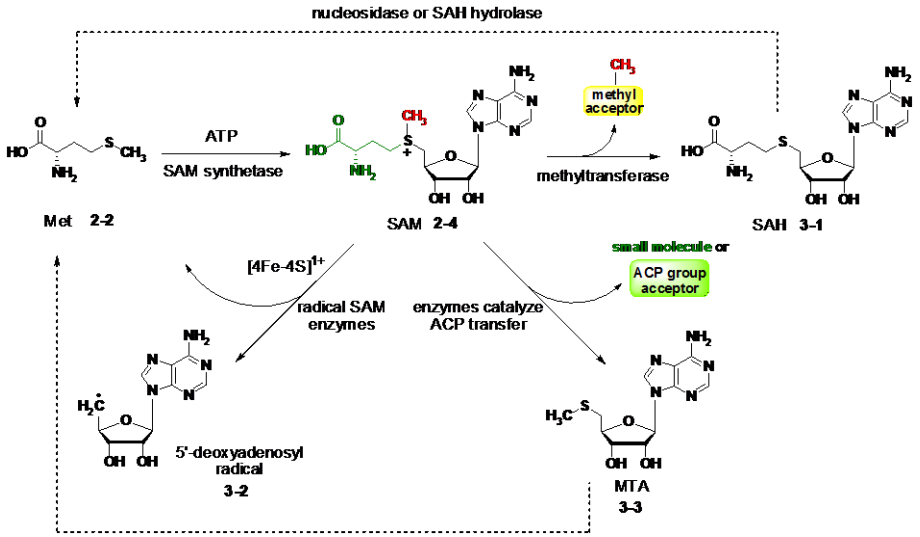

Figure 3-1: Schematic diagram for the SAM cycle. The dotted line indicates multiple steps in between the conversion of two molecules.

SAM used as an electrophile: group transfer

The most striking component of the structure of SAM is the sulfonium group, which makes it no surprise that SAM can act as a good electrophile. In fact, all three carbon-sulfur bonds are prone to nucleophilic attack, resulting in transfer of different moieties of SAM to target molecules.

As a universal cofactor in all kingdoms of life, SAM is also known as the major biological methyl donor for DNA, RNA, proteins, lipids, and small molecules, such as hormones, neurotransmitters, and many natural products.[158] These methylation reactions play important roles in gene regulation, signal-transduction, self-repair, and primary metabolisms. In most cases, the methyl acceptor is a heteroatom or an activated carbon atom and the mechanism is via a typical S_N2 type substitution.[159] During this process, SAM is converted to *S*-adenosylhomocysteine (SAH **3-1**). Several studies have shown that accumulation of this species is both inhibitory and toxic.[160] At the cellular level, SAH can be broken down to adenosine and homocysteine by SAH hydrolase; however, it can also be converted to adenine and *S*-ribosyl-L-homocysteine (SRH) by MTA/SAH nucleosidase. Homocysteine can be utilized to synthesize glutathione (GSH **2-3**), a major physiological antioxidant. It can also be employed by methionine synthase as a substrate to generate methionine. SRH can be further converted to homocysteine and 4,5-dihydroxy-2,3-pentanedione (DPD), a precursor for the universal quorum-sensing signal, autoinducer-2 (AI-2).[161]

Although approximately 95% of the SAM molecules are consumed in methyl transfer reactions,[162] the methyl group is not the only part of SAM that can be transferred. Examples of compounds containing the 3-amino-3-carboxypropyl (ACP) moiety from SAM are listed in Fig. 3-2. These compounds include the bacteria signaling molecules *N*-acylhomoserine lactone (**3-4**) and 3-aminotridec-2-en-4-one (Ea-CAI-1 **3-5**),[163-164] the

antibiotic isonocardicin (**3-6**),[165] the precursor for ethylene biosynthesis in plants 1-aminocyclopropane-1-carboxylic acid (ACC **3-7**),[166] the modified tRNA residues 3-(3-amino-3-carboxypropyl) uridine (acp^{3}U **3-8**)[167] and wybutosine (3-11),[168] the neurotoxic amino acid 2-(3-amino-3-carboxypropyl)-isoxazolin-5-one (**3-9**) from *Lathyrus odoratus,*[169] and polyamines such as spermidine.[170] The by-product from SAM in the ACP group transfer reactions is methylthioadenosine (MTA **3-3**). MTA can be recovered in the methionine cycle, which involves a number of enzymes including MTA/SAH nucleosidase.[160]

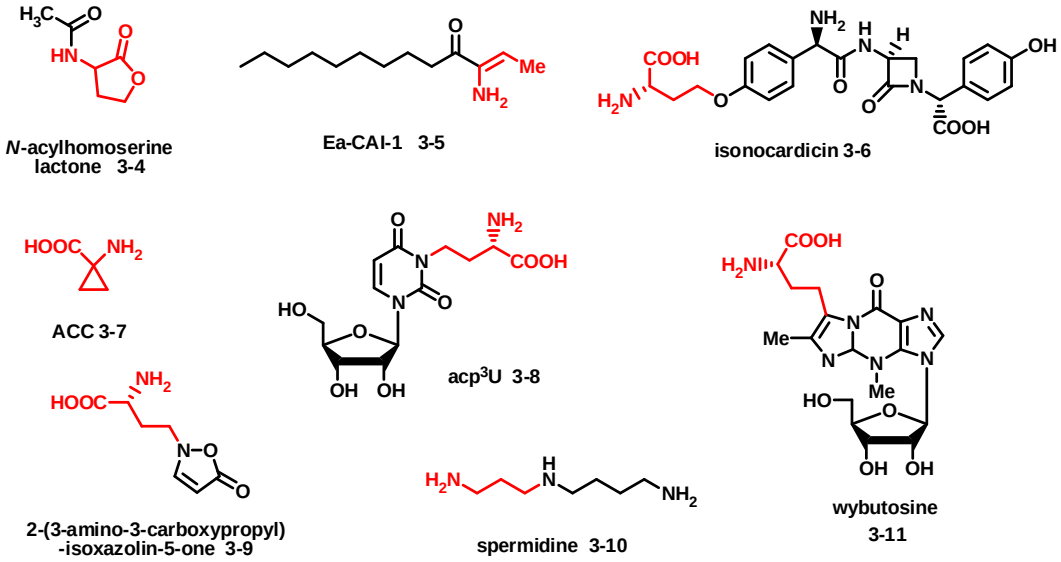

Figure 3-2: Examples of compounds bearing the ACP group from SAM. In the biosynthesis of Ea-CAI-1 and ACC, PLP dependent enzymes are responsible for the transfer of ACP groups. In the biosynthesis of spermidine, enzyme catalyzed SAM decarboxylation occurs first, and then the decarboxylated ACP group is transferred.

The adenosyl group from SAM is less frequently transferred compared to the aforementioned two functional groups, methyl and ACP. One such example is the SAM dependent halogenases shown in Fig. 3-3 A. SalL from the marine bacterium *Salinispora*

tropica and FlA from the soil bacterium *Streptomyces cattleya* catalyze similar reactions using chloride or fluoride as the nucleophile to displace the methionine moiety from SAM.[171-172] Based on the crystal structure of FlA, the finding that both SAM and fluoride are bound in the active site supports the S_N2 type substitution mechanism. The resulting 5'-halo-5'-deoxyadenosine (5'-XDA) is further metabolized and used as a precursor for the biosynthesis of other halogenated metabolites. Another case is the attachment of the ribosyl group to the modified tRNA residue tRNA-preQ1 in a reaction catalyzed by QueA as shown in Fig. 3-3 B.[173] In the proposed mechanism, deprotonation at the C5' position of SAM occurs upon binding of the tRNA substrate, leading to the elimination of the adenine.[174] Nucleophilic attack by the amine group of Trna-preQ1 then yields an ylide intermediate. Recyclization and epoxycarbocycle formation leads to the release of methionine and the formation of the epoxyqueuosine-tRNA (tRNA-oQ) product residue. The by-products from SAM in this reaction are methionine and adenine, which can funnel directly into the nucleotide salvage pathway.

SAM used as a nucleophile: SAM ylide

The sulfonium ylides are commonly used in synthetic organic chemistry and have been proposed to be intermediates in a few SAM dependent transformations. Such reactions include the QueA-catalyzed SAM dependent reaction shown in Fig. 3-3 B and the SAM dependent cyclopropane ring formation catalyzed by cyclopropane fatty acid (CFA) synthase shown in Fig. 3-4 A, pathway b. However, the experimental results suggest that the operant mechanism of CFA may not involve the presence of sulfonium ylide intermediate.[175-177]

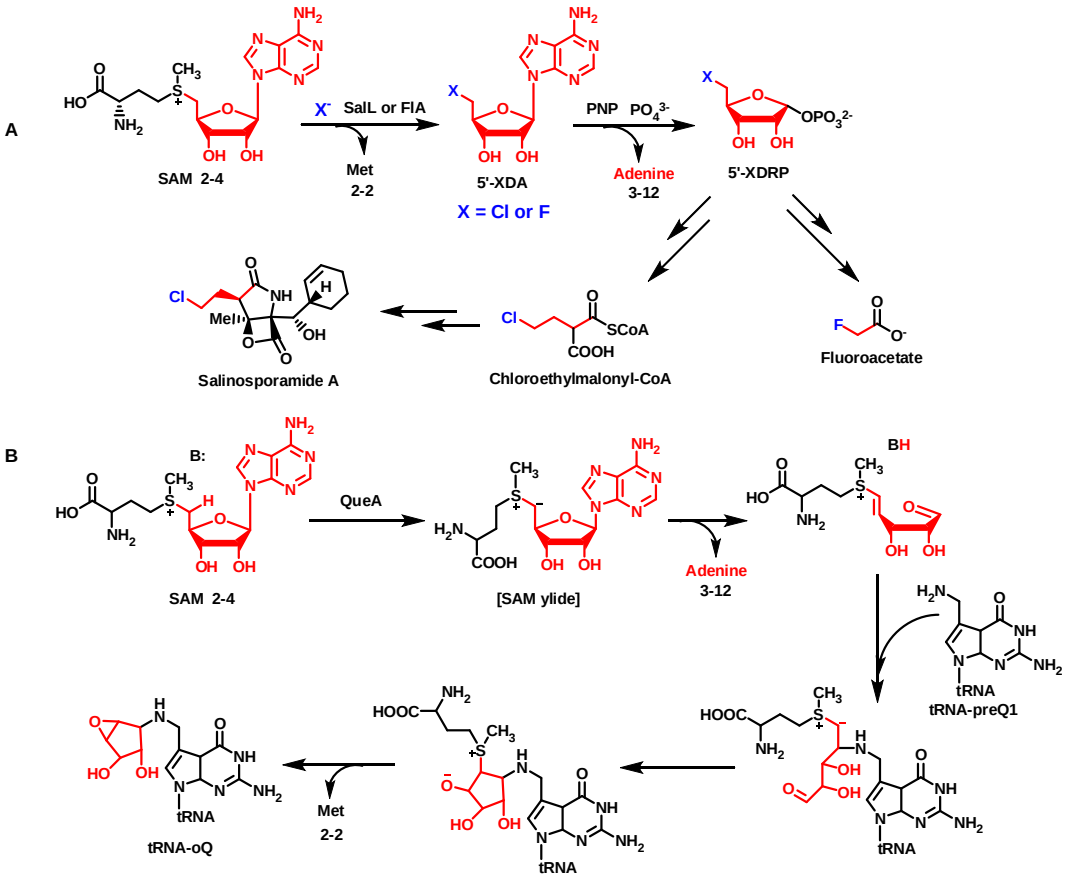

Figure 3-3: Examples of transfer of the adenosyl group from SAM.

Very recently, a study of the CmoA/CmoB enzymes provided more compelling evidence for the existence of a SAM ylide intermediate and its nucleophilic role.[155, 178] As shown in Fig. 3-4 B, 5-oxyacetyl uridine (cmo5U) is a post-transcriptional modified uridine base occurring in several bacterial tRNAs. Early studies showed that inactivation of CmoA or CmoB resulted in the formation of 5-hydroxy uridine (ho5U) instead of cmo5U.[179] In the recent study, a novel metabolite, carboxy-SAM (3-14) was discovered when solving the structure of CmoA.[178] Although a wide variety of SAM analogues designed as the potential tools for macromolecule modification and proteomic analysis

have been synthesized,[180] carboxy-SAM is the first identified SAM analogue existed in nature. Further investigation revealed that prephenate is the source for the carboxylate group on CmoA and CmoB transfers the carboxymethylene group from carboxy-SAM to ho5U.[178] The authors propose that prehenate loses CO_2 and eliminates an hydroxide ion (OH^-) to deprotonate the methyl group of SAM, generating an ylide intermediate. The ylide then reacts with the liberated CO_2 to form carboxy-SAM. The finding that doubly deuterated SAM was formed when triply deuterated SAM was incubated with both CmoA and prephenate further supports this proposal.[178] The by-product from SAM in this reaction is SAH.

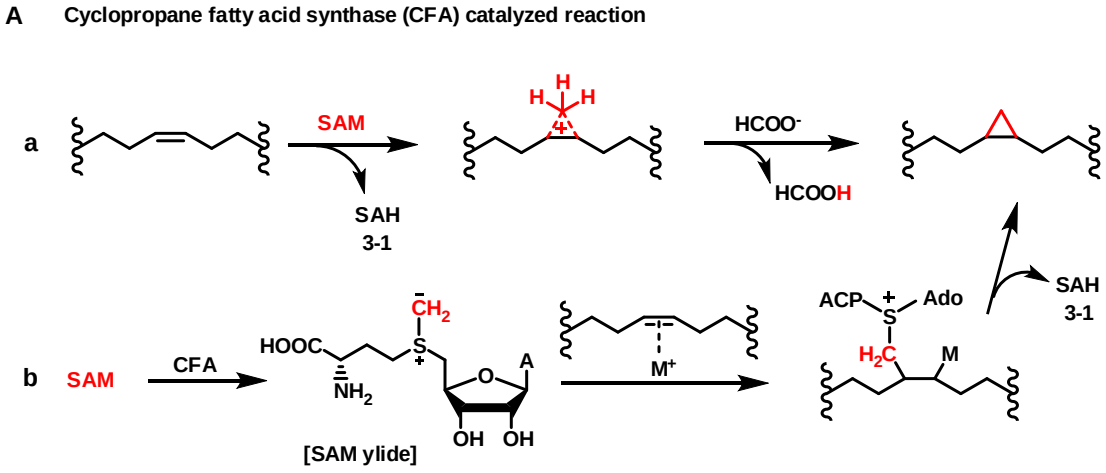

Figure 3-4: Proposed mechanisms for CFA synthase (A) and ComA/ComB (B) catalyzed reactions involving SAM yildes.

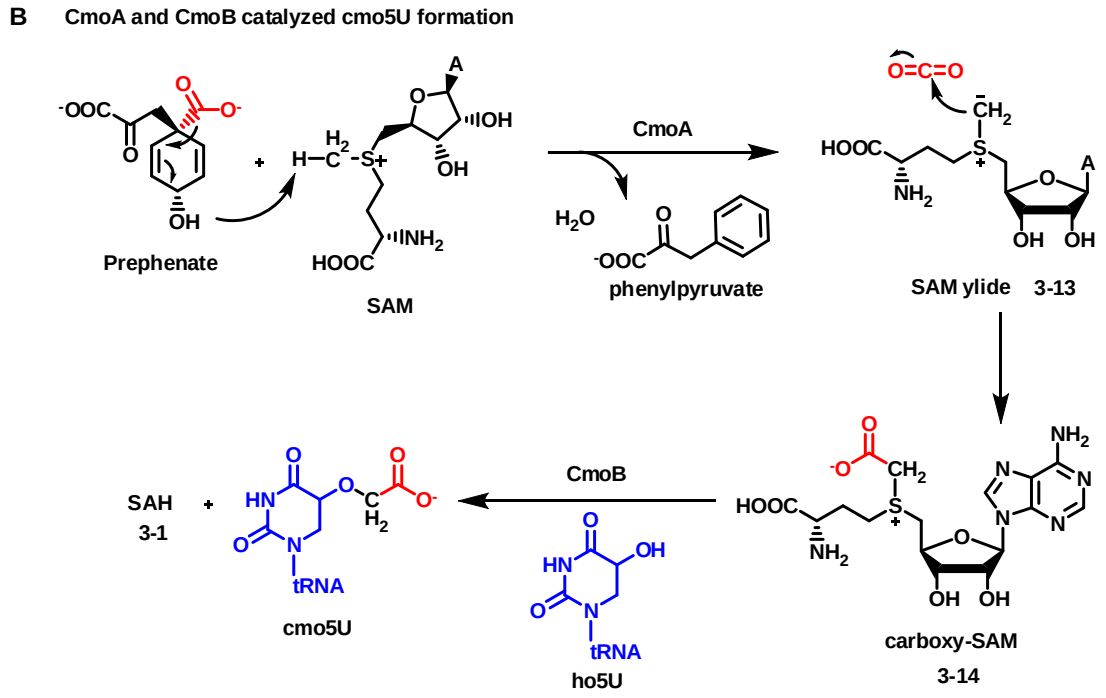

Figure 3-4: Proposed mechanisms for CFA synthase (A) and ComA/ComB (B) catalyzed reactions involving SAM yildes. Current experimental results support pathway a in the case of CFA synthase, although pathway b cannot be fully ruled out. Experimental results are consistent with formation of a SAM ylide intermediate during CmoA/CmoB catalysis.

SAM used as a precursor to radical intermediates: the radical SAM superfamily

The ability of SAM to produce radical intermediates started to be recognized in 1970s with the discovery of lysine 2,3-aminomutase (LAM) from *Clostridium subterminale*.[181] LAM catalyzes the interconversion of L-lysine and L-β-lysine as shown in Fig. 3-5, and requires PLP, SAM, and dithionite for its *in vitro* activity.[181] This type of migration is typical of adenosylcobalamin (coenzyme B_{12}, AdoCbl **3-15**)-dependent rearrangement mediated by AdoCbl-dependent mutases, in which a 5'-deoxy-adenosyl radical (**3-2**) is generated to initiate the radical reaction.[182] However, LAM employs SAM instead of AdoCbl for activity. It is thus puzzling that whether the 5'-deoxy-adenosyl

moiety of SAM functions in the same way. Later studies supported that LAM indeed generates the same radical species (**3-2**) by reductive cleavage of SAM in the presence of $[4Fe\text{-}4S]^{+}$ cluster (**3-16**).[181] In contrast to the elegant structure adenosylcobalamin processes, SAM is thus considered to be "a poor man's adenosylcobalamin".[183]

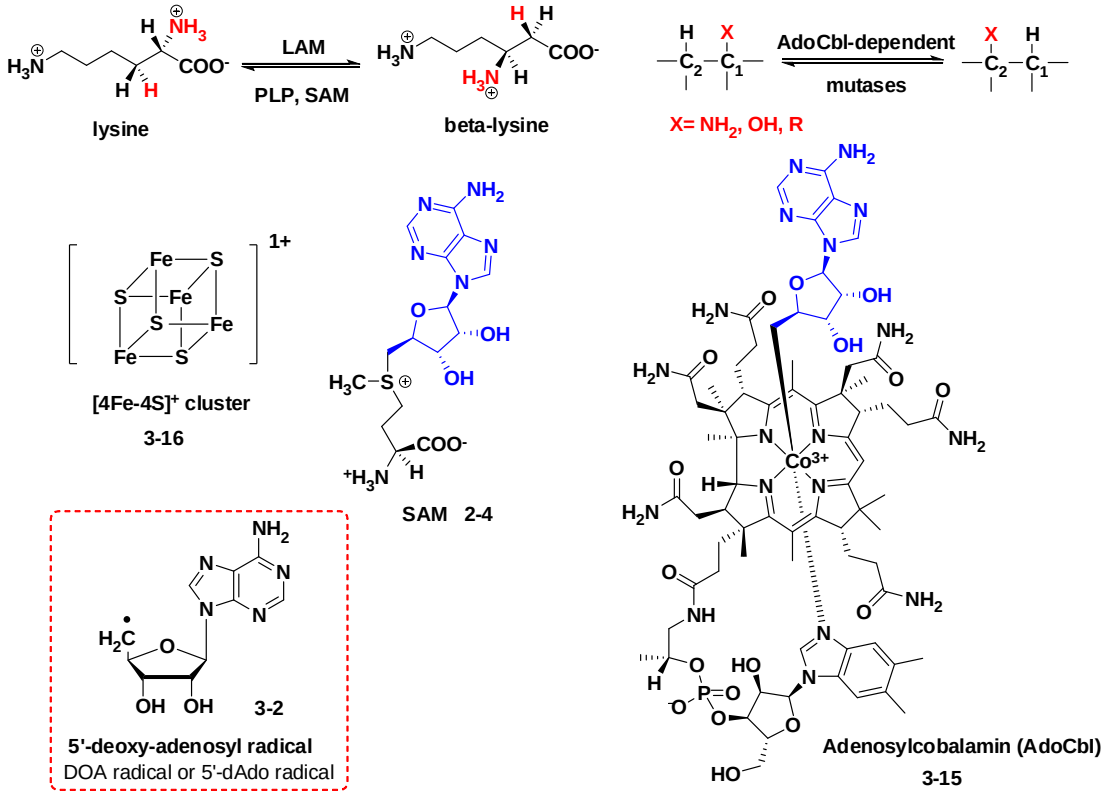

Figure 3-5: Rearrangement reactions mediated by LAM and AdoCbl-dependent mutases. The structures of the cofactors required by these two enzymes are presented and the common 5'-deoxy-adenosyl moiety is shown in blue.

The field underwent a blooming following the publication of bioinformatic studies in 2001 where the radical SAM superfamily was first collectively described.[184] This family contains more than 5000 members[185] that participate in a wide variety of different reactions such as unusual methylation and alkylation reactions, isomerization, sulfur insertion reactions, complex structure formations, anaerobic oxidation, and protein

radical generation. With regard to the types of reactions adenosylcobalamin enzymes mediate (mainly isomerization and elimination reactions), the transformations catalyzed by radical SAM enzymes seem to be much more diverse.[186]

While radical SAM enzymes mediate diverse transformations, they all employ a common mechanism to generate the 5'-deoxy-adenosyl radical as an initiator for the radical transformation as shown in Fig. 3-6.[187] In fact, one distinguishing character of this family is the presence of a [4Fe-4S] cluster coordinated by three conserved cysteines in a Cx_3Cx_2C sequence motif. The fourth iron in the cluster chelates with SAM through its amino acid moiety. Reductive homolysis of the C-S bond at C5' of SAM yields the 5'-deoxy-adenosyl radical (**3-2**) and methionine (**2-2**), concomitant with the oxidation of $[4Fe\text{-}4S]^{1+}$ to $[4Fe\text{-}4S]^{2+}$. The 5'-deoxy-adenosyl radical subsequently abstracts a hydrogen atom from the nominal substrate, resulting in a substrate radical species (**3-17**) that can undergo the radical-mediated transformation as dictated by its interaction and configuration within the enzyme active site. In this process, SAM is reduced to methionine and 5'-deoxy-adenosine (5'-dAdo or DOA **3-18**). Similar to SAH and MTA, 5'-dAdo can also be hydrolyzed by nucleosidases to release adenine (**3-12**).[160]

A recently reported peculiarity in radical SAM mediated catalysis is the reaction catalyzed by Dph2 from *Pyrococcus horikoshii* (PhDph2).[188] Here, the ACP group of SAM is transferred to a histidine residue on the elongation factor 2 (PhEF2) through a radical mechanism (Fig. 3-7). In contrast to canonical radical SAM enzymes, PhDph2 lacks the typical Cx_3Cx_2C motif. However, it still requires a reduced [4Fe-4S] cluster for activity. Biochemical, spectroscopic, and structural studies have revealed that indeed three cysteine residues from different domains of PhDph2 are chelated with the cluster. Another feature that makes PhDph2 unique is that an ACP radical, instead of a typical 5'-dAdo radical is generated. This is supported by the observation of MTA (**3-3**) formation

coupled with the consumption of SAM instead of the typical 5′-dAdo. Besides, 2-amiobutyric acid (ABA **3-20**) and homocysteine sulfinic acid (HSA **3-21**) were detected from the assay in the absence of substrate PhEF2, which correspond to products produced when ACP (**3-19**) radical is reduced by a hydrogen atom or is oxidized by dithionite, respectively.

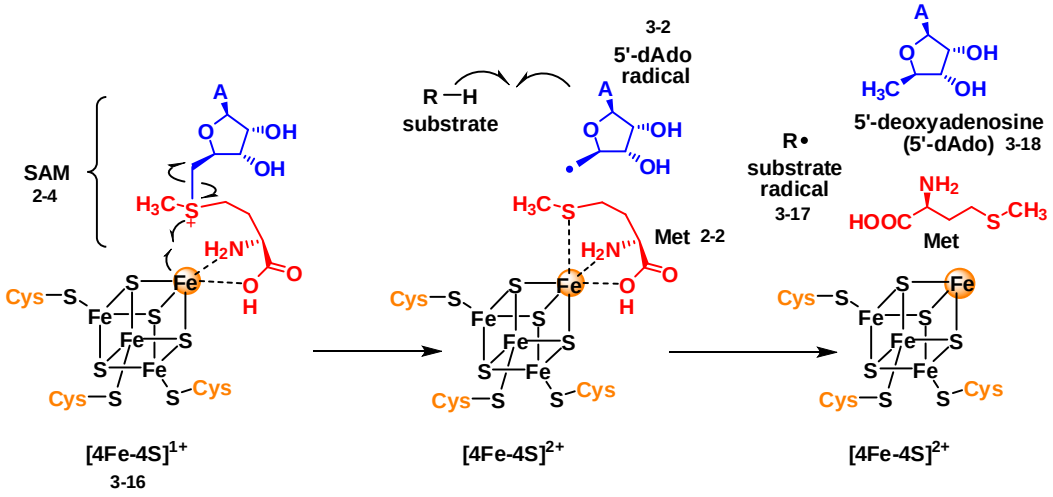

Figure 3-6: Reductive homolysis of SAM in the presence of $[4Fe\text{-}4S]^{1+}$ to generate the 5'-dAdo radical as a reaction initiator. "A" attached to the ribose moiety stands for adenine.

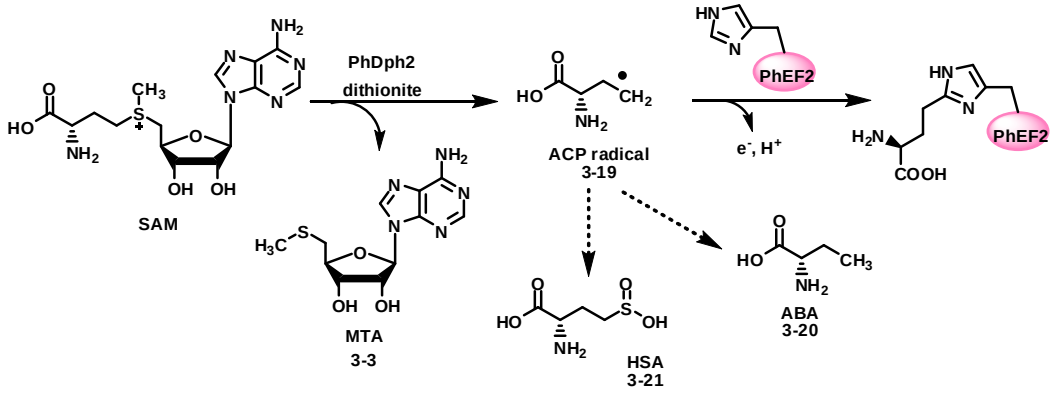

Figure 3-7: Proposed mechanism for PhDph2 catalyzed ACP transfer. The dotted line indicates the product in the absence of the substrate PhEF2.

3.1.2. Radical SAM mediated reactions

In the last decade, the field of radical SAM enzymology has become a treasure trove of new chemistries for study by enzymologists and many reviews have been published recently to address this class of enzymes from different perspectives.[181, 187, 189-195] Prominent members of this family of enzymes are highlighted in this section. Several features of radical SAM enzymes will also be addressed within the different reaction categories, such as variation of the consensus sequence motif, the presence of additional iron-sulfur clusters, mechanistic speculations, stoichiometry, and potential new members.

Isomerases

The radical SAM isomerases identified so far can be divided into two groups. The first group requires the PLP cofactor in addition to the $[4Fe\text{-}4S]^{1+}$ cluster (Fig. 3-8 A and B), while the second group does not need PLP. They all have conserved Cx_3Cx_2C motif and contain one iron-sulfur cluster.

In the first group, lysine 2,3-aminomutase (LAM) is the first radical SAM enzyme to be characterized and is also the most studied.[181] The mechanism of LAM is shown in Fig. 3-9. The substrate radicals, intermediates **1** and **3**, were characterized by electron paramagnetic resonance (EPR) spectroscopy using isotopically labeled substrates and substrate analogues.[186,196-197] Moreover, the 5'-deoxy-adenosine radical was also demonstrated indirectly by characterizing its allylic analogue using EPR spectroscopy.[198] In this reaction, SAM is used catalytically such that it is regenerated after each turnover. A similar mechanism also applies to other PLP-dependent radical SAM mutases such as glutamate 2,3-aminomutase (GAM).[199]

The second group includes enzymes that catalyze isomerization reactions such as spore photoproduct lyase (SPL) and methylornithine synthase (PylB). SPL repairs the major DNA damage spore photoproduct caused by UV irradiation in bacteria endospore

germination process. Specifically, it cleaves the spore photoproduct into two thymines residues as shown in Fig. 3-8 C. The mechanism of this enzyme has been studied for several years and the most recent mechanistic revision is shown in Fig. 3-10.[200-202] In this model, SAM is regenerated via hydrogen atom transfer involving the conserved Cys141 and Tyr99 (potentially Tyr97 is also involved) residues of SPL. PylB catalyzes the transformation of L-lysine to methylornithine in the first step of pyrrolysine biosynthesis (Fig. 3-8 D).[203] Although the crystal structure of this enzyme has been solved with SAM, the iron-sulfur cluster, and the product bound in the active site, *in vitro* activity of this enzyme has not been demonstrated.[204] Therefore, experimental evidence to test the proposed mechanism is still awaited.

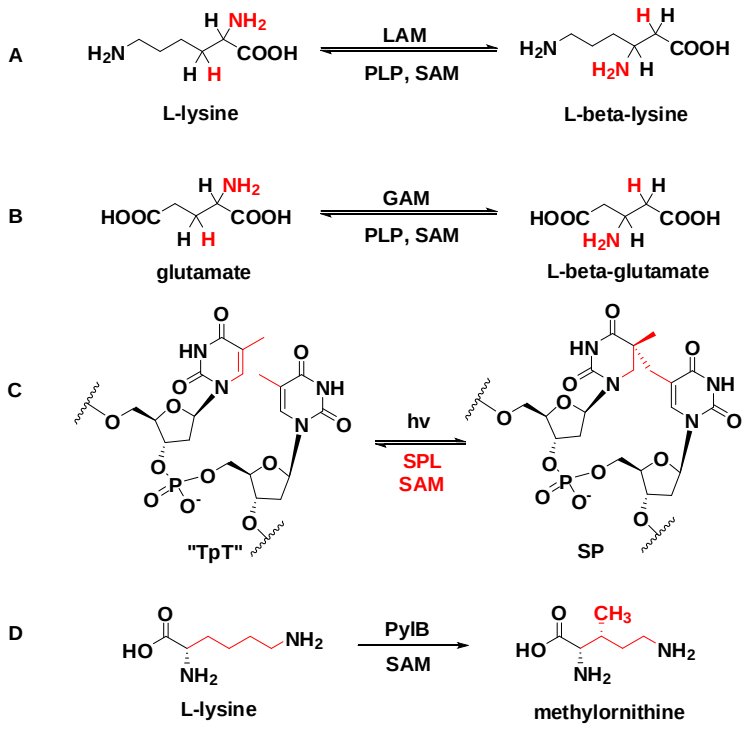

Figure 3-8: Examples of radical SAM enzymes that function as isomerases. In the case of spore photoproduct lyase (SPL), the thymine dimer is a DNA photolesion.

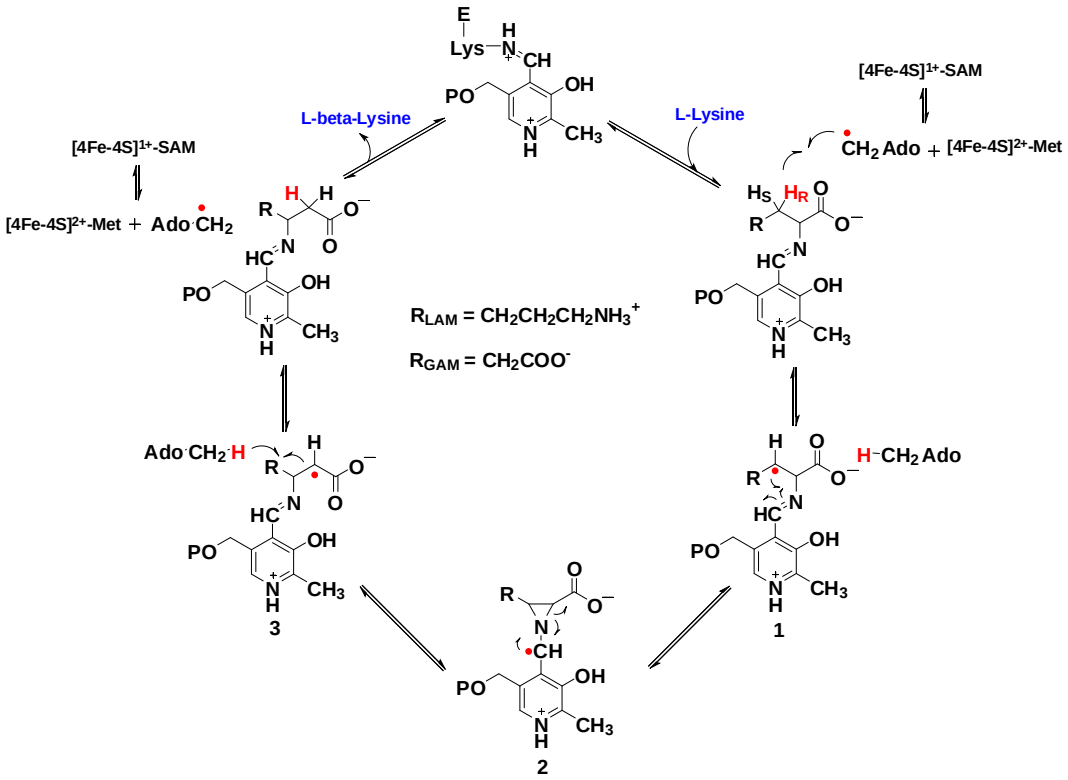

Figure 3-9: Mechanism of LAM catalyzed PLP-dependent isomerization reaction.

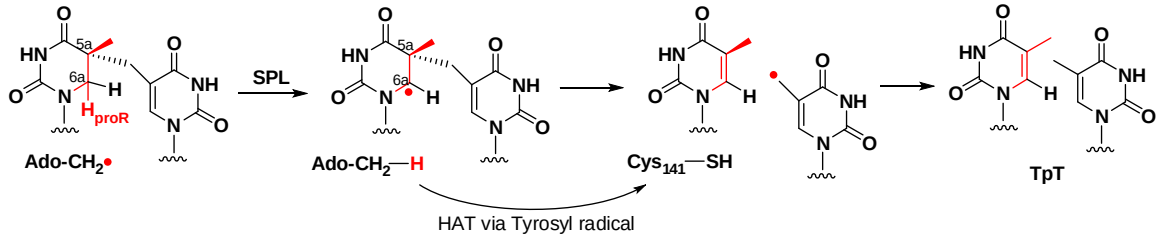

Figure 3-10: Proposed reaction mechanism for SPL from *B. substilis*. HAT stands for hydrogen atom transfer.

Another potential member for this group based on the sequence homology is BlsG from *Streptomyces griseochromogenes* in the Blasticidin S biosynthesis.[205] This enzyme

was proposed to be a PLP-dependent arginine 2,3-aminomutase, although its activity has yet to be reconstituted *in vitro*. Previously, littorine mutase from *Datura stramonium* was proposed to be a putative radical SAM enzyme that catalyzes the rearrangement of littorine to hyoscyamine, a tropane alkaloid produced by some plants that bares anticholinergic activity.[206] However, a more recent gene silencing study suggested this might not be the case and the role of SAM in this reaction is unclear.[207]

Activating enzymes

The glycyl radical enzymes (GREs) are a family of proteins found in anaerobes (Fig. 3-11 A).[189] These enzymes contain a strictly conserved glycine residue that is converted to a glycyl radical by a specific activating enzyme. The resulting glycyl radical is then used to generate a thiyl radical, which ultimately initiates the reaction. The required GRE activating enzymes are radical SAM enzymes that employ the 5'-deoxyadenosyl radical to abstract the hydrogen atom from the conserved glycine residue (Fig. 3-11 B). SAM is consumed with each activation event and reduced to methionine and 5'-deoxyadenosine. The most studied enzyme from this group is pyruvate formate lyase activating enzyme (PFL-Ae). Here, SAM bound to the enzyme has been characterized spectroscopically.[208] It is interesting to point out that all three types of ribonucleotide reductase (RNR) have mechanisms reminiscent of the GREs in which a thiyl radical mediates the elimination of C2' hydroxyl group of the nucleotide.[209] Furthermore, the anaerobic RNR is a member of the GREs class of enzymes and generates the thiyl radical through a glycyl radical, which is in turn generated by a radical SAM activase.

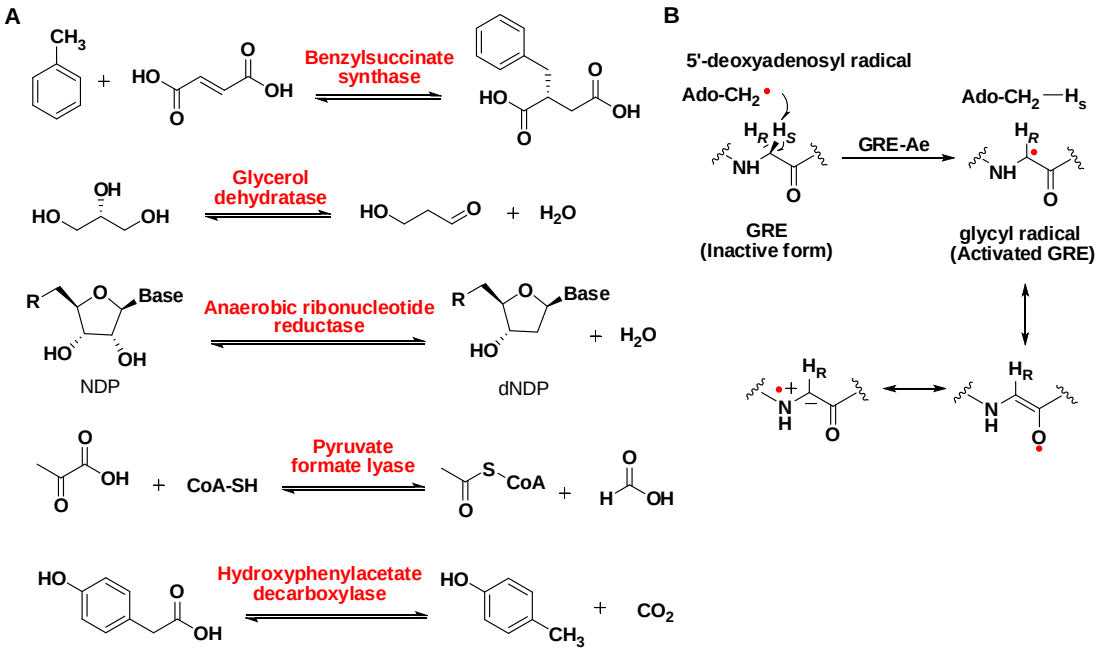

Figure 3-11: Reaction schemes for reported GREs and the activation by GRE-Ae. A. Examples of reported GRE mediated reactions. B. Generation of a glycyl radical on a GRE by radical SAM activating enzyme.

Enzymes catalyze C-S bond formation on unactivated carbon center

As mentioned in Chapter 2, sulfur incorporation in the biological systems may involve only Lewis acid-base chemistry or utilize radical intermediates. So far, enzymes catalyzing radical-mediated sulfur insertion have been all radical SAM enzymes. Recently, couple radical SAM enzymes have also been found to catalyze intramolecular thioether bond formation via a radical mechanism.

Radical SAM enzymes involved in the sulfur insertion reaction can be further divided into two types. The first type includes two members BioB and LipA, which insert sulfur into unactivated C-H bond.[189] They catalyze the sulfur insertion step in the biosynthesis of biotin and lipoic acid, respectively, as shown in Fig. 3-12. BioB is the

most extensively studied case of the radical SAM sulfur insertion enzymes. It contains one [4Fe-4S] cluster, which is responsible for the 5'-deoxy-adenosyl radical formation, and one [2Fe-2S] cluster, which is sacrificed as the sulfur donor.[210] In each reaction cycle, two rounds of reductive cleavage of SAM are coupled to two hydrogen atoms abstraction from dethiobiotin (DTB). In each round, the DTB carbon radical forms a C-S bond with the sulfide sulfur from the [2Fe-2S] cluster and the first hydrogen abstraction occurs at the C9 postition.[211] In case of LipA, the additional iron-sulfur cluster is a [4Fe-4S] cluster rather than a [2Fe-2S] cluster as for BioB. The exact role of this cluster in LipA is not certain although it has been proposed to be cannibalized as the sulfur source for LipA.[126] In both reactions, two SAM molecules are reduced to two 5'-deoxyadenosine during each turnover.

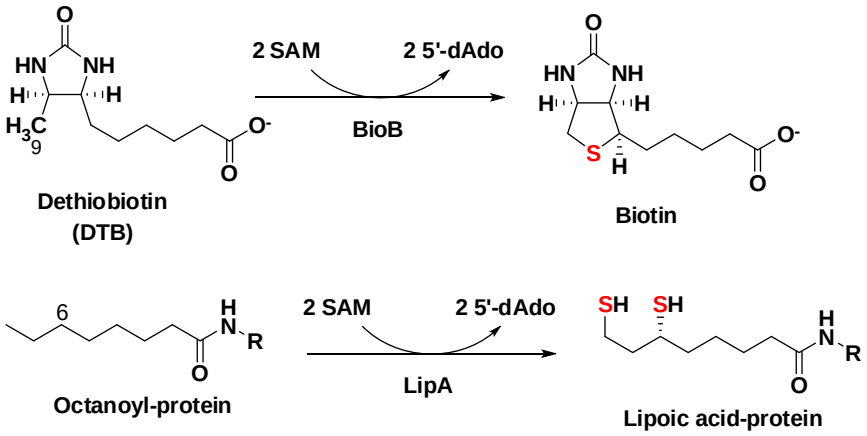

Figure 3-12: BioB and LipA catalyzed sulfur insertion. The number indicates the position from which the 5'-deoxyadenosyl radical abstracts a hydrogen atom to initiate the reaction.

The second type of radical SAM sulfur insertion enzymes is represented by the methylthioltransferase (MTTase). These enzymes catalyze methylthiolation of tRNAs and ribosomal proteins. Typical examples including MiaB, MtaB, and RimO are shown

in Fig. 3-13.[126] The mechanism of MTTase catalysis is hypothesized to involve both radical SAM chemistry and an S_N2 type substitution although the exact order of the two steps is unknown.[126] Similar to BioB and LipA, two SAM molecules are consumed for each enzyme turnover; however, only one of the SAM molecules is reduced to 5'-deoxyadenosine, while the other one is converted to SAH from the S_N2 type methylation. Additionally, all MTTases described to date contain two [4Fe-4S] clusters, and the role of the auxiliary cluster has been proposed to be a sacrificial source of sulfur.[126] Alternatively, instead of destroying the auxiliary cluster, sulfur source could be exogenous sulfur cosubstrate at an open coordination site on the auxiliary cluster.[212]

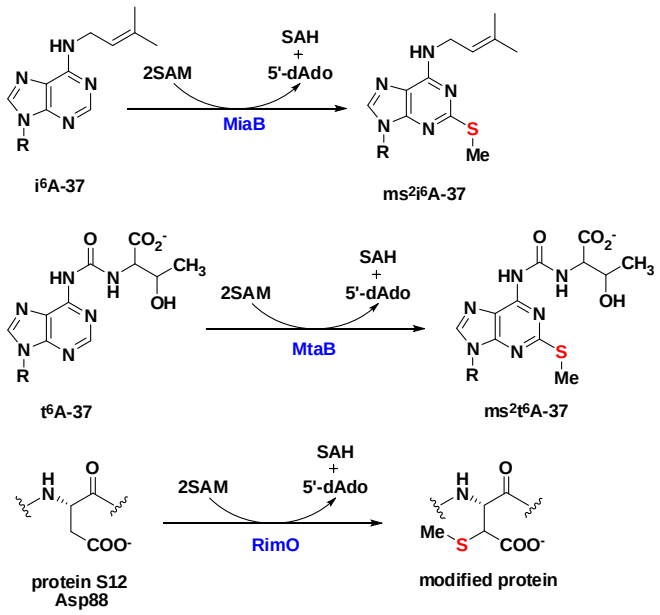

Figure 3-13: Methylthiolation reactions mediated by radical SAM enzymes.

Recently, two radical SAM enzymes have been found to mediate thioether bond formation in the biosynthesis of bacetriocins (see Fig. 3-14).[213-214] They are AlbA in the Subtilosin A biosynthesis and SkfB in the biosynthesis of sporulation killing factor

biosynthesis. Both enzymes have been shown to possess two [4Fe-4S] clusters, and the auxiliary cluster (coordinate by a $Cx_{4-5}Cx_{1-4}C$ motif) has been proposed to function as an electron acceptor.[214] In this reaction, one SAM molecule is converted to 5'-deoxyadenosine with each turnover.[213]

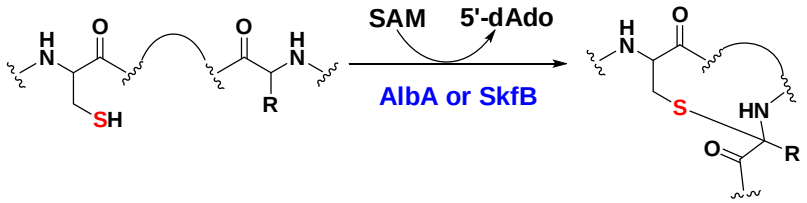

Figure 3-14: Radical SAM mediated thioether bond formation.

Enzymes involved in complex structure formation in cofactor biosynthesis

Several radical SAM enzymes have been reported to be involved in cofactor biosynthesis. These include MoaA (molybdopterin biosynthesis, Fig. 3-15 A),[215-217] HemN (heme biosynthesis, Fig. 3-15 B),[189] ThiH and ThiC (thiamine biosynthesis in anaerobes, Fig. 3-15 C and D),[189] HydG and HydE ([FeFe]-hydrogenase H cluster biosynthesis),[189] PqqE (pyrroloquinoline quinone biogenesis),[218] F_0-synthase (F_{420} cofactor biosynthesis),[219] and MqnC (menaquinone, vitamin K_2 biosynthesis).[220] General reaction schemes based on the most recent studies for these interesting biotransformations are listed in Fig. 3-15 and Fig. 3-16.

MoaA and MoaC mediate the conversion of guanosine 5′-triphosphate (GTP) to cyclic pyranopterin monophosphate (cPMP), the first step in the biosynthesis of molybdopterin cofactor (Moco). MoaA contains two [4Fe-4S] clusters with one located near the *N*-terminus and the other near the *C*-terminus.[221] Structural and spectroscopic studies have revealed that the *N*-terminal cluster, which has a Cx_3Cx_2C motif, is responsible for the 5'-deoxy-adenosyl radical formation, whereas the *C*-terminal cluster,

which has a $Cx_2Cx_{13}C$ motif is bound to substrate.[222] In the early proposal, MoaA was suggested to catalyze the pyranopterin ring formation using a radical mechanism and MoaC was involved in the following intramolecular cyclization.[216] Mechanistic studies of MoaA have shown that the hydrogen atom at C3' position of GTP was abstracted by the 5′-deoxyadenyl radical.[216] Surprisingly, a careful characterization of the MoaA reaction revealed that 3',8-cH$_2$GTP is the actual product of the radical reaction catalyzed by MoaA and MoaC is responsible for the pyranopterin ring formation from 3',8-cH$_2$GTP.[217]

HemN catalyzes stepwise oxidative decarboxylation of coproporphyrinogen III in the oxygen independent biosynthesis of heme (see Fig. 3-15 B).[189] Decarboxylation takes place first at A ring followed by the B ring and hydrogen atom abstraction by 5′-deoxyadenosyl radical occurs at *pro-S* position as labeled in Fig. 3-15 B.[223] Structural and biochemical analysis of HemN showed that two SAM molecules bound to the active site are both required for activity.[224] However, the detailed mechanism is not clear.

During the discussion of bacterial thiamine thiazole biosynthesis in Chapter 2 (Fig. 2-8), it was pointed out that one of the substrates is glycine imine (**3-22**). In anaerobes, this species is formed from tyrosine in a reaction catalyzed by the radical SAM enzyme ThiH as shown in Fig. 3-15 C.[225] Results from kinetic and substrate analogue studies are most consistent with a mechanism involving generation of a tyrosinyl radical. To complete the thiamine biosynthesis in bacteria, another precursor 4-amino-5-hydroxymethyl-2-methylpyrimidine phosphate (HMP-P, **3-24**) is also required.[90] In bacteria, plants, and algae, formation of HMP-P involves another radical SAM enzyme ThiC where aminoimidazole ribonucleotide (AIR, **3-23**) acts as the substrate.[226] ThiC contains one [4Fe-4S] cluster at its *C*-terminus and is chelated by a conserved Cx_2Cx_4C motif instead of the canonical Cx_3Cx_2C motif. In vitro study of ThiC revealed that in each

reaction cycle AIR is converted to HMP-P, carbon monoxide, and formate, concomitant with reduction of one SAM molecule to 5'-dAdo (see Fig. 3-15 D).[227]

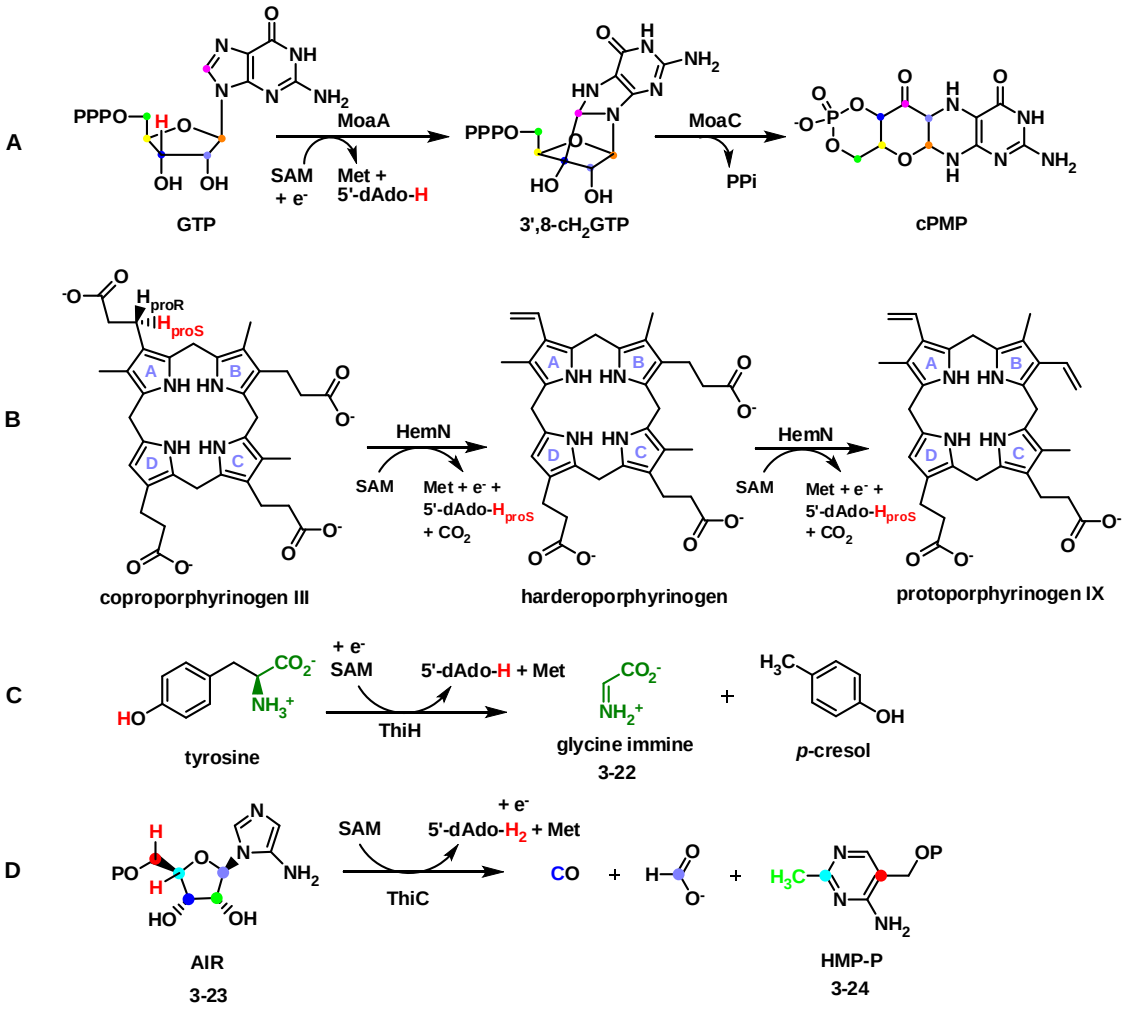

Figure 3-15: Reaction schemes of radical SAM enzymes involves in cofactor biosynthesis. Position of hydrogen abstraction by 5'-deoxyadenosyl radical is indicated by the red color (proposed by the literature based on the isotope labeling results[216,223,225,227]). Other color codes are used to help keep track of the atoms.

[FeFe]-Hydrogenases reversibly reduce protons to molecular hydrogen.[228] They require a metallocofactor called the H-cluster for activity. Biosynthesis of the H-cluster requires three enzymes: two radical SAM enzymes HydE and HydG, as well as the GTPase HydF, where the nascent cofactor is harbored.[229] High sequence similarity between HydG and ThiH, along with initial characterizations for HydG suggested that HydG catalyzes the formation of the CN and CO ligands for the H-cluster assembly as shown in Fig. 3-16 A. However, the substrate for HydE has not been revealed yet.

The PQQ cofactor is found in alcohol and sugar dehydrogenases from gram-negative bacteria.[218] PqqE is a radical SAM enzyme and is one of the six enzymes responsible for PQQ biogenesis. Although activity of PqqE has not been reconstituted *in vitro*, initial studies have shown that it contains two iron-sulfur clusters and can catalyze reductive cleavage of SAM in the presence of dithionite when the substrate is absent.

Two new members of this category are F_0-synthase and MqnC, which are involved in the cofactor biosynthesis of F_{420} and metaquinone, respectively (see Fig. 3-16 B and C).[219-220] The *in vitro* activity of these two radical SAM enzymes have been reconstituted, which has set the foundation for further mechanistic studies.

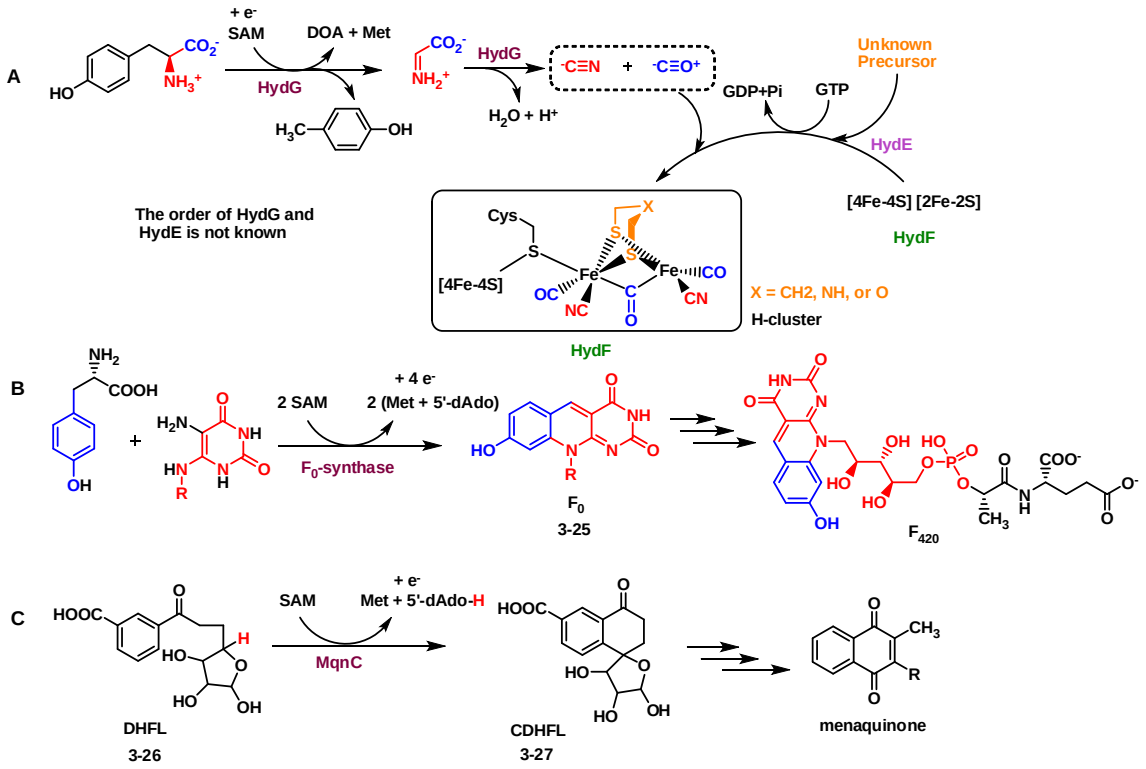

Figure 3-16: Radical SAM enzymes mediated reactions that involving in cofactor biosynthesis. Color codes are used to help keep track of the atoms.

Enzymes involved in purine-based natural products biosynthesis

Radical SAM enzymes involved in this section have been reviewed recently by Vahe Bandarian from the University of Arizona.[193] The 7-deaza-purine core structure occurs in a number of secondary metabolites and modified tRNA residues. The biosynthesis of this moiety starts from GTP, and the radical SAM enzyme QueE catalyzes the complex heterocyclic rearrangement of 6-carboxy-5,6,7,8-tetrahydropterin (CPH_4, **3-28**) to 7-carboxy-7-deazaguanine (CDG, **3-29**) as shown in Fig. 3-17 A.[230] Characterization and kinetic study of QueE have suggested that the enzyme harbors one [4Fe-4S] cluster and that SAM is regenerated after each turnover.

Wybutosine (yW) is found at position 37 of $tRNA_{Phe}$ in eukaryotes and archaea. The biosynthesis of this modified base involves a number of unusual transformations involving SAM as shown in Fig. 3-17 B. Among these SAM-dependent enzymes, TYW1 is a radical SAM enzyme catalyzing the condensation of pyruvate and m^1G with the loss of CO_2.[231] TYW1 likely contains two iron-sulfur clusters and an active site lysine residue has been implicated in the reaction mechanism.[193]

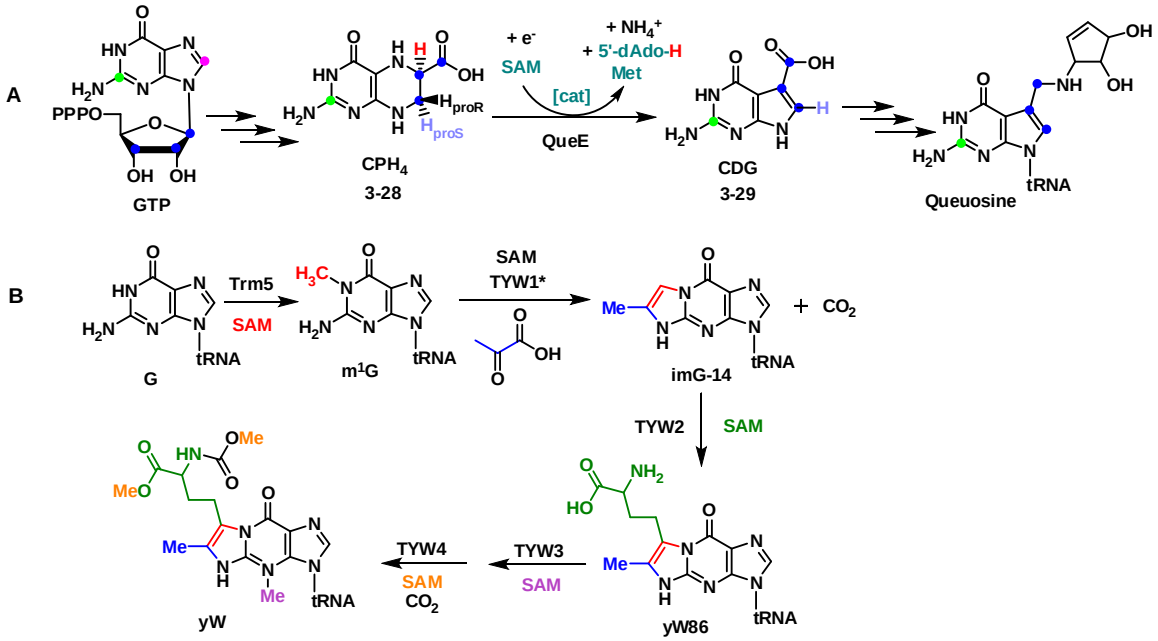

Figure 3-17: Transformations in the biosynthesis of purine-based natural products that involve radical SAM enzymes. Color codes are used to help keep track of the atoms.

Deamination and oxidation

Sulfatases (e.g. AtsA) catalyze the cleavage of sulfate esters via a protein-derived formylglycine (FGly) residue. Formation of this atypical amino acid residue under anaerobic conditions requires a formylglycine synthase (FGS, e.g. AtsB). Anaerobic

FGSs are radical SAM enzymes that catalyze the two-electron oxidation of a specific cysteinyl or seryl residue on the sulfatase substrate enzyme as shown in Fig. 3-18 A.[232] Characterization of AtsB suggests that this enzyme binds three [4Fe-4S] clusters.[232] The auxiliary clusters have been proposed to act as electron acceptors during the catalytic cycle; however, this hypothesis has not been confirmed experimentally.

Two other examples of oxidation and deamination reactions mediated by radical SAM enzymes are found in the biosynthesis of sugar-containing natural products.[187] BtrN catalyzes the oxidation of 2-deoxy-scyllo-inosamine (DOIA, **3-30**) to amino-dideoxy-scyllo-inosose (amino-DOI, **3-31**) in the biosynthesis of 2-deoxystreptamine (DOS), which is found in many aminoglycoside antibiotics (see Fig. 3-18 B). DesII is responsible for the deamination of TDP-4-amino-4,6-dideoxy-D-glucose (**3-32**) that yields TDP-3-keto-4,6-dideoxy-D-glucose (**3-33**) in the biosynthesis of D-desosamine, which is found in many macrolide antibiotics (see Fig. 3-18 C). Interestingly, although DesII catalyzes redox neutral deamination of its natural substrate **3-32**, *in vitro* it can also accept TDP-D-quinovose (**3-33**) and TDP-3-amino-3,6-dideoxy-D-glucose (**3-34**) as substrates; however, and the reaction type changes from redox neutral deamination (or dehydration) to oxidative dehydrogenation. While BtrN contains two iron-sulfur clusters, DesII contains only one.[187] The auxiliary cluster of BtrN was proposed to function as an electron sink although no experimental evidence has been provided.[233]

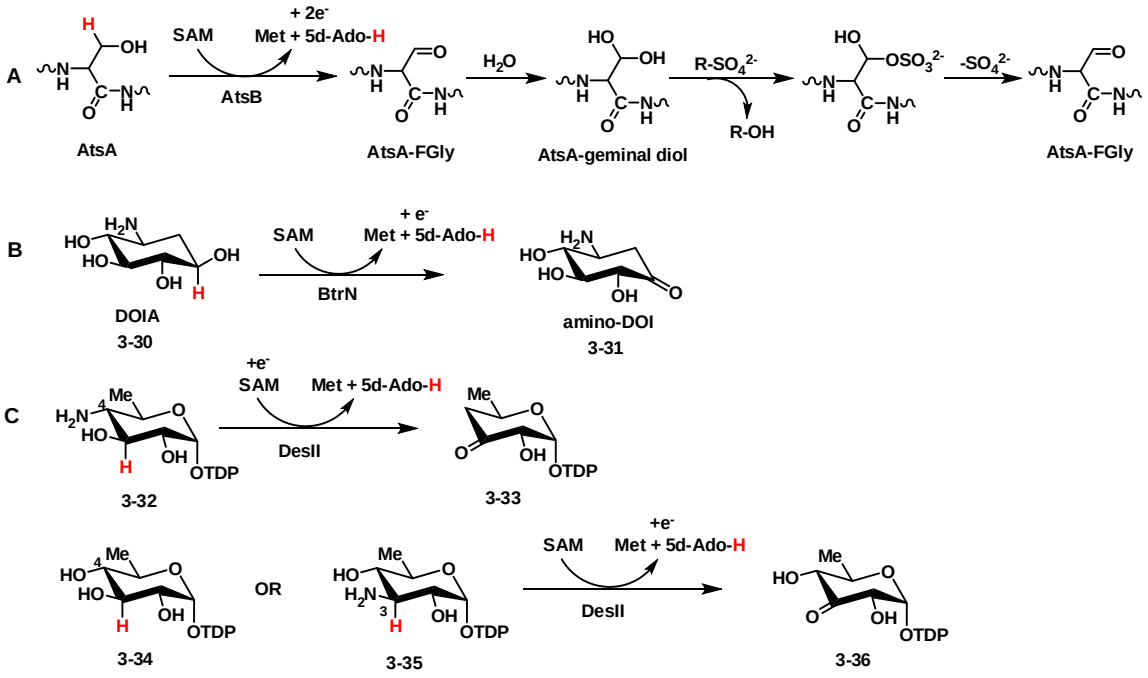

Figure 3-18: Radical SAM enzymes catalyzed oxidation and deamination reactions.

Lyase activity

Several radical SAM enzymes operate as lyases, such as the previously mentioned ThiH and HydG. Other ThiH and HydG homologues have also been reported in other biosynthetic pathways, such as NosL and NocL in the biosynthesis of the 3-methyl-2-indolic acid (MIA, **3-35**) functionality observed in the thiopeptide antibiotics nosiheptide (NOS) and nocathiacin I (NOC-I).[234-235] Both NosL and NocL contain only one canonical [4Fe-4S] cluster, and results from biochemical and spectroscopic studies of NosL and NocL are in agreement with the proposed fragmentation-recombination mechanism shown in Fig. 3-19 A.[234-235]

Another interesting example of a radical SAM lyase is PhnJ from *E. coli*, which catalyzes cleavage of the C-P bond of methylphosphonate (see Fig. 3-19 B). The gene

cluster that encodes this enzyme is involved in the metabolism of alkylphosphonates under condition of phosphate starvation.[236] PhnJ lacks the signature Cx_3Cx_2C motif having instead a $Cx_2Cx_{21}Cx_5C$ motif located near the *C*-terminus. Spectroscopic and biochemical characterizations have revealed that this motif is indeed responsible for coordinating the [4Fe-4S] cluster.[237] Labeling and substrate analogue trapping studies further suggested that PhnJ catalyzed C-P cleavage proceeds via a novel mechanism involving two protein-based radicals intermediates in addition to the 5'-deoxyadenosyl radical intermediate (see Fig. 3-19 C).[237]

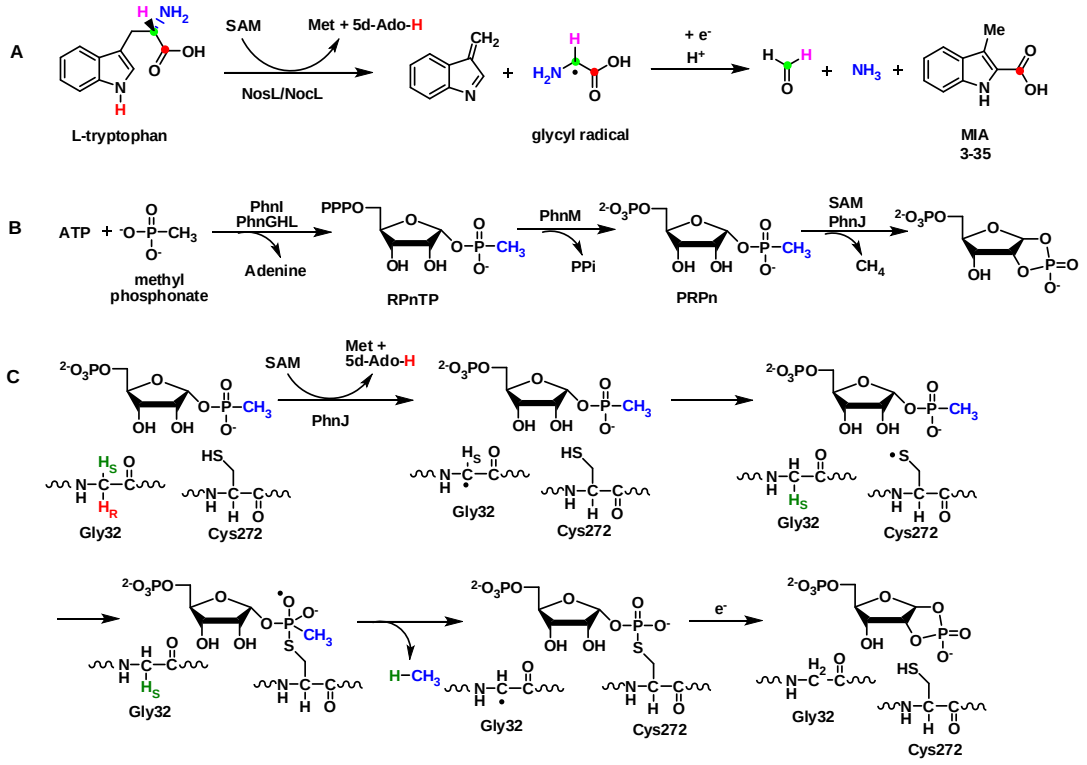

Figure 3-19: Reactions mediated by radical SAM enzymes NosL/NocL and PhnJ.

Methylation

Some radical SAM enzymes are able to catalyze the methylation of unactivated acceptor sites. These enzymes have been further grouped to three different subclasses according to sequence analysis: (A) ribosomal RNA (rRNA) methyltransferases including RlmN, Cfr, and NifB; (B) cobalamin-dependent radical SAM enzymes that contain both a cobalamin binding domain and a canonical radical SAM domain; and (C) enzymes that are likely involved in heteroaromatic substrate methylations and have high sequence similarity to HemN.[238-240]

The functions of RlmN and Cfr were shown in Fig. 3-20 A. RlmN mediates C2 methylation of A2503, which is a housekeeping modification in the bacterial 23S rRNA, whereas Cfr methylates the C8 position, which confers resistance to several antibiotics that target ribosome.[241] Biochemical and structural analysis have suggested the radical mechanism for *E. coli* RlmN shown in Fig. 3-20 B.[242-245] Two SAM molecules are required for the methyl insertion. The first SAM methylates a cysteine residue via a S_N2 type mechanism, and the second one is used to generate a 5'-deoxyadenosyl radical, which abstracts a hydrogen atom from the nascent methyl cysteine residue to initiate the reaction. The other example for this subclass is NifB, which is required for the biosynthesis of the M-cluster found in the active site of nitrogenase.[239] The M-cluster is a metal-sulfur cluster that contains a carbide at its core. Radio labeling experiments demonstrated that the source of the carbide core is SAM.[246] Recently, the activity of NifB has been reconstituted *in vitro* and the mechanism is believed to be similar to that of RlmN although the details remain unclear.[239]

While a few cases have been reported for the *in vitro* reconstitution of activity of subclass B enzymes,[240] no enzyme from subclass C (e.g. NosN) has been reconstituted

in vitro.[247] Currently, the mechanisms for these two subclasses are still unknown and this is one of the most exciting questions regarding radical SAM catalysis.

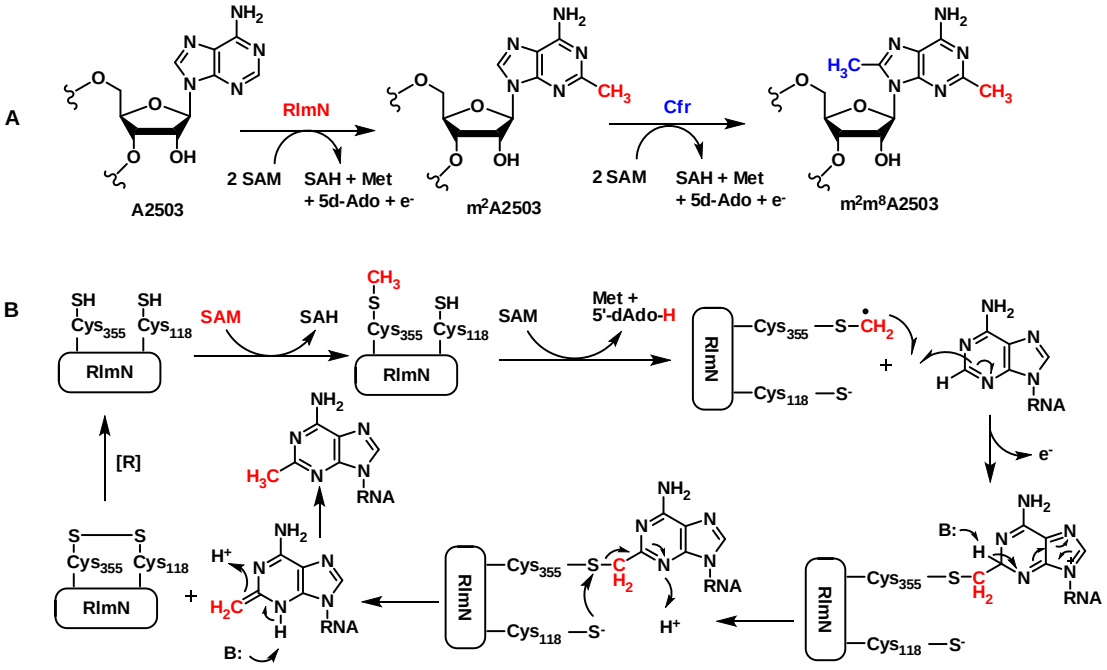

Figure 3-20: RlmN and Cfr catalyzed methyl insertion in the rRNA modification.

3.1.3. Cobalamin-dependent radical SAM enzymes

Occurrence and significance

Cobalamin-dependent radical SAM enzymes were first identified through bioinformatics studies by Sofia *et. al.*.[184] When they analyzed the members in the radical SAM superfamily by their domain architecture in order to predict the function of unknown proteins, they found that a group of proteins appeared to show poor cohesion among all other radical SAM enzymes, which often suggests a divergent function.[184] Compared to other radical SAM members, this group of proteins possesses a long *N*-

terminal extension of ~200 residues containing a cobalamin binding motif in addition to their radical SAM core domain. The aforementioned subclass B radical SAM methyltransferases belong to this group and are proposed to catalyze the methylation at the unactivated carbon centers such as sp^3 hybridized carbons, aromatic heterocycles, and phosphinates.[238] Other members in this group are likely to have distinct functions, such as radical cyclase, which is the predicted function of BchE involved in the chlorophyll biosynthesis.[248]

Several *in vivo* studies have revealed the function of members in this group and the involvement of cobalamine for their activity (e.g. Fom3[249-250], CloN6[251], and PhpK[252]). Very recently, *in vitro* activity of TsrM[253], PhpK[254], and GenK[255] (members of cobalamin-dependent radical SAM enzymes) has also been reconstituted and detail mechanistic investigation for them have just commenced. Therefore, although cobalamin-dependent radical SAM enzymes are likely to mediate diverse and unusual transformations, they have not been fully studied by enzymologists.

Cobalamin-dependent radical SAM enzymes distribute diversely in natural product biosynthesis including antibiotics (e.g. fosfomycin), herbicides (e.g. bialaphos), chemotherapeutic agent (e.g. mitomycin C), and photosynthetic pigments (e.g. bacteriochlorophyll), a lot of which are of clinical and industrial interest.[184] Recently, genomic studies have also found new members invovled in the biosynthesis of ladderanes and polyeheonamides belong to this group.[256-257] Characterization and mechanistic investigation of these enzymes will provide useful information for understanding these important and intriguing chemical transformations.

Reported in vitro reconstitutions

TsrM has been demonstrated to be a tryptophan methyltransferase in the biosynthesis of thiostrepton A, a macrocyclic thiopeptide antibiotic as shown in Fig. 3-21 A.[253] TsrM methylates the C2' position of trptophan (Trp) and the methylation is coupled with the production of SAH. While reconstitution of the iron-sulfur cluster is necessary for TsrM activity, the activity does not appear to be dependent on the reduction of the cluster.[253] When CD_3-SAM was used in the reaction, the product contained three deuterium atoms even in the presence of excess amount of unlabeled methylcobalamin.[253] These observations lead to the hypothesis that TsrM transfers the methyl group from SAM to cobalamin and then to the substrate.[253]

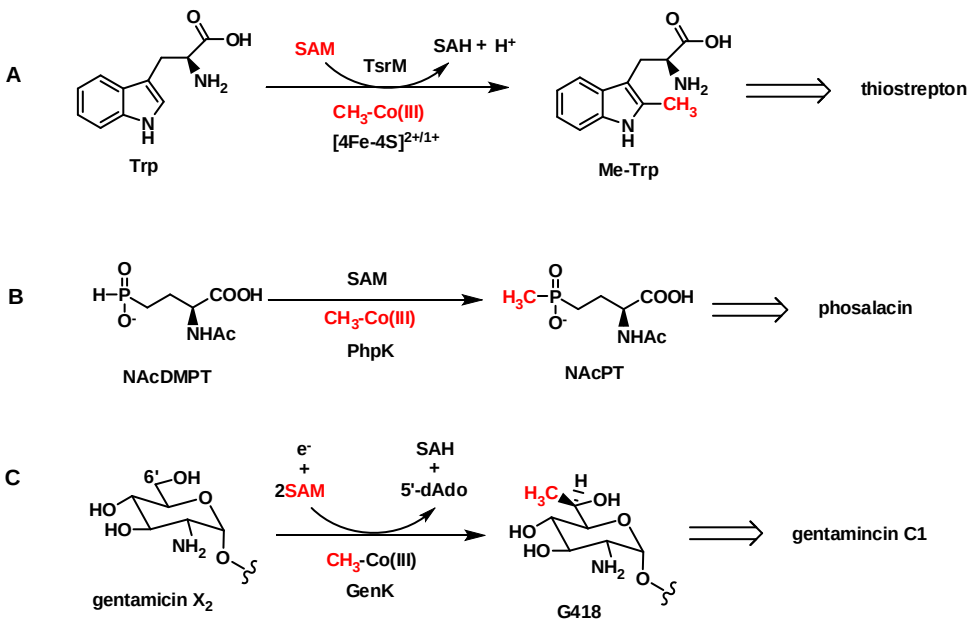

Figure 3-21: Reported *in vitro* reconstitutions for cobalamin-dependent radical SAM enzymes.

PhpK catalyzes the methylation of the phosphorous center of NAcDMPT (*N*-acetyldemethylphosphinothricin) (Fig. 3-21 B) and requires a reduced iron sulfur cluster

unlike TsrM.[254] The methyl donor in this reaction is believed to be methylcobalamin based on the isotope labeling experiments.[254] However, whether SAM is converted to SAH or 5'-dAdo has not been elucidated and the stoichiometry of the reaction is not yet known.[254]

Very recently, another cobalamin-dependent radical SAM methyltransferase GenK (Fig. 3-21 C) in the biosynthesis of gentamicin was characterized *in vitro* by our group.[255] In this case, 5'-dAdo and SAH are produced with the consumption of two SAM molecules upon the methylation of gentamicin X_2 and reduction of the iron-sulfur cluster is necessary.[255] Isotope labeling experiments support the hypothesis that the methyl group of SAM is transferred to cobalamin.[255]

Fom3 from S. wedmorensis and OxsB from B. megaterium NK84-0218

A close homolog of PhpK is Fom3. Fom3 from *Streptomyces fradiae* and *S. wedmorensis* is another putative cobalamin-dependent radical SAM methyltransferase involved in the biosynthesis of fosfomycin. Fosfomycin is an antibiotic with clinical utility against both gram-positive and gram-negative bacteria and acts by perturbing cell wall biosynthesis.[258] With the pioneering work done by Seto's group and recent studies carried out by van der Donk's group, the biosynthetic pathway of fosfomycin in *Streptomyces* has been described as shown in Fig. 3-22.[249-250,259-262] Results from gene disruption and feeding experiments suggest that the biological function of Fom3 is likely to convert 2-hydroxyethylphosphonate (HEP) to 2-hydroxypropyl phosphonic acid (HPP).[249] Methylation at the intrinsically non-nucleophilic alcohol bearing carbon center implies unprecedented chemistry. However, no *in vitro* characterization of this interesting cobalamin-dependent radical SAM enzyme has yet been reported.

OxsB, is one of the few reported cobalamin-dependent enzymes that may mediate intramolecular rearrangement instead of a methylation reaction (see Fig. 3-23 A). OxsB is believed to be the component of the oxetanocin A (OXT-A) biosynthetic pathway that is responsible for the ring contraction that ultimately produces one of the only two known naturally occurring oxetane ring containing nucleosides.[263] OXT-A is isolated from *Bacillus megaterium* NK84-0218 and exhibits antiviral activity against DNA virus species (e.g. herpes simplex virus-II) but not RNA viruses. It also possesses antibacterial activity towards specific strains such as *Staphylococcus aureus 209P*, but not towards most other bacteria, yeast, and fungi.[264] While the other naturally occurring oxetane ring containing nucleoside, albucidin, demonstrates herbicide activity instead.[265] In the past decade, researchers have been successful in synthesizing different oxetanocin analogues for their potential use in drug development.[266-267] However, little is known regarding the biosynthesis of oxetane ring.

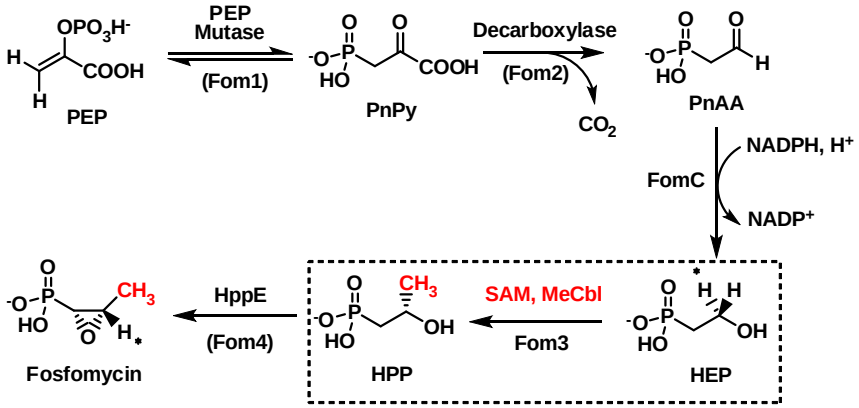

Figure 3-22: Biosynthetic pathway for fosfomycin including the Fom3 catalyzed penultimate step.

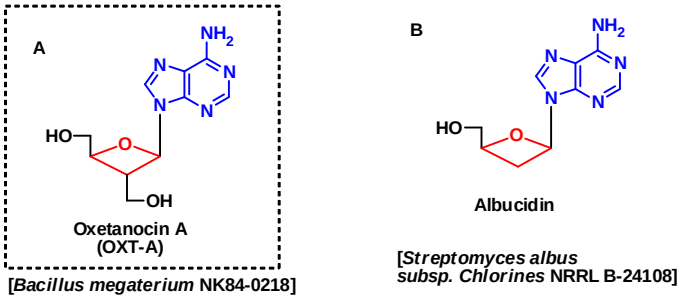

Figure 3-23: Structures and producing strains of oxetane ring containing nucleoside natural products.

3.1.4. Thesis statement

The focus of this chapter is to describe the characterization of two cobalamin-dependent radical SAM enzymes *in vitro*: Fom3 from *S. wedmorensis* and OxsB from *B. megaterium* NK84-0218. Fom3 is a putative methyltransferase that catalyzes C-C bond formation at a non-reactive carbon center. OxsB is likely to be involved in oxetane ring formation using radical SAM chemistry.

Heterologous overexpression of Fom3 in *E. coli* yielded largely insoluble protein. At the beginning, efforts were made to improve the protein solubility via the following methods: (1) variation of media and growth conditions, (2) changes of expression constructs, (3) alteration of the expression host, and (4) revision of the assigned open reading frame for this gene. However, all attempts gave no significant improvements. In the mean time, enzyme activity assays were carried out to discern whether the small amount of soluble Fom3 that could be isolated might exhibit methyltransferase activity. Unfortunately, no activity was found despite these efforts. Inspired by the results from PhpK and GenK studies, more recent attempts to obtain *in vitro* active Fom3 have

focused on refolding the protein from their inclusion bodies. Currently, we are still working on this project and future directions will be discussed.

The challenge for studying OxsB shifted from obtaining soluble protein to identifying the putative substrate. Limited information regarding to the biosynthesis of OXT-A has been reported. Morita *et al.* suggested that four plasmid encoded genes including *oxsB* are likely responsible for the biosynthesis and resistance of OXT-A.[263] Since neither the producing strain nor the plasmid encoding the genes was available, we synthesized the four genes based on the published sequence and overexpressed their encoded proteins in *E. coli*. This allowed the isolation of OxsB along with two putative phosphohydrolases in soluble form. Further biochemical characterization demonstrated that anaerobically reconstituted OxsB catalyzes the homolytic cleavage of SAM in the presence of dithionite and cobalamin to give 5'-sulfinic-adenosine (5'-sAdo) as shown in Fig. 3-24. The mechanism for this uncoupled reaction of OxsB was also investigated. A great deal of effort has also been made to elucidate the substrate of OxsB; however, no clear conclusion can be drawn at this point. The proposed function of OxsB as well as possible biosynthetic pathways of OXT-A will be discussed, and the future direction of this project will be outlined.

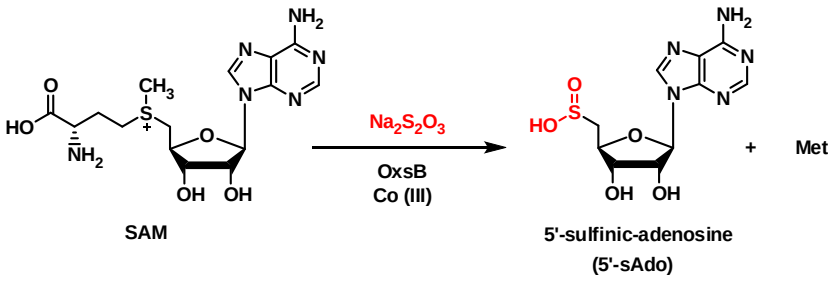

Figure 3-24: Homolytic cleavage of SAM mediated by oxsB as uncoupled reaction.

Cobalamin-dependent radical SAM enzymes participate in diverse biosynthesis pathways and likely catalyze chemically or biochemically unprecedented transformations. Currently, only three members have been characterized *in vitro* and the detail mechanisms of these enzymes are still unclear. Studies carried out in this chapter provide valuable information for understanding this interesting sub-family of radical SAM enzymes and suggest new avenues of future investigation.

3.2. MATERIALS AND METHODS

3.2.1. General

DNA sequencing was performed by the Core Facilities of the Institute of Cellular and Molecular Biology at the University of Texas at Austin. The general methods and protocols for recombinant DNA manipulation were followed according to Sambrook and coworkers.[53] Mass spectra for protein samples was performed at the Mass Spectrometry Core Facility in the College of Pharmacy at the University of Texas at Austin. Mass spectroscopy of isolated small molecules was performed at the Mass Spectrometry Core Facility in the Department of Chemistry and Biochemistry at the University of Texas at Austin.

Materials

The *Escherichia coli* protein expression host strain BL21 star (DE3) was from Invitrogen (Calsbad, CA) and Rosetta II (DE3) was acquired from Novagen (Madison, WI). The 1 kb plus ladder is a product of Invitrogen. DNA markers, restriction enzymes, and T4 DNA ligase were also obtained from Invitrogen. PCR primers were purchased from Integrated DNA Technologies, Inc (Coralville, IA). The plasmid pDB1282, which encodes genes for iron-sulfur cluster biosynthesis, was a generous gift from Professor Dennis Dean at Virginia Polytechnic Institute and State University. Anti-His (*C*-terminal) and Anti-His (*N*-terminal) monoclonal murine antibodies were obtained from Invitrogen. All chemicals and reagents were purchased from Sigma-Aldrich Chemical Co. (St. Louis, MO), Thermo Fisher Scientific (Waltham, MA), or VWR (Radnor, PA), and were used without further purification unless otherwise specified. Amicon® centrifugal filter devices are products of Millipore (Billerica, MA). Sephadex G-25 resin was purchased from GE healthcare (Pittsburgh, PA). Fom3 protein, expressed and/or purified under

specific conditions, was provided by Dr. Yung-nan Liu. *E. coli* flavodoxin (FLD), flavodoxin reductase (FDR),[268] tobacco etch virus (TEV), and 5′-methylthioadenosine/*S*-adenosylhomocysteine nucleosidase (MTAN) enzymes were purified by Dr. Yung-nan Liu. SAM were provided by Dr. Mark W. Ruszczycky. The compounds 2-hydroxyethylphosphonate (HEP) and 2-hydroxypropyl phosphonic acid ((*S*)-HPP), as well as protein HppE (Fom4) were provided by Dr. Wei-chen Chang.[269] Oxetanocin A was synthesized by Dr. Sei-Hyun Choi.

Instrumentation

Most of the instruments used in this chapter have been described in the previous two chapters. In addition, the Corona Charged Aerosol Detector was purchased from ESA-dionex under Thermo Scientific (Sunnyvale, CA). The ÄKTA FPLC system and MonoQ^{TM} column were purchased from GE healthcare (Pittsburgh, PA). The sonic dismemberator model 100 from Thermo Fisher Scientific (Waltham, MA) was used in the glove-box for anaerobic purification. The carousel 5600 slide projector used for illumination is a product of Kodak (Rochester, NY). Centrifugation tubes used for anaerobic purification were obtained from Beckman-Coulter (Arlington Heights, IL). Econo-Pac® 10DG desalting columns were purchased from Bio-Rad (Hercules, CA).

3.2.2. Cloning, expression, and purification of Fom3

Recombinant DNA constructs used to express Fom3 in E. coli system

Recombinant DNA constructs containing *fom3* gene are illustrated in Fig. 3-25. The constructs were designed to increase the solubility of Fom3 and prepared by cloning the *fom3* gene from *S. wedmorensis* into the target expression vector. Sequences of the primers used for cloning the *fom3L* gene (*fom3* with an *N*-terminal extension) were: 5'-ATTACGA**CATATG**AGCACTAAACAGAATCTCATGACGATCGGTTCTCTG-3'

(the restriction site is in bold, and the start codon is underlined) for the forward primer; 5'-CCG**AAGCTT**T*TAG*TACTGGTTTGCGTTCCAC-3' (the stop codon is in italics) for the reverse primer used to prepare a *N*-His_6-tagged construct; and reverse primer 5'-CCG**AAGCTT**GTACTGGTTTGCGTTCCAC-3' used to prepare a *C*-His_6-tagged construct. All Fom3 recombinant DNA constructs contained a kanamycin resistant gene as the antibiotic marker for selection. The published sequence for Fom3 is composed of 1,605 base pairs. Therefore, the following primer was designed for sequencing purposes: 5'-CTGGACCACATCCCGTTCC-3'. The TEV enzyme is a site-specific cysteine protease found in the tobacco etch virus (TEV). It recognizes the sequence "ENLYFQ(G/S)" and the cleavage occurs between Gln and Gly/Ser. In this study, the TEV enzyme was over-expressed and purified as an *N*-His_6-tagged protein. MBP-TEV-Fom3/Fom3L was designed as a self-cleavable fusion protein to increase the solubility of Fom3.[270]

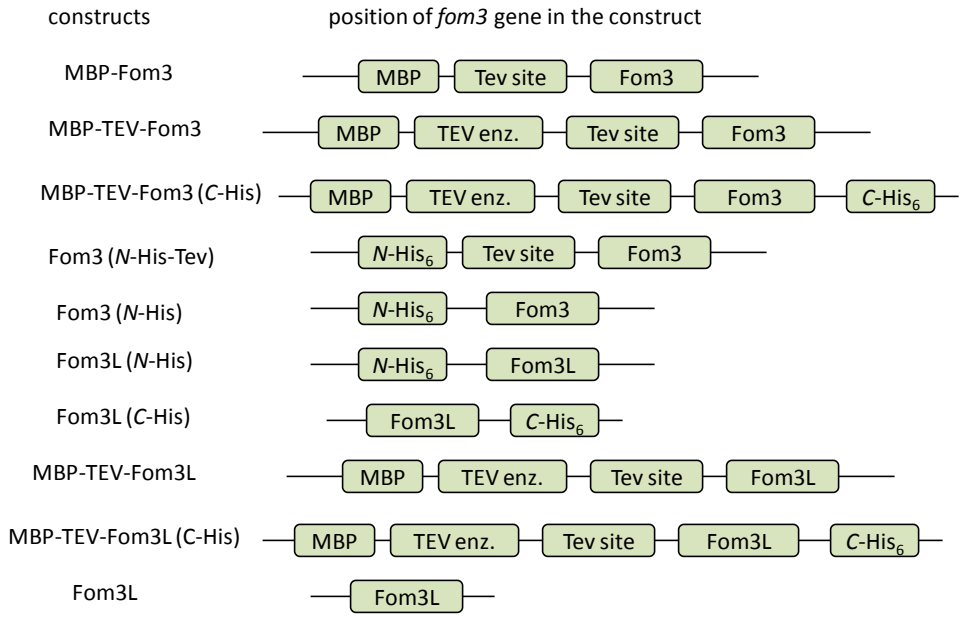

Figure 3-25: Cartoon diagram of different Fom3 constructs.

MBP stands for maltose binding protein, which is commonly used to enhance the solubility of its fused protein in the *E. coli* expression system.[271] "Tev site" stands for TEV enzyme cleavage site. "TEV enz." stands for TEV enzyme.

Conditions for expression and purification of Fom3

A construct encoding the *fom3* gene was co-transformed with plasmid pDB1282 into the target host strain. Plasmid pDB1282 contains a gene cluster that is involved in the iron-sulfur cluster biosynthesis as shown in Fig. 3-26.[272] Equal concentrations of a Fom3 recombinant plasmid and plasmid pDB1282 DNA were added to 100 μL of competent cells (*E. coli* BL21 Star (DE3) or Rosetta II (DE3)) and incubated on ice for 30 min. The procedure to prepare competent cells was identical to that described in Chapter 2. After incubation, the cells were subjected to heat shock at 42 °C for 60 s, followed immediately chilling on ice for 2 min, at which point 500 μL of LB medium was added to the cells. Subsequently, the cells were incubated at 37 °C for 1 h and centrifuged to collect the cell pellet. After decanting the majority of the medium, the cells were resuspended in the remaining 100 μL LB medium and were spread onto a LB-agar plate containing both kanamycin (Kan, 50 μg/mL) and ampicillin (Amp, 100 μg/mL). The resulting LB plate was then incubated at 37 °C for 16 h.

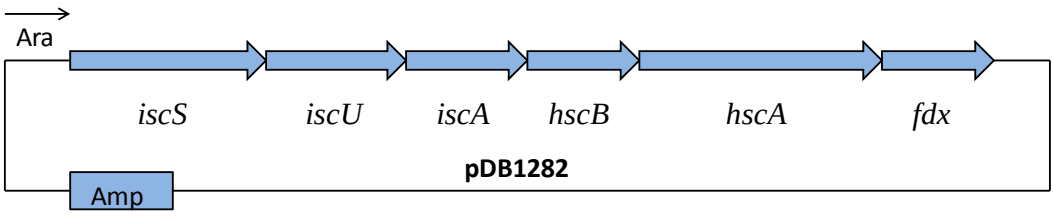

Figure 3-26: Plasmid pDB1282 encodes a gene cluster for ion-sulfur cluster biosynthesis. Expression of the gene cluster can be achieved by addition of L-arabinose. The plasmid contains an ampicillin resistant gene for antibiotic selection.

Typically, an overnight culture of Fom3/pDB1282 grown at 37°C in LB media with kanamycin and ampicillin was used, in a 200-fold dilution, to inoculate 1 L of the same media. The culture was incubated at 37°C with vigorous shaking until the OD_{600} reached 0.2. Expression of iron-sulfur cluster biosynthesis proteins were induced by addition of 0.5 g L-arabinose (Ara), and 40 mg $Fe(NH_4)_2(SO_4)_2$ along with 20 mg L-cysteine were also added to the media to facilitate iron-sulfur cluster biosynthesis. The resulting culture was grown at 30 ºC till the OD_{600} reached at lease 0.6. The culture was then cooled at 4.5 ºC for 2 h and IPTG was added to a final concentration of 0.1 mM to induce expression of the target protein. The culture was then incubated at a specific temperature (18, 22, and 15 °C have been tested, and in most cases 18 °C was used) with slow shaking. After incubation 18 h at 18 ºC, 12 h at 22 ºC, or 22 h at 15 ºC, the cells were harvested by centrifugation at 4 °C and stored at –80 °C until purification.

In some cases, deaerated buffers were used to purify Fom3. To prepare the deaerated buffer, pre-chilled buffer was degassed under vacuum with vigorous stirring for 30 min and saturated with argon gas. This process was repeated three times. The standard Ni-NTA purification procedure was used to isolate His_6-tagged Fom3 proteins. Two buffers have been used in the purification of Fom3: 50 mM Tris buffer (pH 8.0) and 50 mM HEPES buffer (pH 8.0). Other buffer components included 10% glycerol (v/v), 1 mM 2-mercaptoethanol, NaCl (300 mM in lysis buffer, 1 M in wash buffer, 300 mM in elution buffer, and 50 mM in dialysis buffer). In lysis buffer, 1 mM phenylmethanesulfonyl fluoride (PMSF) was added before use. In some cases, detergent (1% Triton X-100 (v/v)) was also added to the buffer in order to increase the solubility of Fom3. After dialysis, proteins were flash frozen and stored at –80 °C before reconstitution. Protein concentrations was determined by Bradford assay.[52] Protein expression and purification was evaluated by 12% SDS-PAGE. Urea (4 M final

concentration) was added to the samples that contained crude cell lysate or cell pellet in order to solubilize the inclusion bodies.

Purification of non-tagged Fom3 from MBP fusion protein

Non-tagged Fom3 was obtained from *in vitro* TEV enzyme cleavage of the MBP-Fom3 fusion protein. First, the standard Ni-NTA procedure was used to purify the MBP-Fom3 fusion protein. After dialysis, the MBP-Fom3 fusion protein was co-incubated at 4 ºC for 16 h with the TEV enzyme, which had been purified separately as an *N*-His_6 tagged protein. The resulting protein mixture (*C*-His_{10} tagged MBP, Fom3, and *N*-His_6 tagged TEV) was then loaded onto a Ni-NTA column and the flow through, which theoretically should have contained only the non-His tagged Fom3, was collected and concentrated. Fom3 obtained from this procedure had two additional amino acids "GH" at the *N*-terminus compared to wild type enzyme.

Anaerobic purification of Fom3

Water and buffers used in anaerobic purifications were prepared by stirring the degassed buffer in the glove-box overnight under the anaerobic condition. All steps were carried out in the glove-box except for centrifugation. When Fom3 was purified anaerobically, lysozyme (1 mg/mL) and DNAases (1 μg/mL) were also added to the lysis buffer. The cell lysis was incubated in the glove-box for 30 min surrounded by ice packs. After incubation, the resulting mixture was sonicated using a benchtop dismembrator. The resulting cell lysis was transferred to centrifugation tubes equipped with an additional seal in the cap to prevent air exchange outside of the glove-box. After centrifugation at 20,000 × g for 20 min, the sealed tube was opened in the glove-box and the supernatant was transferred to a small beaker chilled with ice pack. In some instances the supernatant was assayed directly as cell free extract. Ammonium sulfate was then

added slowly to the supernatant with gentle stirring until the final concentration reached to 30% saturation. The sample was incubated for one more hour and centrifuged. After centrifugation, the resulting pellet was washed with 50 mM HEPES buffer pH 8.0 and re-suspended in (HEPES 50 mM, pH 8.0, containing 2 mM DTT, and 2% Triton X-100 (v/v)). The Triton X-100 detergent was not included in all trials. The resulting solution was desalted using a G10 pre-packed column.

Fom3 overexpressed in M9 minimal media

M9 minimal media modified according to the protocol for the cobalamin-dependent enzyme MetH[273] was also used as alternative to LB. In order to prepare 1 L of M9 minimal media, 100 mL of 10x M9 buffer, 100 mL of 10x amino acid stock, and 2.5 g of NH_4Cl were added to 780 mL of water and the resulting solution was autoclaved. Next, 10 mL of 20% glucose (w/v, pre-autoclaved), 1 mL of ethanolamine, 1 mL of 1 M $MgCl_2$ (sterilized), 1 mL of a 10 mg/mL solution of thiamine (sterilized), 100 µL of 0.1 M $ZnSO_4$ (sterilized), 0.5 mL of 0.1 M $CaCl_2$ (sterilized), 100 µL of 10,000x micronutrient (sterilized), 3 mg of vitamin B_{12} (cyanide form), 0.5 mL of Amp (100 mg/mL), and 0.4 mL of Kan (50 mg/mL) were added to the media. The 1 L 10x M9 buffer contained 67.9 g Na_2HPO_4, 30 g KH_2PO_4, and 6 g NaCl at pH 7.4. The 10x amino acid stock solution was prepared by dissolving 0.715 g Ala, 0.728 g Arg, 0.6 g Asn, 0.507 g Asp, 0.35g Cys, 0.88 g Glu, 0.875 g Gln, 0.6 g Gly, 0.31 g His, 0.525 g Ile, 1.05g Leu, 0.584 g Lys, 0.6 g Met, 0.66 g Phe, 0.46 g Pro, 10.5 g Ser, 0.475 g Thr, 0.205 g Trp, 0.37 g Try, and 0.705 g Val in 1 L water and adjusting the pH to 7.5. The resulting stock solution was autoclaved for 5 min and stored at 4 °C. BL-21 star DE3 cells harboring the Fom3 expression vector along with the plasmid PDB1282 were grown in 10 mL LB

media overnight at 37 ºC. After centrifugation and decanting the LB media, the cell pellet was used to inoculate the 1 L M9 media.

Reconstitution of Fom3

Reconstitution of purified Fom3 was carried out in the glove-box and anaerobic buffers were used. Except Fom3, all other components used in the reconstitution were brought to the glove box as solids and their corresponding stock solutions were prepared in the glove-box with anaerobic buffers or water. Typical reconstitution procedures for Fom3 are as follows. Approximately 2 mL of protein purified aerobically (including the ones purified with degassed buffers) was stirred in the glove-box at ~ 10 ºC for 3 h to remove all the oxygen dissolved in the protein solution. DTT was then added to a final concentration of 5 mM. After 15 min of incubation, 0.5 mM of SAM (final concentration) was added to the solution. The resulting solution was stirred for another 5 min and then 1.5 mM of $Fe(NH_4)_2(SO_4)_2$ (final concentration) was added in 10 aliquots over 10 min, followed by adding 1.5 mM of Na_2S (final concentration) in 20 aliquots over 20 min. The resulting solution was incubated for an additional 3 h to 5 h, and 0.5 mM MeCbl (final concentration) was then added. The resulting solution was incubated for 1 h in dark. After centrifugation to remove precipitates, the mixture was loaded onto a G10 pre-packed desalting column that was pre-equilibrated with the storage buffer (50 mM HEPES, pH 8.0, 1 mM DTT, 10% glycerol). The colored fractions were collected and checked by Bradford assay. Fractions that had relative high protein content were combined and concentrated with YM10 spin columns in the glove-box. The resulting reconstituted Fom3 was stored in the glove box at approximately 10 ºC and used within two days.

3.2.3. Fom3 activity assay

Preparation of Ti(III) citrate solution

The titanium (III) citrate solution was prepared anaerobically from $TiCl_3$ following the protocol of Jarrett and Matthews.[274] In the glove-box, 4.5 mL of 0.2 M sodium citrate was added to 0.5 mL $TiCl_3$ (12% HCl) and stirred for 30 min. Then 1.5 mL of saturated sodium bicarbonate was added slowly to neutralize the solution. Finally, 3.5 mL of 100 mM Tris buffer, pH 7.5 was added and the solution was stirred overnight. The solution was then stored in the dark in the glove-box and used within a month.

Fom3 activity assay conditions

A typical assay of Fom3 activity included the following components: 50 mM HEPES or Tris buffer at pH 8.0, the putative substrate HEP (2–10 mM, measured by weight), SAM (2–10 mM, determined by UV, ε_{260} = 15,400 $M^{-1}cm^{-1}$), MeCbl or OHCbl (0.5–5 mM, determined by weight), DTT (2–10 mM), $MgCl_2$ (1 mM), reconstituted Fom3 protein (5–30 μM, determined by Bradford assay) or anaerobically purified Fom3 (about 80% of the reaction volume was added). One of the following four reducing systems was also included in the assay buffer: (a) 0.3–3 mM Ti(III) citrate solution, (b) 2–10 mM NADPH, 5–20 μM flavodoxin, and 5–20 μM flavodoxin reductase, (c) 0.3–2 mM $RuCl_2$, or (d) 2–10 mM NADPH and 0.5–2 mM methyl viologen. Reactions were incubated in the glove-box at approximately 30 °C for at least 12 h. Samples were then frozen and stored at –80 °C prior to analysis.

A Fom3 reaction mixture was analyzed by first thawing and filtering it using YM10 spin columns at 4 °C to remove the protein. The resulting solution was subjected directly to either HPLC or bioassay analysis. In some cases, the following additional steps were included prior to HPLC or bioassay analysis: (1) samples were concentrated

by lyopholization after removing the protein and then redissolved in 200 μL water, or (2) samples were acidified to pH 4 with HCl after removing the protein and then passed through a small Waters OASIS® MCX cation exchange column to remove the cobalamin and titanium.

Analysis of Fom3 assays: Dionex-HPLC coupled with Corona detector

Reaction progress as defined in terms of the extent of HEP methylation was monitored by HPLC on a Dionex CarboPac PA1 anion exchange column (4 × 250 mm) coupled with a Corona detector. Corona CAD (charged aerosol detector) can detect any nonvolatile or semivolatile analyte with or without a chromophore and is compatible with HPLC system. Therefore, the putative substrate HEP and the expected product (*S*)-HPP can be detected using this detection method since they both possess a monophosphate group but not a chromophore. Typical HPLC programs employed the following gradient. Solvent A is water and solvent B is 200 mM NH_4OAc, pH 7.0. From 0 to 5 min, 12.5% B was used to isocratically. At 5 min, B increased to 25% linearly in 5 min, at which point it was further increased to 32.5% linearly in 30 min, and then to 90% linearly in 2 min. After 5 min, B was decreased back to 12.5% linearly in 2 min, and the column was washed with that mobile phase composition for 6 min before the run was stopped. The flow rate was 1 mL/min, and the UV detector was set at 260 nm whenever dual detection was utilized.

Analysis of Fom3 assays: C18-HPLC coupled with UV detector

The anticipated products SAH and 5'-dAdo from the enzymatic assays were difficult to distinguish using an anion exchange column. Therefore, samples were also subjected to a Varian Microsorb MV 100-5 C18-HPLC chromatography (analytical column dimensions: 4.6 × 250 mm) with UV detection at 260 nm. Column elution was

typically as follows. Solvent A contained 0.1% TFA in water (v/v) and solvent B was methanol. The elution was begun with 5% B for 5 min before increasing B linearly to 35% B in 30 min, where it was maintained isocratic for 6 min. Following the 6 min isoctratic elution, B was decreased linearly back to 5% B in 1 min, where it was maintained isocratic for an additional 4 min before the run was stopped. In some cases, solvent A was replaced with 5 mM NH_4OAc at pH 6.0, while a similar gradient program was used. The flow rate was held constant at 1 mL/min for the duration of the HPLC run.

Analysis of Fom3 assays: bioassay

Another approach to analyze the activity of Fom3 was to use HppE to convert the expected product, (*S*)-HPP, to fosfomycin as shown in Fig. 3-22. Fosfomycin exhibits a strong inhibitory effect on the growth of the *E. coli* K12 strain HW8235.[275] Therefore, if (*S*)-HPP is formed in the Fom3 catalyzed reaction, a coupled enzymatic assay with HppE would result in inhibition of bacterial growth.[275] Specifically, an overnight culture (2 mL) of the *E. coli* K12 strain HW8235 in LB media was mixed with 50 mL of warm, autoclaved LB agar and poured into a Petri dish. After the agar had solidified, sterilized paper discs (13 mm in diameter) were placed on top of the agar. Approximately 20 μL of sample was applied to the paper disc, and the plate was incubated at 37°C for 6-12 h. The diameter of the inhibition zone was then measured by ruler and compared with the results from positive and negative control reactions performed in a parallel manner. A typical reaction volume for this bio-assay was 50 μL, containing 10 μM HppE, 4 mM NADH, 100 μM FAD, 50 μM Fe^{2+}, in 25 mM Tris buffer at pH 7.5 with Fom3 reactions (after anaerobic incubation) or controls (including standards compounds with proper concentration such as fosfomycin, HEP, and HPP). Reactions were carried out

aerobically at 37 °C for 2.5 h and then centrifuged. The resulting supernatant was loaded onto the paper discs directly in 20 µL volume.

3.2.4. Cloning, expression, and purification of four putative ORFs in OXT-A biosynthesis

Design and Cloning of oxsA, oxsB, oxrA, oxrB, and oxsB-3A

Neither the oxetancoin A (OXT-A) producing strain nor the plasmid containing the biosynthetic genes for OXT-A were available at the time this project was started. Therefore, the published genes responsible for the biosynthesis of OXT-A (NCBI, accession No. AB005787, 6.8 kb) were used as a template to design the target expression genes. The free online software FramePlot 2.3.2 was used to analyze the fragment (6.8 kb) and four open reading frames (ORFs) were assigned. For each ORF, the reported sequence was optimized for *E. coli* expression using the online software GeneOptimizer® available through Mr. Gene® (later changed to GeneArt® under Life Technologies, Grand Island, NY) and manually checked to exclude *NdeI*, *HindIII*, *XbaI*, and *SpeI* restriction site sequences as well as poly A (equal to 6 or greater) and poly G (equal to 5 or greater) sequence motifs. Four designed genes (*oxsA*: 593 bp, *oxsB*: 2243 bp, *oxrB*: 987 bp, and *oxrA* 567 bp) were purchased from Mr. Gene®. The four genes were then sub-cloned from the pANY vectors, in which the synthetic genes were encoded, to pET28b(+) vectors using *NdeI*/*HindIII* sites, respectively. The *oxsB* gene was also sub-cloned into the MalE-pET vector (generated in house) to obtain the nearly native protein form (i.e., possessing Gly-His at the *N*-terminus) after TEV cleavage. A triple mutant of OxsB was also prepared using the following primers: 5'-CTGGAAACCAGTCGTGGTGCCGATTATTCACGCGCCACGTTTGCCCCACGTAC CAC-3' as forward primer, and the sequence for the reverse primer was 5'-

GTGGTCACGTGGGGCAAACGTGGCGCGTGAATAATCGGCACCACGACTGGTT TCCAG-3' (the codon for the mutated residue is underlined, three cysteine residues were mutated to alanine residues). Primer 5'-CCGGAGCAATTCTTCGAACGC-3' was designed for sequencing recombinant DNA containing the *oxsB* gene.

Expression and purification of OxsA, OxsB, OxrA, OxrB, and OxsB-3A

Expression and purification procedures for OxsA, OxrA, and OxrB were identical to those used to purify other *N*-His_6 tagged proteins (such as MoeZ and its mutants) as described in Chapter 2. Dialysis buffer contained 50 mM HEPES at pH 8.0, 15% glycerol (v/v), 100 mM NaCl, and 1 mM 2-mercaptoethanol. The lysis buffer was identical to the dialysis buffer but contained 300 mM NaCl and 10 mM imidazole. The wash and elution buffers were also the same as the dialysis buffer but contained 500 mM NaCl and 25 mM imidazole (wash buffer) or 300 mM NaCl and 200 mM imidazole (elution buffer). Protein concentrations were determined by Bradford assay and protein purity was assessed by SDS-PAGE.

OxsB and OxsB-3A have been expressed either with or without the *N*-His_6-tag (with a Gly-His two-amino acid sequence at the *N*-terminus). The protocol and buffer used to purify the *N*-His_6-tagged form of OxsB or OxsB-3A was identical to that described above. For the non-tagged OxsB and Oxs-3A, the general protocol was similar to that used for obtaining the non-tagged Fom3 from the MBP fusion protein. Specifically, expression vector encoding *oxsB* or *oxsB-3A* was co-transformed into *E. coli* BL-21 Star DE3 competent cell with plasmid pDB1282. A 10 mL overnight small culture grown in LB was then used to inoculate 1 LB media containing 60 mg/L of Amp, 20 mg/L of Kan, 3 mg/L vitamin B_{12} (cyanide form), and 1 mL ethanolamine. The culture was incubated at 37 °C with vigorous shaking until the OD_{600} reached to 0.2, at which

point 40 mg/L of $Fe(NH_4)_2(SO_4)_2$, 20 mg/L of L-cysteine hydrocholoride monohydrate, and 0.5 g/L of L-arabinose were added to the media as solid form. The temperature was then decreased to 30 °C and the culture was incubated until the OD_{600} reached to 0.6, whereupon the culture was moved to an ice-water bath for 20 min and approximately 0.15 mM IPTG (as final concentration) was added to the culture. The flask was then sealed with parafilm and covered with aluminum foil and grew at 18 °C with slow shaking for 20 h. The cells were harvested at 45,000 × g by centrifugation, and the cell pellets were collected and stored at –80 °C.

Purification of OxsB and OxsB-3A was carried out aerobically. The cell pellets (approximately 10 g each) were re-suspended in 40 mL lysis buffer (50 mM HEPES, pH 8.0, 300 mM NaCl, 10 mM imidazole, 10% glycerol, 2 mM 2-mercaptoethanol, and 2 mM PMSF). The resulting suspension was sonicated to lyse the cells. The cell lysate was centrifuged, and the supernatant was incubated with Ni-NTA resin at 4 °C in the dark for 1 h. The mixture was then loaded onto a column and washed with 250 mL wash buffer (50 mM HEPES, pH 8.0, 500 mM NaCl, 25 mM imidazole, 10% glycerol, and 2 mM 2-mercaptoethanol). Then approximately 50 mL elution buffer (50 mM HEPES, pH 8.0, 300 mM NaCl, 200 mM imidazole, 5% glycerol, and 2 mM 2-mercaptoethanol) was used to elute the fusion protein. The collected protein was dialyzed (50 mM HEPES, pH 8.0, 100 mM NaCl, 5% glycerol, and 2 mM 2-mercaptoethanol), and a 5% (w/w) solution of *N*-His_6-TEV protease was added. The solution was incubated at 4 °C in the dark for 18 h with gentle agitation. Then the resulting mixture was incubated with Ni-NTA resin again for one hour and loaded onto a column. The flow through was collected with a flow rate of one drop per 5 s and the resin was washed with 20 mL lysis buffer. The combined flow through was re-loaded onto the same resin one more time and the flow through was collected again with a flow rate of one drop per 10 s. The OxsB (or OxsB-3A) in the flow

through was concentrated using YM10 centrifugal filtration and dialyzed before being flash frozen and stored at –80 °C.

Reconstitution of OxsB and OxsB-3A

Reconstitution of OxsB and OxsB-3A were performed in the anaerobic glove-box. Two typical protocols were applied for OxsB reconstitution. The first one is identical to the one described for Fom3 reconstitution. The second one is modified slightly based on the published protocol for the DesII radical SAM enzyme.[272] Before reconstitution, about 5 mg OxsB was thawed on ice and transferred to two 2 mL pre-chilled conical vials. The sample was brought into the glove-box and surrounded by ice packs. The enzyme was then diluted with pre-chilled anaerobic buffer (40 mM HEPES, pH 8.0) and stirred for 1.5 h with the cap off to deaerate. Following the deaeration, the solution was incubated for 15 min with 5 mM DTT (100 mM stock in anaerobic water). The solution was incubated for 5 min with 1 mM SAM (from Sigma, 100 mM in water determined by weight). The solution was then made to contain 2 mM $Fe(NH_4)_2(SO_4)_2$ by adding 100 μL of a 40 mM stock in anaerobic water over 10 min. This was followed by the addition of 100 μL of a 40 mM stock of Na_2S in 100 mM HEPES (pH 8.0) over 20 min to make the reconstitution mixture 2 mM in Na_2S. The resulting solution was incubated for additional 3 h at approximately 10 °C with gentle stirring. After centrifugation to remove any precipitant, the mixture of roughly 4 mL was loaded onto a Sephadex-G25 column pre-equilibrated with 25 mM HEPES at pH 8.0 and eluted with the same pre-chilled buffer. Dark colored fractions were pooled and combined to a final volume of 3 mL. The concentration of protein was determined by Bradford assay. The reconstituted enzyme was kept in the glove-box at approximately 10 °C.

3.2.5. Basic characterization of reconstituted OxsB

UV-vis spectroscopic characterization of iron-sulfur clusters

All the steps were performed in the glove-box unless otherwise specified. A typical sample volume for UV-vis spectrophotometry was approximately 120 μL. All stock solutions were prepared in the glove-box using anaerobic water or buffer. Stock solutions of different types of cobalamin (i.e., methylcobalamin, adenosylcobalamin, hydroxocobalamin, and cyanocobalamin) were kept in the dark on ice.

Iron titration

The iron content of OxsB was determined by the assay developed by Fish with slight modifications and carried out under aerobic conditions.[276] The standard curve was determined using $Fe(NH_4)_2(SO_4)_2$. Typically, 200 μL of sample (containing standard iron solution or diluted protein) was rapidly mixed with 100 μL freshly prepared $KMnO_4$ solution (1:1 mixture (v:v) of 1.2 M HCl and 0.285 M $KMnO_4$) and incubated at 60 °C for 2 h. The samples were then centrifuged, and 20 μL of iron-chelating reagent (containing 6.5 mM ferrozine, 13.1 mM neocuproine, 2 M ascorbic acid, and 5 M ammonium acetate in water, stored in the dark at room temperature and used within three weeks of preparation) was added and vortexed quickly. After incubation at room temperature for 1 h, the resulting solutions were centrifuged again and loaded into the 96-well plate (200 μL per well). The absorbance of the samples was measured at 562 nm.

Sulfur titration

The labile sulfur content of OxsB was determined by a colorimetric assay developed by Beinert and was performed aerobically.[139] The standard curve was determine using Na_2S (prepared from dissolving stock solution in 0.1 M NaOH). A volume of 160 μL standard or diluted protein was added to 40 μL EDTA (100 mM, pH

7.5) and incubated at room temperature for 1 h. A freshly prepared 1% zinc acetate solution (600 μL) was mixed with the sample at the bottom of the tube, followed by 30 μL of 3M NaOH. The mixture was vortexed until the slight pink color became homogeneous. After incubation at room temperature for 1 h, 150 μL of 0.1% *N,N*-dimethyl-*p*-phenylenediamine monohydrochloride (DMPD) in 5 M HCl was pipetted slowly to the bottom end of the tube. Next, 30 μL of 23 mM $FeCl_3$ in 1.2 M HCl was added and mixed rapidly to generate a colorless solution. The resulting solution was incubated at room temperature for at least 30 min whereupon a blue color develops. After centrifugation, 200 μL per well of supernatant was added to the 96-well plate and a plate reader was used to record the absorbance at 670 nm.

Corrinoid content determination

The concentration of cobalamin in a sample of OxsB (as isolated or reconstituted) was estimated using the UV-vis absorbance of cyanocobalamin.[277] This was accomplished by adding 5 μL of 1 M KCN in 0.1 M NaOH to 110 μL of the protein sample, and allowing the mixture to incubate at 90 °C for 20 min. The resulting solution was centrifuged and analyzed by UV-vis spectrophotometry. The absorption at 367nm and 580 nm was recorded and ε_{580} = 10,130 $M^{-1}cm^{-1}$ was used to determine the concentration of cobalamin in the sample. This assay was performed aerobically.

3.2.6. HPLC assay of OxsB activity

Non-tagged OxsB (also called (GH)-OxsB) was assayed for activity using HPLC. A typical assay solution of (GH)-OxsB activity included the following components: 0.2 mM SAM, 1 mM DTT, 1 mM sodium dithionite, and 50 μM reconstituted OxsB (using method 1 with iron, sulfide, and OHCbl). The incubation was performed in 50 mM HEPES buffer at pH 8.0 under anaerobic conditions for 4 h. Enzyme was removed by

YM10 filtration and the resulting solution was subjected to HPLC using a C18 column. The UV detector was set to 260 nm with a flow rate of 1 mL/min. Solvent A was composed of 1% NH_4OAc in water (w/v) at pH 5.0 (adjust with CH_3COOH). Solvent B was CH_3CN. A linear gradient from 2% B to 20% B in 18 min was used. Any new HPLC peak observed following the incubation compared with controls that did not have SAM, dithionite, or enzyme was isolated and dried by rotary evaporation. The sample was then re-dissolved in water to obtain a UV-vis absorption spectrum before submission to the MS facility for ESI-MS analysis. The dithionite concentration was determined by absorbance at 315 nm using an extinction coefficient of 8,043 $M^{-1}cm^{-1}$.[278]

3.2.7. Substrate screening for OxsB

A collection of commercially available purine nucleosides was used to screen for OxsB activity as shown in Fig. 3-27. Typical reaction conditions included the test substrate (0.2 to 0.5 mM), SAM (0.4 to 1 mM), OHCbl (0.1 to 0.5 mM), reconstituted OxsB (50 μM to 200 μM) and reductant (1 mM to 2 mM). As the case of Fom3, different reductants were tried including: (1) dithionite, (2) NADPH with flavodoxin and flavodoxin reductase, (3) NADPH with DTT and methyl viologen, (4) Ti(III) citrate, and (5) $RuCl_2$. Reactions were carried out in the glove-box with 50 mM HEPES buffer (pH 8.0), 1 mM $MgCl_2$ and 2 mM DTT for a period of time ranging from 2 to 18 h.

Two types of work-up were applied to these reactions. The first method was to directly remove the protein by YM10 spin column, and the filtrate was analyzed directly by HPLC with UV detection. This method was used for the test substrates without a phosophate group. For test substrates containing a phosphate group, the reaction mixture was incubated with phosphodiesterase (PDE) and/or alkaline phosphatase (ALP) for 1 h at 37 ºC. Next, a three-fold excess of MeOH (v/v) was added to the reaction mixture to

precipitate all the enzymes. The supernatant was dried by using a speed vacuum concentrator and re-dissolved in water before HPLC analysis.

In some trails, OxsA and/or OxrB were also added after or during the OxsB reaction. When these two enzymes were added, a deaeration step was performed first by gently stirring about 0.5 mL OxsA or OxrB purified aerobically in the glove-box at about 10 ºC for 1 h. On some occasions, methylthioadenosine nucleosidase (MTAN) was used to hydrolyze any SAH, 5′-deoxyadenosine, and MTA to avoid potential product inhibition.[210]

HPLC conditions used to assay for OXT-A were as follows: solvent A was 1% NH_4OAc (w/v) in water at pH 5.0, and solvent B was CH_3CN. The run was begun with a 5 min of 2% B. A linear gradient from 2% to 10% B in 18 min began at 5 min, followed by a 10% to 35% B linear gradient in 9 min. Isocratic elution of 35% B for 2 min was then followed by a return to 2% B linearly in 2 min. The column was the reequilibrated with 2% B for 5 min. A C18 column was used coupled with UV detector set at 260 nm at flow rate of 1 mL/min.

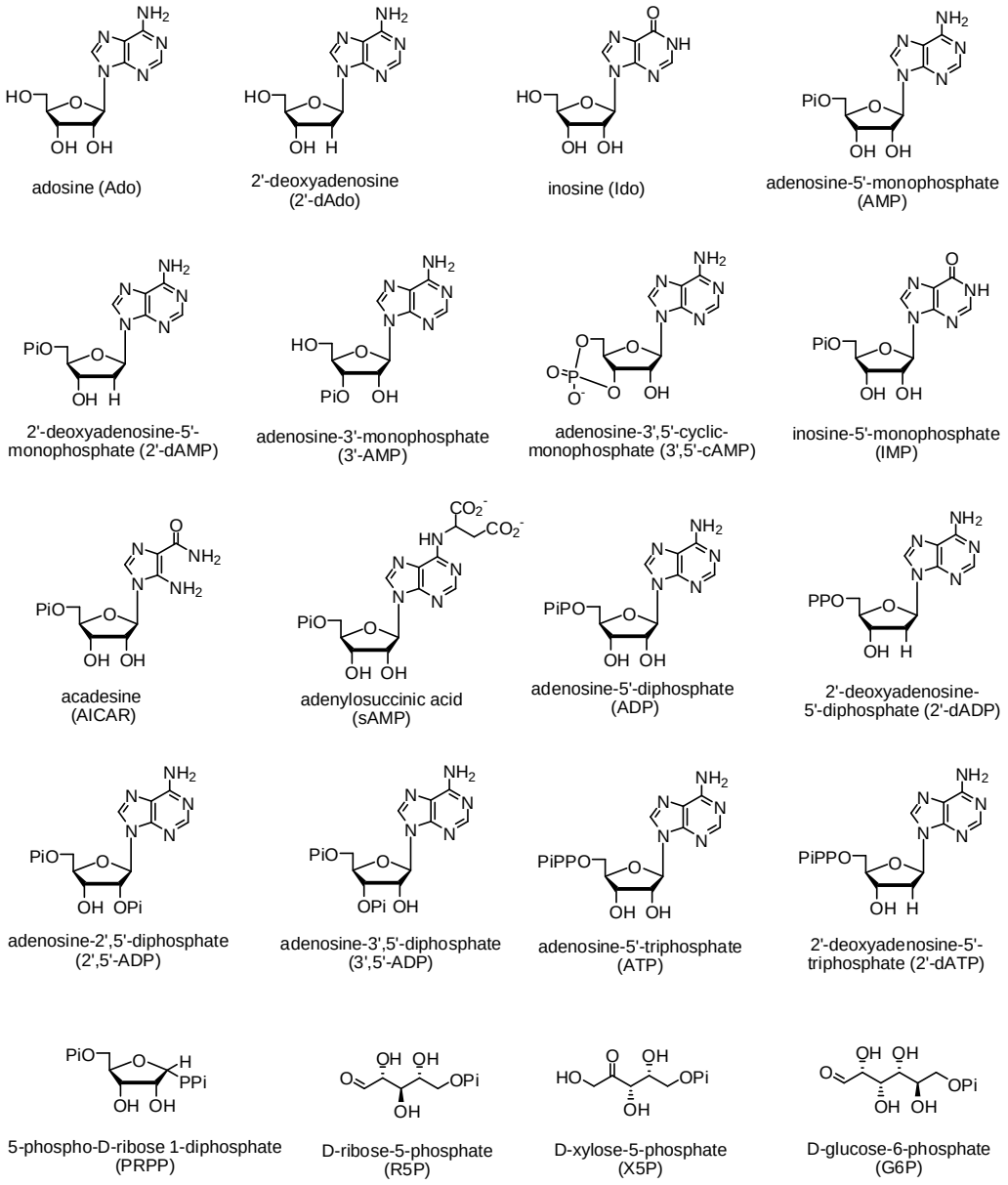

Figure 3-27: Lists of compounds tested as a potential substrate for OxsB.

3.2.8. Kinetic characterization of the deamination activity of (GH)-OxsB

Metal dependence study

To examine the metal dependence of the (GH)-OxsB catalyzed deamination reaction, parallel reactions were set up with 10 µL reconstituted or as isolated (GH)-

OxsB, 250 μM adenosine (Ado), and none or one of the following metals: (1) 1.5 mM $MgCl_2$, (2) 1.5 mM $CaCl_2$, (3) 1.5 mM $MnCl_2$, (4) 0.2 mM $ZnSO_4$, or (5) 0.2 mM $Fe(NH_4)_2(SO_4)_2$ in 25 mM HEPES buffer at pH 8.0. The reaction was incubated in the glove-box for 2 h at 30 ºC. After removal of the enzyme by YM10 filtration, the resulting solution was analyzed by HPLC using a C18 column with the UV detector set at 254 nm. The flow rate was 1 mL/min. The solvent system was the same as the one used for the assay of OXT-A. The following gradient program was applied: 2% B from 0 to 2 min, 2% to 10% B in 18 min, 10% to 30% B in 5 min, 30% B to 2% B in 2 min, and 2% B isocratic until 32 min.

Oxygen dependence study

The reactions to examine the oxygen dependence of (GH)-OxsB mediated deamination were performed under the following conditions: 25 mM HEPES, pH 8.0, 300 μM Ado, and 20 μM reconstituted (GH)-OxsB or as-isolated (GH)-OxsB. Reactions were performed both anaerobically and aerobically. Aerobic reactions were run by bringing an aliquot of reconstituted (GH)-OxsB out of the glove-box and mixing under exposure to air for 10 min. The reaction was then performed under aerobic conditions. The reactions were incubated at 37 ºC for 2.5 h and the enzyme was removed by filtration. Reactions were analyzed using the same method as that used to investigate metal dependence.

Preliminary kinetic characterization of the deamination activity

A modified quenching method and assay conditions were used to measure rates of deamination. In these assays, 0.05 mM, 0.1 mM, 0.15 mM, 0.2 mM, 0.4 mM, and 0.8 mM of adenosine was incubated with 10 μM reconstituted OxsB at 35 °C for 47 min. The reaction was quenched by the addition of a three-fold volume excess of MeOH. The

precipitates were the removed by centrifugation, and the supernatant was dried in a speed vacuum concentrator. The resulting solution was analyzed by the HPLC using an analytical C18 column and the elution method described above.

3.2.9. Studies of OxsB mediated homolysis cleavage of SAM

(GH)-OxsB reconstituted in the absence of OHCbl was incubated with different forms of cobalamin (i.e., MeCbl, OHCbl, AdoCbl, and CNCbl). Typical reaction conditions were 25 mM HEPES at pH 8.0, 0.2 mM SAM, 0.5 mM dithionite, 10 μM of reconstituted (GH)-OxsB (using the method that OHCbl was omitted), and 50 μM of the given cobalamin. Additionally, reactions were run in the absence of cobalamin as well as in the presence of 50 μM KCN. The reactions were carried out anaerobically for 2 h, frozen, and stored at –80 ºC before analysis. Enzyme was removed by YM10 filtration before HPLC. An aliquot was taken before addition of enzyme and analyzed by HPLC as well. All reactions and sample aliquots were maintained under the cover of aluminum foil as much as possible.

Samples were analyzed by HPLC with a C18 analytical column. The solvent system was similar to that used for the assay of OXT-A. The UV detector was set at 260 nm, and the flow rate was maintained at 1 mL/min. The gradient program used for the assay was as follow: 2% B from 0 to 5 min, 2% to 10% B in 18 min, 10% to 25% B in 15 min, 25% B to 2% B in 2 min, and isocratic at 2% B until 45 min.

3.3. Results and Discussion

3.3.1. Purification of different Fom3 constructs expressed in *E. coli*

Despite several attempts to increase the solubility of Fom3, the results have not been very satisfactory. For example, modification of the growth temperature had little impact. In terms of media, both M9 minimal media and 1 M sorbitol with LB conditions have been tested in addition to typical LB media. In all cases, no changes were apparent in the fraction of soluble Fom3.

The MBP-Fom3 construct yielded soluble MBP-Fom3 fusion protein when expressed in *E. coli* BL21 Star DE3 as shown in Fig. 3-28, lanes 2 and 3. However, the fusion protein was prone to degradation during the purification even with the addition of protease inhibitor PMSF (lane 4). After performing TEV enzyme cleavage for 18 h at 4.5 °C, protein precipitation was observed. After removal of the precipitates, the resulting protein solution was loaded to a Ni-NTA column and the flow through (which was supposed to contain only no tagged Fom3, 536 aa, 60,568 Da) was collected and concentrated. Multiple bands were detected in this fraction as shown in lane 7. The small band marked by the arrow in this lane might be Fom3 based on its position on the SDS-PAGE gel. However, without any tag, it could not be confirmed by western blot.

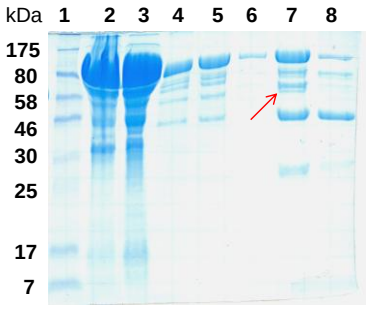

12% SDS-PAGE gel:

1. Protein Marker
2. MBP-Fom3 cell lysis
3. MBP-Fom3 supernatant after sonication
4. MBP-Fom3 fusion protein after first Ni-NTA column
5. MBP-Fom3 fusion protein dialysis before addition of TEV enzyme
6. After TEV cleavage before second Ni-NTA column
7. After second Ni-NTA column, flow through fraction collected
8. After second Ni-NTA, elution fraction collection

Figure 3-28: 12% SDS-PAGE gel of MBP-Fom3 expression and purification with TEV treatment.

Two constructs that contain the TEV enzyme encoded gene in the vector were then designed to overcome the degradation problem observed during the *in vitro* cleavage of MBP. Expression of the constructs yielded Fom3 without an affinity tag and Fom3 with a *C*-terminal His_6 tag. Fom3 without affinity tag was designed to address the possibility that the His tag would interfere with Fom3 activity. Fom3 with a *C*-terminal His_6 tag was designed for the purpose of western blotting to ensure the existence of target protein after purification. SDS-PAGE gels for Fom3 (*C*-His tagged) purified by affinity column chromatography and Fom3 (without affinity tag) isolated anaerobically using ammonium sulfate precipitation are shown in Fig. 3-29. Again, in both cases, only a very small amount of soluble Fom3 could be obtained. Similar results were obtained when the corresponding *N*-His_6 tagged constructs were considered instead.

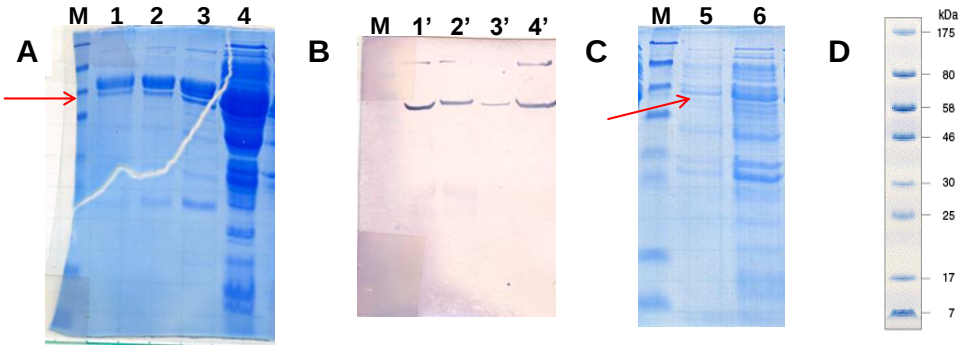

Figure 3-29: 12% SDS-PAGE of purified Fom3 from the *in vivo* TEV cleavage system.

(A) SDS-PAGE of purified Fom3 from construct MBP-TEV-Fom3 (*C*-His). Lane 1 was after Ni-NTA purification; lane 2 was isolated protein after reconstitution in the glove-box; lane 3 was supernatant after sonication; lane 4 was cell lysate. (B) Anti-*C*-His tag western-blot of the SDS-PAGE gel of A. Lane 1' to 4' corresponding to lane 1 to 4 in (A). (C) SDS-PAGE of anaerobically purified Fom3 from overexpression of construct MBP-TEV-Fom3. Lanes 5 and 6 correspond to two fractions after ammonium sulfate precipitation, reconstitution, and desalting. (D) Pre-stained protein marker used in the gels. The red arrow indicates the position of Fom3 on the SDS-PAGE based on the western result (small band under the third line of the marker). The higher molecular weight band on the western blot suggests the presence of MBP-TEV-Fom3 fusion protein that has not been cleaved by the TEV enzyme.

One possible reason for producing insoluble Fom3 in the *E. coli* system was incorrect assignment of the open reading frame, which happened occasionally.[279] When we re-examined the possible open reading frame of Fom3 including other possible start codons for *Streptomyces* such as TTG, second possible assignment was identified as shown in Fig. 3-30. The alternative *fom3* gene sequence contained extra six amino acid residues "MSTKQNL" at the *N*-terminus and the protein encoded by this sequence was denoted Fom3L.

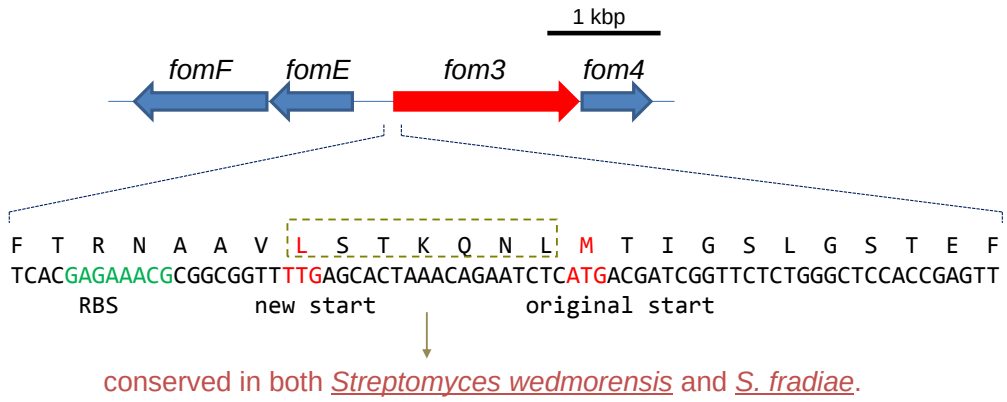

Figure 3-30: Revision of the Fom3 open reading frame assignment. RBS stands for ribosomal binding site.

New constructs containing the Fom3L sequence were prepared, and the results obtained from purification of the *C*-His tagged Fom3L are shown in Fig. 3-31. Although the solubility of the *C*-His tagged Fom3L was slightly better compared to the previous results, a large portion of the protein remained in the inclusion bodies as indicated by lane 3 in Fig. 3-31.

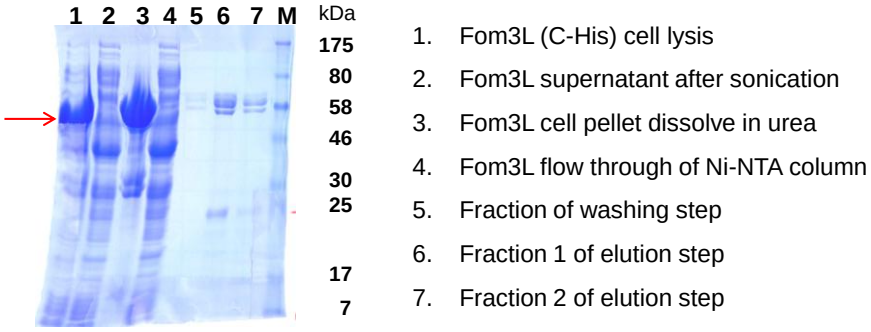

Figure 3-31: 12% SDS-PAGE gel of Fom3L with a *C*-terminal His_6 tag. After removal of methionine, this protein was expected to contain 553 amino acid residues with an expected mass of 62,565 Da. The area pointed by the arrow is where Fom3L is located according to a western blot. The big band in lanes 1 and 3 suggested that the solubility of the protein was still poor and majority of the protein was in the inclusion bodies. In the purified fractions (lane 6 and 7), Fom3L is the second major band. Bands blow 25 kDa are likely resulted from degradation of Fom3L.

3.3.2. Results of purification of Fom3 from other hosts

S. lividans and Baculovirus (Bac-to-Bac® expression system from Invitrogen) were two other hosts used for the overexpression of Fom3. A Fom3 encoding gene was first cloned to a shuttle vector and then transformed into the target host. Expression of Fom3 in insect cells containing the recombinant bacmid DNA gave inconsistent results and the best obtained result was shown in Fig. 3-32 A. The expression level of Fom3 in *S. lividans* was poor (see Fig. 3-32 B). In both hosts, Fom3 was expressed in its native form.

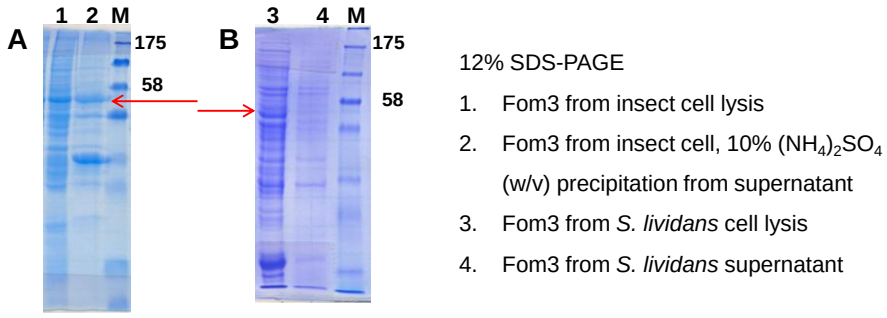

Figure 3-32: 12% SDS-PAGE of Fom3 overexpressed in other hosts. (A) Fom3 overexpression in insect cell. (B) Fom3 overexpression in *S. lividans*. The red arrow indicated the position of Fom3 appeared on the 12% SDS-PAGE.

3.3.3. Summary of results from Fom3 activity assays

Fom3 has been proposed to catalyze the methylation of HEP to generate (*S*)-HPP as shown in Fig. 3-33. To test this hypothesis, a Dionex column coupled with a Corona detector was used to monitor the formation of (*S*)-HPP and the consumption of HEP in the presence of Fom3. The primary sequence of Fom3 places it in the cobalamin-dependent group of radical SAM enzymes. Given the reaction mechanism proposed, it is reasonable to predict that the byproduct from consumption of SAM could be 5'-dAdo, SAH, or both. Therefore, to detect and distinguish 5'-Ado and SAH, a C18 column coupled with a UV detector was employed. During the study, it was observed that the sensitivity of the corona for HEP and (*S*)-HPP was relatively poor (around mM range); therefore, a more sensitive bioassay was also developed.

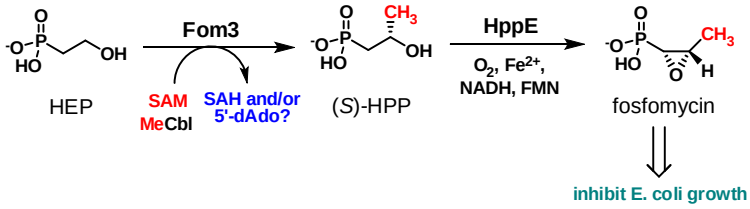

Figure 3-33: Reaction scheme for the proposed function of Fom3 based on the *in vivo* study.[249]

Summary of Fom3 activity examination

Results for the assays to detect Fom3 activity are briefly summarized in Table 3-1. Basically, attempts to obtain active Fom3 in a repeatable manner were not successful. On a few occasions, when MBP-TEV-Fom3 was expressed in insect cells and isolated anaerobically, very small peaks eluted from HPLC showed retention times corresponding to (*S*)-HPP, SAH, and 5'-dAdo as shown in Fig. 3-34 and Fig. 3-35. However, the amount was very small (less than 1% conversion) and the results were not reproducible. Moreover, the bioassay designed to detect (*S*)-HPP gave negative results for the reaction using the cell-free extract of MBP-TEV-Fom3 from insect cells.

Validation of three detection methods

An example of an HPLC trace to detect HPP formation using Dionex-Corona HPLC is shown in Fig. 3-34. In this method, HEP appeared as an asymmetric peak when the concentration is above 10 mM. Although the exact retention time changed slightly between different injections, coinjection of standard HEP and (*S*)-HPP using this method always resulted in baseline separation of the two peaks, and (*S*)-HPP elutes approximately 2 min prior to HEP.

A representative HPLC chromatograph to detect SAH and 5'-dAdo using C18-UV HPLC was shown in Fig. 3-35 A. In this method, SAH eluted 6 min prior to 5'-dAdo. Occasionally, a small peak eluted at a retention time similar to that of SAH was detected from the Fom3 assay (as shown in Fig. 3-35 B). However, it also appeared in the control reaction where substrate HEP was omitted, suggesting even though small amount of SAH may exist in the assay, it did not originate from the methylation reaction.

Expression	Purification and Assay	Results
MBP-TEV-Fom3 from *E. coli* and insect cell	Anaerobically purified using $(NH_4)_2SO_4$ precipitation method. The crude mixture after desalting step used Ti(III) citrate as reductant.	In a few trials, a very small peak (less than 1% of the substrate) was found to have similar retention time as (*S*)-HPP standard in the Dionex-Corona analysis. Very small peaks eluted at the same retention time with SAH and 5'-dAdo were found in the few samples.
MBP-TEV-Fom3 (*C*-His) from *E. coli*	Both aerobic purification and reconstitution, anaerobic purification using $(NH_4)_2SO_4$ precipitation methods have been tested, using Ti(III) citrate as reductant.	A very small peak (less than 1% of the substrate) was found to have similar retention time as (*S*)-HPP standard when using anaerobic purification. A small peak eluting at the same retention time as SAH was detected in some samples.
Fom3 from *S. lividans*	Anaerobically purified using $(NH_4)_2SO_4$ precipitation method. Both Ti(III) citrate and NADPH/FLD/FDR system have been tested for activity.	Negative results from Dionex-Corona HPLC. A small peak that has similar retention time as SAH was detected in reactions with and without substrate HEP. Negative results from bioassay.
MBP-TEV-Fom3L (*C*-His) from *E. coli*	Both aerobic purification and reconstitution, anaerobic purification using $(NH_4)_2SO_4$ precipitation methods have been tested. Three reductants have been examined: Ti(III) citrate, $RuCl_2$, and NADPH/FLD/FDR system.	Negative results from Dionex-Corona method. Small peak that has similar retention time as SAH was detected in reactions with or without substrate HEP. Besides, negative results from bioassay.
Fom3L (*N*-His) and Fom3L (*C*-His) from *E. coli*	Both aerobic purification and reconstitution, anaerobic purification using $(NH_4)_2SO_4$ precipitation methods have been tested, using Ti(III) citrate as reductant.	Negative results from bioassay.
Fom3 or Fom3L with or without *N*-His tag co-expressed with FomD	Anaerobically purified using $(NH_4)_2SO_4$ precipitation method. The crude mixture after desalting step used Ti(III) citrate as reductant.	Negative results from bioassay.

Tabel 3-1: Brief summary of assays used to test the activity of Fom3. FLD/FDR stands for flavodoxin/flavodoxin reductase. MV stands for methyl viologen. FomD is one of the ORFs found in the fosfomycin biosynthetic gene cluster. The function of FomD is not known, but there has been some speculations that it may be related to Fom3 maturation or reactivation.[261]

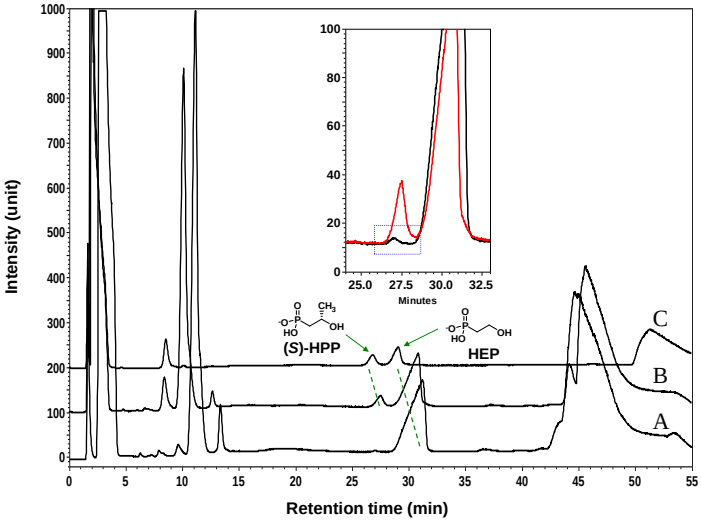

Figure 3-34: Representative HPLC traces using Dionex-Corona HPLC to monitor formation of HPP from HEP. Trace A: tested Fom3 reaction. Trace B: the same tested Fom3 reaction co-injected with 1 mM (*S*)-HPP. Trace C: standards co-injection containing 1 mM (*S*)-HPP and 2 mM HEP. The inserted chromatograph is the overlay of traces A and B. The boxed area around 27.5 min shows a small peak that has a retention time similar to that of HPP.

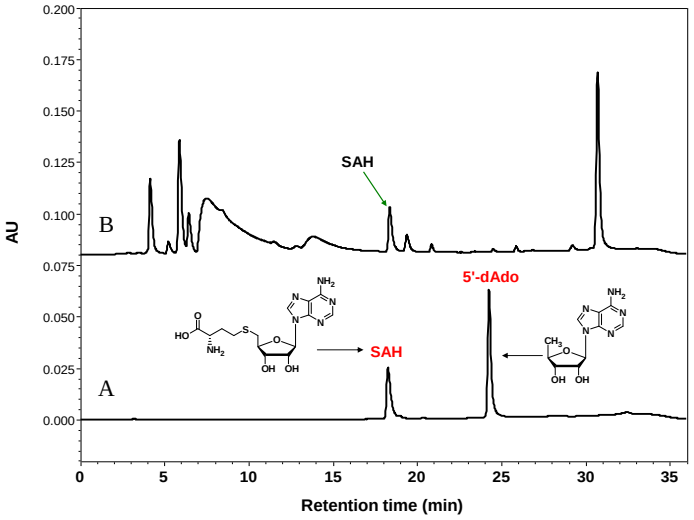

Figure 3-35: HPLC chromatographs for detection of SAH and 5'-dAdo using C18-UV HPLC.

(A) Mixture of 0.1 mM SAH and 0.15 mM 5'-dAdo standards. (B) A representative Fom3 reaction. The green arrow points to a peak that has retention time similar to SAH. This was verified by coinjection with the standard; however, it also appears in the control reactions.

A bioassay based on inhibition zones of *E. coli* K12 strain HW8235 grown on LB agar plate was developed utilizing authentic fosfomycin. This assay was effective at the concentrations of fosfomycin as low as 10 μM (Fig. 3-36, inserted plot, triangle). As HPP can be converted to fosfomycin by HppE, detection of HPP from the Fom3 assay can be alternatively achieved using this bioassay. When HPP standard was treated under HppE assay condition, the inhibition pattern was identical to the authentic fosfomycin, especially at lower concentration (see Fig. 3-36, square), suggesting the bioassay was also effective to detect HPP. Considering the detection limit of HPP is about 500 μM using Dionex-Corona HPLC method, bioassay is actually more sensitive. As a negative control, HEP at different concentrations were tested under the HppE assay condition to ensure no false positive results. As shown in Fig. 3-36 (circle), as long as the amount of HEP was lower than 15 mM (300 nmol in the plot), no inhibition zone was observed. Besides, positive controls where 50 μM (1 nmol in the plot) of HPP was added to the tested Fom3 reaction were performed in parallel to ensure components from Fom3 assay did not inhibit the activity of HppE.

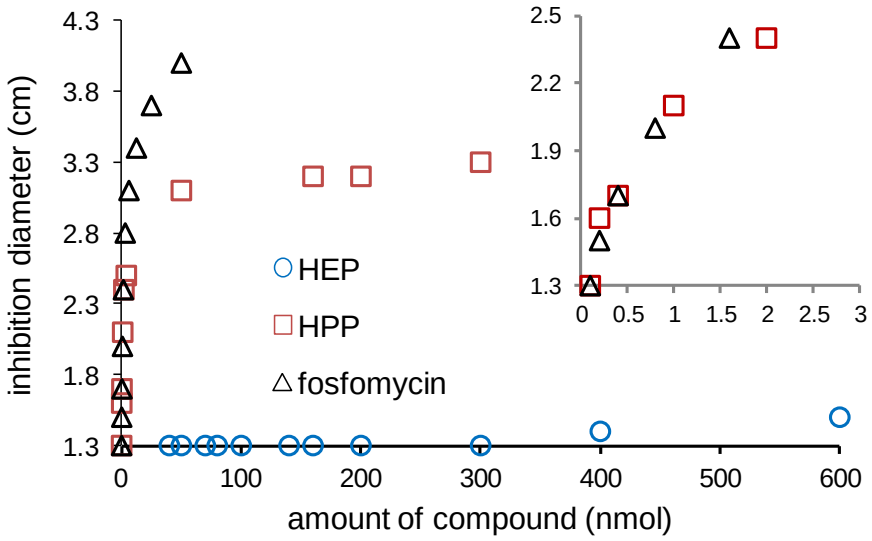

Figure 3-36: Validation of bioassay by plotting the amount of authentic fosfomycin, as well as HEP and HPP under HppE assay condition versus the size of the inhibition zone. The paper disc used in the bioassay is 1.3 cm, therefore, visible inhibition zone needs to be 1.4 cm or larger. The inserted plot is the blow up of the low concentration region.

3.3.4. Analysis of the ORFs responsible for the biosynthesis of OXT-A

Little is known regarding the biosynthesis of OXT-A. So far, biosynthetic study of this compound has been halted at the gene isolation stage.[263] Morino et al. revealed that production and resistance of OXT-A is lost when a 51.5-kb plasmid named pOXT1 is absent from the producing strain.[263] Reintroduction of this plasmid to the mutant strain that did not contain pOXT1 restored both OXT-A production and resistance.[263] Further cloning experiments suggested that a 6.8-kb fragment of the pOXT1 plasmid is sufficient for the high production of OXT-A, and the published sequence is only for this fragment.[263] Four ORFs are assigned in this plasmid (see Fig. 3-37). BLAST results for these ORFs are summarized in Table 3-2.

Figure 3-37: Plasmid-borne genes for the biosynthesis of OXT-A.

gene	putative conserved domain	protein homologue and origin	identity/ similarity (%)
oxsA	Metal dependent phosphohydrolase with conserved 'HD' motif	5'-nucleotidase [*Desmospora sp.* 8437]	32/53
oxsB	B_{12} binding domain and radical SAM domain	radical SAM family protein [*Frankia sp.* CcI3]	30/45
oxrB	Metal dependent phosphohydrolase with conserved 'HD' motif	hypothetical protein BFZC1_14638 [*Lysinibacillus fusiformis* ZC1]	50/71
oxrA	pentapeptide repeats protein	pentapeptide repeats protein YybG [*Bacillus megaterium* QM B1551]	86/94

Table 3-2: Sequence similarity analysis of the four genes in pOXT1.

Based on the BLAST results, putative functions for the four proteins can be assigned: two phosphohydrolases (OxsA and OxrB), one B_{12}-dependent radical SAM enzyme that may be involved in an intramolecular rearrangement (OxsB), and one regulation protein (OxrA). Since these four proteins are sufficient for OXT-A biosynthesis and resistance, one simple and straightforward hypothesis is that OxsB may modify a purine nucleoside phosphate metabolite, while OxsA and/or OxrB may catalyze hydrolysis of the phosphate group(s). It is also possible that OxsB alone is adequate for the biosynthesis of OXT-A, and the phosphohydrolases prevent accumulation of phosphorylated OXT-A, which is likely toxic to the host.[280]

3.3.5. Expression and purification of OxsA, OxsB, OxrA, OxrB, and OxsB-3A

N-His$_6$-OxsA (213 aa, 24,696 Da), *N*-His$_6$-OxsB (763 aa, 88,587 Da), and OxsB-3A (763 aa, 88,491 Da) showed good expression in *E. coli* BL21 Star DE3 and soluble protein can be obtained at more than 30 mg/L culture as shown in Fig. 3-38 (lanes 3, 7, and 8, respectively). Moreover, the purity of OxsB could be improved by gel filtration chromatography using FPLC and a monoQ column (see lane 6, Fig. 3-38). *N*-His$_6$-OxrB (344 amino acid residues, 40,044 Da) overexpressed as major band as shown in Fig. 3-38, lane1. The protein (lane 2) can be obtained in soluble form although the yield was not as high as OxsA or OxrB (approximately 3 mg/L culture). *N*-His$_6$-OxrA (204 residues, 22,870 Da) was not soluble although the expression was good (lane 5 and lane 4). Non-tagged OxsB was also obtained with decent yield and purity using a MBP fusion protein and TEV cleavage (lane 11). This latter protein will be referred to as (GH)-OxsB (746 residues, 86,765 Da).

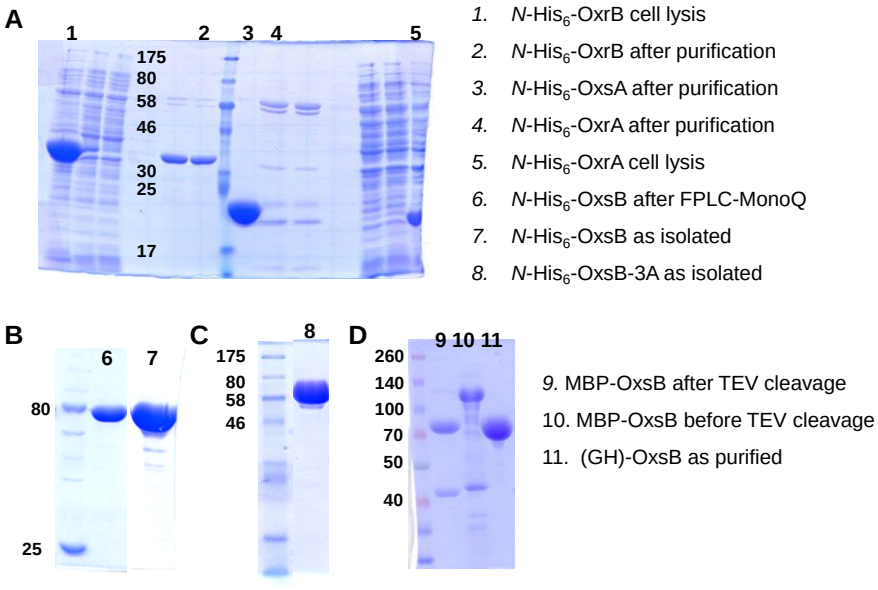

Figure 3-38: SDS-PAGE for OxsA, OxsB, OxrA, OxrB, and OxsB-3A overexpressed in *E. coli*.

(A) 12% SDS-PAGE for OxrA and OxrB expression and purification as well as purified OxsA. (B) 10% SDS-PAGE for purified *N*-His_6-OxsB. (C) 12% SDS-PAGE for purified *N*-His_6-OxsB-3A. (D) 10% SDS-PAGE for purified (GH)-OxsB obtained from TEV cleavage of MBP-OxsB.

3.3.6. Basic characterization of OxsB

UV-vis spectroscopic characterization

Anaerobically reconstituted (GH)-OxsB exhibited a reddish brown color and a broad absorption from 400 to 480 nm, along with a shoulder at 310 nm as shown in Fig. 3-39 (solid line). These UV-vis absorption patterns are nearly identical to those of several reported B_{12}- and iron-sulfur cluster containing proteins, which are not radical SAM enzymes.[277,281] Upon the addition of dithionite, the absorption at 400 nm decreased, consistent with the reduction of $[4Fe\text{-}4S]^{2+}$ to $[4Fe\text{-}4S]^{+}$, which is the active form of the cluster for radical SAM enzymes.[281] Cob(II)alamin has a characteristic absorption around 450 to 470 nm, while Cob(I)alamin and Cob(III)alamin absorb at 390 nm and 360 nm, respectively.[277] The weak broad absorption around 370 nm observed in the as-purified (GH)-OxsB suggests that there was a small amount of cobalamin bound to the enzyme, likely in the 3+ oxidation state. In the spectrum of the reconstituted (GH)-OxsB, absorptions around 310 and 450 nm imply that the reconstituted cobalamin is in the 2+ oxidation state. (GH)-OxsB was estimated to have two $[4Fe\text{-}4S]^{2+}$ clusters using ε_{410} = 15,000 $M^{-1}cm^{-1}$ for $[4Fe\text{-}4S]^{2+}$ and ε_{280} = 101,190 $M^{-1}cm^{-1}$ for (GH)-OxsB.[221]

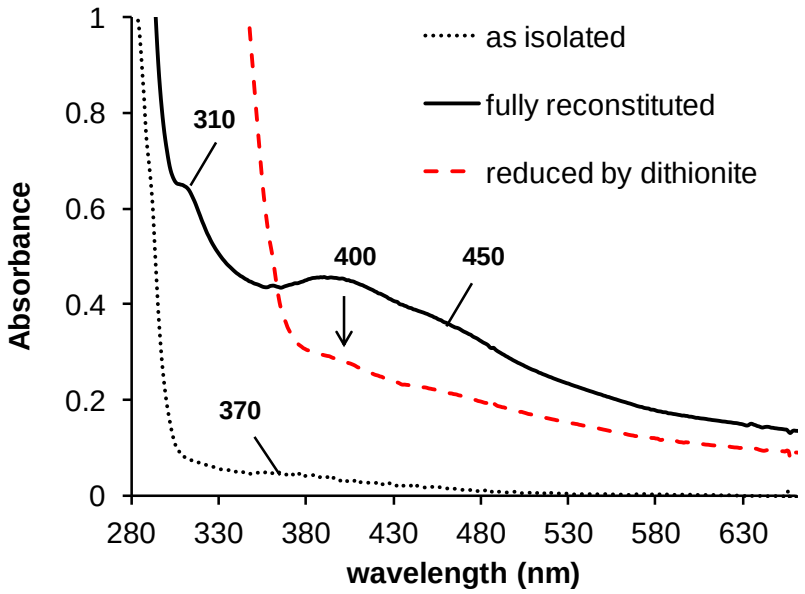

Figure 3-39: Ultraviolet–visible absorbance spectrum of (GH)-OxsB. Dotted line denotes 10 μM (GH)-OxsB following aerobic isolation, solid line denotes 15 μM (GH)-OxsB reconstituted with iron, sulfide, and OHCbl, and dashed line denotes reconstituted enzyme after reduction with 1 mM sodium dithionite. The protein was in 50 mM HEPES buffer at pH 8.0.

Results of iron and sulfide titration

As shown in Fig. 3-40, reconstituted (GH)-OxsB contained 8.5 ± 0.2 mol of iron per mole of protein, suggesting that (GH)-OxsB contains two [4Fe-4S] clusters. This result is in agreement with the corresponding estimate using UV-vis spectroscopy mentioned above. Furthermore, sulfide content in the same batch of reconstituted (GH)-OxsB was determined to be 7.8 ± 0.2 mol of sulfide per mole of protein (see Fig. 3-41), which is consistent with the result from iron titration. Analysis of the (GH)-OxsB sequence indicated that this result is reasonable, because (GH)-OxsB contains 11 cysteines. Moreover, there is a $Cx_2Cx_{17}C$ sequence motif at the *N*-terminal region of OxsB (Fig. 3-42), which is similar to the auxiliary cluster chelating motif of MoaA ($Cx_2Cx_{13}C$).[221]

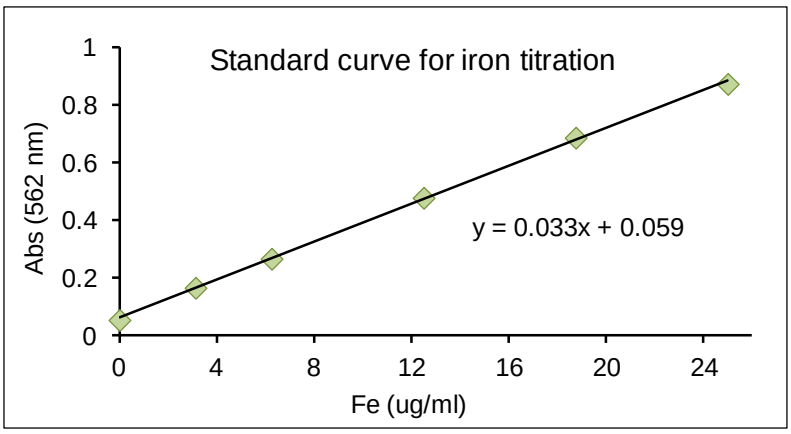

Figure 3-40: Determination of iron content of reconstituted (GH)-OxsB. Standards and samples were assayed in parallel. The enzyme concentration was determined by Bradford assay using BSA as the standard.

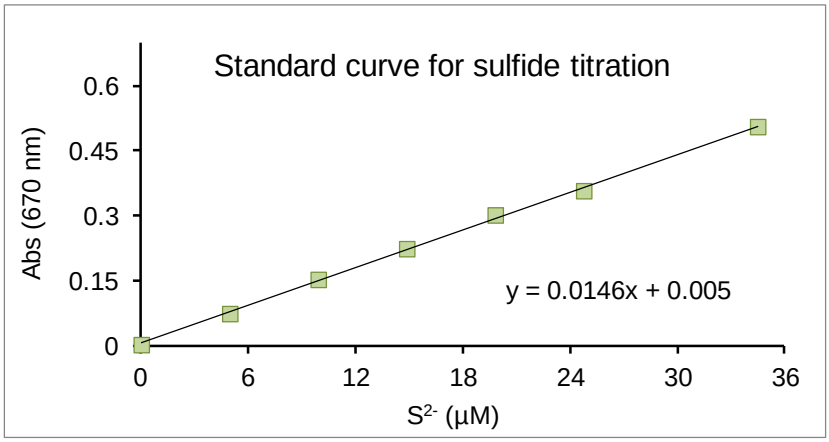

Figure 3-41: Determination of sulfide content of reconstituted (GH)-OxsB. Standards and samples were assayed in parallel. The enzyme concentration was determined by Bradford assay using BSA as the standard.

```
        10          20          30          40          50          60
GHMQTYLSTK SIEYYLKELK EIFSQIWLKP SEIEKRCEEL FKRSKEFDYK RILVSGETDN

        70          80          90         100         110         120
TTLYVIEDSS KIHVFSPNRD LRENPLLMRW HPSWYEIESK EIYYKCFLSC EELYEHLELP

       130         140         150         160         170         180
TVTLVNLCVI ENFPIPRLNL STGTLSSYLR KEQLAKVELI DMQVGTTINQ IIKNLLDSQP

       190         200         210         220         230         240
DIIGLSVNFG QKKLAFEILD LIYSHIENGD LSSIITVGNV IPSFSPEQFF ERYPSLLICD

       250         260         270         280         290         300
KEGEYTLRDL IKMLKKELKL DEVNGISYVD ESGEVKHNVA ETVNFKEEVP TPSLDILGEI

       310         320         330         340         350         360
SKFRGALTLE TSRGCDYSRC TFCPRDHKLR SWRPLSVEQT LKQLDDILRA GKHFNIKPHI

       370         380         390         400         410         420
YMADEEFIGE LPNGTEAQRI IDICEGLLKR EEKIKFDFAA RADSVYEPKR TKEWNVERLK

       430         440         450         460         470         480
MWHYCALAGA DRIFIGVESG SNQQLKRYGK GTTSEQNIIA LRLVSALGIN LRIGFIMFDQ

       490         500         510         520         530         540
LMKGLDNLKE NLDFLERTDA LMKPIDIGDM TYEELYDKLL NDKEFIEKHK TGKPVYTIVS

       550         560         570         580         590         600
YMLASMEILM NTPYSRMVQL TERKEEVNLI MNDGKPDMNM GRYATSFVDK TNGNLSEACQ

       610         620         630         640         650         660
MWIDSNFGVM YTIKSLHKVA NPREKKKLYS YMETHREISH FLLKYLVYNL SPDKESQIIL

       670         680         690         700         710         720
SDFLRMHSME HILDNSKINV GDGSKENILN VMTNWQLIME KLLRDVEADL NKGIITDSED

       730         740
HRLHNTLKRW FSDMGNWSLI NAYELN
```

Figure 3-42: Sequence of (GH)-OxsB. The sequence highlighted in yellow (Cx_4Cx_2C) is the canonical radical SAM iron-sulfur cluster binding motif. The sequence highlighted ($Cx_2Cx_{17}C$) in blue is the proposed binding motif for the second iron-sulfur cluster. The underlined sequence with amino acids in red is the cobalamin binding motif.

Results of cobalamin content determination

As shown in Fig. 3-43, the cobalamin content in the reconstituted (GH)-OxsB (reconstitution with Fe^{2+}, S^{2-}, and OHCbl) was determined by estimating the formation of cyanocobalamin when the sample was treated with KCN.[277] As a positive control, OHCbl was also treated with KCN under similar conditions. After treatment, the protein solution showed a distinct absorption pattern and the cobalamine content was estimated to be 0.6 ± 0.01 mol of cobalamin per mole of protein using ε_{580} = 10,130 $M^{-1}cm^{-1}$.

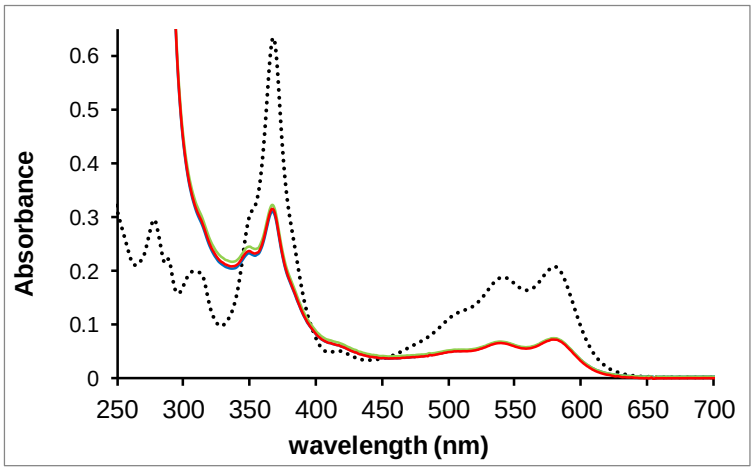

Figure 3-43: Ultraviolet–visible spectra of reconstituted (GH)-OxsB (solid lines) and OHCbl (dashed line) treated with KCN.

3.3.7. Results of substrate screening

A collection of commercially available purine nucleoside metabolites (see Fig. 3-27) were screened as putative substrates for OxsB. Three different criteria for positive hits were formulated: (1) formation of OXT-A, (2) increase of SAH or 5′-dAdo in the enzymatic reaction mixture compared to the control reaction where the putative substrate was omitted, (3) change in the HPLC trace of the sample versus control where one component from the corresponding sample mixture, such as reconstituted OxsB,

reductant, or putative substrate was omitted from the control. Unfortunately, neither the formation of OXT-A nor an increase of 5′-dAdo (and/or SAH) upon the addition of substrate was observed in any case. Expected products are baseline separated by C18-HPLC as shown in Fig. 3-44.

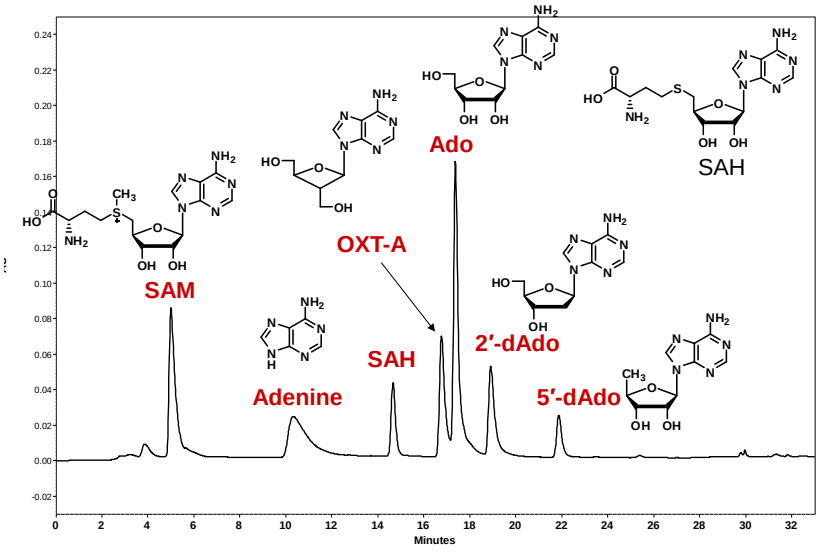

Figure 3-44: Representative HPLC trace to show the separation of several standards.

However, three test compounds did show an overall change in HPLC elution profile versus their controls. They are adenosine (Ado), 2′-deoxy-adenosine (2′-dAdo), and adenylosuccinic acid (sAMP). All three compounds showed consumption of the substrate and a new peak that increases over time in the presence of reconstituted OxsB. The new peaks observed in the reactions of OxsB with Ado and 2′-dAdo reactions were isolated. UV-vis and ESI-MS data suggested that these two peaks are inosine and 2′-deoxy-inosine, respectively. This was further confirmed by coinjection with a commercial standard of inosine and enzymatically generated 2′-deoxy-inosine using adenosine deaminase. These observations indicated that reconstituted OxsB might

possess deamination activity toward Ado and 2′-dAdo. In the sAMP reaction, the new product coeluted with AMP, suggesting that OxsB might exhibit adenylosuccinate lyase activity. However, further studies of these reactions showed that although formation of the deamination product required the presence of reconstituted OxsB, it was independent of SAM. Therefore, these reactions do not appear to involve radical SAM chemistry.

3.3.8. Deamination activity from OxsB

Several experiments were carried out to evaluate the deamination activity of OxsB in a more detailed manner. As shown in Fig. 3-45, when (GH)-OxsB was reconstituted without OHCbl, the deamination still occurred, however, the relative activity decreased when the enzyme was not reconstituted with iron and sulfide. This observation led to the hypothesis that the deamination activity is dependent on reconstitution of the iron-sulfur clusters.

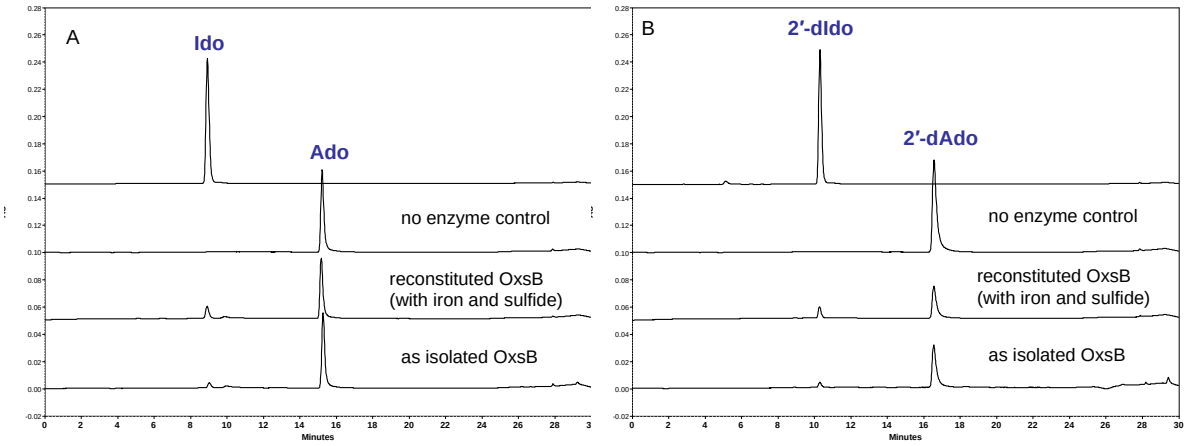

Figure 3-45: Representative HPLC traces for deamination activity. (A) Adenosine is converted to inosine when (GH)-OxsB was present. Furthermore, reconstituted (GH)-OxsB seemed have better activity than as-isolated (GH)-OxsB. (B) A similar phenomenon was observed for reactions with 2'-dAdo.

Extents of deamination were also considered in the presence of different divalent metal ions. As shown in Table 3-3, in the absence of added metal ion, a roughly 2.5-fold increase in extent of turnover over 2 h was observed with reconstituted enzyme compared to as-isolated enzyme. There appeared to be no significant effect on extent of turnover in the presence of divalent metal ions such as Mg^{2+}, Mn^{2+}, Zn^{2+}, Ca^{2+}, and Fe^{2+}, although Ca^{2+} was only considered with reconstituted (GH)-OxsB and Fe^{2+} was only considered with apo enzyme. The fraction of reaction for the deamination reaction was determined using equation 3.1 to account for the difference in extinction coefficients between adenosine and inosine at 254 nm. (Ado: ε_{254} = 13731 $M^{-1}cm^{-1}$, and Ido: ε_{254} = 10493 $M^{-1}cm^{-1}$, estimated by the UV absorption of commercial standards)

Equation 3.1 $$f = \frac{p_I/\varepsilon^I_{254}}{p_I/\varepsilon^I_{254} + p_A/\varepsilon^A_{254}}$$

condition	reconstituted OxsB	as isolated OxsB
no metal added	29%	13%
1.5 mM $MgCl_2$	25%	11%
1.5 mM $CaCl_2$	23%	na
1.5 mM $MnCl_2$	14%	6.4%
0.2 mM $ZnCl_2$	3.9%	1.3%
0.2 mM $Fe(NH_4)_2(SO_4)_2$	na	13%

Table 3-3: Fractions of reaction for the deamination of adenosine by reconstituted (GH)-OxsB and as isolated (GH)-OxsB preparations in the presence of different divalent metal ions. All reactions were run once in parallel. “na” indicates the reaction was not run.

Preliminary results from metal dependency study are consistent with the hypothesis that the iron-sulfur clusters rather than simply the presence of a divalent metal ion is responsible for the deamination activity of OxsB. To further test this hypothesis, an assay was performed in the presence of molecular oxygen using adenosine as the substrate. The fraction of reaction was calculated based on equation 3.1 mentioned above. Three sets of reactions were performed on different days to have an idea of the variance in the measurements. The average results for the fractions of the reaction are listed in Table 3-4. Apparently, OxsB reconstituted under anaerobic conditions resulted in more extensive turnover, suggesting that the deamination activity is sensitive to the presence of molecular oxygen. This is also consistent with our hypothesis that the iron-sulfur cluster is important for deamination activity.

condition	reconstituted OxsB (%)	as isolated OxsB (%)
anaerobic reaction	20 ± 6	6 ± 2
aerobic reaction	6 ± 1	3.3 ± 0.6

Table 3-4: Average fractions of reaction for the deamination of adenosine by reconstituted (GH)-OxsB and as isolated (GH)-OxsB preparations in the presence and absence of molecular oxygen.

Although the deamination reaction seemed to be related to the presence of intact iron-sulfur clusters, the rate was rather slow compared to commercial adenosine deaminases. In order to more quantitatively evaluate this activity, the steady state kinetic parameters were determined using the method of initial rates. The kinetic assays were performed under steady-state conditions at 35 °C. The data was fitted to the Michaelis-Menten equation 3.2 as shown in Fig. 3-46. The value of k_{cat}/K_M was estimated to be 1.4

$\times$ 10^{-5} $\mu M^{-1}s^{-1}$, which is indeed much slower in comparison to other adenosine deaminases (e.g., kinetic parameters for calf adenosine deaminases are as follow: k_{cat} = 250 s^{-1}, K_M = 30 μM, k_{cat}/K_M = 8.3 $\mu M^{-1}s^{-1}$).[282] The metal and oxygen sensitivity of the OxsB deaminase activity implies a requirement for intact iron-sulfur clusters; however, the relatively low level of this deaminase activity and the observation that it does not require SAM suggest that this is likely a side reaction of OxsB.

Equation 3.2 $$v_i = k_{cat} s_i e_0 / (K_M + s_i)$$

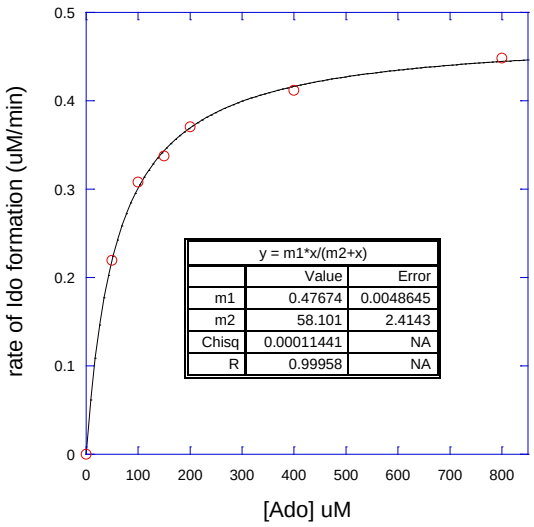

Figure 3-46: Plot of initial rates of inosine formation versus adenosine concentration in the reconstituted OxsB mediated deamination reaction. The k_{cat} value was calculated to be 8 $\times$ 10^{-4} s^{-1}, and the K_M value was calculated to be 60 μM based on the fitting.

3.3.9. Homolytic cleavage of SAM catalyzed by reconstituted OxsB

Identification of 5'-sulfinic-adenosine

Reductive cleavage of SAM mediated by reconstituted OxsB was also examined in the absence of substrate, because generation of the 5'-deoxy-adenosyl radical from

homolytic cleavage of SAM by $[4Fe\text{-}4S]^{1+}$ may not necessarily require the presence of substrate. The resulting radical could abstract a hydrogen atom from the solvent to form 5'-dAdo in a manner uncoupled from the native reaction. Such extensive uncoupling has also been reported for a number of other radical SAM enzymes where the physiological substrates are not known.[218,283-284]

As shown in Fig. 3-47 (everything), in the presence of (GH)-OxsB (reconstituted with Fe^{2+}, $S^{2-}$and OHCbl) and dithionite, SAM (eluted around 8.5 min) disappeared and two new peaks showed up with a major peak eluted at approximately 9.8 min and a minor one at around 16.8 min, a retention time close to where 5'-dAdo eluted. Coinjection with authentic 5'-dAdo confirmed the latter peak coeluted with the standard. Furthermore, this peak also vanished after treatment of the reaction mixture with MTAN, which is a nucleosidase that is known to remove the purine base from 5'-dAdo.[210] These observations indicated that 5'-dAdo is slowly formed during coincubation of reconstituted (GH)-OxsB with SAM. To identify the other major peak, the peak with a retention time of 9.8 min was isolated from the reaction mixture by HPLC and subjected to UV-vis and ESI-MS analysis. The UV-vis spectrum showed this peak has a maximum absorption at 260 nm, suggesting the adenine base was still intact. Mass analysis indicated that this peak has a neutral mass of 315 Da by both positive mode and negative ionization mode (see Fig. 3-48). Therefore, the most reasonable hypothesis for the identity of this species is a 5'-sulfinic-adenosine as shown in the box in Fig. 3-48. Although NMR data is still required for the final characterization of this major peak, there is precedence for the formation of sulfinic acid adduct in other radical SAM reactions, such as PhEF2 and SPL-C141A mutant.[188,285] Therefore, this finding demonstrates that reconstituted OxsB is able to catalyze the reductive homolysis of SAM, which is a key characteristic of radical SAM enzymes.

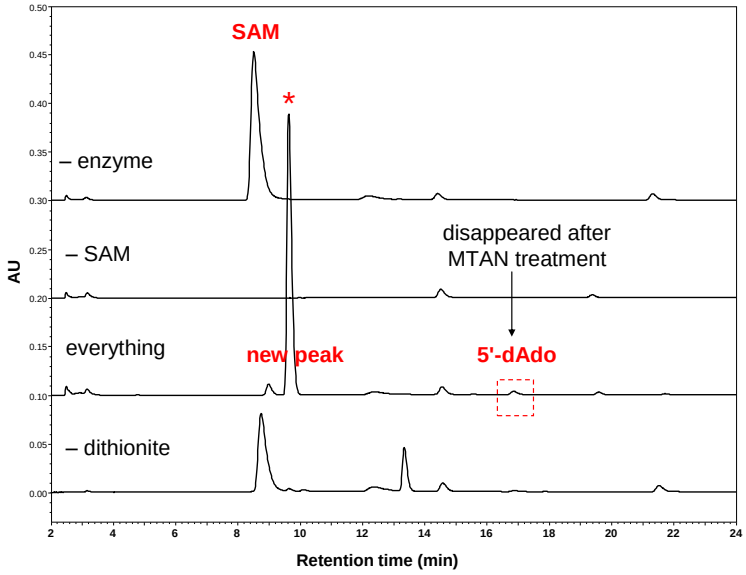

Figure 3-47: HPLC chromatograph showing OxsB mediated homolytic cleavage of SAM. "Everything" included 0.2 mM SAM, 50 µM (GH)-OxsB reconstituted with iron, sulfide, and OHCbl, 1 mM dithionite, and 1 mM DTT in 50 mM HEPES buffer, pH 8.0. (The major new peak was labeled as "new peak" marked with a star sign. The boxed peak was the latter peak suggested to be 5'-dAdo by coinjection and MTAN treatment.

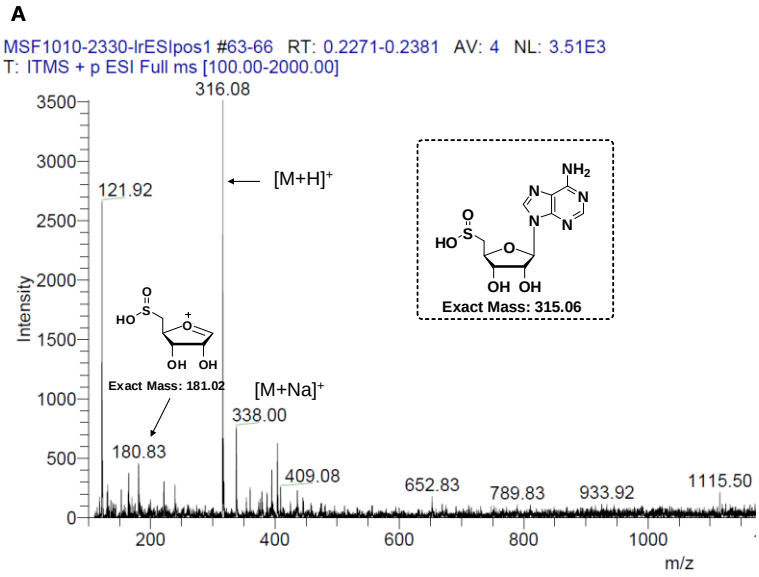

Figure 3-48: ESI-MS spectra of 5'-sulfinic-adenosine isolated from the uncoupled reaction of (GH)-OxsB and SAM. A is in positive mode.

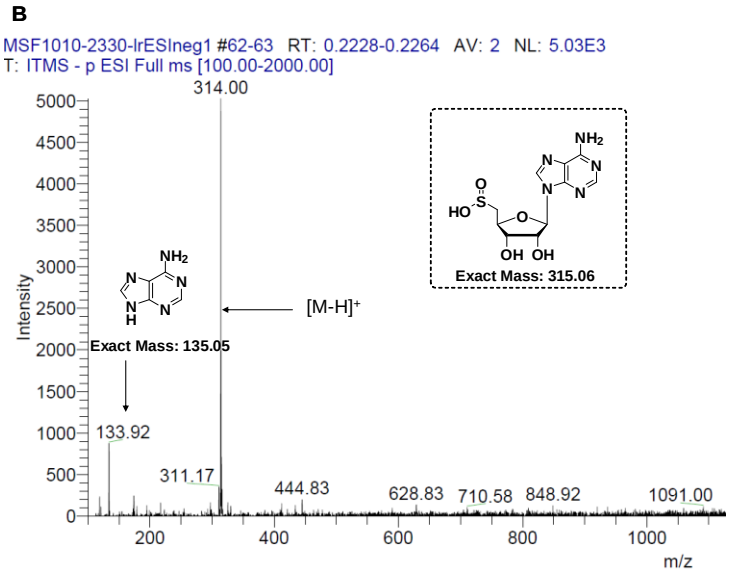

Figure 3-48: ESI-MS spectra of 5'-sulfinic-adenosine isolated from the uncoupled reaction of (GH)-OxsB and SAM. B is in negative mode.

Effects from different cobalamin forms and mechanistic hypothesis

All other uncoupled reactions reported for the radical SAM enzymes so far produce 5′-deoxy-adenosine instead of 5′-sulfinic-adenosine (5'-sAdo). Therefore, it is of interest to determine whether cobalamin plays any role in this unexpected reaction. To address this issue, (GH)-OxsB reconstituted with only iron and sulfide was used and different forms of cobalamin were added during the reaction. Indeed, the presence of cobalamin was required for the formation of 5'-sAdo (see Fig. 3-49). However, it appeared that there is no preference for any specific form of cobalamin, even the relatively inert CNCbl could also be used. In all cases, another new peak eluting with a retention time shorter than that of OHCbl was observed even in the absence of enzyme. UV-vis spectroscopic analysis of different cobalamins in the presence of dithionite and absence of enzyme revealed that this peak is likely to be SO_3Cbl (characterized by its

UV-vis spectrum[285] and coinjection with a positive control prepared by mixing OHCbl and Na_2SO_3).

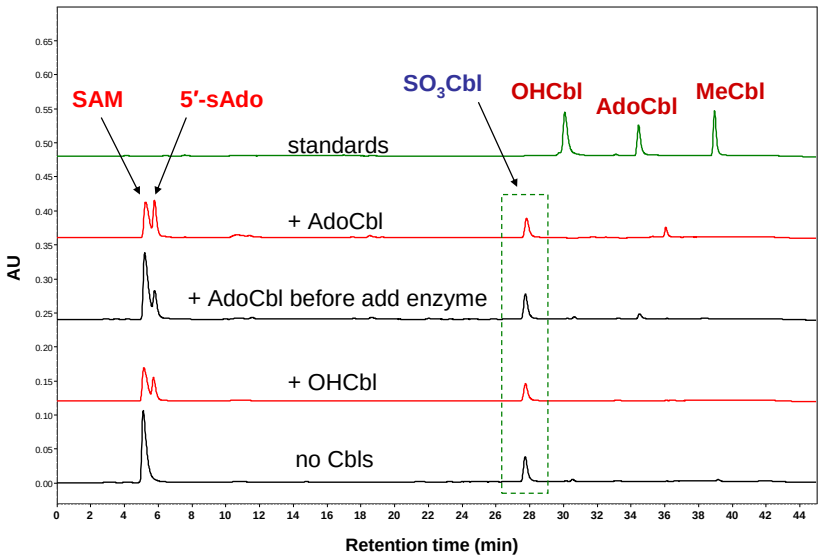

Figure 3-49: Representative HPLC traces following incubation of different cobalamins with SAM and (GH)-OxsB. Each Cbl form was analyzed by HPLC before and after addition of (GH)-OxsB reconstituted with only iron and sulfide. Reactions with the enzyme were incubated for 2 h prior to HPLC.

Another unexpected observation was that when AdoCbl was incubated with dithionite, 5'-sAdo was formed even in the absence of enzyme. We rationalized this observation as the result from photolysis of AdoCbl, which has been well documented.[286-287] Our hypothesis is that photolysis of AdoCbl results in the formation of 5'-deoxy-adenosyl radical, which then reacts with dithionite to generate 5'-sAdo. To test this hypothesis, the nonenzymatic reaction between AdoCbl and dithionite was incubated either in the dark or illuminated with white light. As shown in Fig. 3-50, compared to the reaction carried out in the dark, illumination greatly increased the formation of 5'-sAdo. Furthermore, when illumination of AdoCbl occurred prior to the addition of dithionite, no 5'-sAdo generation was detected. Instead, another peak with a later retention time was

observed. This peak also appeared in the control reaction where dithionite was omitted (see Fig. 3-50, "with light – dithionite"). The identity of this peak is predicted to be 5'-deoxy-5',8-cycloadenosine (5',8-cAdo), based on the reported anaerobic decomposition product from AdoCbl photolysis.[286-287]

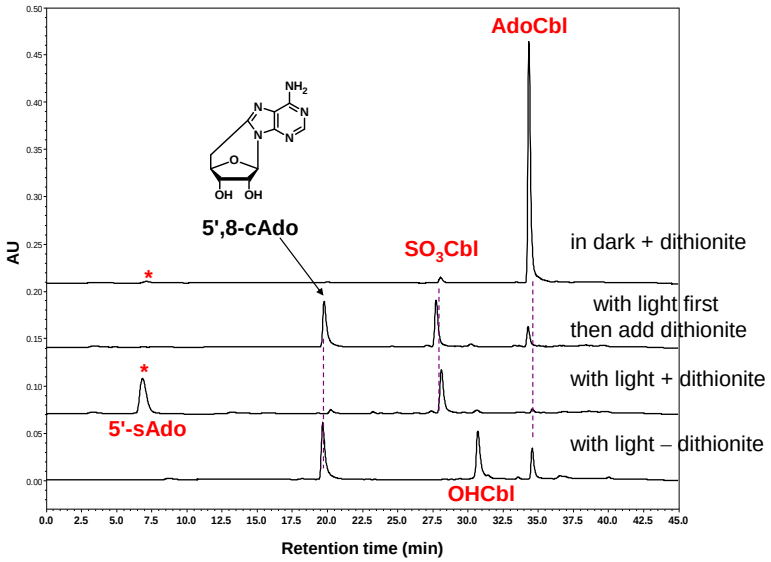

Figure 3-50: HPLC traces of nonenzymatic generation of 5'-sAdo from AdoCbl.

The nonenzymatic reaction led us to several hypotheses regarding the mechanism of homolytic cleavage of SAM catalyzed by the reconstituted OxsB. One mechanism for the formation of the 5'-sAdo is via photolysis of AdoCbl reacting with dithionite directly. In this case, AdoCbl is produced by the enzyme and subsequently photolyzed to the 5'-deoxy-adenosyl radical, which reacts with dithionite as shown in Fig. 3-51 A. Alternatively, the 5'-deoxy-adenosyl radical generated via reductive homolysis of SAM in the OxsB active site may react directly with dithionite (see Fig. 3-51 B). In this scenario a cobalamin is required to activate the enzyme in some fashion that facilitates the reductive homolysis. Instead of reacting with dithionite directly, the 5'-deoxy-adenosyl radical may also react with a $SO_2^{\cdot-}$Cbl(II) complex as shown in Fig. 3-51 C. The

formation of $SO_2^{\cdot}$Cbl(II) can be readily observed by UV-vis when OHCbl is incubated with dithionite, and it subsequently decomposes to SO_3Cbl(III) upon prolonged incubation as has been previously reported.[285]

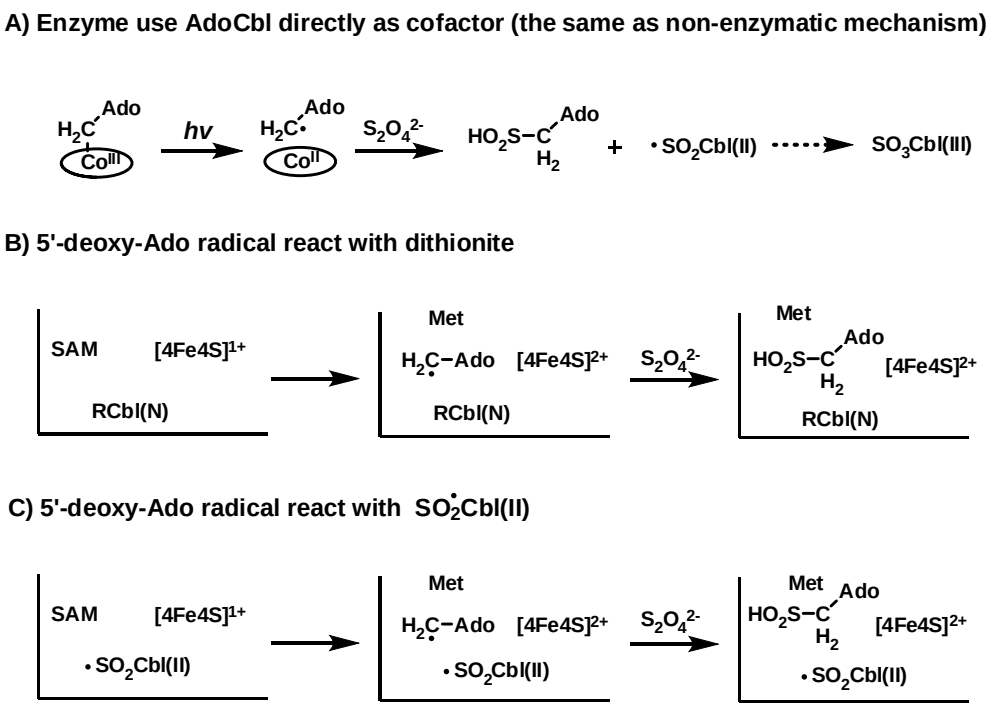

Figure 3-51: Mechanistic hypotheses for the synthesis of 5'-sulfinic-adenosine by reconstituted OxsB (with iron and sulfide) in the presence of cobalamin and $Na_2S_2O_4$. "RCbl(N)" denotes an unspecified cobalamin and redox state.

3.4. DISCUSSION AND FUTURE DIRECTION

The role of *S*-adenosyl-L-methionine (SAM) as a major biological methyl donor has been appreciated for decades. More recently, SAM has been shown to function as a cosubstrate in diverse radical reactions that delineate the radical SAM superfamily of enzymes. Within this family, one group named cobalamin-dependent radical SAM enzymes include members from diverse biosynthesis pathways that are believed to utilize both radical SAM chemistry as well as B_{12} chemistry to complete their catalytic cycles and thus represent an untapped source of novel biochemistry.[240] In this chapter, two cobalamin-dependent radical SAM enzymes from different biosynthesis pathways have been investigated. Fom3 from *Streptomyces wedmorensis* is a putative *C*-methyltransferase involved in the biosynthesis of the clinical relevant antibiotic fosfomycin. OxsB from *Bacillus megaterium* NK84-0218 is proposed to participate in the biosynthesis of oxetanocin A, which is an antiviral nucleoside that bears a rare oxetane ring moiety.

Gene deletion studies combined with feeding experiments suggested that Fom3 methylates the unactivated sp^3 hybridized carbon center at the C2 position of 2-hydroxyethylphosphonate (HEP) to generate 2-hydroxypropyl phosphonic acid (HPP).[249] Two mechanisms suggested by the early feeding experiments can be envisioned for this intriguing methylation as shown in Fig. 3-52.[255,260,288] In both mechanisms, SAM is reductively cleaved concomitant with oxidation of the iron-sulfur cluster to generate the 5'-deoxy-adenosyl radical, which subsequently abstracts the *pro-R* hydrogen atom at C2 position of HEP. In pathway A, the substrate radical can accept the methyl radical from MeCbl, leading to the formation of (*S*)-HPP and cob(II)alamin. The resulting cob(II)alamin can be reduced to cob(I)alamin, which acts as the nucleophile in a methyl transfer reaction with SAM to regenerate MeCbl. This mechanism is similar to the

reductive methylation that takes place during the re-activation of methionine synthase.[289] All other reported cobalamin dependent methyltransferases, however, employ a two electron transfer mechanism, leaving such a mechanism without precedent. Alternatively, the substrate radical can also undergo deprotonation to give a ketyl radical (pathway B), which is an accepted intermediate in a number of other enzyme reactions.[290-291] Nucleophilic attack by the resonance form of the ketyl radical to MeCbl yields the product radical and cob(I)alamin. The product radical can be quenched by an electron and proton, resulting in the formation of HPP. While cob(I)alamin can be used directly by SAM to regeneration MeCbl.

To actually distinguish these two mechanisms, the *in vitro* reconstitution of Fom3 activity is required. Three different analytical methods have been developed to analyze the *in vitro* Fom3 assay: (a) Dionex-Corona HPLC system to detect HEP and HPP, (b) C18-UV HPLC system to detect SAH and 5'-dAdo, and (c) bioassay that uses the enzyme HppE to generate fosfomycin from the proposed Fom3 product. However, in no case has activity for Fom3 been demonstrated definitively. One possible reason is the large amount of protein that forms inclusion bodies upon overexpression, such that the soluble portion is insufficient for observing activity. Different strategies to improve Fom3 solubility have been tried but the results have not been satisfactory. Given the reported successes with *in vitro* reconstitution of PhnK and GenK from inclusion bodies,[254-255] further efforts to obtain active Fom3 will focus on using different refolding methods to obtain soluble Fom3.

OxsB is one of the few members of the cobalamin-dependent group of radical SAM enzymes that may catalyze a reaction other than methylation. The challenge for characterizing OxsB is the limited information available from prior *in vivo* studies. Four

genes including OxsB are reported to be involved in oxetanocin A biosynthesis; however, no additional information regarding to their individual functions is available.[263]

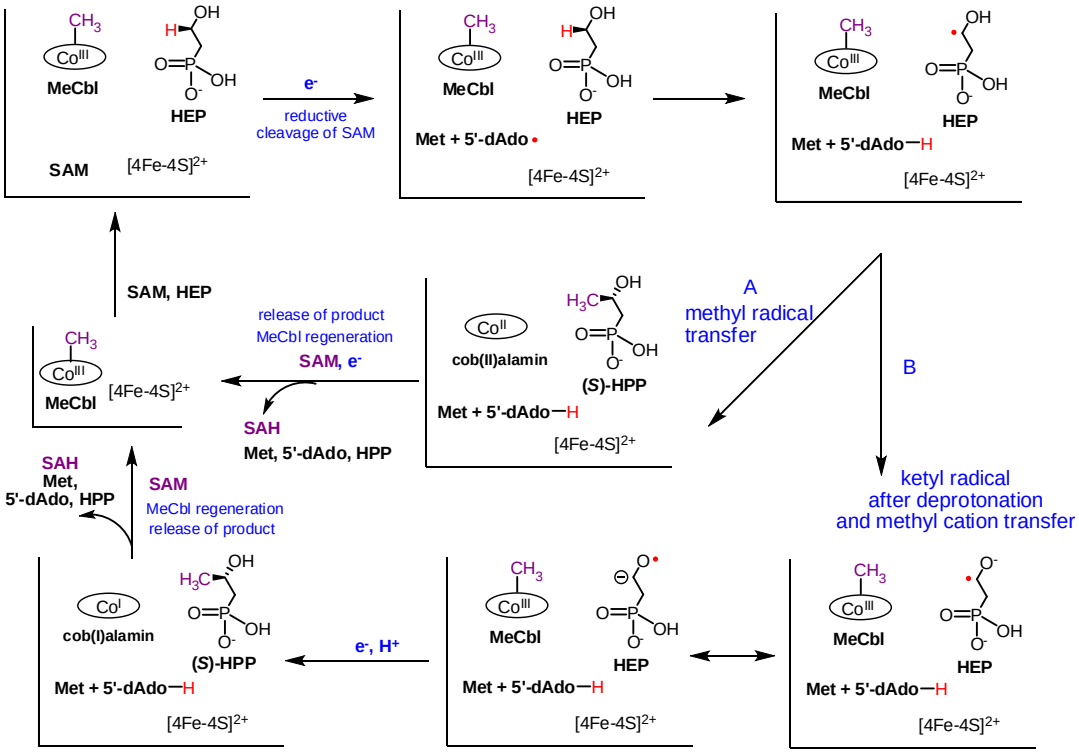

Figure 3-52: Proposed mechanisms for Fom3 mediated methylation at an unactivated carbon center.

In this chapter, successful heterologous overexpression of the oxetanocin A biosynthetic proteins encoded by these four genes was described. Furthermore, three of them were purified as soluble forms including OxsB. OxsB anaerobically reconstituted with iron, sulfide, and OHCbl contains 8.5 ± 0.2 mol of iron, 7.8 ± 0.2 mol of sulfide, and 0.6 ± 0.01 mol of cobalamin per mole of protein determined by titration assays. This result, combined with the UV-vis spectroscopic analysis, suggested that reconstituted OxsB is likely to contain two [4Fe-4S] clusters and one cobalamin center.

A collection of commercially available purine nucleoside metabolites were tested as possible substrates for OxsB. However, no *in vitro* production of oxetanocin A has been observed. Unexpectedly, OxsB could catalyze the deamination of adenosine to inosine, and 2'-deoxy-adenosine to 2'-deoxy-inosine. Further investigation of this activity suggests that this activity is dependent on the reconstitution of the iron-sulfur clusters. However, the activity is about five orders of magnitude slower than typical adenosine deaminases, which suggests that this is likely to be a side reaction of OxsB.

An encouraging discovery from reconstituted OxsB is that the enzyme can catalyze reductive homolysis of SAM, which is a characteristic property of radical SAM enzymes. When the reconstituted enzyme was incubated with SAM and dithionite, 5'-sulfinic-adenosine was generated at the cost of SAM. To my knowledge, this is the first example of a 5'-deoxy-adenosyl sulfinic adduct in radical SAM catalyzed reactions. Moreover, cobalamin was found to be necessary for the generation of this adduct. Several mechanisms have been proposed based on the serendipitous finding that the 5'-sulfinic adenosine can be generated via photo-induced homolysis of AdoCbl in the presence of dithionite. The above mentioned characterizations of OxsB have set the stage for further investigation of its function. Modified assays along with investigation of the other three enzymes involved in the biosynthesis of oxetanocin A will be used in future efforts to identify the substrate of OxsB.

References

1. Kiessling, L. L., and Splain, R. A. (2010) Chemical Approaches to Glycobiology, *Annu. Rev. Biochem.* 79, 619-653.

2. Thibodeaux, C. J., Melançon, C. E., and Liu, H.-w. (2008) Natural-product sugar biosynthesis and enzymatic glycodiversification, *Angew. Chem. Int. Ed. Engl.* 47, 9814-9859.

3. Lin, C.-I, McCary, R. M., and Liu, H.-w. (2013) The biosynthesis of nitrogen-, sulfur-, and high-carbon chain-containing sugars, *Chem. Soc. Rev.* 42, 4377-4407.

4. Peltier, P., Euzen, R., Daniellou R., Nugier-Chauvin, C., and Ferrières, V. (2008) Recent knowledge and innovations related to hexofuranosides: structure, synthesis and applications, *Carbohydr. Res.* 343, 1897-1923.

5. Taha, H. A., Richards, M. R., and Lowary, T. L. (2013) Conformational Analysis of Furanoside-Containing Mono- and Oligosaccharides, *Chem. Rev.* 113, 1851-1876.

6. Pan, F., Jackson, M., Ma Y., and McNeil, M. (2001) Cell wall core galactofuran synthesis is essential for growth of mycobacteria, *J. Bacteriol.* 183, 3991-3998.

7. Gandhi, N. R., Nunn, P., Dheda, K., Schaaf, H. S., Zignol, M., van Soolingen, D., Jensen, P., and Bayona J. (2010) Multidrug-resistant and extensively drug-resistant tuberculosis: a threat to global control of tuberculosis, *Lancet* 375, 1830-1843.

8. Dykhuizen, E. C., May, J. F., Tongpenyai, A., and Kiessling L. L. (2008) Inhibitors of UDP-galactopyranose mutase thwart mycobacterial growth, *J. Am. Chem. Soc.* 130, 6706-6707.

9. Peltier, P., Beláňová, M., Dianišková, P., Zhou, R., Zhang, R. B., Pearcey, J. A., Joe, M., Brennan, P. J., Nugier-Chauvin, C., Ferrières, V., Lowary, T. L., Daniellou, R., and Mikušová, K. (2010) Synthetic UDP-furanose as potent inhibitors of mycobacterial galactan biogenesis, *Chem. Biol.* 17, 1356-1366.

10. Richards, M. R., and Lowary, T. L. (2009) Chemistry and biology of galactofuranose-contianing plolysaccharides, *ChemBioChem.* 10, 1920-1938.

11. Mennink-Kersten, M., Ruegebrink, D., Wasei, N., Melchers, W., and Verweij, P. E. (2006) In vitro release by *Aspergillus fumigates* of galactofuranose antigens, 1, 3-β-D-glucan, and DNA, surrogate markers used for diagnosis of invasive aspergillosis, *J. Clin. Microbiol.* 44, 1711-1718.

12. Chlubnova, I., Legentil, L., Dureau, R., Pennec, A., Almendros, M., Daniellou, R., Nugier-Chauvin, C., and Ferrières, V. (2012) Specific and non-specific enzymes for furanosyl-containing conjugates: biosynthesis, metabolism, and chemo-enzymatic synthesis, *Carbohydr. Res.* 356, 41-46.

13. Zhang, Q., and Liu, H.-w. (2000) Galactopyranose mutase from *Escherichia coli*: an unusual role of reduced FAD in its catalysis, *J. Am. Chem. Soc.* 122, 9065-9070.

14. Poulin, M. B., Nothaft, H., Hug, I., Feldman, M. F., Szymanski, C. M., and Lowary, T. L. (2010) Characterization of a Bifunctional Pyranose-Furanose Mutase from *Campylobacter jejuni* 11168, *J. Biol. Chem.* 285, 493-501.

15. St Michael, F., Szymanski, C. M., Li, J., Chan, K. H., Khieu, N. H., Larocque, S., Wakarchuk, W. W., Brisson, J. R., and Monteiro, M. A. (2002) The structures of the lipooligosaccharide and capsule polysaccharide of Campylobacter jejuni genome sequenced strain NCTC 11168, *Eur. J. Biochem.* 269, 5119-5136.

16. Wang, Q., Ding, P., Perepelov, A. V., Xu, Y., Wang, Y., Knirel, Y. A., Wang, L., and Feng, L. (2008) Characterization of the dTDP-D-fucofuranose biosynthetic pathway in *Escherichia coli* O52, *Mol. Microbiol.* 70, 1358-1367.

17. Konishi, T., Takeda, T., Miyazaki, Y., Ohnishi-Kameyama, M., Hayashi, T., O'Neill, M. A., and Ishii, T. (2007) A plant mutase that interconverts UDP-arabinofuranose and UDP-arabinopyranose, *Glycobiology*, 17, 345-354.

18. Konishi, T., Ohnishi-Kameyama, M., Funane, K., Miyazaki, Y., Konishi, T., and Ishii, T. (2010) An arginyl residue in rice UDP-arabinopyranose mutase is required for catalytic activity and autoglycosylation, *Carbohydr. Res.* 345, 787-791.

19. Levengood, M. R., Splain, R. A., and Kiessling, L. L. (2011) Monitoring processivity and length control of a carbohydrate polymerase, *J. Am. Chem. Soc.* 133, 12758-12766.

20. Nassau, P. M., Martin, S. L., Brown, R. E., Weston, A., Monsey, D., McNeil, M. R., and Duncan, K. (1996) Galactofuranose biosynthesis in *Escherichia coli* K-12: identification and cloning of UDP-galactopyranose mutase, *J. Bacteriol.* 178, 1047-1052.

21. Köplin, R., Brisson, J.-R., and Whitfield, C. (1997) UDP-Galactofuranose precursor required for formation of the lipopolysaccharide O antigen of *Klebsiella pneumonia* serotype O1 is synthesized by the product of the $rfbD_{KPO1}$ gene, *J. Biol. Chem.* 272, 4121-4128.

22. Weston, A., Stern, R. J., Lee, R. E., Nassau, P. M., Monsey, D., Martin, S. L., Scherman, M. S., Besra, G. S., Duncan, K., and McNeil, M. R. (1998) Biosynthetic origin of mycobacterial cell wall galactofuranosyl residues, *Tuber. Lung Dis.* 78, 123-131.

23. Oppenheimer, M., Valenciano, A. L., and Sobrado, P. (2011) Biosynthesis of galactofuranose in kinetoplastids: novel therapeutic targets for treating leishmaniasis and chagas' disease, *Enzyme Res.* 2011, 415976.

24. Dhatwalia, R., Singh, H., Oppenheimer, M., Karr, D. B., Nix, J. C., Sobrado, P., and Tanner, J. J. (2012) Crystal structures and small-angle x-ray scattering analysis of UDP-galactopyranose mutase from the pathogenic fungus *Aspergillus fumigates*, *J. Biol. Chem.* 287, 9041-9051.

25. Lienhart, W.-D., Gudipati, V., and Macheroux, P. (2013) The human flavoproteome, *Arch. Biochem. Biophys*. 535, 150-162.

26. Mansoorabadi, S. O., Thibodeaux, C. J., and Liu, H.-w. (2007) The diverse roles of flavin coenzymes-nature's most versatile thespians, *J. Org. Chem.* 72, 6329-6342.

27. Walsh, C. T. and Wencewicz, T. A. (2013) Flavoenzymes: Versatile catalysts in biosynthetic pathways, *Nat. Prod. Rep.* 30, 175-200.

28. Chen, H, Guo, Z., and Liu, H.-w. (1998) Biosynthesis of Yersiniose: Attachment of the two-carbon branched-chain is catalyzed by a thiamine pyrophosphate-dependent flavoprotein, *J. Am. Chem. Soc.* 120, 11796-11797.

29. Bornemann, S. (2002) Flavoenzyms that catalyse reactions with no net redox change, *Nat. Prod. Rep.* 19, 761-772.

30. Calveras, J., Thibodeaux, C. J., Mansoorabadi, S. O., and Liu, H.-w. (2012) Stereochemical studies of the type II isopentenyl diphosphate-dimethylallyl diphosphate isomerase implicate the FMN coenzyme in substrate protonation, *Chembiochem.* 13, 42-46.

31. Thibodeaux, C. J., Chang, W. C., and Liu, H.-w. (2010) Linear free energy relationships demonstrate a catalytic role for the flavin mononucleotide coenzyme of the type II isopentenyl diphosphate:dimethylallyl diphosphate isomerase, *J. Am. Chem. Soc.* 132, 9994-9996.

32. Sobrado, P. (2012) Noncanonical reactions of flaboenzymes, *Int. J. Mol. Sci.* 13, 14219-14242.

33. Kommoju, P. R., Bruckner, P. C., Ferreira, P., and Jorns, M. S. (2009) Probing the role of active site residues in NikD, an unusual amino acid oxidase that catalyzes an aromatization reaction important in nikkomycin biosynthesis, *Biochemistry* 48, 6951-6962.

34. Yu, Q., Schaub, P., Ghisla, S., Al-Babili, S., Krieger-Liszkay, A., and Beyer, P. (2010) The lycopene cyclase CrtY from *Pantoea ananatis* (formerly *Erwinia uredovora*) catalyzes an FAD_{red}-dependent non-redox reaction, *J. Biol. Chem.* 285, 12109-12120.

35. Razeto, A., Mattiroli, F., Carpanelli, E., Aliverti, A., Pandini, V., Coda, A., and Mattevi, A. (2007) The crucial step in ether phospholipid biosynthesis: structural basis of a noncanonical reaction associated with a peroxisomal disorder, *Structure* 15, 683-692.

36. Nenci, S., Piano, V., Rosati, S., Aliverti, A., Pandini, V., Fraaije, M. W., Heck, A. R., Edmondson, D. E., and Mattevi, A. (2012) Precursor of ether phospholipids is synthesized by a flavoenzyme through covalent catalysis, *Proc. Natl. Acad. Sci. U.S.A.* 109, 18791-18796.

37. Hamdane, D., Argentini, M., Cornu, D., Myllykallio, H., Skouloubris, S., Hui-Bon-Hoa, G., and Golinelli-Pimpaneau, B. (2011) Insights into folate/FAD-dependent tRNA methyltransferase mechanism: role of two highly conserved cysteines in catalysis, *J. Biol. Chem.* 286, 36268-36280.

38. Hamdane, D., Argentini, M., Cornu, D., Golinelli-Pimpaneau, B., and Fontecave, M. (2012) FAD/Folate-dependent tRNA methyltransferase: Flavin as a new methyl-transfer agent, *J. Am. Chem. Soc.* 134, 19739-19765.

39. Barlow, J. N., Girvin, M. E., and Blanchard, J. S. (1999) Positional isotope exchange catalyzed by UDP-galactopyranose mutase, *J. Am. Chem. Soc.* 121, 6968-6969.

40. Barlow, J. N. and Blanchard, J. S. (2000) Enzymatic synthesis of UDP-(3-deoxy-3-fluoro)-D-galactose and UDP-(2-deoxy-2-fluoro)-D-galactose and substrate activity with UDP-galactopyranose mutase, *Carbohydr. Res.* 328, 473-480.

41. Zhang, Q. and Liu, H.-w. (2001) Mechanistic investigation of UDP-galactopyranose mutase from *Escherichia coli* using 2- and 3-fluorinated UDP-galactofuranose as probes, *J. Am. Chem. Soc.* 123, 6756-6766.

42. Huang, Z., Zhang, Q., Liu, H.-w. (2003) Reconstitution of UDP-galactopyranose mutase with 1-deaza-FAD and 5-deaza-FAD: analysis and mechanistic implications, *Bioorg. Chem.* 31, 494-502.

43. Soltero-Higgin, M., Carlson, E. E., Gruber, T. D., and Kiessling, L. L. (2004) A unique catalytic mechanism for UDP-galactopyranose mutase, *Nat. Struct. Mol. Biol.* 11, 539-543.

44. Caravno, A., Sinaÿ, P., and Vincent, S. P. (2006) 1,4-Anhydrogalactopyranose is not an intermediate of the mutase catalyzed UDP-galactopyranose/furanose interconversion, *Bioorg. Med. Chem. Lett.* 16, 1123-11125.

45. Gruber, T. D., Westler, W. M., Kiessling, L. L., and Forest, K. T. (2009) X-ray crystallography reveals a reduced substrate complex of UDP-galactopyranose mutase poised for covalent catalysis by flavin, *Biochemistry* 48, 9171-9173.

46. Yuan, Y., Bleile, D. W., Wen, X., Sanders, D. A., Itoh, K., Liu, H.-w., and Pinto, B. M. (2008) Investigation of binding of UDP-Gal*f* and UDP-[3-F]Gal*f* to UDP-galactopyranose mutase by STD-NMR spectroscopy, molecular dynamics, and CORCEMA-ST calculations, *J. Am. Chem. Soc.* 130, 3157-3168.

47. Itoh, K., Huang, Z., and Liu, H.-w. (2007) Synthesis and analysis of substrate analogues for UDP-galactopyranose mutase: implication for an oxocarbenium ion intermediate in the catalytic mechanism, *Org. Lett.* 9, 879-882.

48. Partha, S. K., Sadeghi-Khomani, A., Slowshi, K., Kotake, T., Thomas, N. R., Jakeman, D. L., and Sanders, D. A. (2010) Chemoenzymatic synthesis, inhibition studies, and x-ray crystallographic analysis of the phosphono analog of UDP-Gal*p* as an inhibitor and mechanistic probe for UDP-Galactopyranose mutase, *J. Mol. Biol.* 403, 578-590.

49. Fullerton, S. W. B., Daff, S., Sanders, D. A., Ingledew, W. J., Whitfield, C., Chapman, S. K., and Naismith, J. H. (2003) Potentiometric analysis of UDP-galactopyranose mutase: stabilization of the flavosemiquinone by substrate, *Biochemistry*, 42, 2104-2109.

50. Desvergnes, S., Desvergnes, V., Martin, O. R., Itoh, K., Liu, H.-w., and Py, S. (2007) Stereoselective synthesis of beta-1-C-substituted 1,4-dideoxy-1,4-imino-D-galactitols and evaluation as UDP-galactopyranose mutase inhibitors, *Bioorg. Med. Chem.* 15, 6443-6449.

51. Liautard, V., Desvergnes, V., Itoh, K., Liu, H.-w., and Martin, O. R. (2008) Convergent and stereoselective synthesis of iminosugar-containing Gal*f* and UDP-Gal*f* mimicks: evaluation as inhibitors of UDP-Gal mutase, *J. Org. Chem.* 73, 3103-3115.

52. Bradford, M. M. (1976) A rapid and sensitive method for the quantitation of microgram quantities of protein utilizing the principle of protein-dye binding, *Anal. Biochem.* 72, 248-254.

53. Sambrook, J., and Russell, D. W. (2001) *Molecular cloning*: A laboratory mamual, 3rd ed. Cold Spring Harbor Laboratory Press, Plainview, NY.

54. Eaton, J. W. (2002), GNU Octave manual, Network Theory Limited.

55. Liu, Z., Zhang, J., Chen, X., and Wang, P. (2002) Combined biosynthetic pathway for de novo production of UDP-galactose: catalysis with multiple enzymes immobilized on agarose beads, *ChemBioChem.* 3, 348-355.

56. Hayashi, T., Murray, B. W., Wang, R., and Wong, C.-H. (1997) A chemoenzymatic synthesis of UDP-(2-deoxy-2-fluoro)-galactose and evaluation of its interaction with galactosyltransferase, *Bioorg. Med. Chem.* 5, 497-500.

57. Creutz, C., and Sutin, N. (1974) Kinetics of the reactions of sodium dithionite with dioxygen and hydrogen peroxide, *Inorg. Chem.* 13, 2041-2043.

58. Meynial, I., Paquet, V., and Combes, D. (1995) Simultaneous separation of nucleotides and nucleotide sugars using an ion-pair reversed-phase HPLC: application for assaying glycosyltransferase activity, *Anal. Chem.* 67, 1627-1631.

59. Walsh, C. (1986) Naturally occurring 5-deazaflavin coenzymes: biological redox roles, *Acc. Chem. Res.* 19, 216-221.

60. Midelfort, C. F., and Rose, I. A. (1976) A stereochemical method for detection of ATP terminal phosphate transfer in enzymatic reactions. Glutamine synthetase, *J. Biol. Chem.* 251, 5881-5887.

61. Mullins, L. S., and Raushel, F. M. (1995) Positional isotope exchange as probe of enzyme action, *Method Enzymol.* 249, 398-425.

62. Seber, G. A. F. and Wild, C. J. (2003) *Nonlinear Regression*, Wiley-Interscience, New Jersey.

63. Cleland, W. W. (1967) The statistical analysis of enzyme kinetic data, *Adv. Enzymol.* 29, 1-32.

64. Johnson, M. L. (1994) Use of least-squares techniques in biochemistry, *Method. Enzymol.* 240, 1-22.

65. Draper, N. R. and Smith, H. (1998) *Applied regression analysis*, Wiley-Interscience, New York, 3rd edition.

66. Taft, R. W., Jr., Ehrenson, S., Lewis, I. C., and Glick, R. E. (1959) Evaluation of resonance effects on reactivity by application of the linear inductive energy relationship. VI. Concerning the effects of polarization and conjugation on the mesomeric order, *J. Am. Chem. Soc.* 81, 5352-5361.

67. Hansch, C., Leo, A., and Taft, R. W. (1991) A survey of Hammett substituent constants and resonance and field parameters, *Chem. Rev.* 91, 165-195.

68. Taft, R. W., Jr. (1960) Sigma values from reactivities, *J. Phys. Chem.* 64, 1805-1815.

69. Edmondson, D. E., and Ghisla, S. (1999) Electronic effects of 7 and 8 ring substituents as predictors of flavin oxidation-reduction potentials, In *Flavins and Flavoproteins*, pp. 71-76, Agency for Scientific Publications, Berlin.

70. Yorita, K., Misaki, H., Palfey, B. A., and Massey, V. (2000) On the interpretation of quantitative structure-function activity relationship data for lactate oxidase, *Proc. Natl. Acad. Sci. U.S.A.* 97, 2480-2485.

71. Roth, J. P., Wincek, R., Nodet, G., Edmondson, D. E., McIntire, W. S., and Klinman, J. P. (2004) Oxygen isotope effects on electron transfer to O_2 probed using chemically modified flavins bound to glucose oxidase, *J. Am. Chem. Soc.* 126, 15120-15131.

72. Legrand, Y. M., Gray, M., Cooke, G., and Rotello, V. M. (2003) Model systems for flavoenzyme activity: relationships between cofactor structure, binding, and redox properties, *J. Am. Chem. Soc.* 125, 15789-15795.

73. Ritchie, C. D. and Sager, W. F. (1964) An examination of structure-reactivity relationships. In *Prog. Phys. Org. Chem.*, Cohen, S. G., Streitweiser, A., and Taft, R. W., eds., volume 2, pp. 323-400.

74. Cleland, W. W. (1975) Partition analysis and the concept of net rate constants as tools in enzyme kinetics, *Biochemistry* 14, 3220-3224.

75. Oppenheimer, M., Valenciano, A. L., Kizjakina, K., Qi, J., and Sobrado, P. (2012) Chemical mechanism of UDP-galactopyranose mutase from *Trypanosoma cruzi*: a potential drug target against Chagas' disease, *PLoS One.* 7, e32918.

76. Veerapen, N., Yuan, Y., Sanders, D. A. R., and Pinto, B. M. (2004) Synthesis of novel ammonium and selenonium ions and their evaluation as inhibitors of UDP-galactopyranose mutase, *Carbohydr.Res.* 339, 2205-2217.

77. Caravano, A., Vincent, S. P., and Sinaÿ, P. (2004) Efficient synthesis of a nucleoside-diphospho-exo-glycal displaying time-dependent inactivation of UDP-galactopyranose mutase, *Chem. Commun.* 10, 1216-1217.

78. Caravano, A., Dohi, H., Sinaÿ, P., and Vincent, S. P. (2006) A new methodology for the synthesis of fluorinated *exo*-glycals and their time-dependent inhibition of UDP-galactopyranose mutase, *Chem. Eur. J.* 12, 3114-3123.

79. Mueller, E. G. (2006) Trafficking in persulfides: delivering sulfur in biosynthetic pathways, *Nat. Chem. Biol.* 2, 185-194.

80. Gustilo, E. M., Vendeix, F. A. P., and Agris, P. F. (2008) tRNA's modifications bring order to gene expression, *Curr. Opin. Microbiol.* 11, 134-140.

81. Mohan, S., and Pinto, B. M. (2007) Zwitterionic glycosidase inhibitors: salacinol and related analogues, *Carbohydr. Res.* 342, 1551-1580.

82. Tang, G.-L., Cheng, Y.-Q., Shen, B. (2004) Leinamycin biosynthesis revealing unprecedented architectural complexity for a hybrid polyketide synthase and nonribosomal peptide synthetase, *Chem. Biol*. 11, 33-45.

83. Taori, K., Paul, V. J., and Luesch, H. (2008) Structure and activity of largazole, a potent antiproliferative agent from the Floridian marine cyanobacterium *Symploca sp.*, *J. Am. Chem. Soc.* 130, 1806-1807.

84. Sasaki, E. (2011) Biosynthetic studies of thiosugar-containing natural products, BE-7585A and lincomycin A, dissertation, University of Texas at Austin.

85. Arnison, P. G., Bibb, M. J., Bierbaum, G., Bowers, A. A., Bugni, T. S., Bulaj, G., Camarero, J. A., Campopiano, D. J., Challis, G. L., Clardy, J., Cotter, P. D., Craik, D. J., Dawson, M., Dittmann, E., Donadio, S., Dorrestein, P. C., Entian, K. D., Fischbach, M. A., Garavelli, J. S., Göransson, U., Gruber, C. W., Haft, D. H., Hemscheidt, T. K., Hertweck, C., Hill, C., Horswill, A. R., Jaspars, M., Kelly, W. L., Klinman, J. P., Kuipers, O. P, Link, A. J., Liu, W., Marahiel, M. A., Mitchell, D. A., Moll, G. N., Moore, B. S., Müller, R., Nair, S. K., Nes, I. F., Norris, G. E., Olivera, B. M., Onaka, H., Patchett, M. L., Piel, J., Reaney, M. J., Rebuffat, S., Ross R. P., Sahl, H. G., Schmidt, E. W., Selsted, M. E., Severinov, K., Shen, B., Sivonen, K., Smith, L., Stein, T., Süssmuth, R. D., Tagg, J. R., Tang, G. L., Truman, A. W., Vederas, J. C., Walsh, C. T., Walton, J. D., Wenzel, S. C. Willey, J. M., van der Donk, W. A. (2013) Ribosomally synthesized and post-translationally modified peptide natural products: overview and recommendations for a universal nomenclature, *Nat. Prod. Rep.* 30, 108-160.

86. Ravilious, G. E., and Jez, J. M. (2012) Structural biology of plant sulfur metabolism: From assimilation to biosynthesis, *Nat. Prod. Rep.* 29, 1138-1152.

87. Liu, Y., Beer, L. L., and Whitman, W. B. (2012) Sulfur metabolism in archaea reveals novel processes, *Environ. Microbiol.* 14, 2632-2644.

88. Liu, Y. Dos Santos, P. C., Zhu, X., Orlando, R., Dean, D. R., Söll, D., and Yuan, J. (2012) Catalytic mechanism of Sep-tRNA:Cys-tRNA synthase: sulfur transfer is mediated by disulfide and persulfide, *J. Biol. Chem.* 287, 5426-5433.

89. Burns, K. E., Baumgart, S., Dorrestein, P. C., Zhai, H., McLafferty, F. W., and Begley T. P. (2005) Reconstitution of a new cysteine biosynthetic pathway in *Mycobacterium tuberculosis*, *J. Am. Chem. Soc.* 127, 11602-11603.

90. Begley, T. P., Ealick, S. E. and McLafferty, F. W. (2012) Thiamin biosynthesis: still yielding fascinating biological chemistry, *Biochem. Soc. Trans.* 40, 555-560.

91. Chatterjee, A., Abeydeera, N. D., Bale1, S., Pai, P.-j., Dorrestein, P. C., Russell, D. H., Ealick, S. E., and Begley, T. P. (2011) Saccharomyces cerevisiae THI4p is a suicide thiamine thiazole synthase, *Nature* 478, 542-546.

92. Geu-Flores, F., Olsen, C. E., and Halkier, B. A. (2009) Towards engineering glucosinolates into non-cruciferous plants, *Planta. 229,* 261-270.

93. Ikeuchi, Y. Shigi, N. Kato, J., Nishimura, A., and Suzuki, T. (2006) Mechanistic insights into multiple sulfur mediators sulfur relay by involved in thioruidine biosynthesis at tRNA wobble positions, *Mol. Cell.* 21, 97-108.

94. Peters, J. W. and Broderick, J. B. (2012) Emerging paradigms for complex iron-sulfur cofactor assembly and insertion, *Annu. Rev. Biochem.* 81, 429-450.

95. Bordo, D. and Bork, P. (2002) The rhodanese/Cdc25 phosphatase superfamily: sequence-structure-function relations, *EMBO Rep.* 3, 741-746.

96. Cipollone, R., Ascenzi, P. and Visca, P. (2007) Common themes and variations in the rhodanese superfamily, *IUBMB Life. 59,* 51-59.

97. Krepinsky, K., and Leimkühler, S. (2007) Site-directed mutagenesis of the active site loop of the rhodanese-like domain of the human molybdopterin synthase sulfurase MOCS3. Major differences in substrate specificity between eukaryotic and bacterial homologs, *FEBS. J.* 274, 2778-2787.

98. Wolfe, M. D., Ahmed, F., Lacourciere, G. M., Lauhon, C. T., Stadtman, T. C., and Larson, T. J. (2004) Functional diversity of the rhodanese homology domain: the Escherichia coli ybbB gene encodes a selenophosphate-dependent tRNA 2-selenouridine synthase, *J. Biol. Chem.* 279, 1801-1809.

99. Liu, Y., Zhu, X., Nakamura, A., Orlando, R., Söll, D., and Whitman, W. B. (2012) Biosynthesis of 4-thiouridine in tRNA in the methogenic archaen *Methanococcus maripaludis*, *J. Biol. Chem.* 287, 36683-36692.

100. Dahl, J. U., Urban, A., Bolte, A., Sriyabhaya, P., Donahue, J. L., Nimtz, M., Larson, T. J., and Leimkühler, S. (2012) The identification of a novel protein involved in molybdenum cofactor biosynthesis in *Escherichia coli*, *J. Biol. Chem.* 286, 35801-35812.

101. Martinez-Gomez, N. C., Palmer, L. D., Vivas, E., Roach, P. L., and Downs, D. M. (2011) The rhodanese domain of ThiI is both necessary and sufficient for synthesis of the thiazole moiety of thiamine in *Salmonella enteric*, *J. Bacteriol.* 193, 4582-4587.

102. Wright, C. M., Christman, G. D., Snellinger, A. M., Johnston, M. V., and Mueller, E. G. (2006) Direct evidence for enzyme persulfide and disulfide intermediates during 4-thiouridine biosynthesis, *Chem. Commun.* 3104-3106.

103. Krishnamoorthy, K. and Begley, T. P. (2010) A reagent for the detection of protein thiocarboxylates in the bacterial proteome: lissamine rhodamine B sulfonyl azide, *J. Am. Chem. Soc.* 132, 11608-11612.

104. Hochstrasser, M. (2009) Origin and function of ubiquitin-like proteins, *Nature* 458, 422-429.

105. Wang, C. Y., Xi, J., Begley, T. P., and Nicholson, L. K. (2001) Solution structure of ThiS and implications for the evolutionary roots of ubiquitin, *Nat. Struct. Biol. 8,* 47-51.

106. Rudolph, M. J., Wuebbens, M. M., Rajagopalan, K. V., and Schindelin, H. (2001) Crystal structure of molybdopterin synthase and its evolutionary relationship to ubiquitin activation, *Nat. Struct. Biol. 8,* 42-46.

107. Burroughs, A. M., Iyer, L. M., and Aravind, L. (2009) Natural history of the E1-like superfamily: implication for adenylation, sulfur transfer and ubiquitin conjugation, *Proteins* 75, 895-910.

108. Schwartz, A. L., and Ciechanover, A. (2009) Targeting proteins for destructuion by the ubiquitin system: implications for human pathobiology, *Annu. Rev. Pharmacol. Toxicol.* 49, 73-96.

109. Leidel, S., Pedrioli, P. G. A., Bucher, T., Brost, R., Costanzo, M., Schmidt, A., Aebersold, R., Boone, C., Hofmann, K., and Peter, M. (2009) Ubiquitin-related modifier Urm1 acts as a sulphur carrier in thiolation of eukaryotic transfer RNA, *Nature 458*, 228-232.

110. van der Veen, A. G., Schorpp, K., Schlieker, C., Buti, L., Damon, J. R., Spooner, E., Ploegh, H. L., and Jentsch, S. (2011) Role of the ubiquitin-like protein Urm1 as a noncanonical lysine-directed protein modifier, *Proc. Natl. Acad. Sci. U.S.A. 108*, 1763-1770.

111. Chowdhury, M. M., Dosche, C., Löhmannsröben, H., and Leimkühler, S. (2012) Dual role of the molybdenum cofactor biosynthesis protein MOCS3 in tRNA thiolation and molybdenum cofactor biosynthesis in humans, *J. Biol. Chem.* 287, 17297-17307.

112. Miranda, H. V., Nembhard, N., Su, D., Hepowit, N., Krause, D. J., Pritz, J. R., Phillips, C., Soll, D., and Maupin-Furlow, J. A. (2011) E1-and ubiquitin-like proteins provide a direct link between protein conjugation and sulfur transfer in archaea, *Proc. Natl. Acad. Sci. U.S.A. 108*, 4417-4422.

113. Shigi, N. (2012) Post-translational modification of cellular proteins by a ubiquitin-like protein in Bacteria, *J. Biol. Chem.* 287, 17568-17577.

114. Xi, J., Ge, Y., Kinsland, C., McLafferty, F. W., and Begley, T. P. (2001) Biosynthesis of the thiazole moiety of thiamin in Escherichia coli: Identification of an acyldisulfide-linked protein-protein conjugate that is functionally analogous to the ubiquitin/E1 complex, *Proc. Natl. Acad. Sci. U.S.A. 98*, 8513-8518.

115. Dorrestein, P. C., Zhai, H. L., McLafferty, F. W., and Begley, T. P. (2004) The biosynthesis of the thiazole phosphate moiety of thiamin: The sulfur transfer mediated by the sulfur carrier protein ThiS, *Chem. Biol. 11*, 1373-1381.

116. Leimkuhler, S., Wuebbens, M. M., and Rajagopalan, K. V. (2001) Characterization of *Escherichia coli* MoeB and its involvement in the activation of molybdopterin synthase for the biosynthesis of the molybdenum cofactor, *J. Biol. Chem. 276*, 34695-34701.

117. Marelja, Z., Stocklein, W., Nimtz, M., and Leimkuhler, S. (2008) A novel role for human Nfs1 in the cytoplasm -Nfs1 acts as a sulfur donor for MOCS3, a protein involved in molybdenum cofactor biosynthesis, *J. Biol. Chem. 283*, 25178-25185.

118. Voss, M., Nimtz, M., and Leimkühler, S. (2011) Elucidation of the dual role of mycobacterial MoeZR in molybdenum cofactor biosynthesis and cysteine biosynthesis, *PLoS. One.* 6, e28170.

119. Krishnamoorthy, K., and Begley, T. P. (2011) Protein thiocarboxylate-dependent methionine biosynthesis in *Woinella succinogenes*, *J. Am. Chem. Soc.* 133, 379-386.

120. Shigi, N., Sakaguchi, Y., Asai, S., Suzuki, T., and Watanabe, K. (2008) Common thiolation mechanism in the biosynthesis of tRNA thiouridine and sulphurcontaining cofactors, *EMBO J. 27*, 3267-3278.

121. Furukawa, K., Mizushima, N., Noda, T., and Ohsumi, Y. (2000) A protein conjugation system in yeast with homology to biosynthetic enzyme reaction of prokaryotes, *J. Biol. Chem. 275*, 7462-7465.

122. Lewis, T. A., Cortese, M. S., Sebat, J. L., Green, T. L., Lee, C. H., and Crawford, R. L. (2000) A Pseudomonas stutzeri gene cluster encoding the biosynthesis of the CCl4-dechlorination agent pyridine-2,6-bis(thiocarboxylic acid), *Environ. Microbiol. 2*, 407-416.

123. Cortese, M. S., Caplan, A. B., and Crawford, R. L. (2002) Structural, functional, and evolutionary analysis of moeZ, a gene encoding an enzyme required for the synthesis of the *Pseudomonas* metabolite, pyridine-2,6-bis(thiocarboxylic acid), *BMC Evol. Biol. 2*, 8.

124. Godert, A. M., Jin, M., McLafferty, F. W., and Begley, T. P. (2007) Biosynthesis of the thioquinolobactin siderophore: An interesting variation on sulfur transfer, *J. Bacteriol. 189*, 2941-2944.

125. Jarrett, J. T. (2005) The novel structure and chemistry of iron-sulfur clusters in the adenosylmethionine-dependent radical enzyme biotin synthase, *Arch. Biochem. Biophys.* 433, 312-321.

126. Booker, S. J., Cicchillo, R. M., and Grove, T. L. (2007) Self-sacrifice in radical Sadenosylmethionine proteins, *Curr. Opin. Chem. Biol. 11*, 543-552.

127. Zhang, Q., and Yu, Y. (2012) Thioether crosslinkages created by a radical SAM enzyme, *Chembiochem.* 13, 1097-1099.

128. Sasaki, E., Ogasawara, Y., and Liu, H.-w. (2010) A biosynthetic pathway for BE-7585A, a 2-thiosugar-containing angucycline-type natural product, *J. Am. Chem. Soc.* 132, 7405-7417.

129. Sasaki, E. and Liu, H.-w. (2010) Mechanistic studies of the biosynthesis of 2-thiosugar: evidence for the formation of an enzyme-bound 2-ketohexose intermediate in BexX-catalyzed reaction, *J. Am. Chem. Soc.* 132, 15544-15546.

130. Matthies, A., Rajagopalan, K. V., Mendel, R. R., and Leimkühler, S. (2004) Evidence for the physiological role of a rhodanese-like protein for the biosynthesis of the molybdenum cofactor in humans, *Proc. Natl. Acad. Sci. U. S. A.* 101, 5946-5951.

131. Schmitz, J., Chowdhury, M. M., Hänzelmann, P., Nimtz, M., Lee, E. Y., Schindelin, H., and Leimkühler, S. (2008) The sulfurtransferase activity of Uba4 presents a link between ubiquitin-like protein conjugation and activation of sulfur carrier proteins, *Biochemistry* 47, 6479-6487.

132. Matthies, A., Nimtz, M., and Leimkühler, S. (2005) Molybdenum cofactor biosynthesis in humans: identification of a persulfide group in the rhodanese-like domain of MOCS3 by Mass Spectrometry, *Biochemistry* 44, 7912-7920.

133. Hochstrasser, M. (2000) Evolution and function of ubiquitin-like protein-conjugation systems, *Nat. Cell. Biol.* 2, E153-E157.

134. Boutureira, O., Bernardes, G. J., Fernández-González, M., Anthony, D. C., and Davis, B. G. (2012) Selenenylsulfide-linked homogeneous glycopeptides and glycoproteins: synthesis of human "hepatic Se metabolite A", *Angew. Chem. Int. Ed.* 50, 1-6.

135. Kinsland, C., Taylor, S. V., Kelleher, N. L., McLafferty, F. W. and Begley, T. P. (1998) Overexpression of recombinant proteins with a *C*-terminal thiocarboxylate: implications for protein semisynthesis and thiamin biosynthesis, *Protein Sci.* 7, 1839-1842.

136. Pecci, L., Pensa, B., Costa, M., Cignini, P. L., and Cannella, C. (1976) Reaction of rhodanese with dithiothreitol, *Biochim. Biophys. Acta* 445, 104-111.

137. Sörbo, B. (1957) Enzymic transfer of sulfur from mercatopyruvate to sulfate or sulfinates, *Biochim. Biophys. Acta* 24, 324-329.

138. Riddles, P. W., Blakeley, R. L., and Zerner, B. (1983) Reassessment of Ellman's reagent, *Methods Enzymol.* 91, 49-60.

139. Beinert, H. (1983) Semi-micro methods for analysis of labile sulfide and of labile sulfide plus sulfane sulfur in unusually stable iron-sulfur proteins, *Anal. Biochem.* 131, 373-378.

140. Chen, J.-s., and Mortenson, L. E. (1977) Inhibition of methylene blue formation during determination of the acid-labile sulfide of iron-sulfur protein samples containing dithionite, *Anal. Biochem.* 79, 157-165.

141. Kosower, E. M. and Kosower, N. S. (1995) Bromobimane probes for thiols, *Methods. Enzymol.* 251, 133-148.

142. Burns, J. A., Butler, J. C., Moran, J. and Whitesides, G. M. (1991) Selective reduction of disulfides by tris-(2-carboxyethyl)-phosphine, *J. Org. Chem.* 56, 2648-2650.

143. Yang, W., Di Vizio, D., Kirchner, M., Steen, H., and Freeman, M. R. (2010) Proteome scale characterization of human *S*-acylated proteins in lipid raft-enriched and non-raft membranes, *Mol. Cell. Proteomics.* 9, 54-70.

144. Lauhon, C. T., and Kambampati, R. (2000) The *iscS* gene in *Escherichia coli* is required for the biosynthesis of 4-thiourifine, thiamin, and NAD, *J. Biol. Chem.* 275, 20096-20103.

145. Hirel, P. H., Schmitter, M. J., Dessen, P., Fayat, G., and Blanquet, S. (1989) Extent of *N*-terminal methionine excision from *Escherichia coli* proteins is governed by the side-chain length of the penultimate amino acid, *Proc. Natl. Acad. Sci. U. S. A.* 86, 8247-8651.

146. Geoghegan, K. F., Dixon, H. B. F., Rosner, P. J., Hoth, L. R., Lanzetti, A. J., Borzilleri, K. A., Marr, E. S., Pezzullo, L. H., Martin, L. B., LeMotte, P. K., McColl, A. S., Kamath, A. V., and Stroh, J. G. (1999) Spontaneous alpha-*N*-6-phosphogluconoylation of a "His tag" in *Escherichia coli*: The cause of extra mass of 258 or 178 Da in fusion proteins, *Anal. Biochem. 267*, 169-184.

147. Kaiser, J. T., Bruno, S., Clausen, T., Huber, R., Schiaretti, F., Mozzarelli, A., and Kessler, D. (2003) Snapshots of the cystine lyase C-DES during catalysis: Studies in solution and in the crystalline state, *J. Biol. Chem. 278*, 357-365.

148. Campanini, B., Schiaretti, F., Abbruzzetti, S., Kessler, D., and Mozzarelli, A. (2006) Sulfur mobilization in cyanobacteria: The catalytic mecahnism of Lcystine C-S lyase (C-DES) from synechocystis, *J. Biol. Chem. 281*, 38769-38780.

149. Omi, R., Kurokawa, S., Mihara, H., Hayashi, H., Goto, M., Miyahara, I., Kurihara, T., Hirotsu, K. and Esaki, N. (2010) Reaction mechanism and molecular basis for selenium/sulfur discrimination of selenocysteine lyase, *J. Biol. Chem.* 285, 12133-12139.

150. Mihara, H., Kurihara, T., Yoshimura, T., Soda, K. and Esaki, N. (1997) Cysteine sulfinate desulfinase, a NIFS-like protein of *Escherichia coli* with selenocysteine lyase and cysteine desulfurase activities: gene cloning, purification, and characterization of a novel pyridoxal enzyme, *J. Biol. Chem.* 272, 22417-22424.

151. Quaderer, R., Sewing, A., and Hilvert, D. (2001) Selenocysteine-mediated native chemical ligation, *Helv. Chim. Acta.* 84, 1197-1206.

152. Hondal, R. J., Nilsson, B. L., and Raines, R. T. (2001) Selenocysteine in native chemical ligation and expressed protein ligation, *J. Am. Chem. Soc.* 123, 5140-5141.

153. Newton, G. L., Buchmeier N., and Fahey, R. C. (2008) Biosynthesis and functions of mycothiol, the unique protective thiol of actinobacteria, *Microbiol. Mol. Biol. Rev.* 72, 471-494.

154. Iyer, L. M., Burroughs, A. M., and Aravind, L. (2006) The prokaryotic antecedents of the ubiquitin-signaling system and the early evolution of ubiquitin-like β-grasp domains, *Genome Biol.* 7, R60.

155. Landgraf, B. J. and Booker, S. J. (2013) Biochemistry: The ylide has landed, *Nature* 498, 45-47.

156. Cantoni, G. L. (1952) The nature of the active methyl donor formed enzymatically from L-methionine and adenosinetriphosphate, *J. Am. Chem. Soc.* 74, 2942-2943.

157. Markham, G. D., Hafner, E. W., Tabor, C. W., and Tabor, H. (1980) *S*-adenosylmethionine synthetase from *Escherichia coli, J. Biol. Chem.* 255, 9082-9092.

158. Fontecave, M., Atta, M., and Mulliez, E. (2004) *S*-adenosylmethionine: nothing goes to waste, *Trends Biochem. Sci.* 29, 243-249.

159. Lin, H. (2011) *S*-Adenosylmethionine-dependent alkylation reactions: When are radical reactions used? *Bioorg. Chem.* 39, 161-170.

160. Parveen, N. and Cornell, K. A. (2011) Methylthioadenosine/*S*-adenosylhomocysteine nucleosidase, a critical enzyme for bacterial metabolism, *Mol. Microbiol.* 79, 7-20.

161. Federle, M. J. (2009) Autoinducer-2-based chemical communication in bacteria: complexities of interspecies signaling, *Contrib. Microbiol.* 16, 18-32.

162. Loenen, W. A. (2006) *S*-adenosylmethionine: jack of all trades and master of everything? *Biochem. Soc. Trans.* 34, 330-333.

163. Val, D. L. and Cronan, J. E. Jr (1998) *In vivo* evidence that *S*-adenosylmethionine and fatty acid synthesis intermediates are the substrates for the LuxI family of autoinducer synthetases, *J. Bacteriol.* 180, 2644-2651.

164. Wei, Y., Perez, L. J., Ng, W.-l., Semmelhack, M. F., and Bassler, B. L. (2011) Mechanism of vibrio cholerae autoinducer-1 biosynthesis, *ACS Chem. Biol.* 6, 356-365.

165. Reeve, A. M., Breazeale, S. D. and Townsend, C. A. (1998) Purification, characterization, and cloning of an *S*-adenosylmethionine-dependent 3-amino-3-carboxypropyltransferase in nocardicin biosynthesis, *J. Biol. Chem.* 273, 30695-30703.

166. Thibodeaux, C. J., Chang, W.-c., and Liu, H.-w. (2012) Enzymatic chemistry of cyclopropane, epoxide, and aziridine biosynthesis, *Chem. Rev.* 112, 1681-1709.

167. Nishimura, S., Taya, Y., Kuchino, Y., and Ohashi, Z. (1974) Enzymatic synthesis of 3-(3-amino-3-carboxypropyl) uridine in *Escherichia coli* phenylalanine transfer RNA: transfer of the 3-amino-3-caeboxypropyl group from *S*-adenosylmethionine, *Biochem. Biophys. Res. Commun.* 57, 702-708.

168. Umitsu, M., Nishimasu, H., Noma, A., Suzuki, T., Ishitani, R., and Nureki, O. (2009) Structural basis of AdoMet-dependent aminocarboxypropyl transfer reaction catalyzed by tRNA-wybutosine synthesizing enzyme, TYW2, *Proc. Natl. Acad. Sci. USA* 106, 15616-15621.

169. Ikegami, F., Sakai, R., Ishikawa, T., Kuo, Y. H., Lambein, F., and Murakoshi, I. (1993) Biosynthesis *in vitro* of 2-(3-amino-3-carboxypropyl)-isoxazolin-5-one, the neurotoxic amino acid in *Lathyrus odoratus*, *Biol. Pharm. Bull.* 16, 732-734.

170. Ikeguchi, Y., Bewley, M. C., and Pegg, A. E. (2006) Aminopropyltransferases: function, structure and genetics, *J. Biochem.* 139, 1-9.

171. Eustáquio, A. S., Pojer, F., Noel, J. P., and Moore, B. S. (2008) Discovery and characterization of a marine bacterial SAM-dependent chlorinase, *Nat. Chem. Biol.* 4, 69-74.

172. Dong, C., Huang, F., Deng, H., Schaffrath, C., Spencer, J. B., O'Hagan, D., and Naismith, J. H. (2004) Crystal structure and mechanism of a bacterial fluorinating enzyme, *Nature* 427, 561-565.

173. Iwata-Reuyl, D. (2003) Biosynthesis of the 7-deazaguanosine hyper modified nucleosides of transfer RNA, *Bioorg. Chem.* 31, 24-43.

174. van Lanen, S. G. and Iwata-Reuyl, D. (2003) Kinetic mechanism of the tRNA-modifying enzyme *S*-adenosylmethionine:tRNA ribosyltransferase-isomerase (QueA), *Biochemistry* 42, 5312-5320.

175. Iwig, D. F., Grippe, A. T., McIntyre, T. A., and Booker, S. J. (2004) Isotope and elemental effects indicate a rate-limiting methyl transfer as the initial step in the reaction catalyzed by Escherichia coli cyclopropane fatty acid synthase, *Biochemistry* 43, 13510-13524.

176. Yuan, Y., and Barry, C. E. (1996) A common mechanism for the biosynthesis of methoxy and cyclopropyl mycolic acids in Mycobacterium tuberculosis, *Proc. Natl. Acad. Sci. USA* 93, 12828-12833.

177. Molitor, E. J. Paschal, B. M. and Liu, H.-w. (2003) Cyclopropane fatty acid synthase from *Escherichia coli*: enzyme purification and inhibition by vinylfluorine and epoxide-containing substrate analogues, *ChemBioChem* 4, 1352-1356.

178. Kim, J., Xiao, H., Bonanno, J. B., Kalyanaraman, C., Brown, S., Tang, X., Al-Obaidi, N. F., Patskovsky, Y., Babbitt, P. C., Jacobson, M. P., Lee, Y. S., and Almo, S. C. (2013) Structure-guided discovery of the metabolite carboxy-SAM that modulates tRNA function, *Nature* 498, 123-126.

179. Nasvall, S. J., Chen, P., and Björk, G. R. (2004) The modified wobble nucleoside uridine-5-oxyacetic acid in tRNAPro(cmo5UGG) promotes reading of all four proline codons *in vivo*, *RNA* 10, 1662-1673.

180. Struck, A. W., Thompson, M. L., Wong, L. S., and Micklefield, J. (2012) *S*-adenosyl-methionine-dependent methyltransferases: highly versatile enzymes in biocatalysis, biosynthesis and other biotechnological applications, *ChemBioChem* 13, 2642-2655.

181. Frey, P. A., Hegeman, A. D., and Ruzicka, F. J. (2008) The radical SAM superfamily, *Crit. Rev. Biochem. Mol. Biol.* 43, 63-88.

182. Marsh, E. N., and Meléndez, G. D. (2012) Adenosylcobalamin enzymes: theory and experiment begin to converge, *Biochim. Biophys. Acta.* 1824, 1154-1164.

183. Frey, P. A. (1993) Lysine 2,3-aminomutase: is adenosylmethionine a poor man's adenosylcobalamin? *FASEB J.* 7, 412-470.

184. Sofia, H. J., Chen, G., Hetzler, B. G., Reyes-Spindola, J. F., and Miller, N. E. (2001) Radical SAM, a novel protein superfamily linking unresolved steps in familiar biosynthetic pathways with radical mechanisms: functional characterization using new analysis and information visualization methods, *Nucleic Acids Res.* 29, 1097-1106.

185. Stubbe, J. (2011) Biochemistry: The two faces of SAM, *Science,* 332, 544-545.

186. Frey, P. A. and Magnusson, O. T. (2003) *S*-Adenosylmethionine: a wolf in sheep's clothing, or a rich man's adenosylcobalamin? *Chem. Rev.* 103, 2129-2148.

187. Ruszczycky, M. W., Ogasawara, Y., and Liu, H.-w. (2012) Radical SAM enzymes in the biosynthesis of sugar-containing natural products, *Biochim. Biophys. Acta.* 1824, 1231-1244.

188. Zhang, Y., Zhu, X., Torelli, A. T., Lee, M., Dzikovski, B., Koralewski, R. M., Wang, E., Freed, J., Krebs, C., Ealick, S. E., and Lin, H. (2010) Diphthamide biosynthesis requires an organic radical generated by an iron-sulphur enzyme, *Nature* 465, 891-896.

189. Challand, M. R., Driesener, R. C. and Roach, P. L. (2011) Radical *S*-adenosylmethionine enzymes: Mechanism, control and function, *Nat. Prod. Rep.* 28, 1696-1721.

190. Zhang, Q. and Liu, W. (2011) Complex biotransformations catalyzed by radical *S*-adenosylmethionine enzymes, *J. Biol. Chem.* 286, 30245-30252.

191. Hiscox, M. J., Driesener, R.C., and Roach, P. L. (2012) Enzyme catalyzed formation of radicals from *S*-adenosylmethionine and inhibition of enzyme activity by the cleavage products, *Biochim. Biophys. Acta.* 1824, 1165-1177.

192. Dowling, D. P., Vey, J. L., Croft, A. K., and Drennan, C. L. (2012) Structural diversity in the AdoMet radical enzyme superfamily, *Biochim. Biophys. Acta.* 1824, 1178-1195.

193. Bandarian, V. (2012) Radical SAM enzymes involved in the biosynthesis of purine-based natural products, *Biochim. Biophys. Acta.* 1824, 1245-1253.

194. Duffus, B. R., Hamilton, T. L., Shepard, E. M., Boyd, E. S., Peters, J. W., and Broderick, J. B. (2012) Radical AdoMet enzymes in complex metal cluster biosynthesis, *Biochim. Biophys. Acta.* 1824, 1254-1263.

195. Shisler, K. A., and Broderick, J. B. (2012) Emerging themes in radical SAM chemistry, *Curr. Opin. Struct. Biol.* 22, 701-710.

196. Ballinger, M. D., Frey, P. A., and Reed, G. H. (1992) Structure of a substrate radical intermediate in the reaction of lysine 2,3-aminomutase, *Biochemistry* 31, 10782-10789.

197. Wu, W., Lieder, K. W., Reed, G. H., and Frey, P. A. (1995) Observation of a second substrate radical intermediate in the reaction of lysine 2,3-aminomutase: a radical centered on the beta-carbon of the alternative substrate, 4-thia-L-lysine, *Biochemistry* 34, 10532-10537.

198. Magnusson, O. Th., Reed, G. H. and Frey, P. A. (2001) Characterization of an allylic analogue of the 5'-deoxyadenosyl radical: an intermediate in the reaction of lysine 2,3-aminomutase, *Biochemistry* 40, 7773-7782.

199. Ruzicka, F. J. and Frey, P. A. (2007) Glutamate 2,3-aminomutase: a new member of the radical SAM superfamily of enzymes, *Biochim. Biophys. Acta* 1774, 286-296.

200. Yang, L., Nelson, R. S., Benjdia, A., Lin, G., Telser, J., Stoll, S., Schlichting, I. and Li, L. (2013) A radical transfer pathway in spore photoproduct lyase, *Biochemistry* 52, 3041-3050.

201. Yang, L., Lin, G., Nelson, R. S., Jian, Y., Telser, J. and Li, L. (2012) Mechanistic studies of the spore photoproduct lyase via a single cysteine mutation, *Biochemistry* 51, 7173-7188.

202. Buis, J. M., Cheek, J., Kalliri, E. and Broderick, J. B. (2006) Characterization of an active spore photoproduct lyase, a DNA repair enzyme in the radical *S*-adenosylmethionine superfamily, *J. Biol. Chem.* 281, 25994-26003.

203. Gaston, M. A., Zhang, L., Green-Church, K. B. and Krzycki, J. A. (2011) The complete biosynthesis of the genetically encoded amino acid pyrrolysine from lysine, *Nature* 471, 647-650.

204. Quitterer, F., List, A., Eisenreich, W., Bacher, A., and Groll, M. (2011) Crystal structure of methylornithine synthase (PylB): insights into the pyrrolysine biosynthesis, *Angew. Chem. Int. Ed.* 50, 1-5.

205. Cone, M. C., Yin, X., Grochowski, L. L., Parker, M. R. and Zabriskie, T. M. (2003) The blasticidin S biosynthesis gene cluster from *Streptomyces griseochromogenes*: sequence analysis, organization, and initial characterization, *ChemBioChem* 4, 821-828.

206. Layer, G., Kervio, E., Morlock, G., Heinz, D. W., Jahn, D., Retey, J. and Schubert, W. (2005) Structural and functional comparison of HemN to other radical SAM enzymes, *Biol. Chem.* 386, 971-980.

207. Li, R., Reed, D. W., Liu, E., Nowak, J., Pelcher, L. E., Page, J. E., and Covello, P. S. (2006) Functional genomics analysis of alkaloid biosynthesis in *Hyoscyamus niger* reveals a cytochrome P450 involved in littorine rearrangement, *Chem. Biol.* 13, 513-520.

208. Duschene, K. S., Veneziano, S. E., Silver, S. C., and Broderick, J. B. (2009) Control of radical chemistry in the AdoMet radical enzymes, *Curr. Opin. Chem. Biol.* 13, 74-83.

209. Marsh, E. N., Patterson, D. P., and Li, L. (2010) Adenosyl radical: reagent and catalyst in enzyme reactions, *ChemBioChem*. 11, 604-612.

210. Farrar, C. E., Siu, K. K., Howell, P. L., and Jarrett, J. T. (2010) Biotin synthase exhibits burst kinetics and multiple turnovers in the absence of inhibition by products and product-related biomolecules, *Biochemistry* 49, 9985-9996.

211. Farrar, C. E., and Jarrett, J.T. (2009) Protein residues that control the reaction trajectory in *S*-adenosylmethionine radical enzymes: mutagenesis of asparagine 153 and aspartate 155 in Escherichia coli biotin synthase, *Biochemistry* 48, 2248-2258.

212. Forouhar, F., Arragain, S., Atta, M., Gambarelli, S., Mouesca, J. M., Hussain, M., Xiao, R., Kieffer-Jaquinod, S., Seetharaman, J., Acton, T. B., Montelione, G. T, Mulliez, E., Hunt, J. F., and Fontecave, M. (2013) Two Fe-S clusters catalyze sulfur insertion by radical-SAM methylthiotransferases, *Nat. Chem. Biol.* 9, 333-338.

213. Flühe, L., Knappe, T. A., Gattner, M. J., Schäfer, A., Burghaus, O., Linne, U., and Maraheil, M. A. (2012) The radical SAM enzyme AlbA catalyzes thioether bond formation in substilosin A, *Nat. Chem. Biol.* 8, 350-357.

214. Flühe, L., Burghaus, O., Wieckowski, B. M., Giessen, T. W., Linne, U., and Marahiel, M. A. (2013) Two [4Fe-4S] clusters containing radical SAM enzyme SkfB catalyze thioether bond formation during the maturation of the sporulation killing factor, *J. Am. Chem. Soc.* 135, 959-962.

215. Hänzelmann, P., and Schindelin, H. (2006) Binding of 5'-GTP to the *C*-terminal FeS cluster of the radical S-adenosylmethionine enzyme MoaA provides insights into its mechanism, *Proc. Natl. Acad. Sci. U.S.A.*103, 6829-6834.

216. Mehta, A. P., Hanes, J. W., Abdelwahed, S. H., Hilmey, D. G., Hänzelmann, P., and Begley, T. P. (2013) Catalysis of a new ribose carbon-insertion reaction by the molybdenum cofactor biosynthetic enzyme MoaA, *Biochemistry* 52, 1134-1136.

217. Hover, B. M., Loksztejn, A., Ribeiro, A. A., and Yokoyama, K. (2013) Identification of a cyclic nucleotide as a cryptic intermediate in molybdenum cofactor biosynthesis, *J. Am. Chem. Soc.*135, 7019-7032.

218. Wecksler, S. R., Stoll, S., Tran, H., Magnusson, O. T., Wu, S., King, D., Britt, R. D. and Klinman, J. P. (2009) Pyrroloquinoline quinone biogenesis: demonstration that PqqE from *Klebsiella pneumoniae* is a radical SAM enzyme, *Biochemistry* 48, 10151-10161.

219. Decamps, L., Philmus, B., Benjdia, A., White, R., Begley, T. P., and Berteau, O. (2012) Biosynthesis of F_0, precursor of the F_{420} cofactor, requires a unique two Radical-SAM domain enzyme and tyrosine as substrate, *J. Am. Chem. Soc.* 134, 18173-18176.

220. Cooper, L. E., Fedoseyenko, D., Abdelwahed, S. H., Kim, S.-H., Dairi, T., and Begley, T. P. (2013) *In vitro* reconstitution of the radical *S*-adenosylmethionine enzyme MqnC involved in the biosynthesis of futalosine-derived menaquinone, *Biochemistry* 52, 4592-4594.

221. Hänzelmann, P., Hernández, H. L., Menzel, C., García-Serres, R., Huynh, B. H., Johnson, M. K., Mendel, R. R., and Schindelin, H. (2004) Characterization of MOCS1A, an oxygen-sensitive iron-sulfur protein involved in human molybdenum cofactor biosynthesis, *J. Biol. Chem.* 279, 34721-34732.

222. Lees, N. S., Hänzelmann, P., Hernandez, H. L., Subramanian, S., Schindelin, H., Johnson, M. K., and Hoffman, B. M. (2009) ENDOR spectroscopy shows that guanine N1 binds to [4Fe-4S] cluster II of the *S*-adenosylmethionine-dependent enzyme MoaA: mechanistic implications, *J. Am. Chem. Soc.* 131, 9184-9185.

223. Rand, K., Noll, C., Schiebel, H. M., Kemken, D., Dülcks, T., Kalesse, M., Heinz, D. W., and Layer, G. (2010) The oxygen-independent coproporphyrinogen III oxidase HemN utilizes harderoporphyrinogen as a reaction intermediate during conversion of coproporphyrinogen III to protoporphyrinogen IX, *Biol. Chem.* 391, 55-63.

224. Layer, G., Grage, K., Teschner, T., Schünemann, V., Breckau, D., Masoumi, A., Jahn, M., Heathcote, P., Trautwein, A. X., and Jahn, D. (2005) Radical *S*-adenosylmethionine enzyme coproporphyrinogen III oxidase HemN: functional features of the [4Fe-4S] cluster and the two bound *S*-adenosyl-L-methionines, *J. Biol. Chem.* 280, 29038-29046.

225. Challand, M. R., Martins, F. T., and Roach, P. L. (2010) Catalytic activity of the anaerobic tyrosine lyase required for thiamine biosynthesis in *Escherichia coli*, *J. Biol. Chem.* 285, 5240-5248.

226. Chatterjee, A., Li, Y., Zhang, Y., Grove, T. L., Lee, M., Krebs, C., Booker, S. J., Begley, T. P., and Ealick, S. E. (2008) Reconstitution of ThiC in thiamine pyrimidine biosynthesis expands the radical SAM superfamily, *Nat. Chem. Biol.* 4, 758-765.

227. Chatterjee, A., Hazra, A. B., Abdelwahed, S., Hilmey, D. G., and Begley, T. P. (2010) A "radical dance" in thiamin biosynthesis: mechanistic analysis of the bacterial hydroxymethylpyrimidine phosphate synthase, *Angew. Chem. Int. Ed.* 49, 8653-8656.

228. Bethel, R. D., and Darensbourg, M. Y. (2013) Bioinorganic chemistry: Enzymes activated by synthetic components, *Nature* 499, 40-41.

229. Shepard, E. M., McGlynn, S. E., Bueling, A. L., Grady-Smith, C. S., George, S. J., Winslow, M. A., Cramer, S. P., Peters, J. W., and Broderick, J. B. (2010) Synthesis of the 2Fe subcluster of the [FeFe]-hydrogenase H cluster on the HydF scaffold, *Proc. Natl. Acad. Sci. U.S.A.*107, 10448-10453.

230. McCarty, R. M., Krebs, C., and Bandarian, V. (2013) Spectroscopic, steady-state kinetic, and mechanistic characterization of the radical SAM enzyme QueE, which catalyzes a complex cyclization reaction in the biosynthesis of 7‑deazapurines, *Biochemistry* 52, 188-198.

231. Young, A. P., and Bandarian, V. (2011) Pyruvate is the source of the two carbons that are required for formation of the imidazoline ring of 4-demethylwyosine, *Biochemistry* 50, 10573-10575.

232. Grove, T. L., Lee, K.-H., St. Clair, J., Krebs, C., and Booker, S. J. (2008) *In vitro* characterization of AtsB, a radical SAM formylglycine-generating enzyme that contains three [4Fe-4S] clusters, *Biochemistry* 47, 7523-7538.

233. Grove, T. L., Ahlum, J. H., Sharma, P., Krebs, C., and Booker, S. J. (2010) A consensus mechanism for radical SAM-dependent dehydrogenation? BtrN contains two [4Fe-4S] clusters, *Biochemistry* 49, 3783-3785.

234. Zhang, Q., Li, Y., Chen, D., Duan, L., Shen, B., and Liu, W. (2011) Radical-mediated enzymatic carbon chain fragmentation-recombination, *Nat. Chem. Biol.* 7, 154-160.

235. Zhang, Q., Chen, D., Lin, J., Liao, R., Tong, W., Xu, Z. and Liu, W. (2011) Characterization of NocL involved in thiopeptide Nocathiacin I biosynthesis: a [4Fe-4S] cluster and the catalysis of a radical *S*-adenosylmethionine enzyme, *J. Biol. Chem.* 286, 21287-21294.

236. Kamat, S. S., Williams, H. J., and Raushel, F. M. (2011) Intermediates in the transformation of phosphonates to phosphate by bacteria, *Nature* 480, 570-573.

237. Kamat, S. S., Williams, H. J., Dangott, L. J., Chakrabarti, M., and Raushel, F. M. (2013) The catalytic mechanism for aerobic formation of methane by bacteria, *Nature* 497, 132-136.

238. Zhang, Q., van der Donk, W. A., and Liu, W. (2012) Radical-mediated enzymatic methylation: a tale of two SAMs, *Acc. Chem. Res.* 45, 555-564.

239. Wiig, J. A., Hu, Y., Lee, C. C., and Ribbe, M. W. (2012) Radical SAM-dependent carbon insertion into the nitrogenase M-cluster, *Science* 337, 1672-1675.

240. Fujimori, D. G. (2013) Radical SAM-mediated methylation reactions, *Current Opinion in Chemical Biology* 17, 597-604.

241. Yan, F., LaMarre, J. M., Röhrich, R., Wiesner, J., Jomaa, H., Mankin, A. S., and Fujimori, D. G. (2010) RlmN and Cfr are radical SAM enzymes involved in methylation of ribosomal RNA, *J. Am. Chem. Soc.* 132, 3953-3964.

242. Grove, T. L., Benner, J. S., Radle, M. I., Ahlum, J. H., Landgraf, B. J., Krebs, C., and Booker, S. J. (2011) A radically different mechanism for *S*-adenosylmethionine dependent methyltransferases, *Science* 332, 604-607.

243. Boal, A. K., Grove, T. L., McLaughlin, M. I., Yennawar, N. H., Booker, S. J., and Rosenzweig, A. C. (2011) Structural basis for methyl transfer by a radical SAM enzyme, *Science* 332, 1089-1092.

244. Grove, T. L., Radle, M. I., Krebs, C., and Booker, S. J. (2011) Cfr and RlmN contain a single [4Fe-4S] cluster, which directs two distinct reactivities for *S*-adenosylmethionine: methyl transfer by S_N2 displacement and radical generation, *J. Am. Chem. Soc.* 133, 19586-19589.

245. McCusker, K. P., Medzihradszky, K. F., Shiver, A. L., Nichols, R. J., Yan, F., Maltby, D. A., Gross, C. A., and Fujimori, D. G. (2012) Covalent intermediate in the catalytic mechanism of the radical *S*-adenosyl-L-methionine methyl synthase RlmN trapped by mutagenesis, *J. Am. Chem. Soc.* 134, 18074-18081.

246. Spatzal, T., Aksoyoglu, M., Zhang, L., Andrade, S. L. A., Schleicher, E., Weber, S., Rees, D. C., and Einsle, O. (2011) Evidence for interstitial carbon in nitrogenase FeMo cofactor, *Science* 334, 940.

247. Yu, Y., Duan, L., Zhang, Q., Liao, R., Ding, Y., Pan, H., Wendt-Pienkowski, E., Tang, G., Shen, B., and Liu, W. (2009) Nosiheptide biosynthesis featuring a unique indole side ring formation on the characteristic thiopeptide framework, *ACS Chem. Biol.* 4, 855-864.

248. Brooker, S. J. (2009) Anaerobic functionalization of unactivated C-H bonds, *Curr. Opin. Chem. Biol.* 13, 58-73.

249. Woodyer, R. D., Li, G., Zhao, H., and van der Donk, W. A. (2007) New insight into the mechanism of methyl transfer during the biosynthesis of fosfomycin, *Chem. Commun.* 359-361.

250. Kuzuyama, T., Hidaka, T., Kamigiri, K., Imai, S., and Seto, H. (1992) Studies on the biosynthesis of fosfomycin: 4. The biosynthetic origin of the methyl group of fosfomycin, *J. Antibiot.* 45, 1812-1814.

251. Westrich, L., Heide, L., and Li, S. M. (2003) CloN6, a novelmethyltransferase catalysing themethylation of the pyrrole-2-carboxyl moiety of clorobiocin, *ChemBioChem* 4, 768-773.

252. Kamigiri, K., Hidaka, T., Imai, S., Murakami, T., and Seto, H. (1992) Studies on the biosynthesis of bialaphos (SF-1293): 12. C-P bond formation mechanism of bialaphos: discovery of a P-methylation enzyme. *J. Antibiot.* 45, 781-787.

253. Pierre, S., Guillot, A., Benjdia, A., Sandström, C., Langella, P., and Berteau, O. (2012) Thiostrepton tryptophan methyltransferase expands the chemistry of radical SAM enzymes, *Nat. Chem. Biol.* 8, 957-959.

254. Werner, W. J., Allen, K. D., Hu, K., Helms, G. L., Chen, B. S., and Wang, S. C. (2011) *In vitro* phophinate methylation by PhpK from Kitasatospora phosalacinea, *Biochemistry*, 50, 8986-8988.

255. Kim, H. J., McCarty, R. M., Ogasawara, Y., Liu, Y.-n., Mansoorabadi, S. O., LeVieux, J., and Liu, H.-w. (2013) GenK-catalyzed C-6' methylation in the biosynthesis of gentamicin: isolation and characterization of a cobalamin-dependent radical SAM enzyme, *J. Am. Chem. Soc.* 135, 8093-8096.

256. Strous, M., Pelletier, E., Mangenot, S., Rattei, T., Lehner, A., Taylor, M. W., Horn, M., Daims, H. Bartol-Mavel, D., Wincker, P., Barbe, V., Fonknechten, N., Vallenet, D., Segurens, B., Schenowitz-Truong, C., Médigue, C., Collingro, A., Snel, B., Dutilh, B. E., Op den Camp, H. J. M., van der Drift, C., Cirpus, I., van de Pas-Schoonen, K. T., Harhangi, H. R., van Niftrik, L., Schmid, M., Keltjens, J., van de Vossenberg, J., Kartal, B., Meier, H., Frishman, D., Huynen, M. A., Mewes, H., Weissenbach, J., Jetten, m. S. M., Wagner, M. and Le Paslier, D. (2006) Deciphering the evolution and metabolism of an anammox bacterium from a community genome, *Nature* 440, 790-794.

257. Freeman, M. F., Gurgui, C., Helf, M. J., Morinaka, B. I., Uria, A. R., Oladham, N. J., Sahl, H. G., Mastunaga, S., and Piel, J. (2012) Metagenome mining reveals polytheonamides as posttranslationally modified ribosomal peptides, *Science* 338, 387-390.

258. Marquardt, J. L., Brown, E. D., Lane, W. S., Haley, T. M., Ichikawa, Y., Wong, C. H., and Walsh, C.T. (1994) Kinetics, stoichiometry, and identification of the reactive thiolate in the inactivation of UDP-GlcNAc enolpyruvoyl transferase by the antibiotic Fosfomycin, *Biochemistry* 33, 10646-10651.

259. Hidaka, T., Goda, M., Kuzuyama, T., Takei, N., Kidaka, M., and Seto, H. (1995) Cloning and nucleotide sequence of fosfomycin biosynthetic genes of *Streptomyces wedmorensis*, *Mol. Gen. Genet.* 249, 274-280.

260. Hammerschmidt, F. (1994) Incorporation of L-[methyl-$^{2}H_{3}$]methionine and 2-[hydroxy-^{18}O] hydroxyethylphosphonic acid into fosfomycin in *Streptomyces fradiae*-an unusual methyl transfer, *Angew. Chem. Int. Ed.* 33, 341-342.

261. Woodyer, R. D., Shao, Z., Metcalf, W. M., Thomas, P. M., Kelleher, N. L., Blodgett, J. A., Metcalf, W. W., van der Donk, W. A., and Zhao, H. (2006) Heterologous production of fosfomycin and identification of the minimal biosynthetic cluster, *Chem. Biol.* 13, 1171-1182.

262. Metcalf, W. W. and van der Donk, W. A. (2009) Biosynthesis of phosphonic and phosphinic acid natural products, *Annu. Rev. Biochem*. 78, 65-94.

263. Morita, M., Tomita, K., Ishizawa, M., Takagi, K., Kawamura, F., Takahashi, H., and Morino, T. (1999) Cloning of oxetanocin A biosynthetic and resistance genes that reside on a plasmid of *Bacillus megaterium* strain NK84-0128, *Biosci. Biotechnol. Biochem.* 63, 563-566.

264. Shimada, N., Hasegawa, S., Harada, T., Tomisawa, T., Fujii, A., and Takita, T. (1986) Oxetanocin, a novel nucleoside from bacteria, *J. Antibiot.* 39, 1623-1625.

265. Hahn, D. R., Graupner, P. R., Chapin, E., Gray, J., Heim, D., Gilbert, J. R., and Gerwick, B. C. (2009) Albucidin: a novel bleaching herbicide from *Streptomyces albus subsp. chlorinus* NRRL B-24108, *J. Antibiot.* 62, 191-194.

266. Seki, J., Shimada, N., Takahashi, K., Takita, T., Takeuchi, T., and Hoshino, H. (1989) Inhibition of infectivity of human immunodeficiency virus by a novel nucleoside, oxetanocin, and related compounds, *Antimicrob. Agents Chemother.* 33, 773-775.

267. Gumina, G. and Chu, C. K. (2002) Synthesis of L-oxetanocin, *Org. Lett.* 4, 1147-1149.

268. Szu, P.-h. (2008) The biosynthetic of TDP-D-Desosamine: Characterization and mechanistic studies of DesII, a radical *S*-adenosylmethionine-dependent enzyme, dissertation, University of Texas at Austin.

269. Chang, W.-c. (2011) Mechanistic studies of two iron-containing enzymes that catalyze unusual chemical transformations, dissertation, University of Texas at Austin.

270. Shih, Y.-p., Wu, H.-c., Hu, S.-m., Wang, T.-f., and Wang, A. H.-j. (2005) Self-cleavage of fusion protein in vivo using TEV protease to yield native protein, *Protein Sci.* 14, 936-941.

271. Kapust, R. B. and Waugh, D. S. (1999) *Escherichia coli* maltose-binding protein is uncommonly effective at promoting the solubility of polypeptides to which it is fused, *Protein Sci.* 8, 1668-1674.

272. Szu, P. H., Ruszczycky, M. W., Choi, S. H., Yan, F., and Liu, H.-w. (2009) Characterization and mechanistic studies of DesII: a radical *S*-adenosyl-L-methionine enzyme involved in the biosynthesis of TDP-D-desosamine, *J. Am. Chem. Soc.* 131, 14030-14042.

273. Bandarian, V. and Matthews, R. G. (2001) Quantitation of rate enhancements attained by the binding of cobalamin to methionine synthase, *Biochemistry* 40, 5056-5064.

274. Jarrett, J. T., Goulding, C. W., Fluhr, K., Huang, S., and Matthews, R. G. (1997) Purification and assay of cobalamin-dependent methione synthase from *Escherichia coli.*, *Methods in Enzymology*, 281, 196-213.

275. Feng, Y., Munos, J. W., Liu, P. and Liu, H.-w. (2006) Biosynthesis of fosfomycin, re-examination and re-confirmation of a unique Fe(II) and NAD(P)H-dependent epoxidation reaction, *Biochemistry* 45, 11473-11481.

276. Fish, W. W. (1988) Rapid colorimetric micromethod for the quantitation of complexed iron in biological samples, *Meth. Enzymol.* 158, 357-364.

277. Krasotkina, J., Walters, T., Maruya, K. A., and Ragsdale, S. W. (2001) Characterization of the B_{12}- and iron-sulfur-containing reductive dehalogenase from *Desulfitobacterium chlororespirans*, *J. Biol. Chem.* 276, 40991-40997.

278. Creutz, C. and Sutin, N. (1974) Kinetics of the reactions of sodium dithionite with dioxygen and hydrogen peroxide, *Inorg. Chem.* 13, 2041-2043.

279. Kim, H. J., Ruszczycky, M. W., Choi, S. H., Liu, Y.-n., and Liu, H.-w. (2011) Enzyme-catalysed [4+2] cycloaddition is a key step in the biosynthesis of spinosyn A, *Nature* 473, 109-112.

280. Nagahata, T., Kitagawa, M., and Matsubara, K. (1994) Effect of oxetanocin G, a novel nucleoside analog, on DNA synthesis by Hepatitis B Virus virions, *Antimicrob. Agents Chemother.* 38, 707-712.

281. Ragsdale, S. W., Lindahl, P. A., and Müncks E. (1987) Mössbauer, EPR, and optical studies of the corrinoid/iron-Sulfur protein involved in the synthesiosf acetyl coenzyme A by *Clostridium thermoaceticum*, *J. Biol. Chem.* 262, 14289-14297.

282. Cercignani, G. and Allegrini, S. (1991) On the validity of continuous spectrophotometric assays for adenosine deaminase activity: A critical reappraisal, *Anal. Biochem.* 192, 312-315.

283. Paraskevopoulou, C., Fairhurst, S. A., Lowe, D. J., Brick, P. and Onesti, S. (2006) The Elongator subunit Elp3 contains a Fe_4S_4 cluster and binds *S*-adenosylmethionine, *Mol. Microbiol.* 59, 795-806.

284. Duschene, K. S. and Broderick, J. B. (2010) The antiviral protein viperin is a radical SAM enzyme, *FEBS Lett.* 584, 1263-1267.

285. Salnikov, D. S., Silaghi-Dumitrescu, R., Makarov, S. V., van Eldik, R., and Boss, G. R. (2011) Cobalamin reduction by dithionite: evidence for the formation of a six-coordinate cobalamin(II) complex, *Dalton Trans.* 40, 9831-9834.

286. Hogenkamp, H. P. C. (1963) A cyclic nucleoside derived from coenzyme B_{12}, *J. Biol. Chem.* 237, 1950-1952.

287. Schwartz, P. A. and Frey, P. A. (2007) 5'-peroxyadenosine and 5'-peroxyadenosylcobalamin as intermediates in the aerobic photolysis of adenosylcobalamin, *Biochemistry* 46, 7284-7292.

288. Hammerschmidt, F. (1992) Biosynthesis of natural products with a P-C bond: 9. Synthesis and incorporation of (*S*)-2-hydroxy-[2-^{2}H]ethylphosphonic and (*R*)-2-hydroxy-[2-^{2}H]ethylphosphonic acid into fosfomycin by *Streptomyces fradiae*, *Liebigs Ann. Chem.* 553-57.

289. Matthews, R. G. (2001) Cobalamin-dependent methyltransferases, *Acc. Chem. Res.* 34, 681-689.

290. Ruszczycky, M. W., Choi, S.-h., and Liu, H.-w. (2013) EPR-kinetic isotope effect study of the mechanism of radical-mediated dehydrogenation of an alcohol by the radical SAM enzyme DesII, *Proc. Natl. Acad. Sci. U.S.A.* 110, 2088-2093.

291. Kim, J., Darley, D. J., Buckel, W., and Pierik, A. J. (2008) An allylic ketyl radical intermediate in clostridial amino-acid fermentation, *Nature* 452, 239-242.

Vita

He (Grace) Sun was born in Tianjin, China, and is the only child of her parents. Grace graduated from Tianjin No. 3 High School in July, 2001 and attended the College of Pharmaceutical Science and Technology at Tianjin University during her undergraduate studies. After completing the junior division in two years, she joined Prof. Kang Zhao's laboratory and began her research work: synthesis of phenylaminoimidazoisoquinolin-9-one derivatives as potential tyrosine kinase inhibitors. In 2005, Grace was admitted to the graduate program in the Department of Chemistry at Washington State University where she began her graduate studies under the supervision of Prof. Zhaohui (Sunny) Zhou. There she coauthored two research publications describing the development of novel methodologies for characterizing methylation reactions for use in proteomic analyses. After obtaining an M.S. degree in chemistry in 2007, Grace decided to pursue her doctoral studies at the University of Texas at Austin (College of Pharmacy, Medicinal Chemistry division) and joined Prof. Hung-wen (Ben) Liu's group in January of 2008. She received the Competitive Graduate Scholarship from the College of Pharmacy in her second year and was a teaching assistant for courses in medicinal chemistry for one year and general chemistry laboratory for two years. Her research on the mechanistic studies of UDP-galactopyranose mutase led to one first-author publication. Several additional research articles from her other projects are currently in preparation.

Permanent email: h.sun@utexas.edu

This dissertation was typed by He Sun.